

NASA CR-66102

D2-84042-2

GPO PRICE \$ \_\_\_\_\_  
CFSTI PRICE(S) \$ \_\_\_\_\_

Hard copy (HC) 7.00  
Microfiche (MF) 1.75

ff 653 July 65

N66 26847

FACILITY FORM 802

(ACCESSION NUMBER)	(THRU)
<u>316</u>	<u>1</u>
(PAGES)	(CODE)
<u>CR-66102</u>	<u>31</u>
(NASA CR OR TMX OR AD NUMBER)	(CATEGORY)



# Synchronous Orbit Study

## Manned Orbital Telescope System

• Aerospace Group • The BOEING Company, Seattle, Washington

Distribution of this report is provided in the interest of information exchange. Responsibility for the

Langley Contractor Reports

A Systems Study of a Manned Orbital Telescope  
Synchronous Orbit Study  
NASA Contract NAS1-3968

ABSTRACT

A comparison study was conducted on operating a 120-inch telescope in a 28.5 degree inclined 24-hour synchronous orbit with a 28.5 degree inclined 250-nautical mile orbit. (This study investigation was an extension of "A Systems Study of a Manned Orbital Telescope," reported in Boeing document D2-84042-1, also identified as NASA Contractor Report CR-66047.) Comparisons of observation time, stability and control, thermal distortion, radiation and micrometeoroids, and costs are made between the two orbits. The study concluded that the Manned Orbital Telescope operating in a synchronous orbit will have considerable advantages with respect to observation time and thermal stability, but the logistics costs will increase.

**A SYSTEM STUDY OF A MANNED ORBITAL TELESCOPE  
SYNCHRONOUS ORBIT STUDY**

D2-84042-2

April 1966

Prepared for  
National Aeronautics and Space Administration  
Langley Research Center  
Hampton, Virginia

Under Contract NAS1-3968

Prepared by  
Aerospace Group  
THE BOEING COMPANY  
Seattle, Washington

Distribution of this report is provided in the interest of  
information exchange. Responsibility for the contents  
resides in the author or organization that prepared it.

D2-84042-2



*Print by end of*



**BLANK PAGE**

## CONTENTS

	<u>Page</u>
1.0 INTRODUCTION	1
2.0 SUMMARY	3
2.1 Concepts and Configurations	3
2.2 Operational Analysis	3
2.3 Structures	3
2.4 Radiation and Micrometeoroid Effects	4
2.5 Attitude Stability and Control	4
2.6 Data Management, Communications, Electrical Power	4
2.7 Cost	5
2.8 General Conclusions and Recommendations	5
3.0 SYNCHRONOUS ORBIT MOT SYSTEM FEASIBILITY	7
3.1 Concept and Configuration Definition	7
3.1.1 System Description	7
3.1.1.1 Typical MORL-MOT Assembly and Operational Sequence	9
3.1.1.2 Attachment Modes	11
3.1.2 Configuration	12
3.1.2.1 Baseline Telescope	14
3.1.2.2 Soft-Gimbal Mode	14
3.1.2.3 Detached Mode	21
3.1.2.4 Logistics Vehicle	27
3.2 Structural Analysis	31
3.2.1 Primary Structure	31
3.2.2 Limit Load Factors	31
3.2.3 Flight Control Comparison	33
3.2.4 Compatibility of Payload with Booster	33
3.2.5 Primary Mirror	38
3.2.5.1 Dynamics	38
3.2.5.2 Stresses	38
3.2.5.3 Deformation	38
3.3 Configuration Mass Analysis	39
3.3.1 Soft-Gimbal Mode	39
3.3.1.1 Mass Analysis Parameters	39
3.3.1.2 MOT Mass Analysis Details	40
3.3.1.3 Orbit Configuration Mass Properties	48
3.3.2 Detached Mode	50
3.3.2.1 Mass Analysis Parameters	50
3.3.2.2 MOT Mass Analysis Details	50
3.3.2.3 Shuttle-Vehicle Mass Analysis	50
3.3.2.4 Orbit Configuration Mass Properties	59

## CONTENTS (Cont.)

	<u>Page</u>
3.3.3 Logistics Vehicle	59
3.3.3.1 Conclusions	59
3.3.3.2 Mass Analysis Parameters	59
3.3.3.3 Mass Analysis Details	60
3.4 Flight Performance Analysis	64
3.4.1 Launch and Rendezvous	68
3.4.1.1 MORL	68
3.4.1.2 MOT and Logistics Vehicle	70
3.4.2 Orbit-Keeping and Stationkeeping	74
3.4.2.1 Perturbations Due to Earth Gravitational Anomalies	75
3.4.2.2 Perturbations Due to Sun and Moon Gravity Forces	75
3.4.2.3 Perturbations Due to Solar Radiation	76
3.4.2.4 Stationkeeping	76
3.4.3 Re-entry	76
3.4.4 Shuttle from Low Earth Orbit	76
3.5 Operational Analysis	77
3.5.1 Observational Limitations	79
3.5.1.1 Occultation by Earth	80
3.5.1.2 Occultation by the Sun	82
3.5.1.3 Occultation by the Moon	82
3.5.1.4 Available Observation Time	85
3.5.2 Functional and Timeline Analysis	85
4.0 OPERATIONAL AND DESIGN COMPARISONS	93
4.1 Thermal Distortion Control	93
4.1.1 Thermal Balance Analysis	93
4.1.1.1 Analysis Technique	99
4.1.1.2 Temperature Distributions	99
4.1.1.3 Conclusions	116
4.1.2 Thermal Distortions	116
4.1.2.1 Primary Mirror	116
4.1.2.2 Secondary Mirror-Support Tube	117
4.1.2.3 Conclusions	117
4.2 Attitude Control	127
4.2.1 Summary and Technical Approach	127
4.2.2 System Description	127
4.2.2.1 Requirements	127
4.2.2.2 Selected Configuration	127
4.2.2.3 CMG Characteristics	130
4.2.2.4 Reaction-Control System	135
4.2.2.5 Sensor Characteristics	136



## CONTENTS (Cont.)

	<u>Page</u>
4.4.2 Communications	237
4.4.2.1 Rf Communications Link	237
4.4.2.2 Laser Communication-Link Considerations	237
4.4.2.3 Photoscan Techniques	238
4.4.2.4 Conclusions and Recommendations	243
4.4.3 Navigation and Guidance	244
4.4.3.1 Synchronous Orbit Navigation and Guidance Profile	245
4.4.3.2 Synchronous Orbit Navigation System	245
4.4.3.3 Synchronous Orbit Rendezvous Guidance Description	251
4.4.3.4 Conclusions and Recommendations	256
4.4.4 Electrical Power	256
4.4.4.1 Soft-Gimbal Mode	257
4.4.4.2 Detached Mode	257
4.4.4.3 Conclusions and Recommendations	262
4.5 Flight-Performance Comparison -- Low Earth Orbit versus Synchronous Orbit	263
4.5.1 Launch and Rendezvous	263
4.5.2 Orbit-Keeping	264
4.5.3 Re-entry	264
4.5.4 Conclusions	264
4.6 Operational Comparison	266
4.6.1 Observation Time	266
4.6.2 Experiment Expendables	268
4.6.3 Conclusions and Recommendations	268
4.7 System Evaluation	273
4.7.1 Comparison Criteria	273
4.7.2 Systems Comparison	274
4.7.2.1 Mode of Operation	274
4.7.2.2 Orbital Altitude	275
4.7.3 General Conclusions and Recommendations	281
4.7.3.1 Mode of Operation	281
4.7.3.2 Operational Altitude	281
4.7.3.3 Recommended Follow-on Studies	282
5.0 REFERENCES	283

## 1.0 INTRODUCTION

The present investigation of the MOT in synchronous orbit is a natural extension of the study of the manned orbital telescope in low Earth orbit as reported in Boeing Document D2-84042-1. Early in that study, it was apparent that there might be significant advantages and disadvantages in going to such an orbit. For example, in a synchronous orbit there is a considerable gain in total observation time and in uninterrupted observation time for a particular target. Also, the cyclic nature of the thermal environment would be largely eliminated, and problems of thermal distortion control are thus reduced. However, such potential advantages might well be offset by difficulties in logistic resupply and crew cycling.

This preliminary comparison was made on the basis of the MOT in a 28.5-degree inclined, 24-hour synchronous orbit and in a low Earth (250-nautical-mile) 28.5-degree inclined orbit. The scientific objectives of the MOT in synchronous orbit remained the same as in low Earth orbit and, hence, will not be recapitulated here. Both the soft-gimbal and detached modes of operation were considered.

Specific objectives of the added study were to:

- 1) Establish the feasibility of placing and maintaining the MOT in a synchronous orbit;
- 2) Make comparisons between low Earth orbit and high Earth orbit in the areas of available observation time, thermal distortions, stability and control requirements, radiation and micrometeoroid protection, data management, communications, and electrical power;
- 3) Recommend the best altitude and mode of operation for the MOT.

The major study constraints are as follows:

- The concept for putting MORL in synchronous orbit shall be that described in Douglas Report SM 46079 except for minor modifications.
- The basic MOT configuration (developed in D2-84042-1) will be launched unmanned and rendezvoused with the MORL, similar to low Earth orbit.
- The launch vehicle for the MOT, MORL, and logistic vehicles will be the Saturn V.
- The orbital configuration for the synchronous orbit will be as similar as possible to the low Earth orbit to facilitate direct comparisons.

Feasibility of placing and maintaining the MOT in synchronous orbit was studied by determining if a reasonable launch configuration could be developed for the various elements of the observatory, including the MOT, MORL, and the logistics vehicle. Problems of putting these elements into synchronous orbit, rendezvousing,

and assembling them into an observatory were examined as were the problems associated with resupplying the observatory. The comparisons in observation time, thermal distortion, etc., were made to identify significant problems or advantages in going to synchronous orbit. To make the picture somewhat more complete, a preliminary cost comparison was added. This cost comparison was based only on booster and booster launch costs because it was assumed that MOT and MORL and logistics vehicle costs would be very nearly equal for high and low Earth orbits.

## 2.0 SUMMARY

Principal results of the synchronous orbit study are summarized below. Evaluation and comparison of the various system concepts investigated during the study are presented in Section 4.7. Detailed discussions of study items are located in pertinent sections of the report.

### 2.1 CONCEPTS AND CONFIGURATION

Operational system concepts and vehicle configurations based on the low-Earth-orbit study were developed for operation in synchronous orbit. No major change in overall operational concept or configurations appears to be necessary. Elimination of the forward telescope doors in the synchronous-orbit configuration is possible because of the brief exposure to Earth's albedo during any one orbit. Relatively minor changes are required with respect to radiation protection and logistics support. Use of the Saturn V as a launch vehicle for the synchronous-orbit system provides a wide margin of weight growth in the MOT system.

The logistics weight requirements for synchronous orbit are less severe than for the low Earth orbit because of the increased margin of booster capability and the reduction by approximately 50 percent of propellants required for attitude control, stationkeeping, and orbit-keeping for a given period of time.

Operation of the MOT coupled to the MORL by a soft-gimbal mount appears to be preferable for the synchronous-orbit case; additional investigation is warranted in this area.

### 2.2 OPERATIONAL ANALYSIS

The operational concepts developed for the low-Earth-orbit system were found to also apply generally to operation in synchronous orbit. Large gains in total observation time and the potential duration of a single exposure are achievable in synchronous orbit. With proper target selection, stellar, galactic, and intergalactic observations from synchronous orbit are possible for 24 hours per orbit, and planetary observations are achievable for 22.4 hours per orbit. This effectively doubles the total observation time available in low Earth orbit and provides for long uninterrupted exposures.

During this study, it was determined that the sensitivity of film to radiation requires its use within approximately 60 days in both the low Earth and synchronous orbits. A functional and timeline analysis for each case was developed to include this consideration.

### 2.3 STRUCTURES

The structural design of the MOT was determined to be compatible with the requirements for launch by the Saturn V and operation in synchronous orbit. Mirror



dynamics and stresses during launch to synchronous orbit were investigated and determined to be equal to or less than those encountered for launch to the low Earth orbit.

Thermal deformation of the primary mirror in synchronous orbit was determined to degrade the telescope performance less than in the low-Earth-orbit case. Total deformation of the mirror is greater in synchronous orbit (resulting in a greater change in focal length); but the root-mean-square deviation from a parabolic surface is nearly negligible because of the nearly constant viewing conditions.

#### 2.4 RADIATION AND MICROMETEOROID EFFECTS

The increased radiation environment in synchronous orbit over that in a low Earth orbit requires addition of approximately 14,200 pounds of shielding in the MORL, including the incorporation of a biowell to protect the crew against solar flares for 180 days. An additional 1000 pounds are required to protect the film for 60 days. This weight penalty is well within the launch capability of the Saturn V.

The primary-mirror performance over a period of 5 years is degraded slightly more in synchronous orbit.

Micrometeoroid effects in either orbit altitude were determined to have nearly negligible effects on the mirror or telescope structure during a normal period of operation.

#### 2.5 ATTITUDE STABILITY AND CONTROL

The external disturbance environment in synchronous orbit was determined and its effects compared with that of the low Earth orbit. The external disturbance torques are two orders of magnitude less in synchronous orbit; this results in a reduction of approximately 50 percent in the control-moment-gyro momentum required — a slight advantage for the synchronous orbit.

Control within the 0.01-arc-second stability required of the telescope appears feasible at either altitude and in either mode of operation.

#### 2.6 DATA MANAGEMENT, COMMUNICATIONS, AND ELECTRICAL POWER

Data management and communications are improved by operation in synchronous orbit in that continuous communication and data transfer to a single ground station are possible. Time delay in data transmission and the amount of redundant data transferred is thus reduced. Also eliminated is the need for a rapidly slewing space-vehicle-borne antenna as is required for the low-Earth-orbit case where considerable relative motion is imposed between the transmitter and receiver.

The electrical power subsystem for the MOT in synchronous orbit is similar to that for the low Earth orbit. However, for the MOT operating in the detached

mode in synchronous orbit, reduction of approximately 40 percent in size of the solar panels and a reduction of approximately 65 percent in battery weight is realized. This is due to the decreased amount of time per orbit spent within the shadow of the Earth.

## 2.7 COST

Operation of the MOT and MORL in synchronous orbit results in an increase in launch vehicle and launch operations cost by a factor of approximately 3.0 over those of the low-Earth-orbit system. However, the usable observation time is approximately doubled, resulting in an effective launch-cost-per-observation-cost increase of 1.5. Consideration of total system cost would reduce this factor still further.

## 2.8 GENERAL CONCLUSIONS AND RECOMMENDATIONS

Results of this study indicate that operation of the manned orbital telescope in synchronous orbit, in the soft-gimbal mode, is preferable unless total budgetary limitations or availability of launch vehicles prohibit inclusion of the Saturn V in the system.

Future studies pertaining to the manned orbital telescope should include:

- 1) Development of a 120-inch primary mirror;
- 2) Detailed investigation of attitude-control-system requirements;
- 3) Further design and evaluation of soft-gimbal hardware;
- 4) Definition and integration of astronomical and astrophysical requirements of the observatory;
- 5) Definition of a development program plan and a detailed costing analysis.

**BLANK PAGE**

### 3.0 SYNCHRONOUS ORBIT MOT SYSTEM FEASIBILITY

#### 3.1 CONCEPT AND CONFIGURATION DEFINITION

This section describes operational and configuration concepts developed for the manned orbital telescope for operation in a 24-hour synchronous orbit. In brief, the overall concept is to operate the MOT in a 28.5-degree inclined, synchronous orbit in conjunction with the Douglas MORL — directly attached to the MORL through a soft-gimbal system or in a detached mode. Support vehicles for the MORL-MOT synchronous orbit system include the following:

- Apollo Command Service Module (CSM) — Used for crew transport and as a command vehicle for the multimission module.
- Douglas Multimission Module — Used as a logistics carrier and launched in conjunction with an Apollo CSM.
- Shuttle Vehicle — Used for transportation in orbit between the MORL and the detached MOT.
- Saturn V — Used to launch MORL-MOT components into synchronous orbit.

##### 3.1.1 System Description

The postulated MOT system for the 24-hour synchronous orbit is an extension of the operational systems and configurations defined in a previous NASA-contracted study (Reference 1). The basic telescope concept is a 120-inch-aperture telescope developed for operation at an altitude of 250 nautical miles. This telescope is operated in conjunction with the synchronous-orbit MORL concept of the Douglas Aircraft Company (Reference 9). The launch vehicle considered in this study extension is the three-stage Saturn V comprised of an S-IC, S-II, and S-IVB, with a payload capability of 79,600 pounds to synchronous orbit, as defined in the Douglas MORL study.

For rendezvous with the MORL in synchronous orbit, the MOT, Apollo, and logistics vehicles are launched into a 100-nautical-mile holding orbit inclined at 28.5 degrees. From here a Hohmann transfer is made to synchronous-orbit altitude for rendezvous with the MORL. The S-IVB (third) stage of the Saturn V is used to perform the transfer maneuver. Propulsion for the MOT final rendezvous corrections is supplied by two 1000-pound thrusters located on the MOT cabin. During the launch of the MOT, an outer fairing and the nose cone are jettisoned after first-stage burnout at approximately 200,000-foot altitude to maximize the payload capability in orbit. The vehicle remains in this configuration until after burnout of the S-IV stage, then separation occurs. The general sequence of launch operations and parts jettisoning is illustrated in Figure 3.1-1.

For the present study, it was assumed that the MORL will be operational by the planned time of first operation of the MOT — approximately 1980.

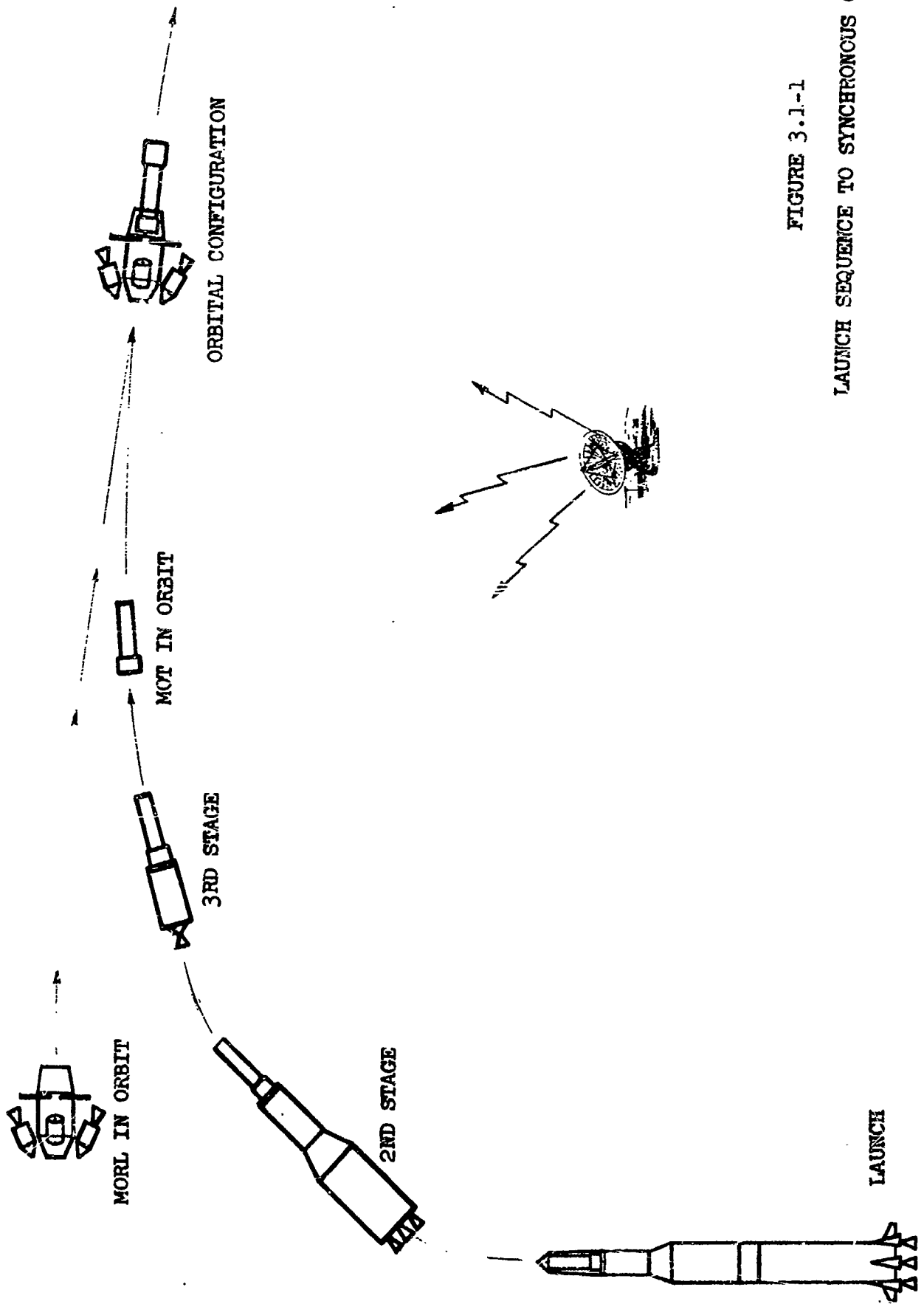


FIGURE 3.1.1-1

LAUNCH SEQUENCE TO SYNCHRONOUS ORBIT

The Douglas 24-hour synchronous-orbit MORL concept has been modified somewhat to meet operational requirements of the telescope. The MORL is required to accommodate a six-man crew for a period of 3 to 5 years. Part of the crew is rotated approximately each 90 days, using a nominal stay time of 180 days for each member. Three-man Apollo command modules are used to transport the crew between Earth and the orbiting MORL. Expendables, other than photographic film, are resupplied approximately every 180 days. Due to the limited stay time for unexposed and unprocessed photographic film, it is resupplied and returned to Earth every 90 days; this is accomplished in conjunction with the crew rotation flights.

For this study, the MORL is modified to enable docking and attachment of the MOT and the docking and repositioning of Apollo command modules, the Moon-mission-size Apollo service module, and logistics modules (Douglas MORL multi-mission modules). Additionally, the MORL is operational in a 28.5-degree-inclined orbit at synchronous-orbit altitude prior to launching the telescope. The telescope is only one of several scientific systems operating in conjunction with the MORL, and operation of the MOT is not the sole purpose for placing the MORL in synchronous orbit. However, in this study attention will be focused on the operation of the telescope. The following sequence of vehicle launchings and returns is postulated to keep the telescope in operation for a typical 1-year period. This sequence is adjusted in minor details (see the functional analysis, Section 3.5) to fit the specific requirements for the analysis. A number of alternate assembly sequences have been reviewed — some including launch of the MORL — but, for all of them, the requirements for operation of the MOT are relatively the same.

#### 3.1.1.1 Typical MORL-MOT Assembly and Operational Sequence —

<u>Time Days</u>	<u>Launch No.</u>	<u>Operation</u>
0		MORL is in orbit with two three-man Apollos and one multi-mission module attached.
0	1	Unmanned MOT launched and rendezvoused with the MORL.
0	2	<ul style="list-style-type: none"> <li>• One three-man Apollo CSM with one logistics multimission module launched and rendezvoused with the MORL. If the MOT is to operate in the detached mode, a shuttle vehicle is included in this launching. For launch, the shuttle vehicle is located in the adapter fairing behind the multimission module.</li> <li>• One three-man Apollo CSM and crew deorbited from the MORL. Each returning crew member has had 180 days stay time in the MORL.</li> <li>• If a shuttle vehicle is included in Launch 2, the multimission module is deorbited with and by the Apollo CSM and</li> </ul>

separated after a sufficient reduction in velocity to ensure its re-entry into the Earth's atmosphere.

- |     |   |  |
|-----|---|--|
| 90  | 3 | <ul style="list-style-type: none"> <li>• One three-man Apollo CSM launched and rendezvoused with the MORL.</li> <li>• One three-man Apollo CSM and crew deorbited from the MORL. Each returning crew member has had 180 days stay time in the MORL.</li> </ul>   |
| 180 | 4 | <ul style="list-style-type: none"> <li>• One three-man Apollo CSM with one logistics multimission module launched and rendezvoused with the MORL.</li> <li>• One three-man Apollo CSM and crew deorbited from the MORL. Each returning crew member has had 180 days stay time in the MORL.</li> <li>• The empty multimission module is deorbited with and by the Apollo CSM and separated after a sufficient reduction in velocity to ensure its re-entry into the Earth's atmosphere.</li> </ul>  |
| 270 | 5 | <ul style="list-style-type: none"> <li>• One three-man Apollo CSM launched and rendezvoused with the MORL.</li> <li>• One three-man Apollo CSM and crew deorbited from the MORL. Each returning crew member has had 180 days stay time in the MORL.</li> </ul>   |
| 360 | 6 | <ul style="list-style-type: none"> <li>• One three-man Apollo CSM with one logistics multimission module launched and rendezvoused with the MORL to continue operation of the MORL-MOT combination into the second year.</li> <li>• One three-man Apollo CSM and crew deorbited from the MORL. Each returning crew member has had 180 days stay time in the MORL.</li> <li>• The empty multimission module is deorbited with and by the Apollo CSM and separated after a sufficient reduction in velocity to ensure its re-entry into the Earth's atmosphere.</li> </ul> |

Summary of Baseline Sequence — For this sequence, the study:

- Assumes that MOT is a supplementary system to MORL in synchronous orbit.
- Assumes a requirement for balanced MORL-MOT configuration during telescope operation.
- Provides for immediate use of MOT after rendezvous with the MORL.
- Requires the following number of vehicles per year for MOT operation:

1	MORL	
1	MOT	
5	Apollos	} One Apollo and one multimission module are for continuation of operations into the second year.
2	Logistics Multimission Modules	
1	Shuttle Vehicle	If detached mode is used.
6	Launch Vehicles	Required to initiate and sustain MOT for 1 year and leave it in condition for second year operations. Five launch vehicles used if second-year operation is not required.

Logistic Support — The Douglas MORL multimission module is employed as the logistics vehicle and is launched in conjunction with an Apollo CSM. The Saturn V payload capability of 79,600 pounds to synchronous orbit allows the resupply cycle to be increased to 180 days rather than the 90 days used for the low-Earth-orbit study.

Film is resupplied each 90 days by including it as part of the logistics module payload each 180 days and as part of the payload on flights for personnel transfer.

3.1.1.2 Attachment Modes — Two modes of attachment during operation of the MOT were considered.

Soft-Gimbal Mode — Operation of the MOT in the soft-gimbal mode is essentially the same for both the synchronous- and low-Earth-orbit cases. After docking the MOT with the MORL, a rigid attachment is made between the MORL and the MOT gimbal support structure, and the boost-phase support structure for the gimbals and spring suspension system is removed. Setup, checkout, and alignment of the MOT scientific instrumentation and optical elements and preparation of the auxiliary equipment and subsystems are done during this period.

Gross positioning of the telescope is made by slewing the MOT-MORL combination to within 0.5 degree of the target (line of sight). One-half degree of angular travel is the approximate limit of the MOT spring suspension and two-axis gimbal system. The spring suspension and gimbal system are unlocked, and fine pointing is achieved using the star-tracking sensors. The MOT attitude-control system subsequently maintains attitude stabilization and pointing to the target.

Repair, maintenance, and logistics procedures for the soft-gimbal-mounted, synchronous-orbit telescope are similar to those for the 250-nautical-mile telescope described in detail in Reference 1.

Detached Mode — When operating in the detached mode, the MOT is separated from the MORL during observation periods. The MOT is launched and rendezvoused with the MORL similar to the procedure for the soft-gimbal mode. Setup, checkout,



and alignment of instrumentation and optical elements and preparation of auxiliary subsystems are done with the MOT rigidly attached to the MORL. During operation, the MOT is separated from the MORL (and is physically free of the station) by a distance of approximately 1 mile. Pointing and attitude control of the telescope is accomplished by systems within the MOT. When separated from the MORL, electrical power for the MOT is furnished by a self-contained system of solar panels and batteries. A shuttle vehicle is used for frequent short-duration trips required between the MORL and the telescope for exchange of film, changing of equipment operation, minor maintenance, etc. For major maintenance and repair activities, the MOT is redocked and rigidly attached to the MORL, providing direct access to the MOT cabin from the MORL via a shirt-sleeve environment.

### 3.1.2 Configuration

The manned orbital telescope system comprises the following major vehicle systems:

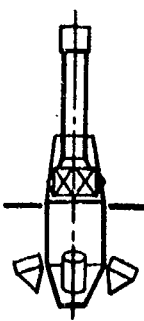
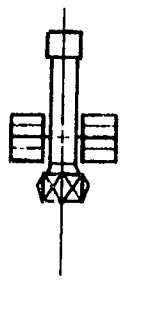
- Manned Orbital Research Laboratory (MORL)
- Manned Orbital Telescope (MOT)
- Apollo Logistics Vehicle
- Shuttle Vehicle (Detached Mode Only)

Conceptual designs of these vehicles, except the MORL, have been developed to support the synchronous-orbit MOT feasibility study. The MORL, Apollo command module, and Apollo service module are injected into synchronous orbit by the three-stage Saturn-V booster. This configuration has been studied by Douglas (Reference 9).

Changes to the MORL subsystems, in addition to those previously defined for the low-Earth-orbit missions, to support the MOT in synchronous orbit are:

- 1) Additional radiation protection for longer duration imposed by the MOT;
- 2) Longer stowage arms to facilitate the combination of Apollo command module, service module, and multimission module;
- 3) Additional structure (possibly) in the MORL docking area to accommodate the Apollo command module and service module.

In general, there is no major modification required of the low-Earth-orbit MOT configuration of Reference 1 to accomplish synchronous-orbit missions. Figure 3.1-2 shows a comparison of the low-Earth- and synchronous-orbit configurations. Differences among the configurations with respect to the star tracker and the MOT boost support structure are not a function of orbital altitude, but are design improvements over the previous (low-Earth-orbit) configuration. It can be concluded that the MORL-MOT combination for the low-Earth orbit is feasible in synchronous orbit with additional radiation shielding for the film and crew in the MORL.

LAUNCH VEHICLE	EARTH RETURN VEHICLE	MULTI-MISSION MODULE (CARGO)	THERMAL CONTROL	STAR TRACKER SYSTEM	ATTITUDE CONTROL SYSTEM	RADIATION SHIELDING	MOT SOLAR PANEL AREA	MOT BOOST SUPPORT STRUC.
 Low Orbit	Saturn IB	Deorbit Propulsion Provided (840 lbs)	Thermal Coating, Insulation, Fwd Doors	8 Star Trackers (Total)	Control Moment Gyros Desat. Prop = 350 lbs (180-Day Supply)	MORL = 1000 lbs MOT = 110 lbs	0 (Power from MORL)	Non-Jettisonable
	Saturn V	Deorbit with Apollo & S/M (4111 lbs Propellant added to S/M)	Thermal Coating Insulation	5 Star Trackers (Total)	Control Moment Gyros Desat. Prop = 5 lbs (180-Day Supply)	MORL = 15,200 lbs MOT = 0	0 (Power from MORL)	Jettisoned* During S-IVB Separation
 Low Orbit	Saturn IB	Deorbit Propulsion Provided (840 lbs)	Thermal Coating, Insulation, Fwd Doors	8 Star Trackers (Total)	Control Moment Gyros Desat. Prop = 350 lbs (180-Day Supply)	MORL = 1000 lbs MOT = 110 lbs	216 sq ft	Non-Jettisonable
	Saturn V	Deorbit with Apollo C/M & S/M (4111 lbs Propellant added to S/M)	Thermal Coating, Insulation	5 Star Trackers (Total)	Control Moment Gyros Desat. Prop = 5 lbs (180-Day Supply)	MORL = 15,200 lbs MOT = 0	132 sq ft	Jettisoned* During S-IVB Separation

\* Denotes Design Improvement Only

FIGURE 3.1-2 CONFIGURATION COMPARISON

Adaptation to the higher-performance launch vehicle is also required for the synchronous-orbit mission.

The following sections describe configuration changes required for operating in a 24-hour synchronous orbit instead of the previously defined 250-nautical-mile low Earth orbit.

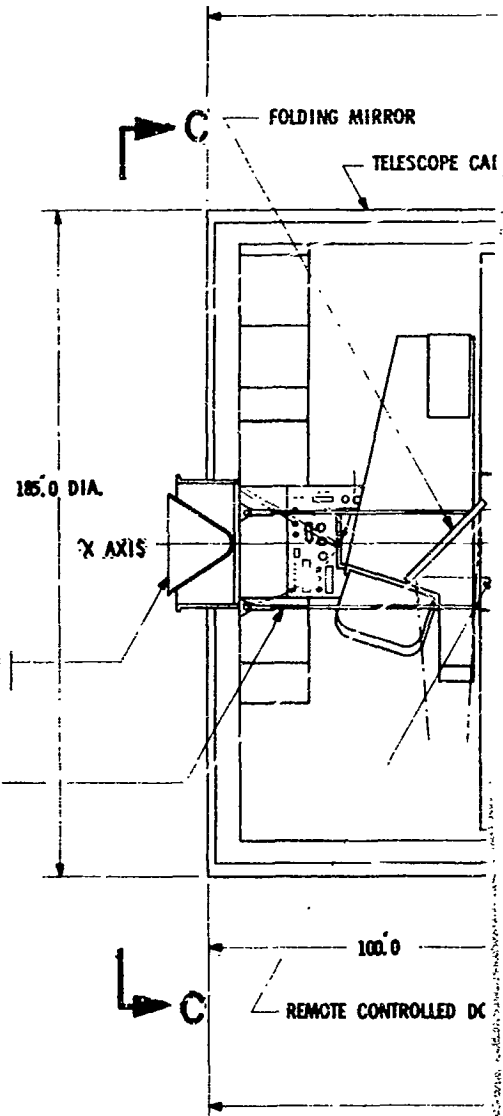
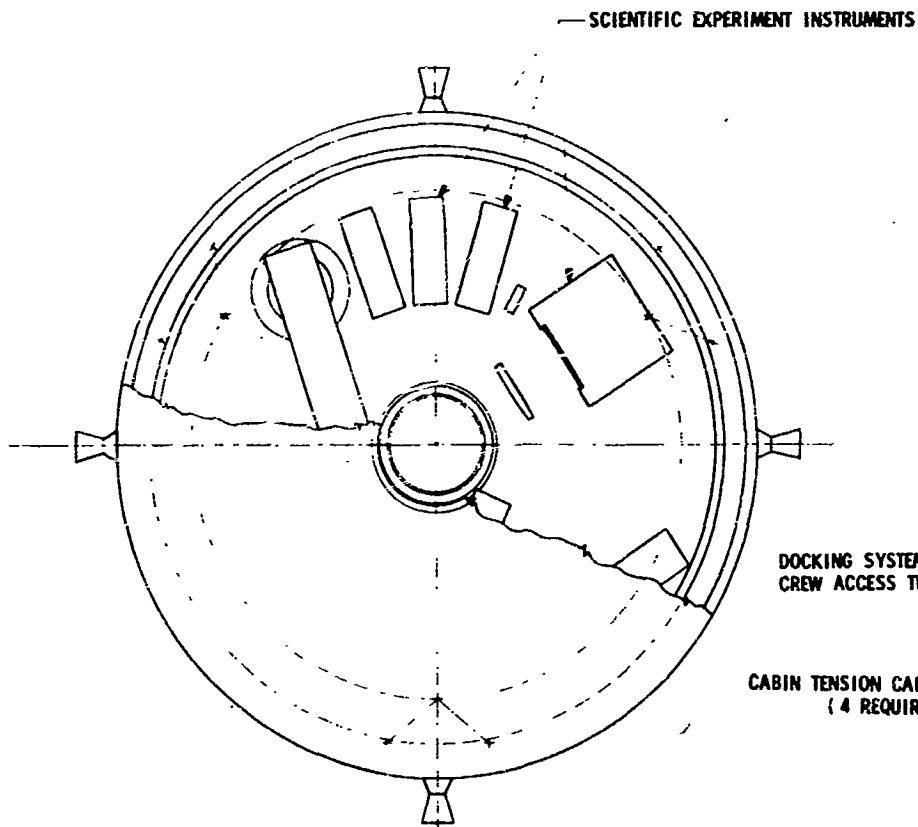
**3.1.2.1 Baseline Telescope** — The baseline telescope-structure concept (Figure 3.1-3) for synchronous orbit is essentially the same as for low Earth orbit. The design objective is to provide environmental protection and structural support for all optical and instrumentation systems during launch and orbital operation. Detailed descriptions of the subsystems and a structural analysis of the low-Earth-orbit configuration are described in Section 5.0 of Reference 1.

Modifications to the low-Earth-orbit baseline telescope to achieve the synchronous-orbit configuration are listed below:

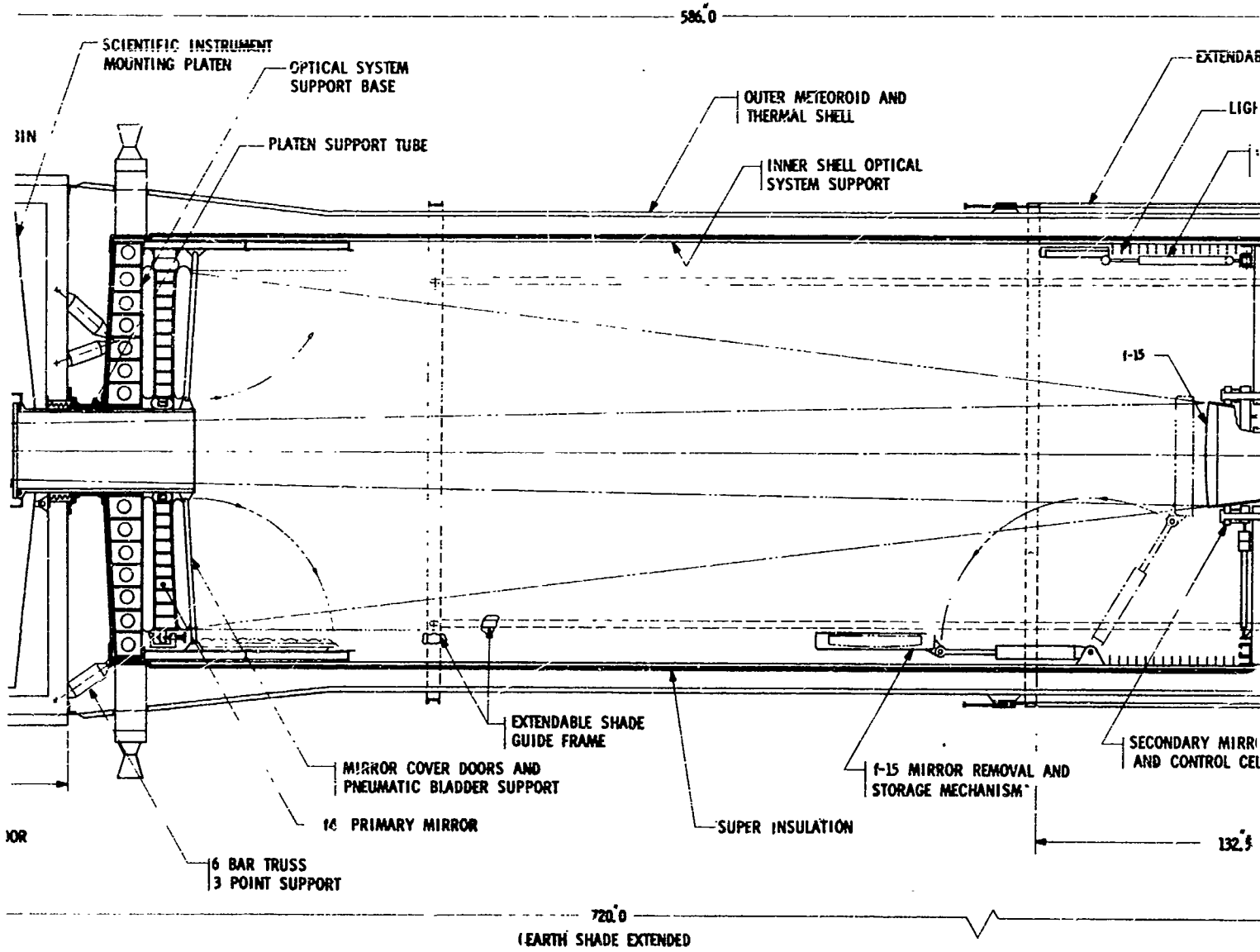
- The doors located on the front of the telescope are eliminated as a result of the reduced thermal distortions in the higher orbit. The Earth shade can also be eliminated from the thermal point of view, but is retained to minimize the amount of stray light entering the telescope tube.
- The two 1000-pound rendezvous engines mounted on the aft end of the telescope cabin are canted 28.5 degrees outboard with respect to the optical axis, so that the thrust axis is passing through the telescope's center of gravity even if one engine fails. In the low-Earth-orbit configuration, the mounting position of these engines is limited because the telescope is positioned lower inside the S-IVB equipment section, and the engines were mounted parallel to the optical axis to avoid interference between the S-IVB equipment and the MOT rendezvous engines.
- Arrangement of star trackers for the guidance system has been modified. This is an improvement rather than a requirement for the synchronous-orbit mission. Two clusters of three star trackers, specified for the low-Earth-orbit configuration, are replaced by two single star trackers; a single star tracker is added at the forward end of the telescope. These trackers, together with the two unchanged single trackers of the baseline telescope, provide a coverage of 360 degrees perpendicular to the optical axis and 90 degrees conical coverage parallel to the optical axis.

**3.1.2.2 Soft-Gimbal Mode** — Conceptual designs of orbital and launch configurations for the soft-gimbal mode are shown in Figures 3.1-4 and 3.1-5. These figures show the overall vehicle size and relative size and location of the major components and subsystems.

In the soft-gimbal mode, the concept uses a two-axis gimbal located at the MOT's center of gravity, and the outer gimbal ring is mounted in a soft spring suspension system that provides a soft spring rate for six degrees of freedom. The



15/16



15/16 (2)

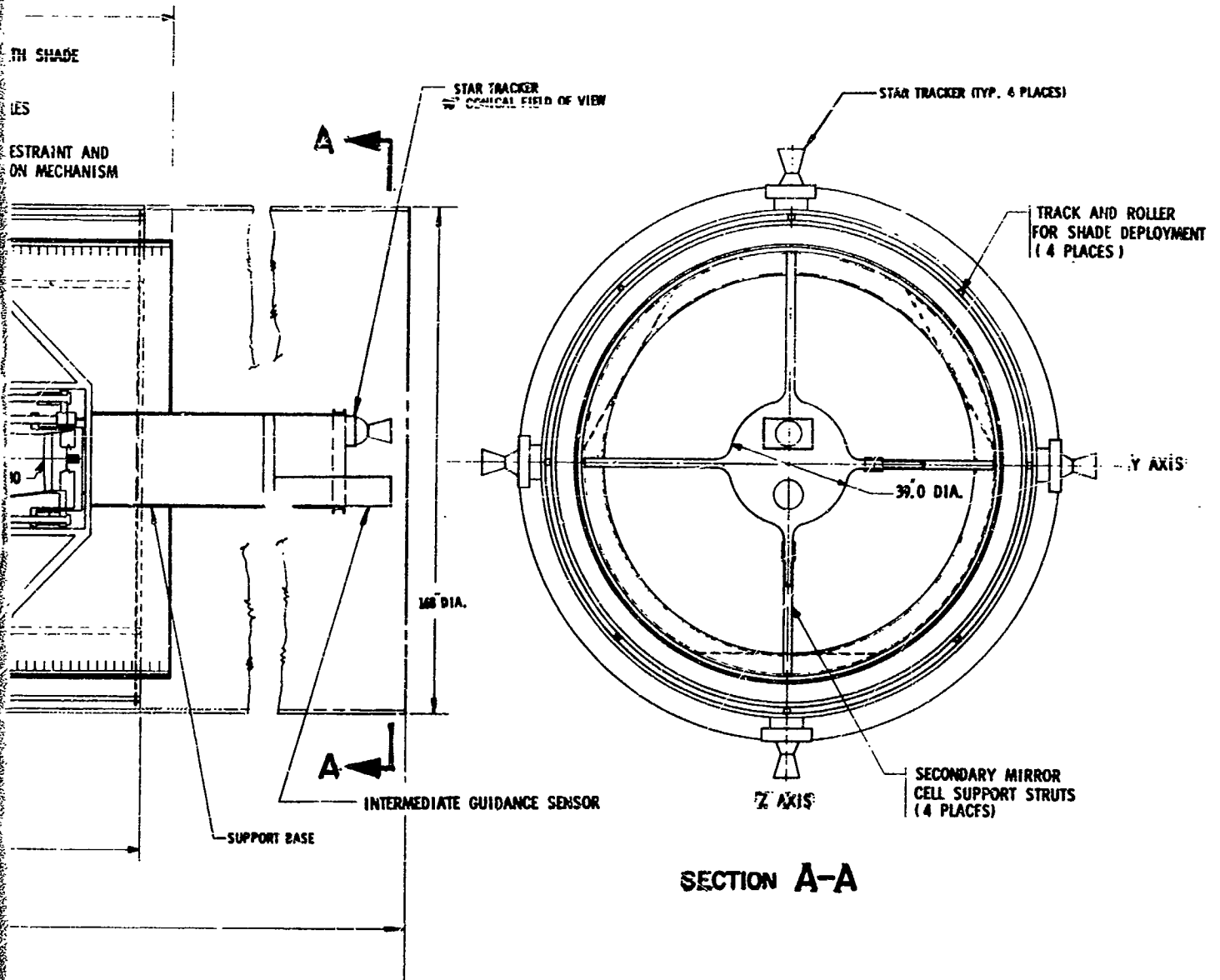
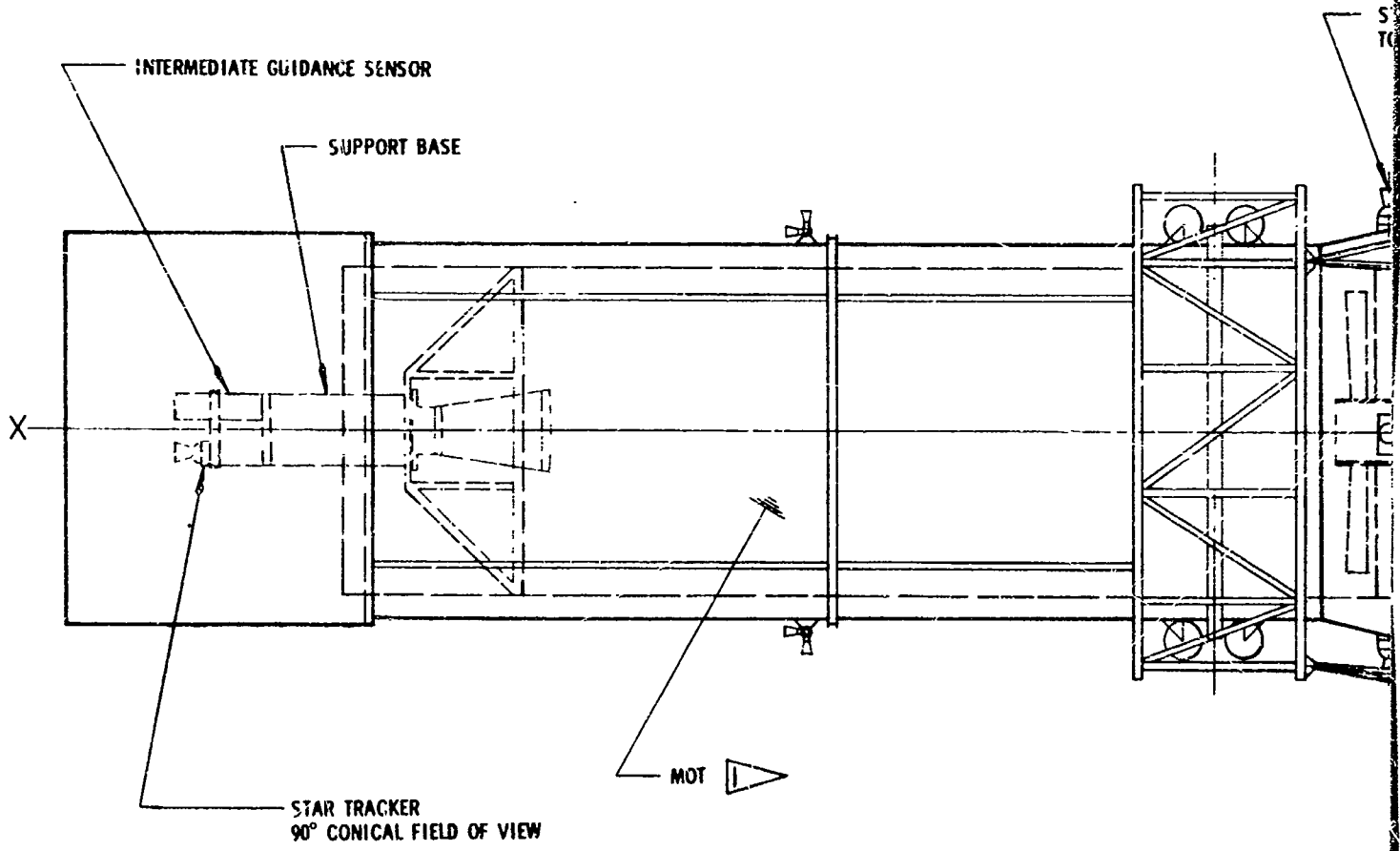


FIGURE 3.1-3  
BASELINE CONFIGURATION  
120 INCH MANNED ORBITAL TELESCOPE

3

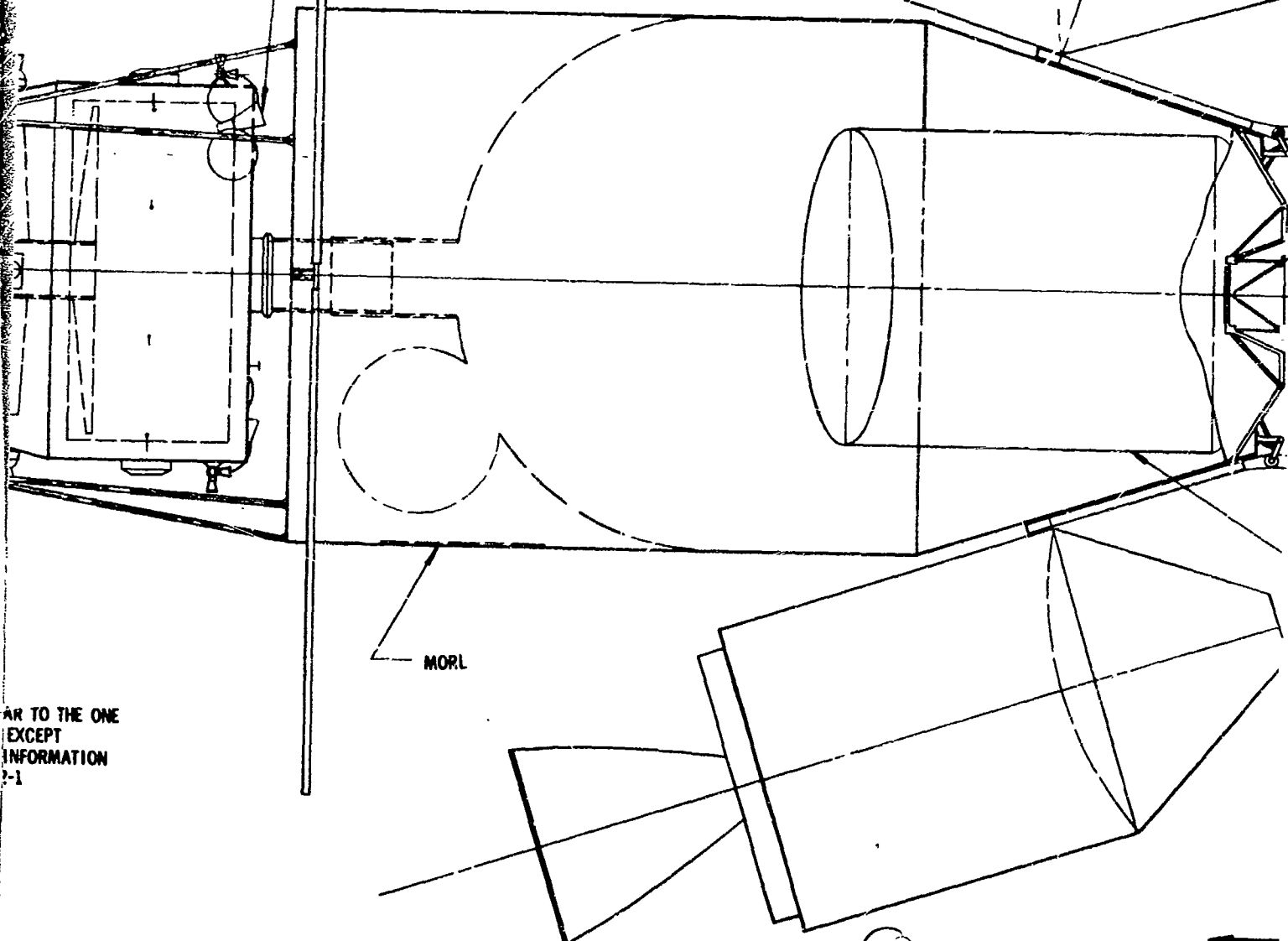


▲ THIS CONFIGURATION IS SIMILAR  
 DEVELOPED FOR THE LOW ORBIT  
 AS NOTED. FOR OTHER DETAIL  
 SEE FIGURE 5.2-3 DUC. 92-8404

17/1/8

RENDEZVOUS PROPULSION  
1000 LB. THRUST ENGINE  
600 LB. PROPELLANT (N<sub>2</sub>O<sub>4</sub>, AERO-50)  
(2 PLACES)

TAR TRACKER (4 REQUIRED)  
TOTAL FIELD OF VIEW 360°



VAR TO THE ONE  
EXCEPT  
INFORMATION  
2-1

19118

(2)



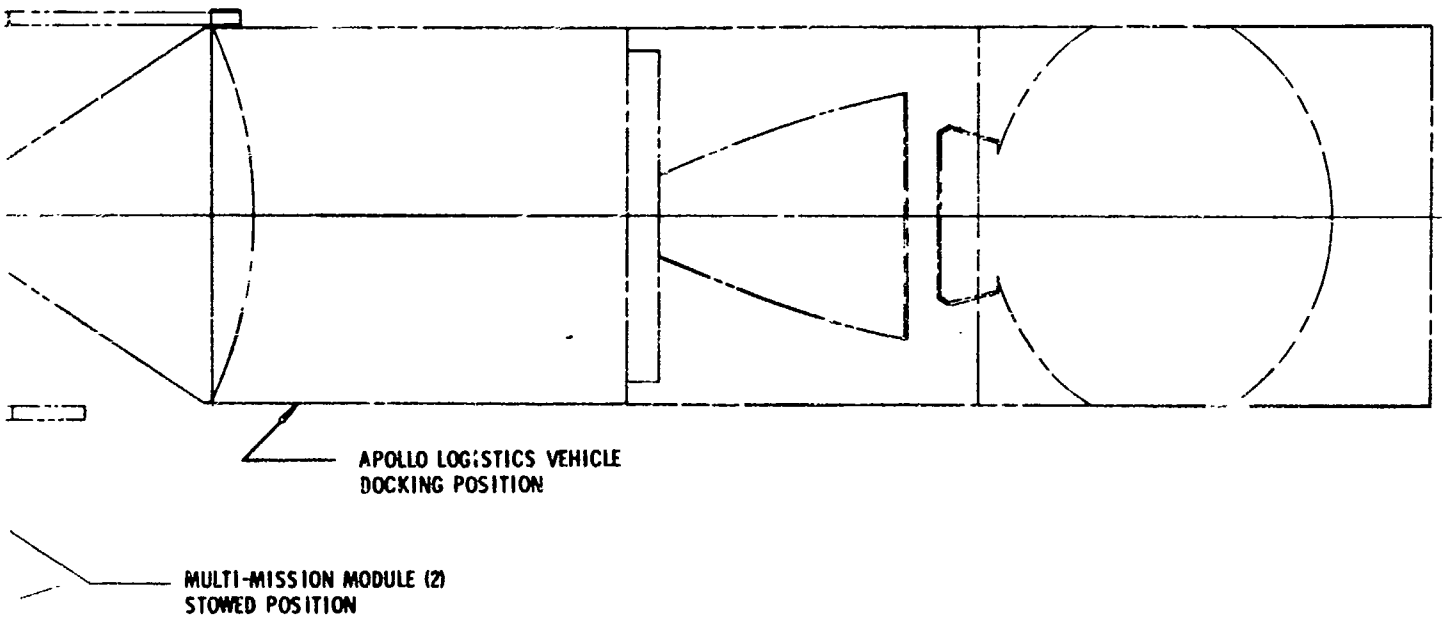
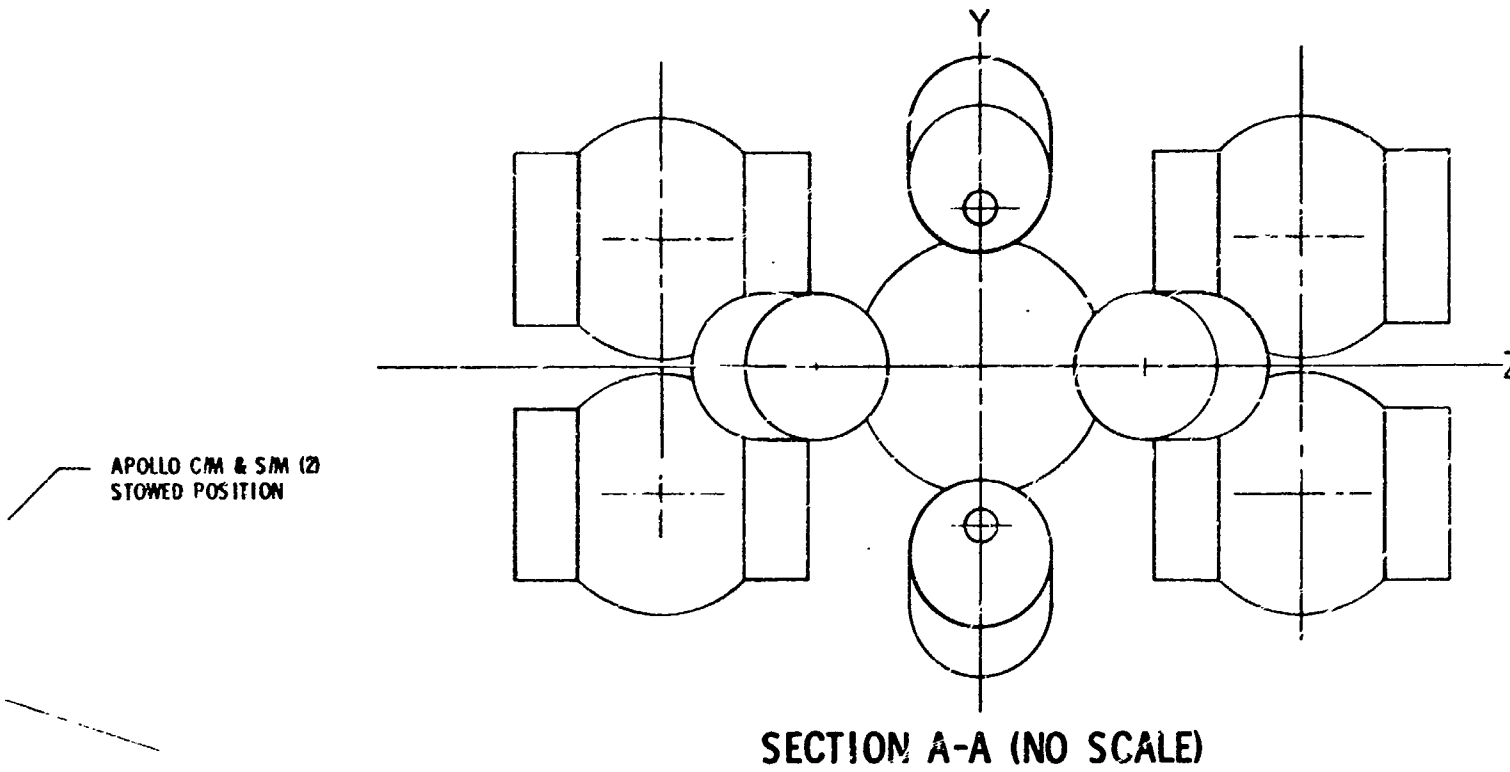
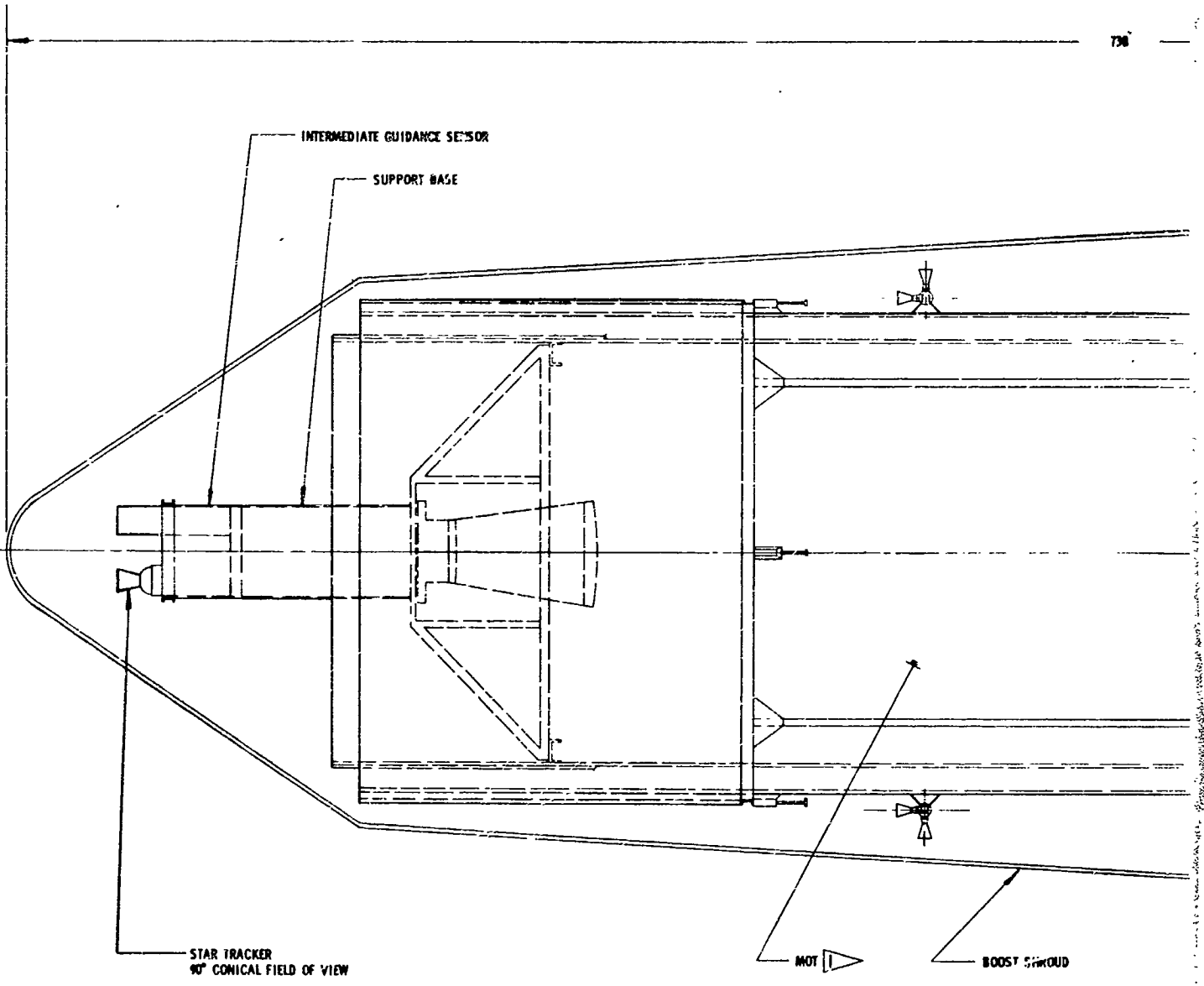


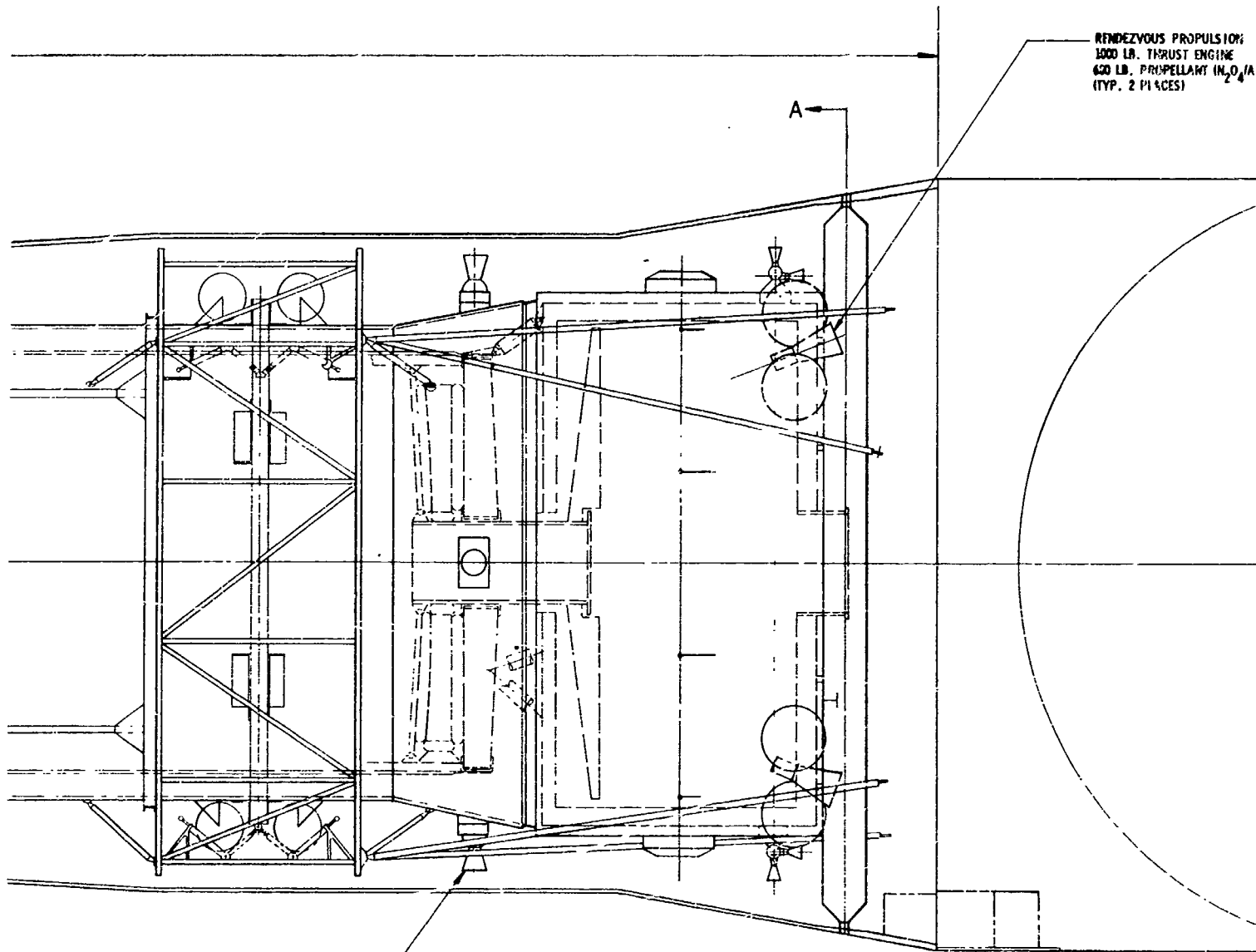
FIGURE 3.1-4  
ORBITAL CONFIGURATION  
120 INCH MANNED ORBITAL TELESCOPE  
SYNCHRONOUS ORBIT  
SOFT GIMBAL MODE

3



DETAIL

19/20



RENDEZVOUS PROPULSION:  
 1000 LB. THRUST ENGINE  
 600 LB. PROPELLANT (N<sub>2</sub>O<sub>4</sub>)  
 (TYP. 2 PLACES)

A

STAR TRACKER (4 REQUIRED)  
 TOTAL FIELD OF VIEW 360°

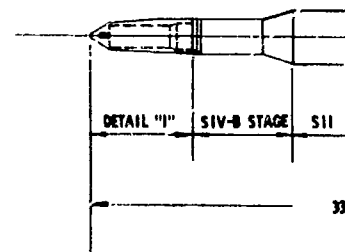
A

BOOST SHROUD  
 SEPARATION PLANE

SIV-B STAGE

ILT

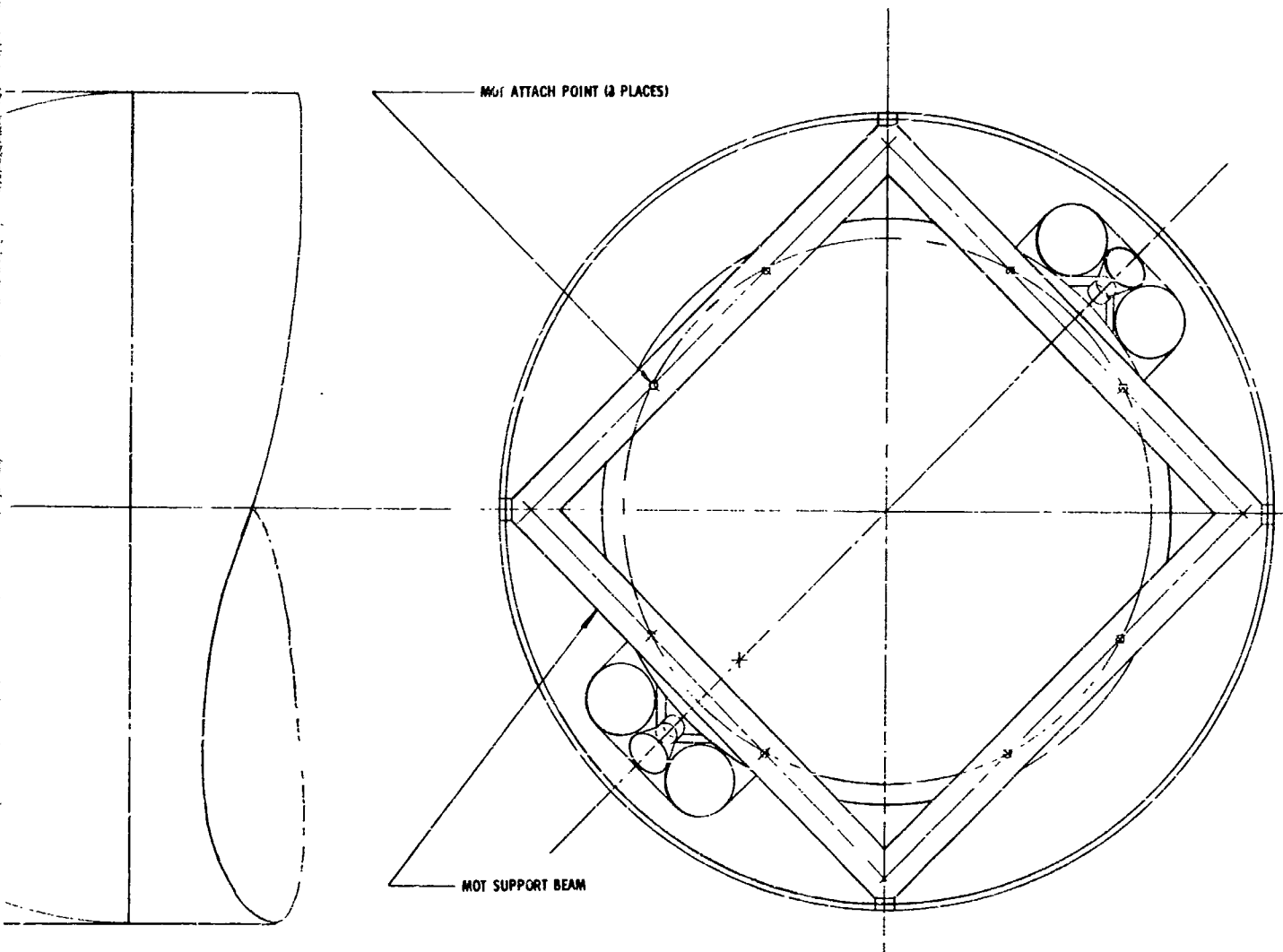
THIS CONFIGURATION IS SIMILAR TO THE  
 LOW ORBIT CONFIG. EXCEPT AS NOTED.  
 FOR OTHER DETAIL INFORMATION  
 SEE FIGURE 5.2-4 DOC. D2-84042-1



NOT LAUNCH

19/20 (2)

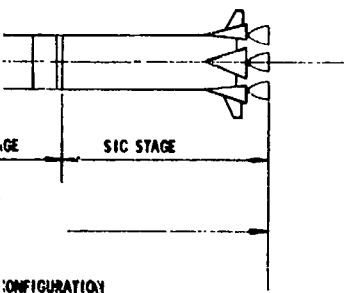
1-50



SECTION A-A

FIGURE 3.1-5

LAUNCH CONFIGURATION  
120 INCH MANNED ORBITAL TELESCOPE  
SYNCHRONOUS ORBIT  
SOFT GIMBAL MODE



spring suspension system is mounted on an open frame truss-type structure which is permanently attached to the MORL. Detailed descriptions of the operations and structural analysis are described in Section 5.0 of Reference 1.

**Orbital Configuration** — This configuration (Figure 3.1-4) is similar to the one developed for the low Earth orbit except for the following items:

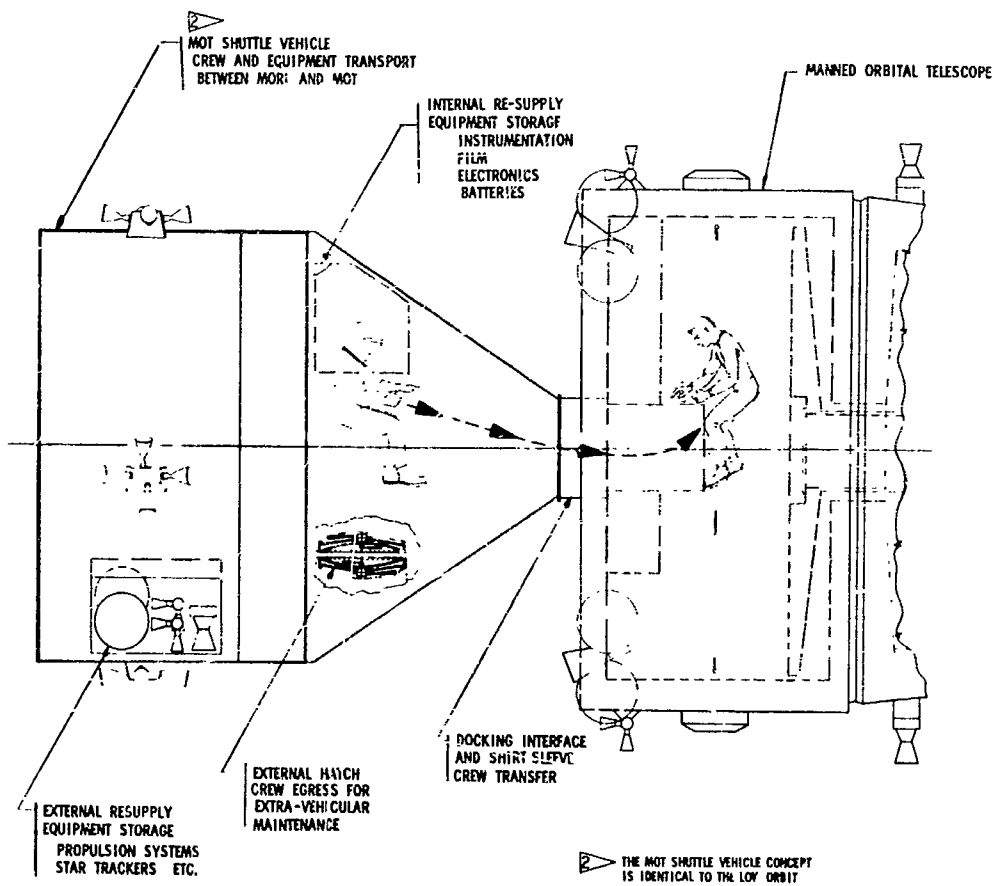
- The Apollo service module is required (for deorbit and return to Earth) instead of the smaller low-Earth-orbit service pack because greater deorbit  $\Delta V$  is required.
- The Apollo and multimission modules storage locations are rotated about the MORL Y axis 45 degrees from the low-Earth-orbit configuration so that the service modules will not interfere with the MORL solar panel rotation.
- The MOT support truss is replaced by a beam system. This beam system will be jettisoned with the S-IVB stage. This configuration provides more space around the periphery of the telescope cabin to mount equipment such as antennas, rendezvous engines, and propellant tanks. Furthermore, some potential installation problems of the soft-gimbal concept have been eliminated. Further design trade studies should be made to determine the optimum support structure.

**Launch Configuration** — The launch configuration of the soft-gimbal concept is shown in Figure 3.1-5. The MOT is installed on top of the three-stage Saturn V booster and is enclosed by a jettisonable shroud. The shroud, which includes the nose cone section, is jettisoned after first-stage burnout to maximize the payload in orbit.

There are three significant differences in this configuration as compared to the low-Earth-orbit case:

- The launch vehicle is a three-stage Saturn V instead of the two-stage Saturn IB that is planned for the low Earth orbit. Payload capability, in addition to the MOT, is 52,565 pounds.
- The shape of the boost shroud is similar to the one designed for the low-Earth-orbit case, except that it is 187 pounds heavier due to the difference in launch environment.
- The MOT is supported on top of a beam-type support structure at eight attachment points. Separation of the MOT from the S-IVB stage is also accomplished at these attachment points. The MOT inertial loads are transferred to the modified Apollo LEM adapter through four support beams.

**3.1.2.3 Detached Mode** — Conceptual designs of the orbital and launch configurations are shown in Figures 3.1-6 and 3.1-7. These configurations show overall vehicle size and relative size and location of major components and subsystems.



RENDEZVOUS PROPULSION  
1,000 POUND ROCKET ENGINE  
(2 PLACES)

DIPOLE-RENDEZVOUS  
& DOCKING

185.0 DIA.  
(REL.)

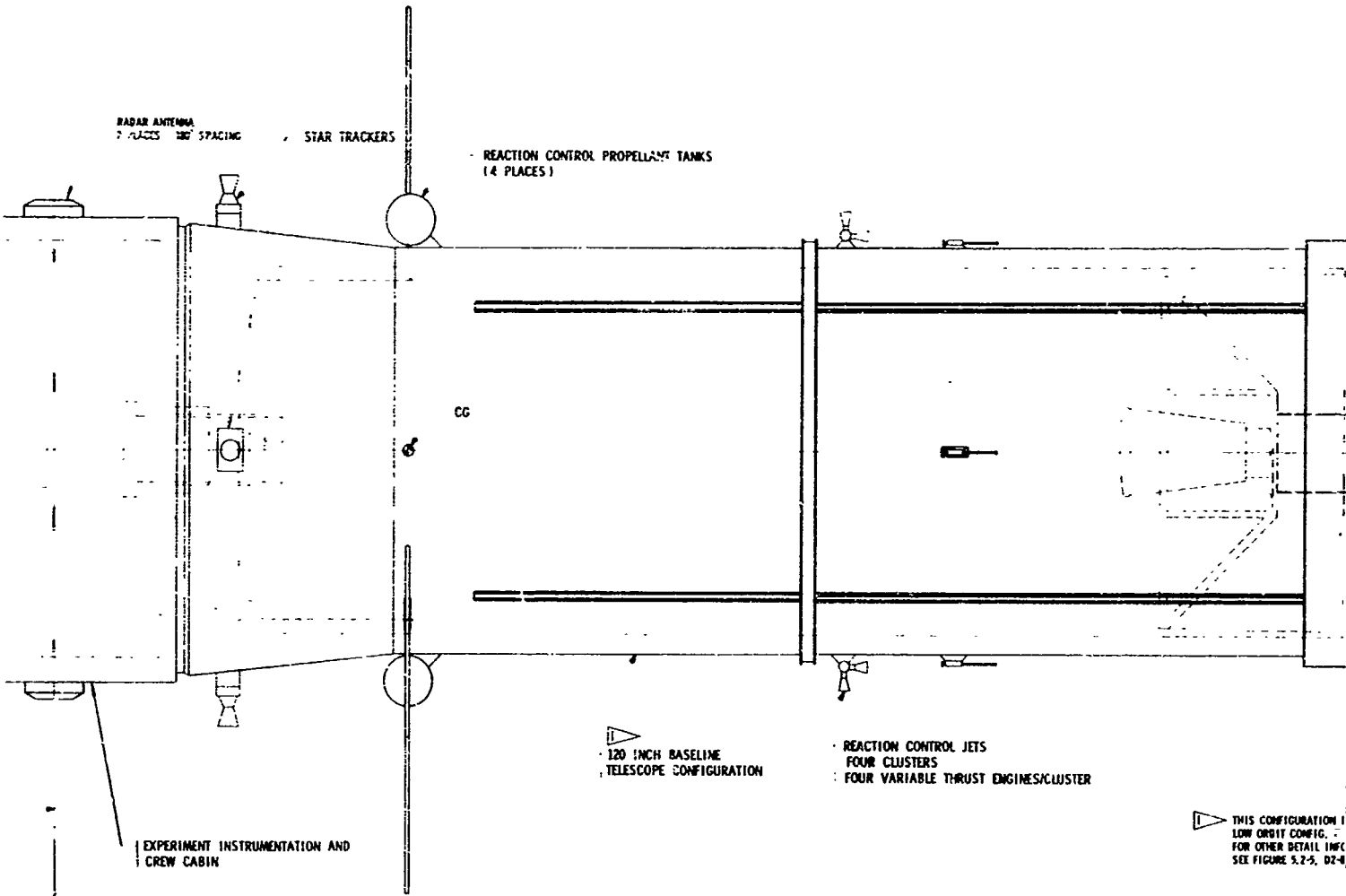
**ORBITAL CONFIGURATION**  
(TELESCOPE MANNED FOR EXPERIMENT  
SET-UP AND MAINTENANCE)

①

23/24

**PRECEDING PAGE BLANK NOT FILLED.**

720.0  
(REF.)



REMOTE CONTROLLED ORBITAL CONFIGURATION  
(UNMANNED DURING EXPERIMENT OBSERVATIONS)

23/29 2

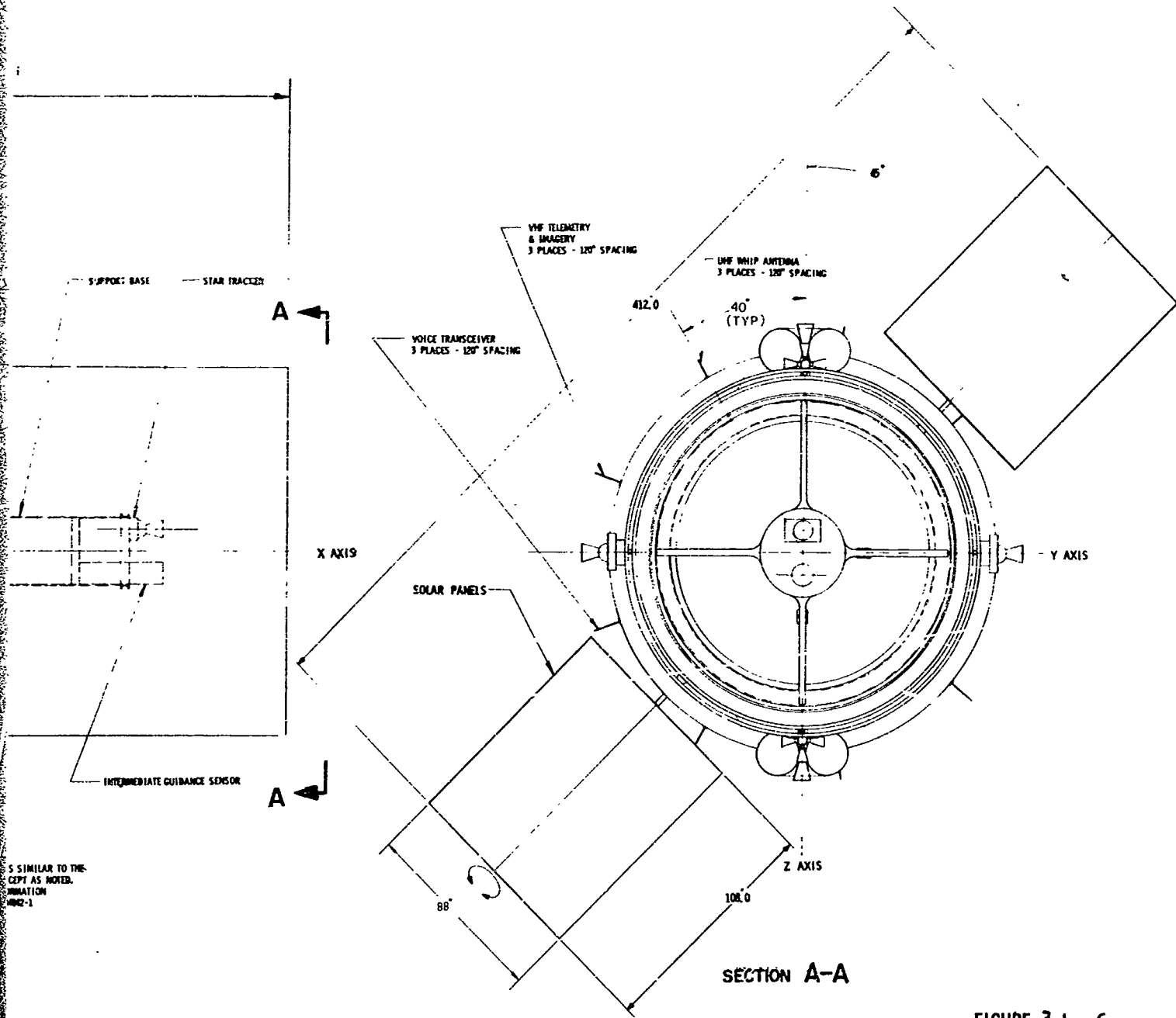
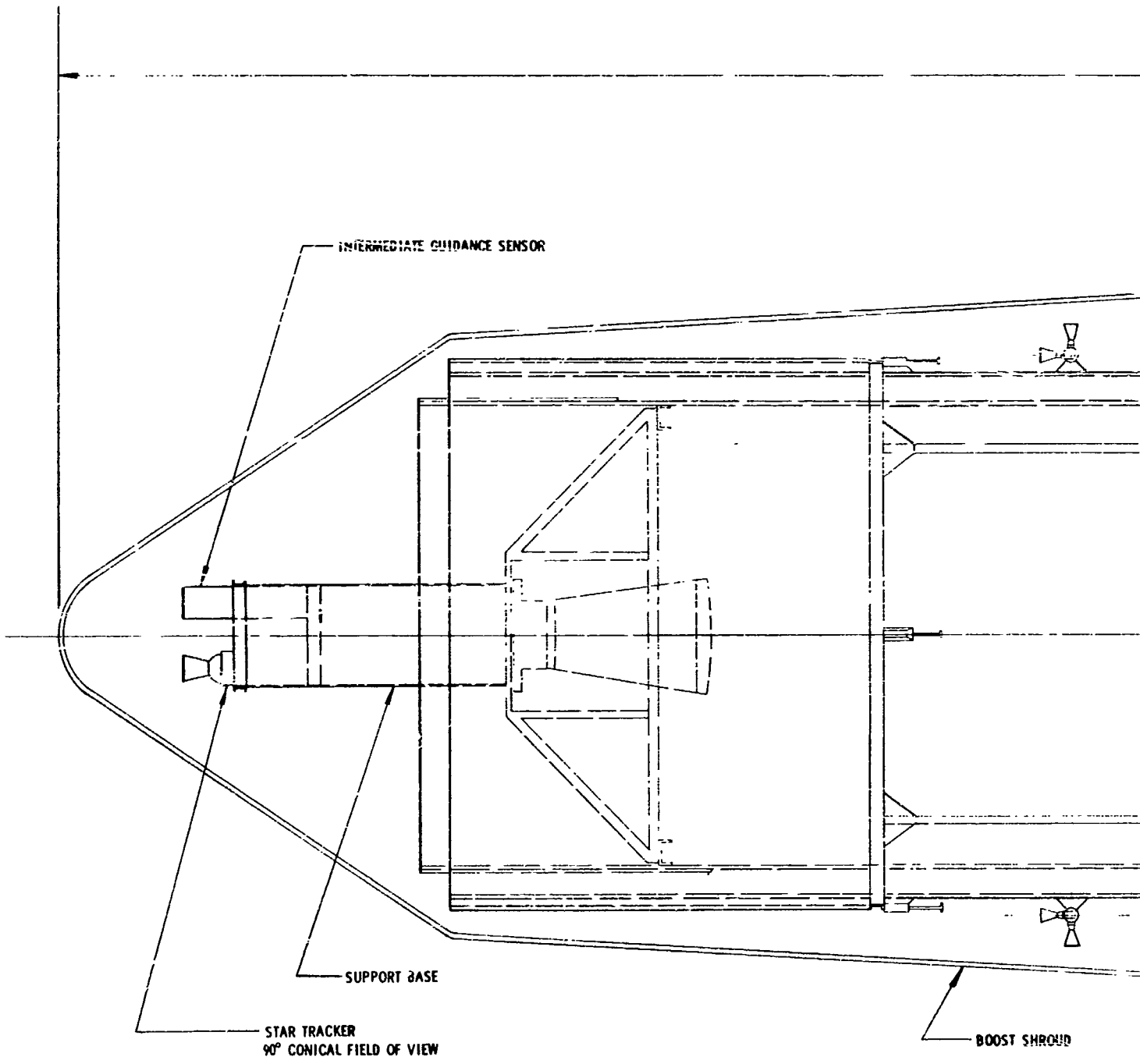


FIGURE 3.1-6  
ORBITAL CONFIGURATIONS  
120 INCH MANNED ORBITAL TELESCOPE  
SYNCHRONOUS ORBIT  
DETACHED MODE





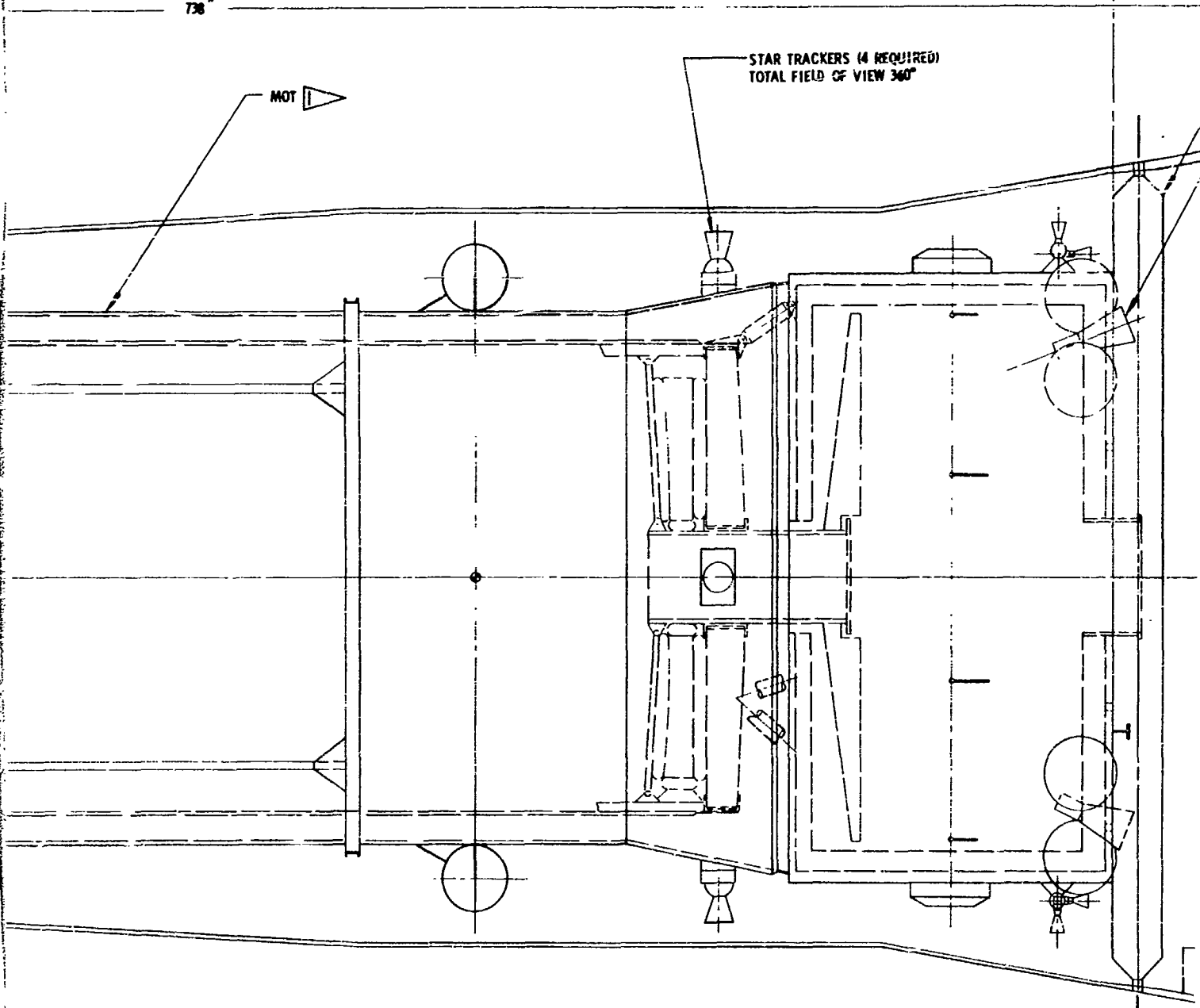
g5g6

MOT & BOOSTER  
SEPARATION PLANE

738"

STAR TRACKERS (4 REQUIRED)  
TOTAL FIELD OF VIEW 360°

MOT



THIS CONFIGURATION IS SIMILAR TO THE  
LOW ORBIT CONFIG. EXCEPT AS NOTED  
FOR OTHER DETAIL INFORMATION. SEE  
FIGURE 5.2-7, D2-84042-1.

BOOST SHROUD  
SEPARATION PL

TAIL "I"

25/90 (2)

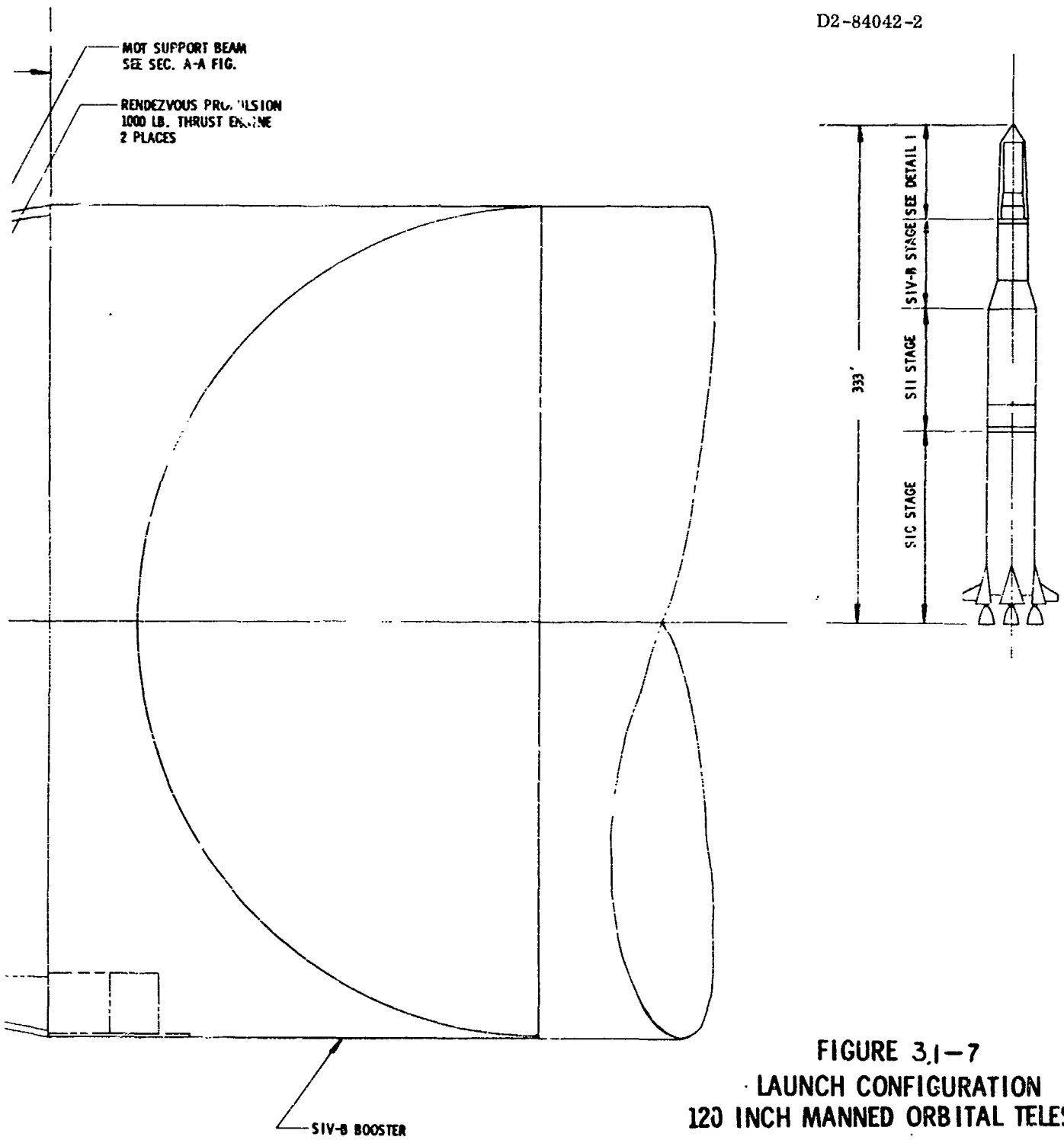


FIGURE 3.1-7  
LAUNCH CONFIGURATION  
120 INCH MANNED ORBITAL TELESCOPE  
SYNCHRONOUS ORBIT  
DETACHED MODE

ANE

3

In the detached mode, the MOT is decoupled for astronomical observations. The MOT is capable of docking with the MORL, but a shuttle vehicle is used for normal operations.

**Orbital Configuration** — Figure 3.1-6 shows the orbital configuration of the MOT when it is detached for astronomical observation. A shuttle vehicle is shown docked to the telescope cabin for experiment setup and maintenance. These concepts are similar to those for the low-Earth-orbit case described in detail in Section 5.0 of Reference 1. Basically, the orbital configuration is essentially the baseline telescope with the addition of reaction control jets, propulsion equipment, and two solar panels. Two single solar panels with an area of 132 square feet are required for synchronous orbit instead of the 216-square-foot foldout panels required for low Earth orbit. Detailed descriptions of these subsystems are included in appropriate sections of this document.

**Launch Configuration** — The launch configuration of the detached mode is shown in Figure 3.1-7. The only changes in this configuration as compared to Figure 3.1-4 are removal of the soft-gimbal structure and addition of solar panels. The arrangement of star trackers in the baseline telescope enables use of the same boost shroud for either launch configuration.

**Shuttle Vehicle** — The conceptual design of the shuttle vehicle is also shown in Figure 3.1-6. This design is similar to the one used for the low-Earth-orbit study. Figure 3.1-8 shows a comparison of shuttle-vehicle concepts for both low Earth and synchronous orbits. Each of the three vehicles has the same basic system requirements for servicing the MOT and, hence, the only difference is the provision of deorbit capability. This provision is not included in the baseline shuttle vehicles for either the low-Earth- or synchronous-orbit case. It may be desirable to add deorbit capability to the shuttle so that emergency Earth return would be possible if the MORL became damaged or if any malfunctions in the docking system occurred. By adding the deorbit capability, a severe weight penalty is incurred (see Section 3.3.2.3).

Configuration C of Figure 3.1-8 is the chosen baseline vehicle for this study. This shuttle vehicle consists of crew and cargo modules. It accommodates two men, logistic equipment, and supporting subsystems. The crew module is an Apollo command module modified by removal of all structures designed for sustaining a crew during launch, re-entry, and landing. The heat shield is also removed, thus leaving only the basic primary structure intact. The cargo module is 100 inches long and 154 inches in diameter. This cylindrical section is permanently attached to the crew module, and a cargo transfer hatch is provided between the crew and cargo modules to facilitate cargo transfer.

**3.1.2.4 Logistics Vehicle** — The logistics vehicle shown in Figure 3.1-9 consists of a modified Apollo command module, Apollo service module, and a Douglas multimission module. The command module is the inflight control center, crew living quarters during ascent and descent, and the re-entry vehicle during return

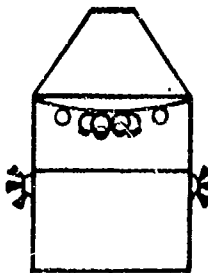
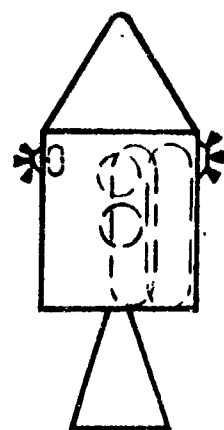
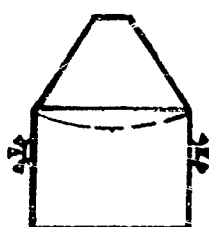
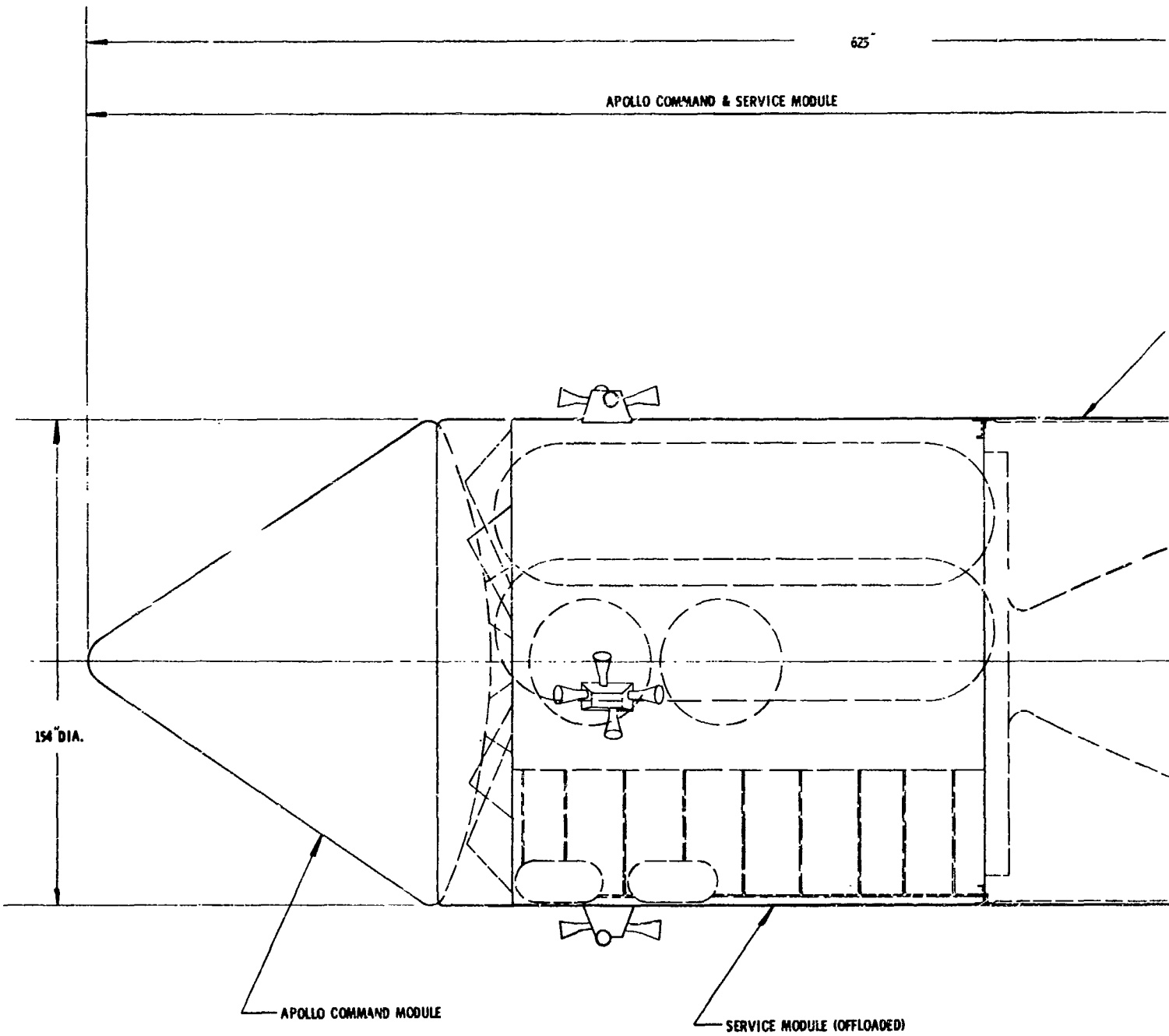
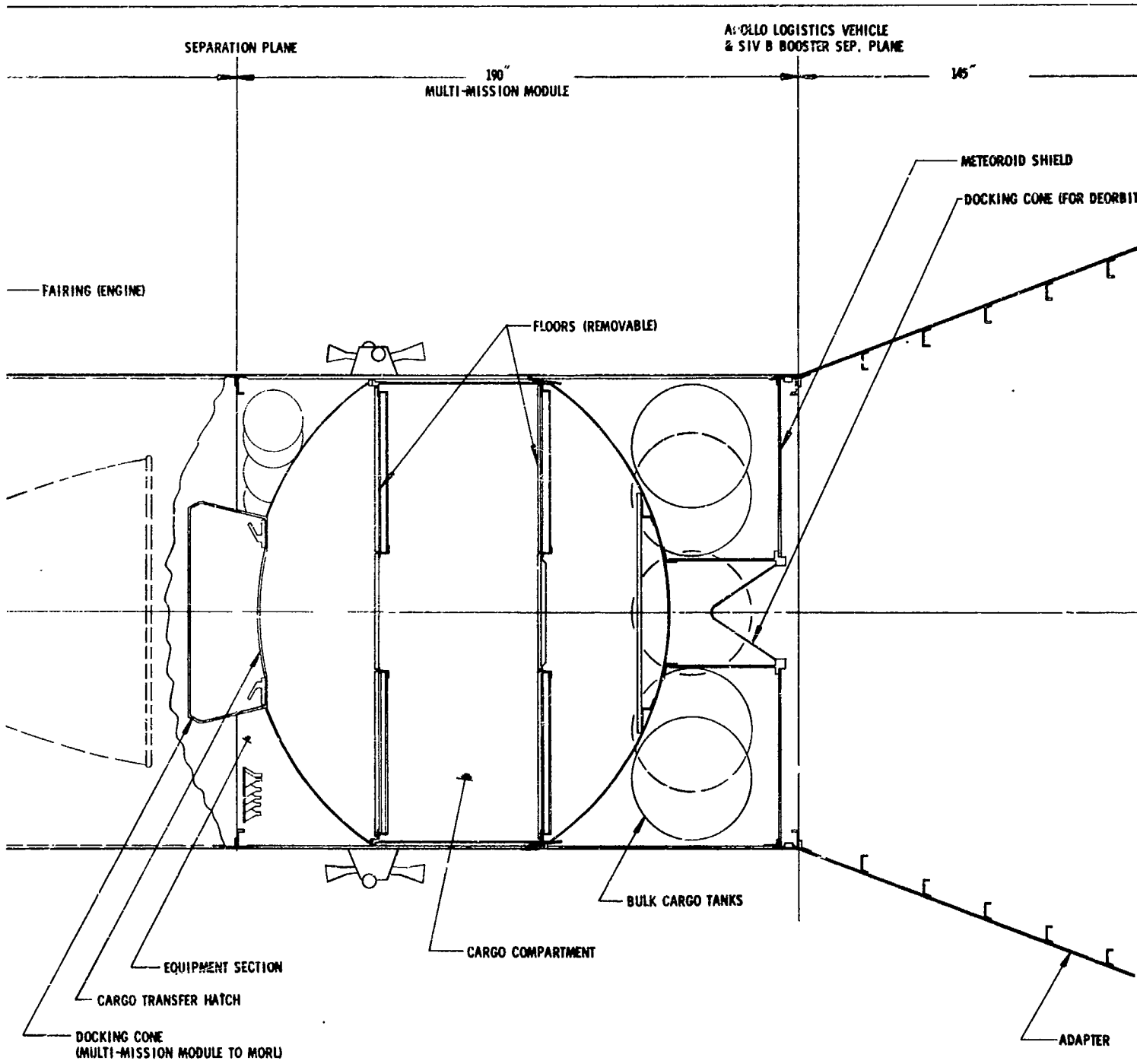
	LOW ORBIT	SYNCHRONOUS ORBIT
<p><b>A</b></p> 	<ul style="list-style-type: none"> <li>● SYSTEM CONSISTS OF AN APOLLO C/M, SERVICE PACK &amp; CARGO MODULE</li> <li>● DEORBIT CAPABILITY</li> <li>● EXTRAVEHICULAR ACTIVITY REQUIRED FOR EQUIPMENT TRANSFER</li> <li>● VEHICLE WT = 16,515 LB TOTAL</li> <li>● PROP. WT - DEORBIT = 1025 LB (SOLID) SHUTTLE = 1060 LB</li> </ul>	
<p><b>B</b></p> 		<ul style="list-style-type: none"> <li>● SYSTEM CONSISTS OF AN APOLLO C/M &amp; SERVICE MODULE (OFF-LOADED)</li> <li>● DEORBIT CAPABILITY</li> <li>● EXTRAVEHICULAR ACTIVITY REQUIRED FOR EQUIPMENT TRANSFER</li> <li>● VEHICLE WT = 37,835 LBS</li> <li>● PROP. WT - DEORBIT = 15,565 LBS SHUTTLE = 2425 LBS</li> </ul>
<p><b>C</b></p> 	<ul style="list-style-type: none"> <li>● SYSTEM CONSISTS OF A MODIFIED APOLLO C/M &amp; CARGO MODULE</li> <li>● NO DEORBIT CAPABILITY</li> <li>● EXTRAVEHICULAR ACTIVITY IS MINIMIZED</li> <li>● VEHICLE WT = 7800 LBS</li> <li>● PROP. WT = 500 LBS</li> </ul>	<p>SAME AS LOW ORBIT</p>

FIGURE 3.1-8 SHUTTLE VEHICLE CONCEPT COMPARISON

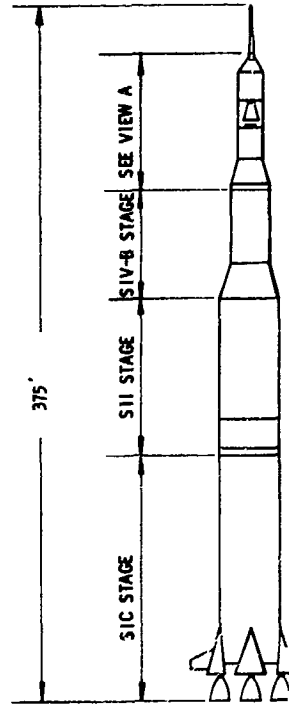
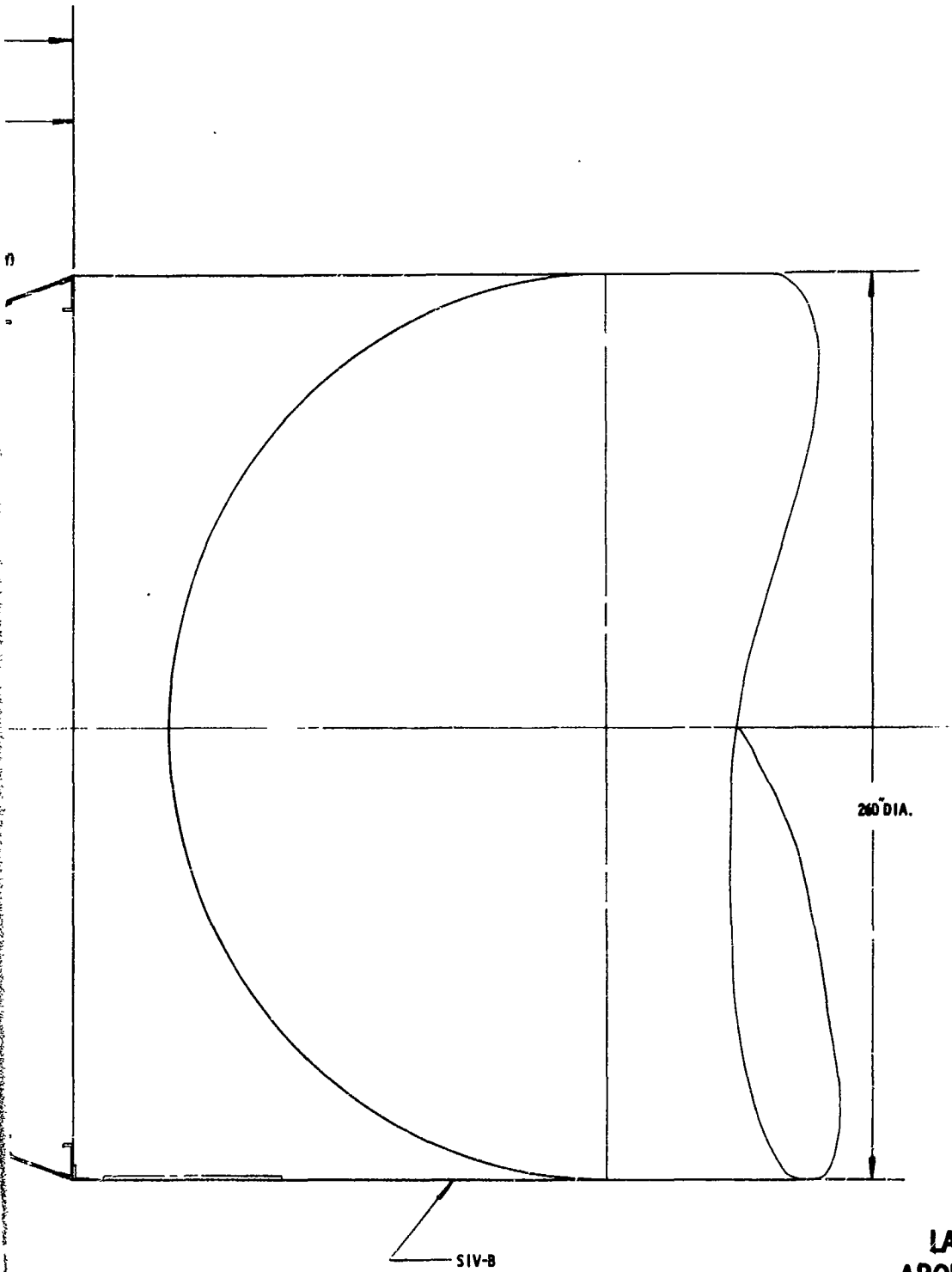


29/30 ①



2

2 9/30



**FIGURE 3.1-9  
LAUNCH CONFIGURATION  
APOLLO LOGISTICS VEHICLE**

3



**BLANK PAGE**

to Earth. The service module provides supporting services (power, environmental control, etc.) for operation of the command module and the deorbit impulse for returning the command module to Earth and for disposing of spent multimission modules. The multimission module provides the cargo volume and the propulsion system for the terminal rendezvous operation with the MORL.

The Apollo command and service modules are modified (from their lunar-mission configurations) to withstand the extended space time of the MOT mission and to interface with the MORL so as to be on a standby basis during their space stay. These modifications were not studied but would be essentially the same as reported by Douglas (Reference 21).

Only two significant modifications are anticipated for the multimission module configuration. One modification is to change the rendezvous engines from a 150-pound thrust level to at least 300 pounds of thrust due to the greater mass involved. The other modification is to add a docking cone, without an access opening, to the lower end of the module to facilitate deorbit as illustrated in Figure 3.1-10. The multimission module is shown in Figure 3.1-9 and is described in detail by Douglas (Reference 21).

The launch vehicle for the logistics vehicle is the three-stage Saturn V. The logistics multimission module is mounted on the S-IVB stage by means of a 145-inch-long adapter section. The adapter is an aluminum skin-stringer-frame structure and provides the load path between the multimission module and the S-IVB stage. A mechanical attachment joint is provided at the lower and upper ends of the adapter. The adapter remains attached to the S-IVB stage at separation.

## 3.2 STRUCTURAL ANALYSIS

### 3.2.1 Primary Structure

Elements of the primary structure for the low-Earth-orbit MOT are listed and identified in Figures 5.2-2 through 5.2-8 of Reference 1.

Elements of the primary structure of the synchronous-orbit MOT are essentially the same as above; differences are discussed in Section 3.1.2.2.

### 3.2.2 Limit Load Factors

The limit load factors given in Reference 1 are derived under the assumptions that thrust cutoff was instantaneous and the dynamic factor for overshoot was 2.50.

The analysis used to derive the limit load factors for the synchronous orbit is based on a beam column (lumped mass) idealization of the gross vehicle, its mass distribution, and a thrust cutoff time of 0.4 second. The limit load factors for launch condition are as shown in the following tabulation:

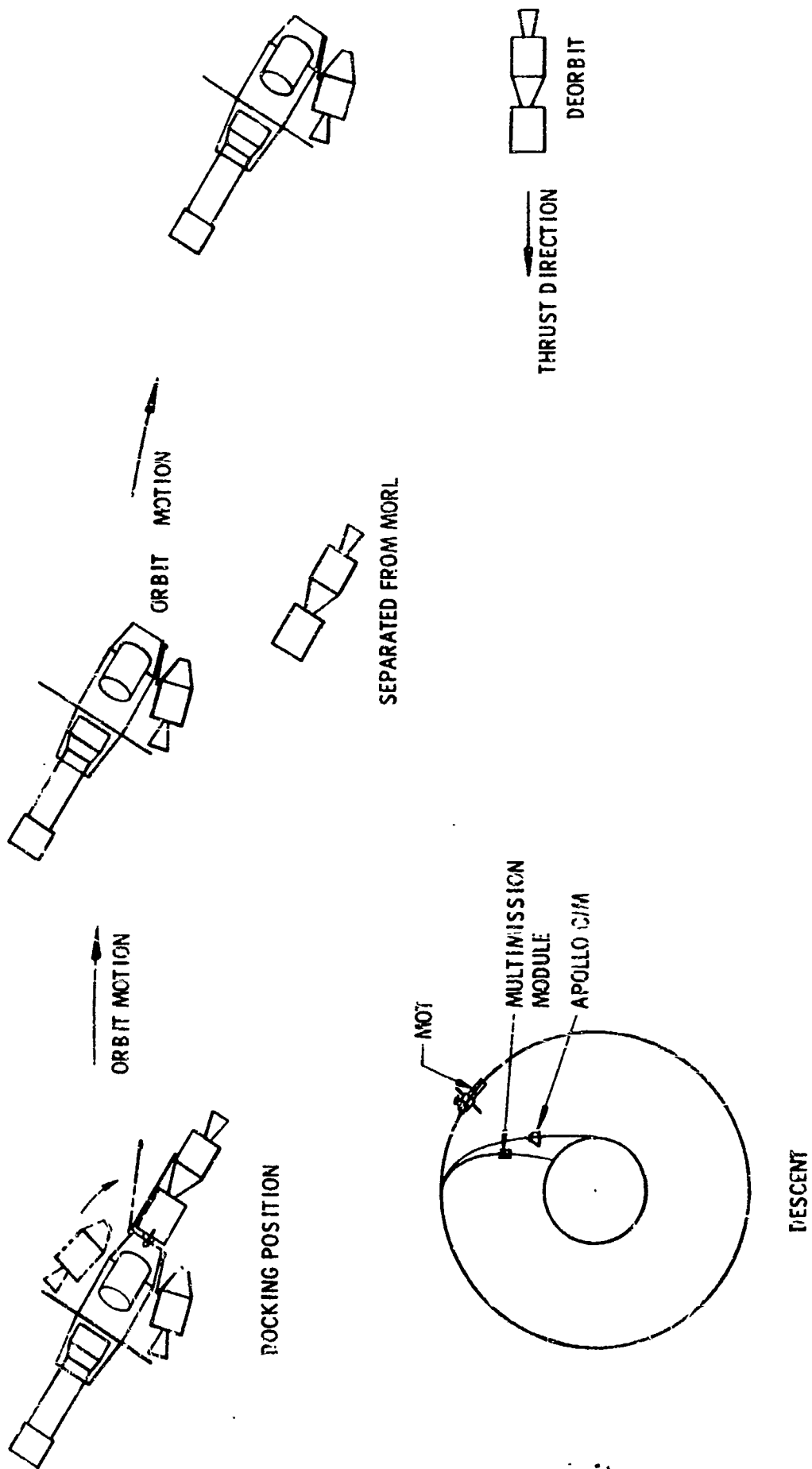


FIGURE 3.1-10 LOGISTICS VEHICLE DEORBIT SEQUENCE

Condition	Limit Load Factor		
	Z	X or Y	Torsion about Z
Launch	+5.6 g	±2 g	0
Stage 1	-2.8 g	±2 g	0
Stage 2	0	0	10 rad/sec <sup>2</sup>
Stage 3	2.7 g	---	0

Loads are obtained by applying these load factors at the center of gravity of each significant mass item with the total load being reacted at the adapter section.

These load factors are used for sizing all primary structural elements.

Light structures, such as solar panels and antennas, must be adequate to withstand not only the above load factors, but must also withstand the following dynamic loading conditions applied separately during launch:

- 1) Vibration environment according to Figure 3.2-1;
- 2) A reverberant acoustic field of 143 db/third octave from 50 to 200 cps with 10 db/octave rolloff below 50 cps and 5 db/octave rolloff above 200 cps.

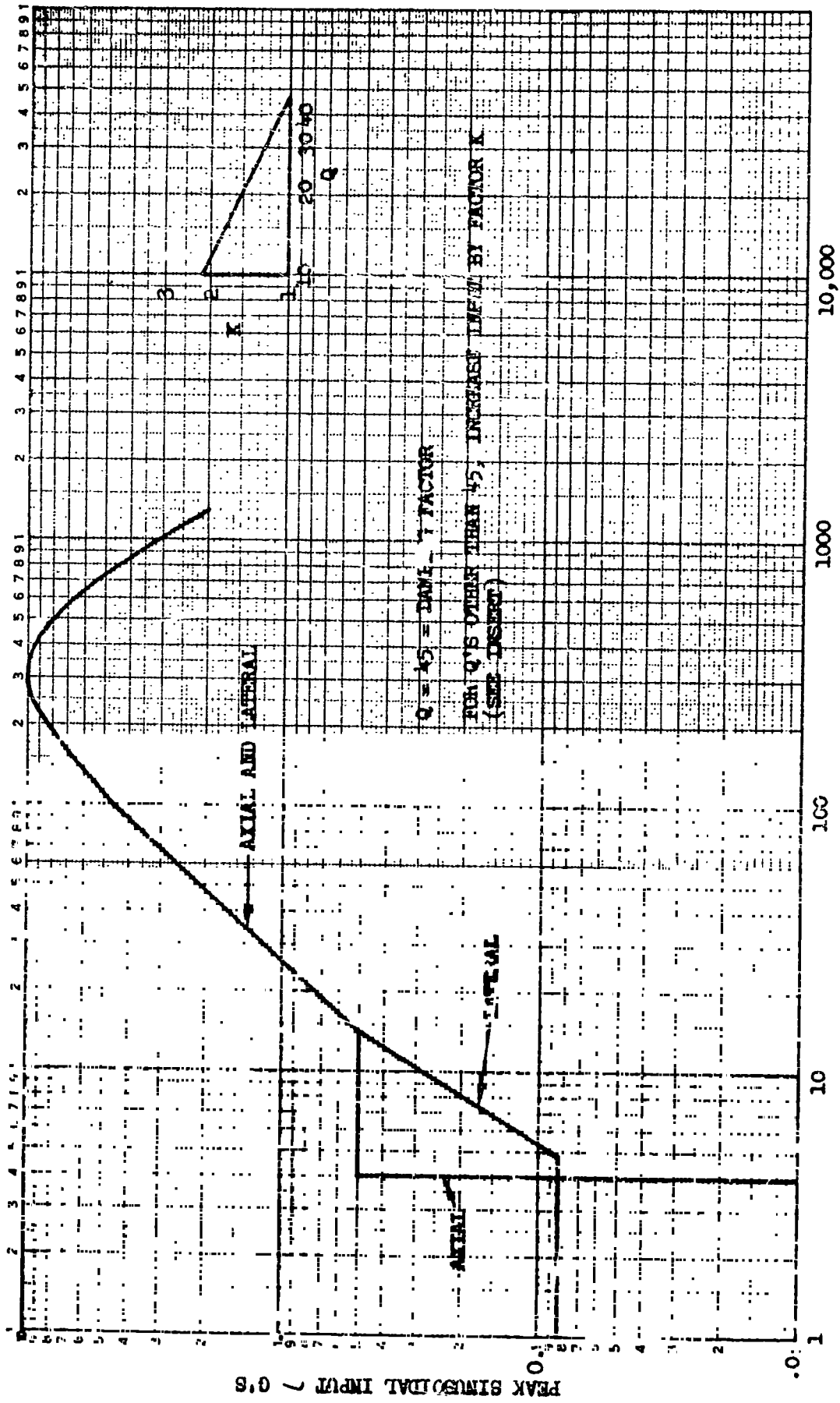
### 3.2.3 Flight Load Comparison

Shear loads, bending moments, and axial loads of the MOT, MORL, and logistics multimission module were calculated for a low-Earth-orbit mission using the Saturn IB launch vehicle and for a synchronous-orbit mission using the Saturn V vehicle. These loads reflect the 95-percent wind criterion for which the Saturn V is designed. All loads presented occur during maximum  $q$  in the trajectory. The maximum  $q$  is 5400 pounds-degree/ft<sup>2</sup> for the Saturn V and 3500 pounds-degree/ft<sup>2</sup> for the Saturn IB. These loads are not sufficiently refined for a detailed structural analysis; but, they are sufficient for comparing effects of the two launch vehicles on the payloads (see Section 3.3).

The limit shear load, bending moments, and axial loads of the MORL, the logistics multimission module, and the MOT were calculated. Those for the MORL, which are the critical ones because of the greater payload weight and vehicle length, are shown in Figures 3.2-2 through 3.2-4. All loads are plotted in respect to the distance forward to the S-IVP and payload interface; this is a reference common to all payloads.

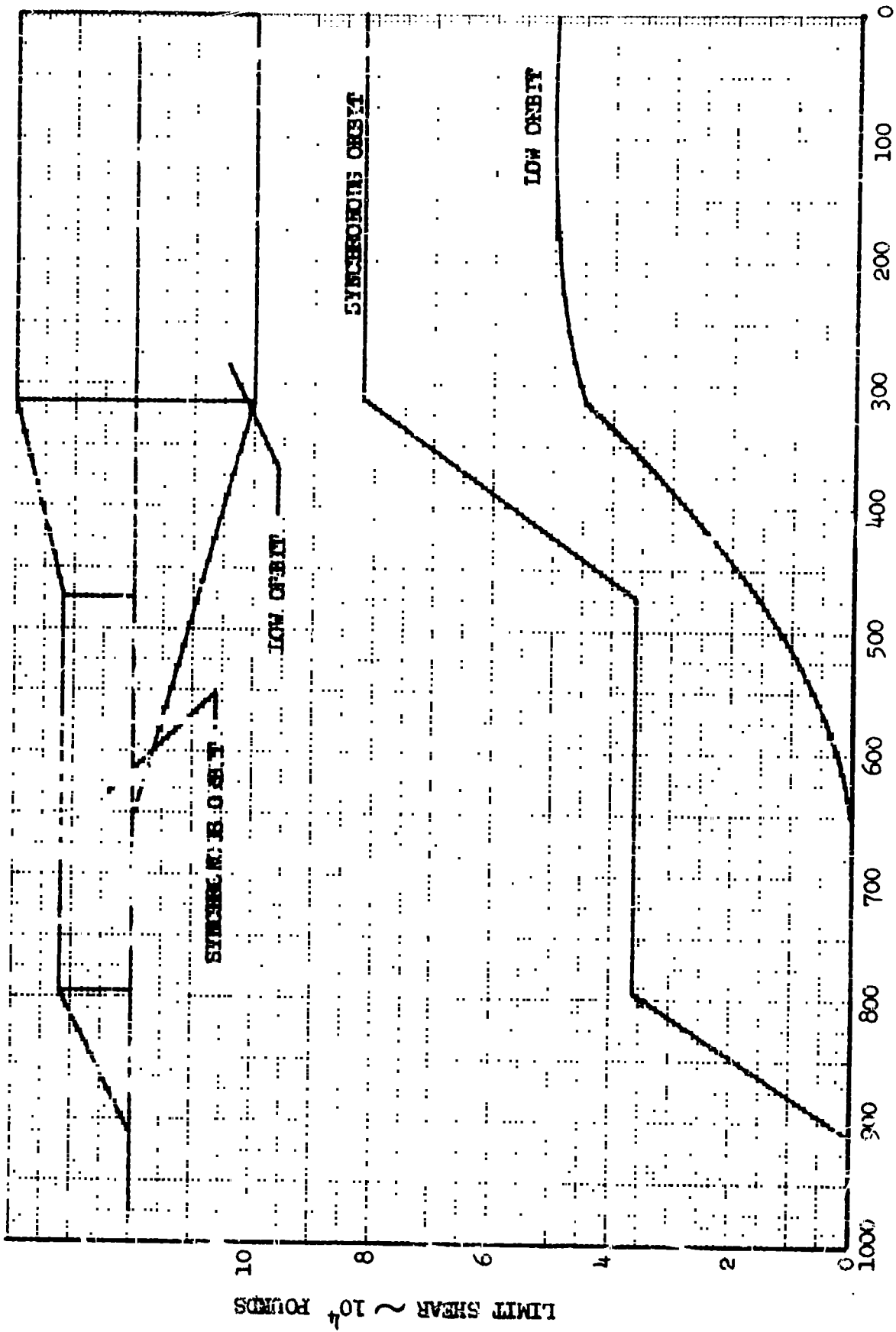
### 3.2.4 Compatibility of Payload with Booster

An attempt has been made to assess the compatibility of the MOT system payload, logistics vehicle, and MORL with the Saturn V launch vehicle. An absolute evaluation of system compatibility is not possible at this time because the strength of the upper stages of the booster is unknown. The loads imposed by the Apollo LOR system are known, however, and these provide a lower limit for stage strength.



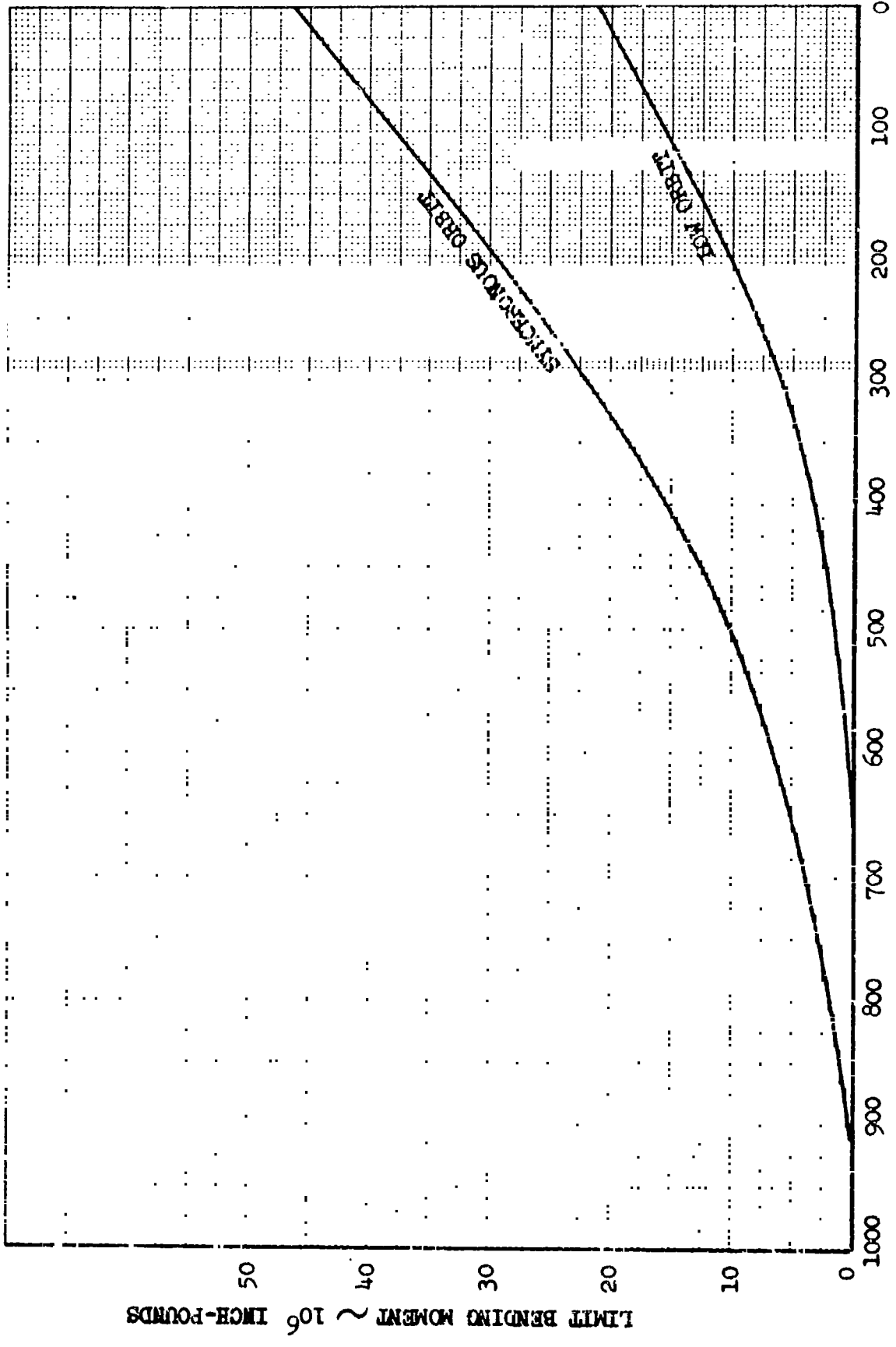
FREQUENCY  $\sim$  CPS

FIGURE 3.2-1 VIBRATION ENVIRONMENT SPECIFICATION FOR LIGHTWEIGHT SUBSYSTEMS



DISTANCE FWD OF MORL - S-IVB INTERFACE ~ INCHES

FIGURE 3.2-2 MORL SHEAR LOAD



DISTANCE FWD OF MORL - S-IV3 INTERFACE ~ INCHES

FIGURE 3.2-3 MORL BENDING MOMENTS

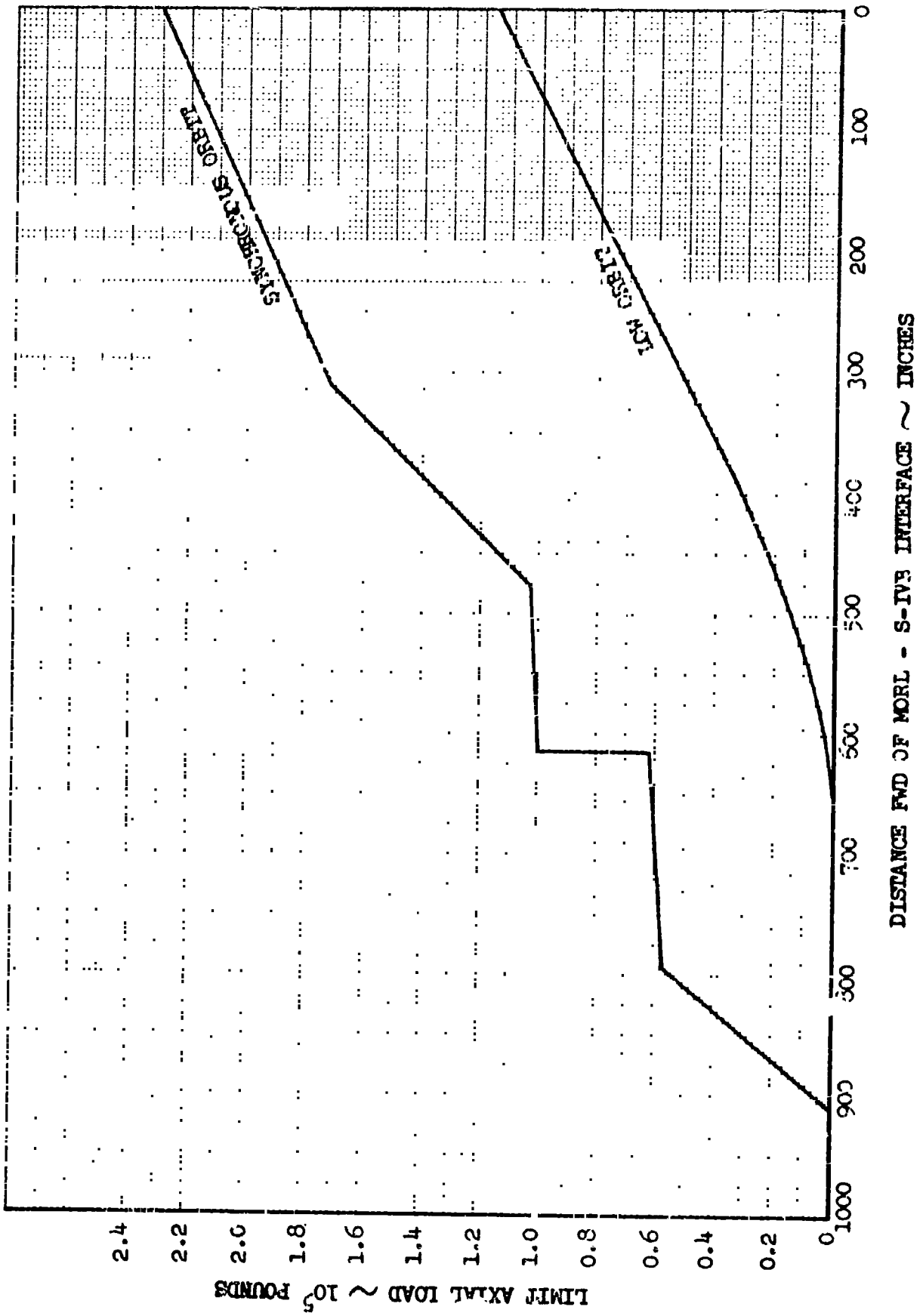


FIGURE 3.2-4 MORL AXIAL LOAD



The loads presented in Section 3.2.3 are based on data taken from Boeing Document D5-10059, "Saturn V Design Data Book for Space Propulsion Systems." Assuming the loads presented in D5-10059 are limit allowable loads, the ratio of bending moment at the S-IVB and payload interface to allowable bending moment and the ratio of equivalent axial load at the interface,  $N_c$ , to the allowable axial load can be made.

	$N_c/N_{c\text{Allowable}}$	$BM/BM_{\text{Allowable}}$
MOT	0.90	0.88
Logistics Vehicle	0.77	0.70
MORL	1.27	1.40

From the above tabulation it is evident that the MOT and logistics vehicle are within the above defined limit allowable loads, with the Saturn V; but, that the MORL exceeds the above defined load limits. It must be emphasized that these figures are conservative since the strength of the S-IVB has been conservatively estimated. More specific statements about compatibility cannot be made until more detailed booster-strength data is available.

### 3.2.5 Primary Mirror

3.2.5.1 Dynamics — The dynamic characteristics of the primary mirror in the synchronous-orbit system are the same as those for the primary mirror of the low-Earth-orbit MOT because the stiffness and mass distribution are the same. These characteristics and analyses are given in Section 5.3.2.2 of Reference 1.

3.2.5.2 Stresses — A discussion of the stress analysis of the primary mirror is presented in Section 5.3.2.3 of Reference 1. This analysis is conservative for the synchronous-orbit MOT because of the lower load factors encountered during launch with the Saturn V (to synchronous orbit) as compared to those for the S-IB (to a 250-nautical-mile orbit).

3.2.5.3 Deformation — Any deformation of the mirror degrades the optical performance of the MOT. Because the mirror is orbiting at zero g, any distortion of the mirror is due to thermal gradients. An analysis of this distortion is presented in Section 4.1.2.

## 3.3 CONFIGURATION MASS ANALYSIS

Analysis of launch configurations required to orbit and sustain the MOT system in synchronous orbit indicates that the launches can easily be accomplished for either mode of the Saturn V booster. Large weight increases over the low-Earth-orbit system occur due to increased radiation shielding, boost structure, and deorbit propellant. These increases are more than offset, however, by the greater boost capability and the decrease in propellant required in orbit. The boost capability is large enough so that fewer launches would actually be required in

synchronous orbit were it not for the desirability of rotating the crew at 90-day intervals and of storing film for short periods of time. The boost capability does make it possible to eliminate one launch by adding an Apollo vehicle to the MORL launch.

This section contains an analysis of mass properties for each of the vehicles in the MOT system. Weights of the MORL and the ferry vehicle are not included in detail. The MORL weight for synchronous orbit has been covered by Douglas (Reference 9), and the ferry vehicle weight will be identical to the logistics vehicle without the multimission module. This section is divided into three parts covering each of the modes and the logistics vehicle. Mass properties for the synchronous orbit are compared to the low-Earth-orbit mass properties in each case.

A 20-percent contingency factor has been added to the operational weights of the MOT and the shuttle vehicle that does not have deorbit capability. This contingency factor was also added to new hardware components in the shuttle vehicle that does have deorbit capability. A lower contingency allowance (equal to 1300 pounds) was applied to the shuttle vehicles with deorbit capability since this is basically an Apollo CSM that has experienced considerable design history.

### 3.3.1 Soft-Gimbal Mode

The mass analysis of the synchronous-orbit, soft-gimbal-mode system includes a revision of the low-Earth-orbit configuration weights so that the weights presented are directly comparable. Design improvements that were developed in the synchronous-orbit study and are also applicable to the low Earth orbit are reflected. Refinements resulting from more definition and greater depth of analysis are also incorporated.

3.3.1.1 Mass Analysis Parameters — Mass analysis of the telescope is based on the following major parameters. Most of these parameters are identical to those used in the low-Earth-orbit study and are repeated here for clarity.

- Inner, outer, and Earth-shade tubes of 1-inch aluminum honeycomb
- Thermal protection of 1-inch superinsulation over inner tube
- Beryllium primary mirror --- cell construction
- Quartz secondary mirrors — solid construction
- Main supports of titanium
- Thermally insulated supports of fiberglass
- Auxiliary boost structure and bladders are removed after initial rendezvous
- Inner and outer gimbal rings of aluminum
- MORL structural truss to gimbal mount carried aboard MOT at launch

- Electrical power for operation provided by MORL
- Atmosphere supply, purification, and pumpdown provided by MORL
- Multipurpose mission module conceived in Boeing studies for NASA — Apollo extension study — is used for the cabin
- Cabin is unpressurized when not occupied
- Cabin atmosphere when occupied is 50-percent  $N_2O_2$  at 7 psia
- Tankage for consumables is sized for 180 days of operation
- Rendezvous-velocity requirement is 426 fps accomplished by two 1000-pound-thrust engines with an  $I_{sp}$  of 300.

3.3.1.2 MOT Mass Analysis Details — Two design improvements that are applicable to either orbit were evolved in the synchronous-orbit study and are reflected in the weights for both orbits as shown in Figure 3.3-1.

One improvement is the rearrangement of star trackers to improve their field of view; only five are now needed instead of the seven previously required. This change requires reconfiguration of the boost shroud, which allows identical shrouds to be used in both the soft-gimbal and detached modes. Because of the star tracker, mounted off the secondary mirror support at the forward end of the telescope, the folding doors used in the low Earth orbit must be modified.

The other improvement is the support of the MOT within the shroud by a rack consisting of four beams under the MOT cabin. This rack replaces the truss that supported the MOT through the sides of the cabin in the previous low-Earth-orbit study. The rack itself is heavier than the truss but, since the attachment points of the rack to the boost adapter are much lower, the increase in weight is offset by a decrease in adapter weight. The rack provides easier separation from the telescope cabin and, therefore, can be staged with the S-IVB stage. In the low-Earth-orbit study, it was assumed that the rendezvous propulsion and ascent batteries would be separated after rendezvous. With incorporation of the rack support system, these items are no longer removed, thus eliminating the problems of separating and deorbiting these items after rendezvous. The revised weights are reflected in the launch mass summary in Figure 3.3-2.

The MOT structure is nearly the same for either orbit. The folding doors covering the front of the telescope are eliminated in the synchronous-orbit configuration. The meteoroid environment is slightly worse in synchronous orbit due to reduction in the Earth shielding factor. The slight increase in flux has a negligible effect on weight, however, since the cabin is unoccupied most of the time and the inherent shielding of the MOT is adequate for the equipment (see Section 4.3.5). The only additional radiation shielding required in synchronous orbit is that to protect film in the cabin. The major structural weight difference is the increase in boost-shroud and adapter weights because of increased flight loads during launch to synchronous orbit (see Section 3.2). The effect of this weight increase is minimized, however, since the shroud is separated at first-stage burnout.

	<u>Low Earth Orbit</u>	<u>Synchronous Orbit</u>
TELESCOPE OPTICS	<u>4343</u>	<u>4343</u>
Primary Mirror	(2205)	(2205)
Mirror	1936	1936
Inner and Outer Cylinders	164	164
Attach Bases and Tangent Bars	105	105
Support Base	(479)	(479)
Floor	129	129
Rings	44	44
Beams	306	306
Platen Support Tube	(314)	(314)
Tube	97	97
Insulation	127	127
Flanges, Rings, and Door	90	90
Folding Mirror Assembly	(171)	(171)
Support Bladders	(61)	(61)
Primary Mirror Doors	(345)	(345)
Cover Doors	264	264
Frames, Hinges, and Attachments	81	81
Secondary Mirror — f/15	(290)	(290)
Secondary Mirror — f/30	(99)	(99)
Secondary Support Truss and Sleeve	(86)	(86)
Secondary Positioning Systems	(53)	(53)
Removal Mechanism — f/15	(90)	(90)
Alignment Control	(150)	(150)
Autocollimators	80	80
Interferometer	25	25
Sensors and Alignment Unit	45	45
STRUCTURE — TELESCOPE	<u>3904</u>	<u>3753</u>
Inner Tube	(1473)	(1473)
Honeycomb	1115	1115
Rings and Fittings	218	218
Outer Ring and Door Fittings	114	114
Light Baffles	26	26
Outer Tube	(1558)	(1558)
Honeycomb	1290	1290
Rings and Fittings	268	268
Telescope Doors	(151)	(0)
Extendable Shade	(523)	(523)
Honeycomb Sandwich	430	430
Actuators and Mounting	60	60
Rings and Fittings	33	33

Figure 3.3-1: MOT OPERATIONAL MASS — GIMBAL MODE

Figure 3.3-1 (Cont.)

	<u>Low Earth Orbit</u>	<u>Synchronous Orbit</u>
Shade Guide Frame	(119)	(119)
Crew Restraint and Positioning	(40)	(40)
Sensor Support Frame	(40)	(40)
<b>STRUCTURE --- CABIN</b>	<u>2694</u>	<u>2694</u>
Cabin-Telescope Interface	(393)	(393)
Outer Wall Attachment	52	52
Six-Bar Truss	27	27
Support Tube Connection	14	14
Platen and Fittings	228	228
Indexing Structure and Mechanisms	72	72
Bulkheads	(1351)	(1351)
Waffle Structure	713	713
Radial Beams	244	244
Intermediate Ring	82	82
Inner Ring and Tunnel	33	63
Seal Ring and Seal	99	99
Fittings and Attachments	150	150
Cylinders	(503)	(503)
Cylinder Skin	310	310
Internal Columns	163	163
Central Head Ties	30	30
Penetrations and Seals	(85)	(85)
Subsystem Support Beams	(72)	(72)
Console Structure	(35)	(35)
Seat, Locomotion, and Restraint	(40)	(40)
<b>STRUCTURE --- GIMBAL MECHANISMS</b>	<u>581</u>	<u>581</u>
Gimbal Mechanisms	(279)	(279)
Outer Gimbal Ring	103	103
Inner Gimbal Ring	99	99
Gimbal Bearings	36	36
Coil Springs	12	12
Actuators and Guides	29	29
Gimbal Truss Structure	(178)	(178)
Support Rings	105	105
Truss Members	41	41
Support Frames	22	22
Attachments	10	10
MOT-MORL Support Truss	(124)	(124)
Truss Structure	82	82
Fittings and Attachments	42	42

Figure 3.3-1 (Cont.)

	<u>Low Earth Orbit</u>	<u>Synchronous Orbit</u>
<b>THERMAL PROTECTION</b>	<u>2912</u>	<u>2912</u>
Inner Tube Insulation	(1922)	(1922)
Shade Insulation	(352)	(352)
Primary Mirror Insulation	(372)	(372)
Platen Support Tube Insulation	(92)	(92)
Cabin Insulation	(84)	(84)
Thermal Coatings	(90)	(90)
<b>ELECTRICAL POWER</b>	<u>405</u>	<u>405</u>
Battery Installation	(127)	(127)
Ag-Zn Batteries	110	110
Installation Provisions	17	17
Regulators	(23)	(23)
Inverters	(60)	(60)
Distribution System	(195)	(195)
<b>REACTION CONTROL SYSTEM</b>	<u>145</u>	<u>120</u>
Engines	(40)	(40)
Propellant Tanks and Residuals	(28)	(8)
Pressurization System	(7)	(2)
Valves, Plumbing, and Fittings	(55)	(55)
Wiring	(15)	(15)
<b>ATTITUDE CONTROL AND STABILIZATION</b>	<u>1137</u>	<u>1011</u>
Sensors	(249)	(249)
Sun Sensors	3	3
Gyro Package	16	16
Star Trackers	120	120
Intermediate Pointing	50	50
Fine Pointing	60	60
Electronics	(528)	(528)
Digital Computer	290	290
Star Tracker	138	138
Analog Computer	50	50
CMG Electronics	45	45
Sensor Gyro Electronics	5	5
Control Moment Gyro	(360)	(234)
X Axis	30	54
Y Axis	165	90
Z Axis	165	90

Figure 3.3-1 (Cont.)

	Low Earth Orbit	Synchronous Orbit
<b>COMMUNICATION AND DATA MANAGEMENT</b>	<u>58</u>	<u>58</u>
Telemetry	(21)	(21)
Vidicon Cameras	(12)	(12)
VHF System	(19)	(19)
Voice Transponder	(6)	(6)
<b>ENVIRONMENTAL CONTROL AND LIFE SUPPORT</b>	<u>238</u>	<u>238</u>
Atmosphere Control	(37)	(37)
Heat Transport	(66)	(66)
Pumps, Accumulators, and Controls	10	10
Cold Plates and HX	30	30
Plumbing and Coolant	26	26
Emergency Repressurization	(90)	(90)
Gaseous Oxygen Tanks	39	39
Gaseous Nitrogen Tanks	38	38
Plumbing and Controls	13	13
Radiator	(45)	(45)
Tubes and Headers	21	21
Fluid System	24	24
<b>RENDEZVOUS PROPULSION</b>	<u>200</u>	<u>185</u>
Engines	(80)	(80)
Propellant Tanks	(58)	(49)
Pressurization System	(40)	(34)
Lines, Fittings, and Valves	(22)	(22)
<b>EXPERIMENTS — f/15</b>	<u>454</u>	<u>454</u>
Low-Dispersion UV Spectrometer	(49)	(49)
Low-Dispersion Spectrograph	(54)	(54)
High-Dispersion UV Spectrometer	(122)	(122)
Wide-Field Camera	(218)	(218)
Vidicon Camera	(11)	(11)
Wiring	(20)	(20)
<b>EXPERIMENTS — f/30</b>	<u>942</u>	<u>942</u>
Thermoelectric Photometer	(24)	(24)
Photoelectric Photometer	(63)	(63)
High-Dispersion IR Spectrometer	(188)	(188)
High-Dispersion Spectrograph	(440)	(440)
Large-Scale Camera	(186)	(186)
Vidicon Camera	(11)	(11)
Intermittent Recorders	(30)	(30)
Wiring	(35)	(35)

Figure 3.3-1 (Cont.)

	<u>Low Earth Orbit</u>	<u>Synchronous Orbit</u>
<b>EXPERIMENT CONTROL SENSORS</b>	<u>495</u>	<u>495</u>
Pointing Sensors	(305)	(305)
Intermediate Pointing	100	100
Photometry Pointing	55	55
Low-Dispersion Pointing	60	60
High-Dispersion Pointing	90	90
Photo Sensors	(110)	(110)
Star-Field Photo	40	40
Planetary Photo	30	30
Planetary Spectrography	40	40
Translation Mechanisms	(35)	(35)
Wiring	(45)	(45)
<b>EXPENDABLES</b>	<u>476</u>	<u>322</u>
Film	(126)	(252)
Film Radiation Protection	(110)	(0)
Propellant	(175)	(57)
EC/SL Expendables	(55)	(55)
Sensor Coolants (Average)	(10)	(10)
<b>SPARES</b>	<u>360</u>	<u>360</u>
<b>CONTINGENCY (20%)</b>	<u>3,867</u>	<u>3,771</u>
<b>TOTAL OPERATIONAL MASS</b>	23,211	22,644



	Low Earth Orbit	Synchronous Orbit
Telescope Optics	4,343	4,343
Structure — Telescope	3,904	3,753
Structure — Cabin	2,694	2,694
Structure — Gimbal System	581	581
Thermal Protection	2,912	2,912
Electrical Power	405	405
Reaction Control System	145	120
Attitude Control and Stabilization	1,137	1,011
Communication and Data Management	58	58
Environmental Control and Life Support	238	238
Rendezvous Propulsion	200	185
Experiments — f/15	454	454
Experiments — f/30	942	942
Experiment Control Sensors	495	495
Expendables	476	322
Spares	360	360
Contingency	3,867	3,771
<b>Total Operational Mass</b>	<b>23,211</b>	<b>22,644</b>
Docking Propellant	120	120
Rendezvous Propellant	1,045	900
<b>Start Rendezvous</b>	<b>24,377</b>	<b>23,664</b>
S-IV and MOT Interstage	1,592	1,610
MOT Support Rack	828	828
<b>Staging Orbit Mass</b>	<b>26,797</b>	<b>26,102</b>
Effective Fairing Mass	631	789
Effective Nose Cone Mass	117	146
<b>EFFECTIVE LAUNCH MASS</b>	<b>27,545</b>	<b>27,037</b>
<b>CAPABILITY</b>	<b>36,000</b>	<b>79,600</b>
<b>EXCESS</b>	<b>+8,455</b>	<b>+52,563</b>

Figure 3.3-2: MOT LAUNCH MASS SUMMARY — GIMBAL MODE

Electrical-power-subsystem weights are the same for either orbit. This subsystem is required for the boost phase only and its size is, therefore, dependent on the time required to reach the orbits. Time spent in parking orbit for the low-Earth-orbit configuration would affect the battery weight; but, for purposes of comparison, it was assumed that time to orbit would be the same for either orbit.

The reaction-control-subsystem weight differs only in the amount of propellant and tankage required. The propellant tanks for the low Earth orbit are sized to contain a 90-day supply (see Section 3.3.3) while a 180-day supply is contained in the synchronous-orbit configuration. Tanks for both configurations contain propellant for initial docking (35 pounds). Attitude-control propellant requirements are very low in synchronous orbit (see Section 4.2).

The only weight difference in the attitude-control-and-stabilization subsystem is in the control-moment-gyro weight. The low-Earth-orbit configuration weights have been updated to include the weight of a digital computer that was inadvertently omitted in the previous report.

The rendezvous-propulsion subsystem for synchronous orbit is identical to that for the low Earth orbit except for the amounts of propellant, pressurant, and tankage required. The synchronous rendezvous requirements are less than those of low Earth orbit because the S-IVB injects the vehicle into orbit — a function performed by the propulsion subsystem in low Earth orbit. Velocity requirements are 426 and 475 fps, respectively, for the synchronous and low Earth orbits. These figures include an allowance of 50 fps for docking; this velocity is attained using the reaction control system. The low-Earth-orbit total rendezvous-velocity requirement was increased from the previous study value of 380 to the above value of 475 fps to reflect a value comparable to the synchronous-orbit requirement.

Experiment weight in synchronous orbit remains unchanged from low-Earth orbit. The low-Earth-orbit experiment weights have been increased to include intermittently operating tape recorders.

Expendable weights reflect a 180-day supply of consumables for the synchronous orbit and a 90-day supply for the low Earth orbit. The 90-day supply period reflects a change from the previous study and is explained in Section 3.3.3. The initial supply of film is also an addition to previously reported weights.

The initial supply of spares, estimated as a 1-year requirement, is included. Spares are replaced by the logistics vehicle as they are used.

Subsystems not included in the preceding discussion have not changed from the previous low-Earth-orbit study.

Weight for reserves, allowances, and contingency is consistent with the policy established in the low-Earth-orbit study.

**3.3.1.3 Orbit Configuration Mass Properties** — Approximate mass properties for the soft-gimbal mode are shown in Figure 3.3-3 and include the center of gravity, center of pressure, and mass moments of inertia. These data were estimated near the start of the synchronous-orbit study for use in determining attitude and stabilization control requirements and the weights shown are, therefore, not consistent with those shown in the preceding section. The effect of the refinements in weight on the remainder of the mass properties is small and, therefore, no iteration was made. The following parameters were used in establishing the mass data:

- Mass properties for MORL without external vehicles were obtained from Douglas Aircraft Company (Reference 16) for low Earth orbit
- The weights used for external vehicles (Apollo and cargo modules) are:

Apollo CM — 10,387 pounds	both orbits
Apollo SM — 20,958 pounds	synchronous orbit only; includes 12,508 pounds of propellant for re-entry
Modified SM — 2640 pounds	low Earth orbit only; includes 1270 pounds solid retropropack for re-entry
Cargo Module — 8300 pounds	both orbits

It was assumed that in either orbit the service module power subsystem would consist solely of batteries, and atmosphere storage would be accomplished with a high-pressure gaseous system. Systems and supplies are adequate for transit between Earth and MORL only.

- Three-man command modules with a 180-day crew-rotation period.
- Additional MORL radiation protection for synchronous orbit (14,200 pounds) was obtained from Douglas (Reference 9) and includes a biowell. It was assumed that equipment in MORL would be relocated so that the center of gravity would be the same as the low-Earth-orbit MORL, and the moments of inertia would be in proportion to weight.
- The Apollos and cargo modules are rotated about the X axis 45 degrees from the low-Earth-orbit configuration for the synchronous orbit so that the service modules will not interfere with solar-cell-panel rotation. These modules lie on the principal axes in the synchronous-orbit configuration.
- The effect of weight differences as a result of differences in attitude-control, power, or other subsystem requirements between the two orbits is not included.
- It is desirable to maintain the same center of gravity of the MORL configuration, including external vehicles, for both the low-altitude and synchronous orbits so that the telescope gimbal design will be the same for both configurations. This necessitates retracting the Apollo docking booms about 40 inches when the Apollos are stowed for the synchronous-orbit configuration.

Orbit	Weight (Pounds)	C. G. (*MORL Sta.)	C. P.		I <sub>Roll</sub> (Slug-Ft <sup>2</sup> )	I <sub>Pitch</sub> (Slug-Ft <sup>2</sup> )	I <sub>Yaw</sub> (Slug-Ft <sup>2</sup> )	I <sub>YZ</sub> (Slug-Ft <sup>2</sup> )
			**YX Plane (MORL Sta.)	ZX Plane (MORL Sta.)				
<b>Synchronous</b>								
MORL	123,490	2,003	1,978	1,835	970,860	609,130	1,025,878	0
MOT	21,965	1,490	1,330	1,330	21,100	157,600	156,800	0
Coupled	145,455	1,926	1,731	1,729	991,960	1,796,890	2,212,840	0
<b>Low Altitude</b>								
MORL	72,654	2,003	1,963	1,811	525,390	424,560	530,900	24,023
MOT	21,965	1,490	1,330	1,330	21,100	157,600	156,800	0
Coupled	94,619	1,884	1,674	1,700	546,490	1,533,010	1,641,550	24,023

\* MORL Station 1714 is on the solar-cell-gimbal axis (stations are given in inches).

\*\* X axis is longitudinal; Z axis is through the solar-cell-gimbal axis. Therefore, the effect of solar cells on center of pressure does not apply to the YX plane. It was assumed that the solar panels are oriented in the ZX plane.

Figure 3.3-3: MASS PROPERTIES COMPARISON — SOFT-GIMBAL MODE

### 3.3.2 Detached Mode

Many of the mass analysis parameters and mass characteristics of the MOT are common in both modes and have been discussed in Section 3.3.1. The discussion of mass analysis of the detached mode, therefore, will be confined to items that are peculiar to this mode.

3.3.2.1 Mass Analysis Parameters — The following parameters apply to the detached mode only:

- Direct entry from shuttle to the MOT cabin without airlock.
- Pumpdown power shared with shuttle.
- Pumpdown system and cooling supplied by the MOT.
- Pumpdown gaseous storage at 500 psia provided by shuttle.
- Electrical power supplied by articulated solar panels, fixed in position during telescope operation, plus silver-cadmium batteries.
- Expendables and storage capability for 180-day operation resupplied by docking to the MORL.

3.3.2.2 MOT Mass Analysis Details — Figures 3.3-4 and 3.3-5 present operational weight and sequential launch weight respectively for the MOT detached mode. The following discussion describes the weight changes that are required for the detached mode in addition to those that are applicable to both modes.

The meteoroid-bumper weight of the MOT cabin was increased in weight slightly to reflect the increased meteoroid flux in synchronous orbit, which results from the decreased Earth blockage factor. This bumper covers the aft end of the MOT cabin, which is protected by MORL in the gimbal mode.

The electrical power subsystem is reduced in synchronous orbit because of the small amount of time that the solar panels are shaded from the Sun by Earth.

The reaction control subsystem is lighter for the detached mode in synchronous orbit than for low Earth orbit because of the reduced disturbance environment. The systems are larger than for the gimballed mode since control must be attained without aid from the MORL and because repeated dockings with the MORL are required. Section 3.3.3 describes the logistics required for each mode.

3.3.2.3 Shuttle-Vehicle Mass Analysis — Figure 3.3-6 shows the shuttle-vehicle weights for the MOT detached mode in both low Earth and synchronous orbits for the three shuttle concepts described in Section 3.1.2. The centerline approach for both orbits is a shuttle vehicle without deorbit or abort capability. This vehicle will be identical for both orbits and consists of a stripped Apollo command module with an attached cargo module. It may be desirable, however, to add deorbit capability to the shuttle so that abort would be possible if the MORL

	<u>Low Earth Orbit</u>	<u>Synchronous Orbit</u>
<b>TELESCOPE OPTICS</b>	<b><u>4343</u></b>	<b><u>4343</u></b>
Primary Mirror	(2205)	(2205)
Mirror	1936	1936
Inner and Outer Cylinders	164	164
Attach Bases and Tangent Bars	105	105
Support Base	(479)	(479)
Floor	129	129
Rings	44	44
Beams	306	306
Platen Support Tube	(314)	(314)
Tube	97	97
Insulation	127	127
Flanges, Rings, and Door	90	90
Folding Mirror Assembly	(171)	(171)
Support Bladders	61	61
Primary Mirror Doors	(345)	(345)
Cover Doors	264	264
Frames, Hinges, and Attachments	81	81
Secondary Mirror — f/15	(290)	(290)
Secondary Mirror — f/30	(99)	(99)
Secondary Support Truss and Sleeve	(86)	(86)
Secondary Positioning Systems	(53)	(53)
Removal Mechanism — f/15	(90)	(90)
Alignment Control	(150)	(150)
Autocollimators	80	80
Interferometer	25	25
Sensor and Alignment Unit	45	45
<b>STRUCTURE — TELESCOPE</b>	<b><u>3880</u></b>	<b><u>3729</u></b>
Inner Tube	(1473)	(1473)
Honeycomb	1115	1115
Rings and Fittings	218	218
Outer Rings and Door Fittings	114	114
Light Baffles	26	26
Outer Tube	(1534)	(1534)
Honeycomb	1290	1290
Rings and Fittings	244	244
Telescope Doors	(151)	(0)
Extendable Shade	(523)	(523)
Honeycomb Sandwich	430	430
Actuators and Mounting	60	60
Rings and Fittings	33	33

Figure 3.3-4: MOT OPERATIONAL MASS — DETACHED MODE

Figure 2.3-4 (Cont.)

	<u>Low Earth Orbit</u>	<u>Synchronous Orbit</u>
Shade Guide Frame	(119)	(119)
Crew Restraint and Positioning	(40)	(40)
Sensor Support Frame	(40)	(40)
<b>STRUCTURE — CABIN</b>	<b><u>2847</u></b>	<b><u>2853</u></b>
Cabin and Telescope Interface	(393)	(393)
Outer Wall Attachment	52	52
Six-Bar Truss	27	27
Support Tube Connection	14	14
Platen and Fittings	228	228
Indexing Structure and Mechanisms	72	72
Bulkheads	(1389)	(1389)
Waffle Structure	792	792
Radial Beams	244	244
Intermediate Ring	82	82
Inner Ring and Tunnel	63	63
Seal Ring and Seal	58	58
Fittings and Attachments	150	150
Cylinders	(503)	(503)
Cylinder Skin	310	310
Internal	163	163
Central Head Ties	30	30
Hatch, Penetrations, and Seals	(105)	(105)
Docking Structure	(195)	(195)
Subsystem Support Beams	(123)	(123)
Console Structure	(35)	(35)
Seat, Locomotion, and Restraint	(40)	(40)
Meteoroid Bumper	(64)	(70)
<b>THERMAL PROTECTION</b>	<b><u>2932</u></b>	<b><u>2932</u></b>
Inner Tube Insulation	(1922)	(1922)
Shade Insulation	(352)	(352)
Primary Mirror Insulation	(372)	(372)
Platen Support Tube Insulation	(92)	(92)
Cabin Insulation	(84)	(84)
Thermal Coatings	(110)	(110)
<b>ELECTRICAL POWER</b>	<b><u>1437</u></b>	<b><u>921</u></b>
Solar Panels	(324)	(196)
Cells, Wiring, and Cover Glass	166	100
Substrate Structure	62	37
Beams and Actuators	57	34
Extension System and Supports	39	24

Figure 3. 3-4 (Cont.)

	Low Earth Orbit	Synchronous Orbit
Battery Installation	(593)	(212)
AgCd (Low), AgZn (Synchronous) Batteries	545	195
Installation Provisions	48	17
Regulators	(75)	(75)
Inverters	(180)	(180)
Battery Chargers	(15)	(8)
Distribution System	(250)	(250)
<b>REACTION CONTROL SYSTEM</b>	<u>165</u>	<u>179</u>
Engines	(40)	(40)
Propellant Tanks and Residuals	(48)	(59)
Pressurization System	(7)	(10)
Valves, Plumbing, and Fittings	(55)	(55)
Wiring	(15)	(15)
<b>ATTITUDE CONTROL AND STABILIZATION</b>	<u>1137</u>	<u>1011</u>
Sensors	(249)	(249)
Sun Sensors	3	3
Gyro Package	16	16
Star Trackers	120	120
Intermediate Pointing	50	50
Fine Pointing	60	60
Electronics	(528)	(528)
Digital Computer	290	290
Star Tracker	138	138
Analog Computer	50	50
CMG Electronics	45	45
Sensor Gyro Electronics	5	5
Control Moment Gyro	(360)	(234)
X Axis	30	54
Y Axis	165	90
Z Axis	165	90
<b>COMMUNICATION, TRACKING, AND DATA MANAGEMENT</b>	<u>123</u>	<u>123</u>
Telemetry	(21)	(21)
Vidicon Cameras	(12)	(12)
VHF System	(19)	(19)
Voice Transponder	(6)	(6)
Rendezvous Radar	(30)	(30)
Antennas, Cables, and Wiring	(35)	(35)



Figure 3.3-4 (Cont.)

	<u>Low</u> <u>Earth Orbit</u>	<u>Synchronous</u> <u>Orbit</u>
<b>ENVIRONMENTAL CONTROL AND LIFE SUPPORT</b>	<u>523</u>	<u>523</u>
Atmosphere Control	(22)	(22)
Atmosphere Recovery	(148)	(148)
Compressor	120	120
Coolers and Plumbing	28	28
Heat Transport	(81)	(81)
Pumps, Accumulators, and Controls	12	12
Cold Plates and Heat Exchanger	35	35
Plumbing and Coolant	29	29
Emergency Repressurization	(90)	(90)
Gaseous Oxygen Tanks	39	39
Gaseous Nitrogen Tanks	38	38
Plumbing and Controls	13	13
Radiator	(182)	(182)
Tubes and Headers	84	84
Fluid System	98	98
<b>RENDEZVOUS PROPULSION</b>	<u>202</u>	<u>187</u>
Engines	(80)	(80)
Propellant Tanks	(59)	(50)
Pressurization System	(41)	(35)
Lines, Fittings, and Valves	(22)	(22)
<b>EXPERIMENTS — f/15</b>	<u>454</u>	<u>454</u>
Low-Dispersion UV Spectrometer	(49)	(49)
Low-Dispersion Spectrograph	(54)	(54)
High-Dispersion UV Spectrometer	(122)	(122)
Wide-Field Camera	(218)	(218)
Vidicon Camera	(11)	(11)
Wiring	(20)	(20)
<b>EXPERIMENTS — f/30</b>	<u>942</u>	<u>942</u>
Thermoelectric Photometer	(24)	(24)
Photoelectric Photometer	(63)	(63)
High-Dispersion IR Spectrometer	(188)	(188)
High-Dispersion Spectrograph	(440)	(440)
Large-Scale Camera	(186)	(186)
Vidicon Camera	(11)	(11)
Intermittent Recorders	(30)	(30)
Wiring	(35)	(35)

Figure 3.3-4 (Cont.)

	<u>Low Earth Orbit</u>	<u>Synchronous Orbit</u>
EXPERIMENT CONTROL SENSORS	<u>495</u>	<u>495</u>
Pointing Sensors	(305)	(305)
Intermediate Pointing	100	100
Photometry Pointing	55	55
Low-Dispersion Pointing	60	60
High-Dispersion Pointing	90	( )
Photo Sensors	(110)	(110)
Star-Field Photo	40	40
Planetary Photo	30	30
Planetary Spectrography	40	40
Translation Mechanisms	(35)	(35)
Wiring	(45)	(45)
EXPENDABLES	<u>794</u>	<u>931</u>
Film	(126)	(252)
Film Radiation Protection	(110)	(0)
Propellant	(483)	(604)
Environmental Control and Life Support Expendables	(65)	(65)
Sensor Coolants (Average)	(10)	(10)
SPARES	<u>452</u>	<u>452</u>
CONTINGENCY (20%)	<u>4143</u>	<u>4011</u>
TOTAL OPERATIONAL MASS	24,869	24,086

	<u>Low Earth Orbit</u>	<u>Synchronous Orbit</u>
Telescope Optics	4,343	4,343
Structure — Telescope	3,880	3,729
Structure — Cabin	2,847	2,853
Thermal Protection	2,932	2,932
Electrical Power	1,437	921
Reaction Control System	165	179
Attitude Control and Stabilization	1,137	1,011
Communication and Data Management	123	123
Environmental Control and Life Support	523	523
Rendezvous Propulsion	202	187
Experiments — f/15	454	454
Experiments — f/30	942	942
Experiment Control Sensors	495	495
Expendables	794	931
Spares	452	452
Contingency	4,143	4,011
	<hr/>	<hr/>
Total Operational Mass	24,869	24,086
Docking Propellant	120	120
Rendezvous Propellant	1,126	944
	<hr/>	<hr/>
Start Rendezvous	26,115	25,150
S-IV and MOT Interstage	1,592	1,610
MOT Support Rack	828	828
	<hr/>	<hr/>
Staging Orbit Mass	28,535	27,586
Effective Fairing Mass	631	789
Effective Nose Cone Mass	117	146
	<hr/>	<hr/>
EFFECTIVE LAUNCH MASS	29,283	28,523
CAPABILITY	36,000	79,600
EXCESS	+6,717	+51,077

Figure 3.3-5: MOT LAUNCH MASS SUMMARY — DETACHED MODE

	<u>No Abort Capability</u>	<u>Abort Capability from Low-Earth Orbit</u>	<u>Abort Capability from Synchronous Orbit</u>
CREW MODULE	(4,200)	(9,675)	(9,675)
Structure	1,860	4,870	4,870
Crew Systems	230	230	230
Electrical Power	410	510	510
Communications	120	370	370
Environmental Control and Life Support	360	360	360
Controls, Displays, and Instrumentation	160	510	510
Navigation and Stability Control	110	620	620
MOT Maintenance Provisions	30	30	30
Docking System	190	190	190
Environmental Control and Life Support Expendables	110	165	165
Penetrations and Leaks	50	50	50
Crew and Equipment	570	570	570
Reaction Control	0	600	600
Earth Landing System	0	600	600
SERVICE AND CARGO MODULE	(2,300)	(5,540)	(26,860)
Structure	1,220	1,790	2,210
Reaction Control and Propulsion	160	445	4,456
Atmosphere Storage System	270	270	270
MOT Stored Atmosphere	150	150	150
Subsystems	0	800	1,784
Shuttle Propellant	500	1,060	2,425
Abort Propellant	0	1,025	15,565
CONTINGENCY	(1,300)	(1,300)	(1,300)
TOTAL SHUTTLE VEHICLE	7,800	16,515	37,835

Figure 3.3-6: SHUTTLE VEHICLE WEIGHT

became damaged during the shuttle operation or if rendezvous with the MORL could not be accomplished. By adding deorbit capability, a severe weight penalty is incurred. The added weight falls in three categories:

- 1) The crew-module structure and subsystems must be made capable of re-entry;
- 2) A retrograde propulsion module must be added;
- 3) Shuttle propellant must be increased to carry the above changes.

When deorbit capability is added, a large difference between shuttle vehicle weight for low Earth orbit and that for synchronous orbit can be seen. It should be noted that none of the three vehicles is optimum from a weight standpoint because they make maximum use of existing Apollo hardware. Optimization of structure, heat shield, propulsion, and subsystem would reduce the weight of each vehicle.

The following major parameters have been used to determine mass requirements of the shuttle vehicle:

- The shuttle is designed for 15 round trips — MORL to MOT to MORL — requiring 15 repressurization cycles of the MOT. Refurbishment is required after 15 round trips.
- Maximum of 1-mile MOT-MORL separation.
- Nominal two-man crew, with overload capability of three.
- Crew-module atmosphere of 50-percent O<sub>2</sub> and 50-percent N<sub>2</sub> at 7 psia.
- Cargo module unpressurized.
- One emergency repressurization of crew module stored aboard.
- Storage capability for 90 percent of MOT recovered atmosphere at 500 psia.
- Atmosphere makeup for 10-percent MOT atmosphere makeup, stored at 3500 psia, for each repressurization cycle.
- No MOT propellant resupply capability — this is a requirement of MOT-MORL docking operation.
- Cargo module cylindrical wall integrated with redundant tube radiator.
- Batteries sized for providing 4000 watt-hours at 80-percent depth of discharge for shuttle use. Re-entry batteries, if required, equivalent to ferry vehicle requirements.
- Apollo service module offloaded for synchronous deorbit with a deorbit  $\Delta V$  capability of 5200 fps in addition to shuttle requirements.
- Shuttle propulsion  $\Delta V$  capability of 650 fps.
- Cargo module staged prior to deorbit for low-altitude configuration and integrated with the service module for the synchronous-orbit configuration.

- Weight contingency of 20 percent is allowed for vehicles without deorbit capability. This same amount (1300 pounds) is used for the other configurations. While these other configurations are heavier, they are comprised of hardware that is more fully developed.

3.3.2.4 Orbit Configuration Mass Properties — Differences between mass properties for the detached-mode MOT configuration in low Earth and synchronous orbits are not large enough to be significant with regard to attitude stability-and-control requirements, considering the stage of design. Therefore, the same properties reported in the low-Earth-orbit study (Reference 1) are applicable. Slight differences caused by the difference in MOT weight and solar panel size will be detectable in later stages of design. MORL mass properties will be similar to those given for the soft-gimbal mode in Section 3.3.1.3.

### 3.3.3 Logistics Vehicle

This section contains a comparative evaluation of the MOT logistic vehicle weights for the gimbal and detached modes in low-altitude and synchronous orbits. Summary weights are presented according to the arrangement of major components at launch. For a more detailed comparison, the weights have been grouped in the categories of structure, propellant, atmosphere, and dry cargo.

3.3.3.1 Conclusions — The logistics vehicle weight requirements for the synchronous orbit are less severe with regard to booster capability than for the low Earth orbit, primarily because of the increased booster capability and decreased propellant cargo requirements for synchronous orbit.

The logistics supply cycle for the low Earth orbit should coincide with crew-rotation launches at 90-day intervals. The synchronous-orbit logistic launches are needed only at every other crew-rotation launch, i. e., at 180-day intervals.

3.3.3.2 Mass Analysis Parameters — The following parameters have been used to derive the mass of the logistics requirements based on a 1-year period.

#### Parameters Common to Both Modes

- 71 film replacement periods of 3 hours each.
- 10 setup and checkout periods of 7.5 hours each.
- 4 scheduled maintenance periods of 3 days each.
- 1 scheduled 4-day period for f/15 to f/30 changeover.
- 15 unscheduled maintenance periods of 1 day or less.
- 0.30 lb/hr MOT atmosphere leakage rate.
- 2.5 lbs per man-day metabolic oxygen rate.

- Command module deorbit  $\Delta V$  for low Earth and synchronous orbits are 500 and 5200 fps. respectively.
- Multimission module deorbit  $\Delta V$  for low Earth and synchronous orbits are 190 and 5000 fps. respectively.
- Service module propulsion  $I_{sp}$  is 305.
- Multimission module propulsion  $I_{sp}$  is 290.
- Command module weight is based on a minimum modified Apollo vehicle.
- Weight contingency is included at the rate of 20 percent on new hardware, excluding cargo and propellant. Calculations of propellant and cargo include contingency allowances.
- Logistics requirements for MORL are according to Douglas reports (Reference 21). Multimission module weights are also derived from this source.
- Film is resupplied at 90-day intervals (coinciding with crew rotation) to limit fogging by radiation.

Parameters for Gimbal Mode Only

- Emergency atmosphere repressurization by MORL, four per year estimated, required for high-leak loss (dump) of cabin atmosphere.

Parameters for Shuttle Mode Only

- 2-hour average shuttle travel time per docking cycle - two men.
- 1-hour average shuttle checkout and maintenance time per docking cycle - one man.
- 1-hour shuttle holding time for MOT pumpdown - two men.
- Spares replacement mass increased (over the gimbal mode) by electrical power equipment and by orbit control equipment.
- Emergency atmosphere for one complete repressurization stored in both the MOT and the shuttle, four replacements per year estimated for MOT plus one while coupled to MORL — two replacements per year for shuttle.
- Shuttle atmosphere leakage rate of 0.25 lb/hr.
- 1-year battery lifetime, replacement has not been included in the 1-year logistics provisions.

3.3.3.3 Mass Analysis Details — Logistics vehicle weights differ markedly between low Earth and synchronous orbits. The cargo requirements for low Earth orbit are higher because of the requirements for attitude control and station and orbit keeping propellant. Conversely, propellant required to deorbit

both the command and multimission modules is much larger for the synchronous orbit. In terms of feet per second required, the requirements for deorbit differ by more than an order of magnitude. The overriding influence with regard to mission accomplishment is booster capability. The Saturn-V capability in synchronous orbit is nearly twice that of the Saturn IB in low Earth orbit. These factors enable a 180-day resupply cycle in synchronous orbit while the low-Earth-orbit resupply cycle is confined to 90 days. In either case, the number of launches required remains the same since a crew rotation schedule of 90 days has been assumed. Figure 3.3-7 is a weight summary that illustrates the effect of orbit altitude on both modes and the effect of time on the low-Earth-orbit vehicle. The following paragraphs discuss weight differences between orbits in more detail.

Structure — Structure weight, as shown in Figure 3.3-8, differs between the configurations for low Earth and synchronous orbits for the following reasons:

- Heavier service module structure is required to contain the additional propellant required.
- An additional adapter section is required between the service module and the multimission module due to the size of the service module engine.
- Multimission module outer cylinder is heavier because:
  - 1) The payload above the cylinder is greater because of the larger service module;
  - 2) The flight load bending moment is greater as a result of the longer configuration and boost-vehicle characteristics (see Section 3.2).

A slight compensating reduction exists because of the lesser acceleration loads imposed by the Saturn V as compared to the Saturn IB.

- Multimission module meteoroid shielding is slightly heavier since the meteoroid flux blockage by Earth is much less at synchronous-orbit altitude.
- Multimission module adapter weight is heavier for the same reasons that the multimission module cylinder is heavier.
- An additional docking port is required on the multimission module in synchronous orbit to facilitate deorbiting. In synchronous orbit, the multimission module is deorbited by the Apollo service module, whereas the low-Earth-orbit configuration contains its own propulsion system for deorbit.

Propellant — Propellant requirements for the low-Earth- and synchronous-orbit configurations, as shown in Figure 3.3-9, differ for the following reasons:

- Command module deorbit- $\Delta V$  requirements are about 5200 fps for the synchronous-orbit configuration compared to 190 fps for the low-Earth-orbit configuration.
- Multimission module deorbit- $\Delta V$  requirements differ by about the same amount as the command module, and deorbit is accomplished by the service module for synchronous orbit as compared to using the multimission module propulsion system for deorbit in the low-Earth-orbit configuration.



	180-Day Supply Cycle			90-Day		
	Low Orbit		Synchronous Orbit	Low Orbit		Detached Mode
	Gimbal Mode	Detached Mode	Gimbal Mode	Detached Mode	Gimbal Mode	Detached Mode
Command Module	(10,387)	(10,387)	(10,387)	(10,387)	(10,387)	(10,387)
Service Module	(2,640)	(2,640)	(25,838)	(26,088)	(2,640)	(2,640)
Inerts	1,824	1,824	8,450	8,450	1,824	1,824
Main Propellant	816	816	17,388	17,638	816	816
Service Module Adapter	(0)	(0)	(755)	(755)	(0)	(0)
Multimission Module	(6,092)	(6,092)	(5,188)	(5,273)	(4,091)	(4,146)
Structure	1,863	1,863	2,500	2,500	1,833	1,833
Subsystems	118	118	118	118	118	118
Propulsion	4,111	4,111	2,570	2,655	2,140	2,195
Cargo	(17,335)	(16,779)	(11,128)	(13,314)	(8,752)	(8,465)
Atmosphere	4,697	5,067	4,697	5,067	2,370	2,545
Dry Cargo	4,688	4,707	4,814	4,833	2,407	2,417
Propellant	7,950	7,005	1,617	3,414	3,975	3,503
Multimission Module Adapter	(745)	(745)	(1,115)	(1,115)	(745)	(745)
Contingency	(1,630)	(1,625)	(1,380)	(1,440)	(1,315)	(1,310)
Launch Weight	38,829	38,268	55,791	58,372	27,930	27,693
Capability	36,000	36,000	79,600	79,600	36,000	36,000
Excess	-2,829	-2,268	+23,809	+21,228	+8,070	+8,307

Figure 3.3-7: LOGISTICS VEHICLE WEIGHT SUMMARY

<u>Item</u>	<u>Low Orbit</u>	<u>Synchronous Orbit</u>
Service Module (Includes Subsystems)	1624	8,450
Service Module Adapter	0	755
Multimission Module Outer Cylinder	866	1,485
Multimission Module Pressurized Section	817	817
Multimission Module Second Docking Port	0	57
Multimission Module Meteoroid Shielding	180	198
Multimission Module Adapter	<u>745</u>	<u>1,115</u>
Total	4432	12,877

Figure 3.3-8: LOGISTICS VEHICLE STRUCTURE WEIGHT

	<u>Low Orbit</u>		<u>Synchronous Orbit</u>	
	<u>Gimbal</u>	<u>Detached</u>	<u>Gimbal</u>	<u>Detached</u>
Service Module Propellant	(816)	(816)	(17,388)	(17,638)
CM Deorbit	816	816	13,168	13,168
MMM Deorbit	0	0	4,220	4,470
MMM Propulsion	(4,111)	(4,111)	(2,570)	(2,655)
Ascent and Rendezvous	2,090	2,090	1,750	1,815
Deorbit	840	840	0	0
Propulsion Inerts	1,181	1,181	820	840
Cargo Propellant	(7,950)	(7,005)	(1,617)	(3,414)
MORL	3,170	3,170	900	900
MORL Caused by MOT	3,335	463	332	0
MOT	350	967	5	604
Shuttle	0	1,440	0	1,440
Tanks and Lines	<u>1,095</u>	<u>965</u>	<u>225</u>	<u>470</u>
Total	12,877	11,932	21,575	23,707

Figure 3.3-9: LOGISTICS VEHICLE PROPELLANT AND STORAGE WEIGHT (180 Days)

- Ascent and rendezvous propellant is different because:
  - 1) In low orbit, all requirements are satisfied by the multimission module propulsion system, while the S-IVB stage provides the requirements up to and including orbit injection for synchronous orbit;
  - 2) The synchronous-orbit rendezvous and docking propellant weight is greater because the mass is greater.
- Propellant supplied to MORL in the form of cargo is much less for the synchronous orbit because of lesser disturbances (orbit keeping, gravity gradient, etc.).
- Cargo propellant required because of MOT is less for synchronous orbit for the same reason as the MORL requirements.
- Shuttle propellant is the same for both orbits.

Atmosphere and Storage — Atmosphere and storage weight, as shown in Figure 3.3-10, does not differ between orbits. A difference between modes, however, is shown since shuttle requirements must be added to the detached mode. The same number of trips into the MOT cabin and the same number of manhours have been assumed for both orbits. This assumption is based on the increased observation time for the synchronous orbit being accommodated by increasing the quantity of film and tape transferred on each trip.

Dry Cargo — Dry-cargo weight is shown in Figure 3.3-10. The only weight difference between orbits is an increase in film and tape for the greater observation time in synchronous orbit. Personal supplies, including food, did not vary. The difference in subsystems is very slight and, therefore, the difference in replacement spares is not discernible. It was assumed that 80 percent of the initial supply of spares would be replaced in a year's time. Figure 3.3-11 shows the logistics requirements for low-Earth orbit with a 90-day resupply cycle. All time-dependent items except film and tape are reduced by one-half from the 180-day weights. Film and tape is resupplied every 90 days regardless of the scheduled resupply time (Sections 3.5.2 and 4.3).

#### 3.4 FLIGHT PERFORMANCE ANALYSIS

The synchronous orbit selected for the MOT is circular and inclined 28.5 degrees to the Earth equatorial plane. The radius of this orbit from the center of the Earth is 22,767 nautical miles and the orbit period is 86,161.25 seconds — about 23 hours and 56 minutes. This orbit period results in the MOT tracing the same ground track on the Earth's surface every orbital period. The ground track is a figure eight symmetrical about the Earth's equator and is illustrated in Figure 3.4-1.

The geographic longitude of the MOT in synchronous orbit is nominally 20°W. This longitude is selected because it:

ATMOSPHERE AND STORAGE WEIGHT				
	Low Earth Orbit		Synchronous Orbit	
	Gimbal	Detached	Gimbal	Detached
		MORL-MOT		Shuttle-MOT
Oxygen for MORL	2315	0	2315	0
Oxygen for MOT	417	431	417	431
Nitrogen for MOT	330	0	330	0
Nitrogen for MOT	305	307	305	307
Oxygen Tanks	955	150	955	150
Nitrogen Tanks	255	125	255	125
Lines and Fittings	120	30	120	30
<b>TOTAL</b>	<b>4697</b>	<b>5067</b>	<b>4697</b>	<b>5067</b>

DRY CARGO				
Food, Personal Items, EC/LS Equipment, and Backpack Supplies	2680	0	2680	0
MORL Spares	1810	0	1810	0
MOT Spares	72	51	72	51
Film and Tape	126	126	252	252
<b>TOTAL</b>	<b>4688</b>	<b>4707</b>	<b>4614</b>	<b>4833</b>

Figure 3.3-10: LOGISTICS CARGO WEIGHT  
(180 Days)

STRUCTURE	(4,402)		
Service Module	1,824		
Multimission Module			
Outer Cylinder	866		
Pressurized Section	817		
Meteoroid Shielding	150		
Adapter	745		
	Gimbal	Detached	
PROPELLANT	(6,934)	(6,262)	
Service Module	816	816	
Multimission Module			
Ascent and Rendezvous	1,330	1,380	
Deorbit	90	90	
Propulsion Inerts	720	725	
MORL Cargo	1,585	1,585	
MORL Caused by MOT	1,668	232	
MOT	175	484	
Shuttle	0	720	
Tanks and Lines	550	230	
	Gimbal	Detached	
		MORL-MOT	Shuttle-MOT
ATMOSPHERE AND STORAGE	(2,370)	(2,545)	
Oxygen for MORL	1,158	1,158	0
Oxygen for MOT	209	75	216
Nitrogen for MORL	165	165	0
Nitrogen for MOT	153	47	154
Storage Tanks, Lines, and Fittings	685	575	155
DRY CARGO	(2,407)	(2,417)	
Food, Personal Items, etc.	1,340	1,340	0
MORL Spares	905	905	0
MOT Spares	36	20	26
Film and Tape	126	0	126
TOTAL	16,113	15,626	

Figure 3.3-11: 90-DAY-SUPPLY LOGISTICS — LOW EARTH ORBIT

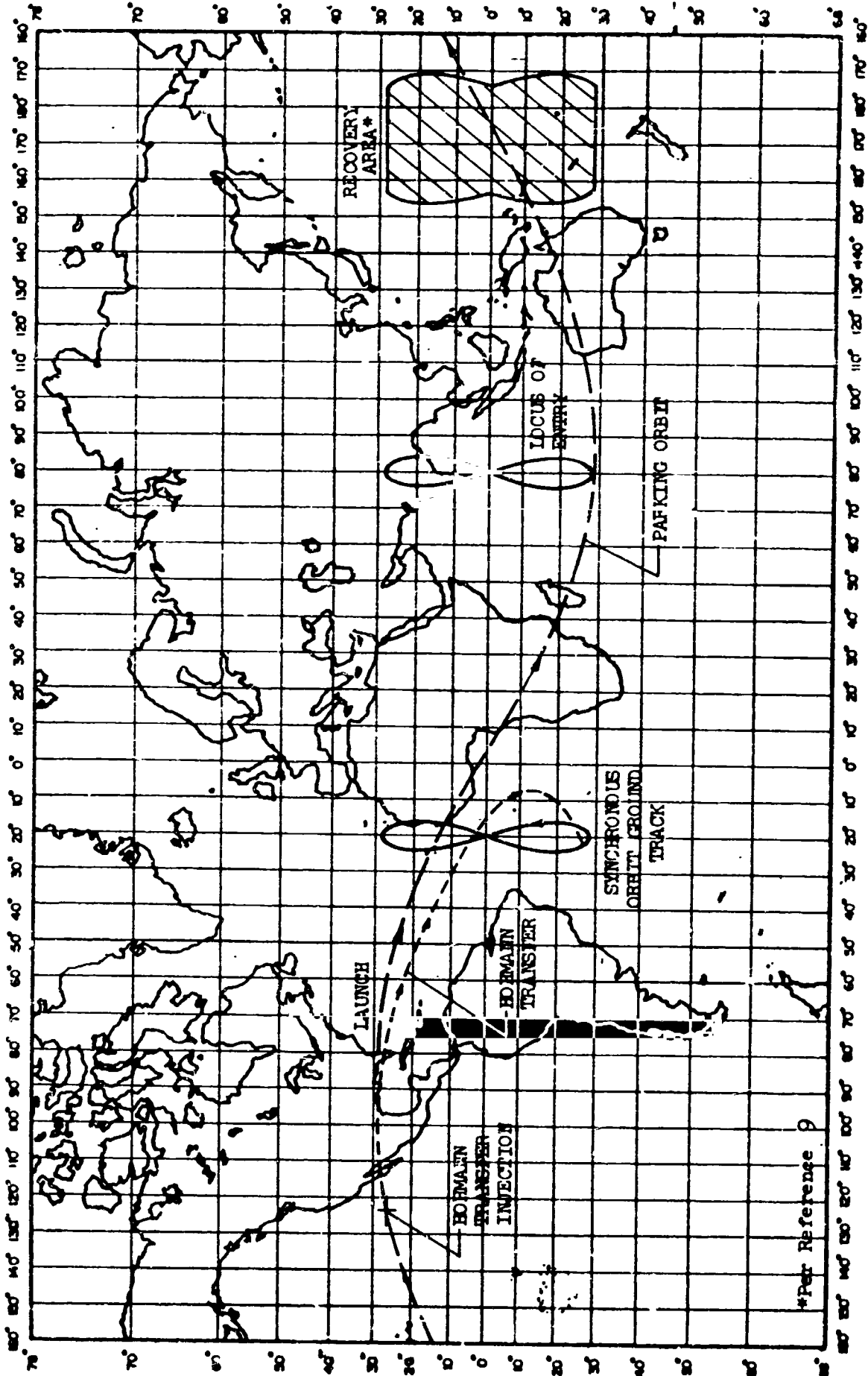


FIGURE 3.4-1 GROUND TRACKS

- 1) Locates the Apollo recovery zone over water, just east of Australia; see Figure 3.4-1 (per re-entry data from Douglas, Reference 9):
- 2) Is favorable for communication with several existing ground stations 100 percent of the time, e.g., Bermuda, Antigua, Ascension;
- 3) Results in good tracking coverage by the existing AMR tracking network during ascent operations by the various vehicles;
- 4) Is one of the four longitudes at which a synchronous orbit is stationary, albeit unstably so, with respect to perturbations due to the Earth's triaxiality (see Section 3.4.2).

The 28.5-degree orbit inclination is favorable for maximizing booster payload for vehicles launched from Kennedy Space Center. This inclination is also favorable for observation of our own galaxy. When the right ascension of the ascending node of the MOT orbit is 6 hours and 40 minutes, the MOT orbit plane is essentially normal to the plane of our galaxy, thereby minimizing the zone of the galactic plane that is occulted by Earth. Once every day an opportunity will exist for due-East launch (maximum payload) into this orbit plane.

The following paragraphs discuss trajectory profiles employed by the various vehicles to achieve the above MOT synchronous orbit. The synchronous orbit is further discussed from the aspect of orbit-keeping.

### 3.4.1 Launch and Rendezvous

3.4.1.1 MORL — The MORL ascent profile is shown in Figure 3.4-2 and consists of boosting into a 100-nautical-mile parking orbit of 28.5-degree inclination, remaining in the parking orbit for 77.5 minutes, and then transferring to the synchronous orbit via a Hohmann transfer. Boost to the parking orbit is achieved with the first two stages of the Saturn-V booster via an east launch out of Cape Kennedy. Boost time is 9 minutes.

The parking orbit is used to reach a position from which the synchronous orbit can be reached via a Hohmann transfer. This position is between Hawaii and the West Coast at 26.4°N latitude and 124°W longitude, see Figure 3.4-1. During the parking orbit coast time, the vehicle is tracked from the surface, the parking orbit is determined, the transfer trajectory is computed, the flight systems are updated, and transfer trajectory instructions are given to the vehicle. The S-IVB stage (third stage of Saturn V) is used to inject into the Hohmann transfer orbit. The nominal  $\Delta V$  required is 8080 fps. The injection maneuver takes 4.5 minutes and 134,000 pounds of propellant. The injection maneuver can be monitored by Guymas, Vandenberg, and/or Houston.

Time in the transfer orbit is 5.25 hours. During this time, the vehicle is tracked from ground stations of the ETR. Insertion into the synchronous orbit requires a nominal  $\Delta V$  of 4855 fps, which is provided by the S-IVB stage. This maneuver

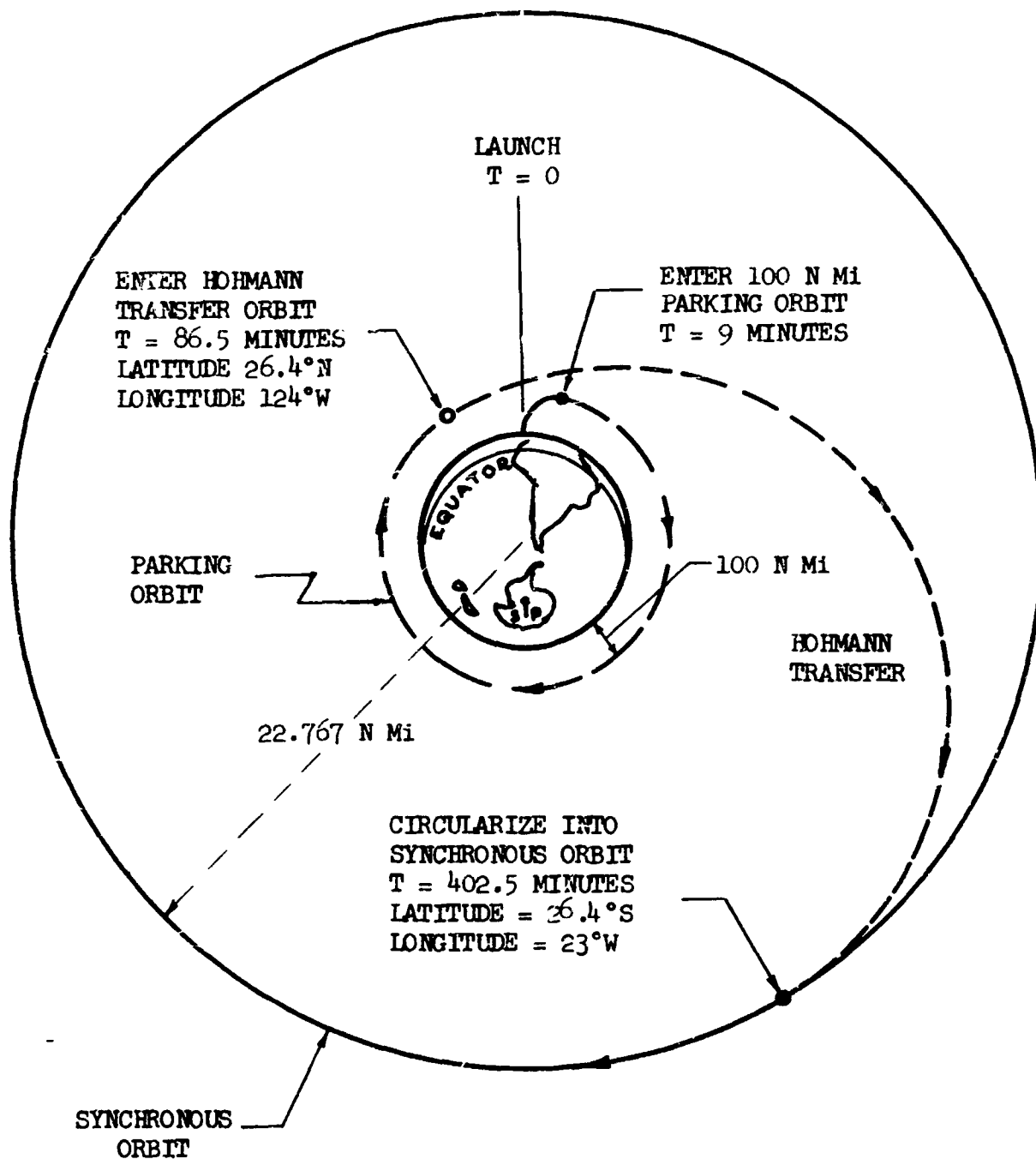


FIGURE 3.4-2: NOMINAL ASCENT PROFILE



takes 1.75 minutes and 50,000 pounds of propellant. Unless there is some use for the S-IV stage structure in the synchronous orbit, it is jettisoned and perturbed into a different orbit (to return the S-IVB stage to Earth requires 5000 fps and to escape the stage requires 4250 fps).

Salient features of the ascent profile are:

- 1) One restart on the S-IVB stage, which is its present design;
- 2) Minimal  $\Delta V$  requirements;
- 3) Good ground tracking and communication coverage throughout ascent;
- 4) Requires no booster modification.

3.4.1.2 MOT and Logistics Vehicle — The ascent profiles of the MOT and logistics vehicle are essentially the same as the MORL ascent profile described in the previous section. This similarity is possible because the target MORL is in a synchronous orbit and because any plane change, introduced with launch window, is deferred until terminal rendezvous. The terminal maneuver then consists of the plane-change maneuver and any remaining guidance and control errors. Figure 3.4-3 diagrams this ascent and rendezvous profile.

The terminal rendezvous maneuver is performed with multiple restart engines aboard the MOT and logistics vehicles at a  $\Delta V$  rate of 175 fps per degree of plane change. Two 1000-pound thrust engines aboard the MOT are sufficient to ensure the rendezvous operation even if one engine fails. The Douglas multimission module design includes a rendezvous propulsion system that uses four 150-pound-thrust engines. These engines should be replaced with larger engines — at least 300-pound thrust — because of the greater payload involved (80,000 versus 30,000 pounds).

Figure 3.4-4 shows launch window versus ideal (errorless) terminal maneuver  $\Delta V$ , i.e., the  $\Delta V$  required for launch window in excess of that required for error corrections. In Section 4.4.3.3, it is shown that a total  $\Delta V$  of 426 fps will correct  $3\sigma$  errors and provide a 2-hour (150 fps) launch window.

The weight of the MOT is about one-third of the payload capability of the Saturn V for a synchronous orbit. As a result, accelerations during the boost of an unbalanced MOT are slightly greater than during boost of the MORL or the logistics systems. At first- and second-stage burnout, where cutoff accelerations are about 5.5 and 3 g's, respectively, the changes in acceleration are insignificant because of the masses involved. At synchronous-orbit insertion, cutoff acceleration of the MOT is 3.25 g's as compared to 2.75 g's for a full payload, which still leaves the first-stage cutoff acceleration as the determining load factor due to thrust-to-weight effects. The only other deleterious effect that an increased cutoff acceleration could have is velocity error introduced through booster cutoff errors. Even if the cutoff error is as much as  $\pm 0.1$  second, the additional velocity error introduced by increasing the cutoff acceleration from 2.75 to 3.25 g's is

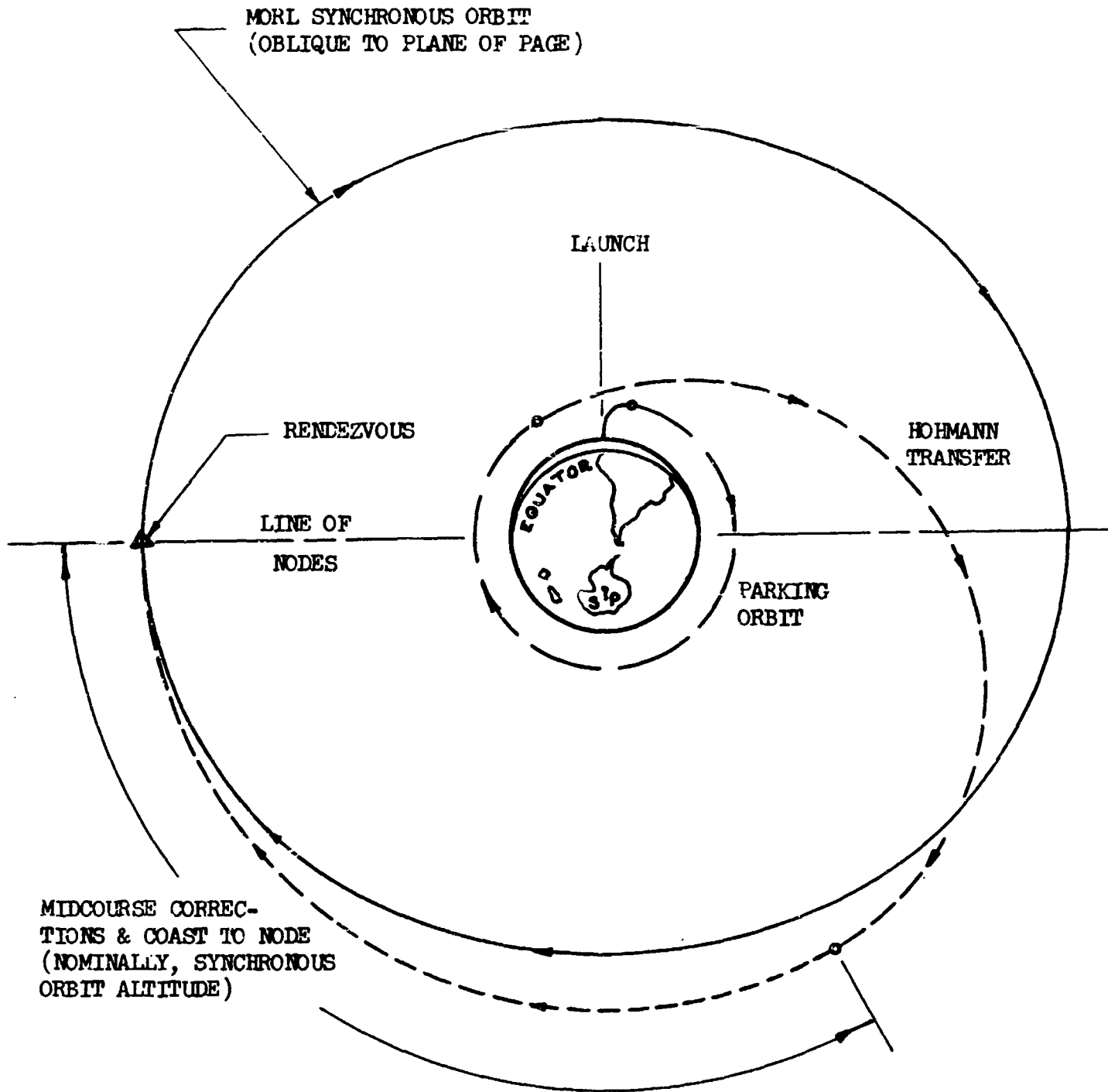


FIGURE 3.4-3: NOMINAL ASCENT & RENDEZVOUS TRAJECTORY PROFILE

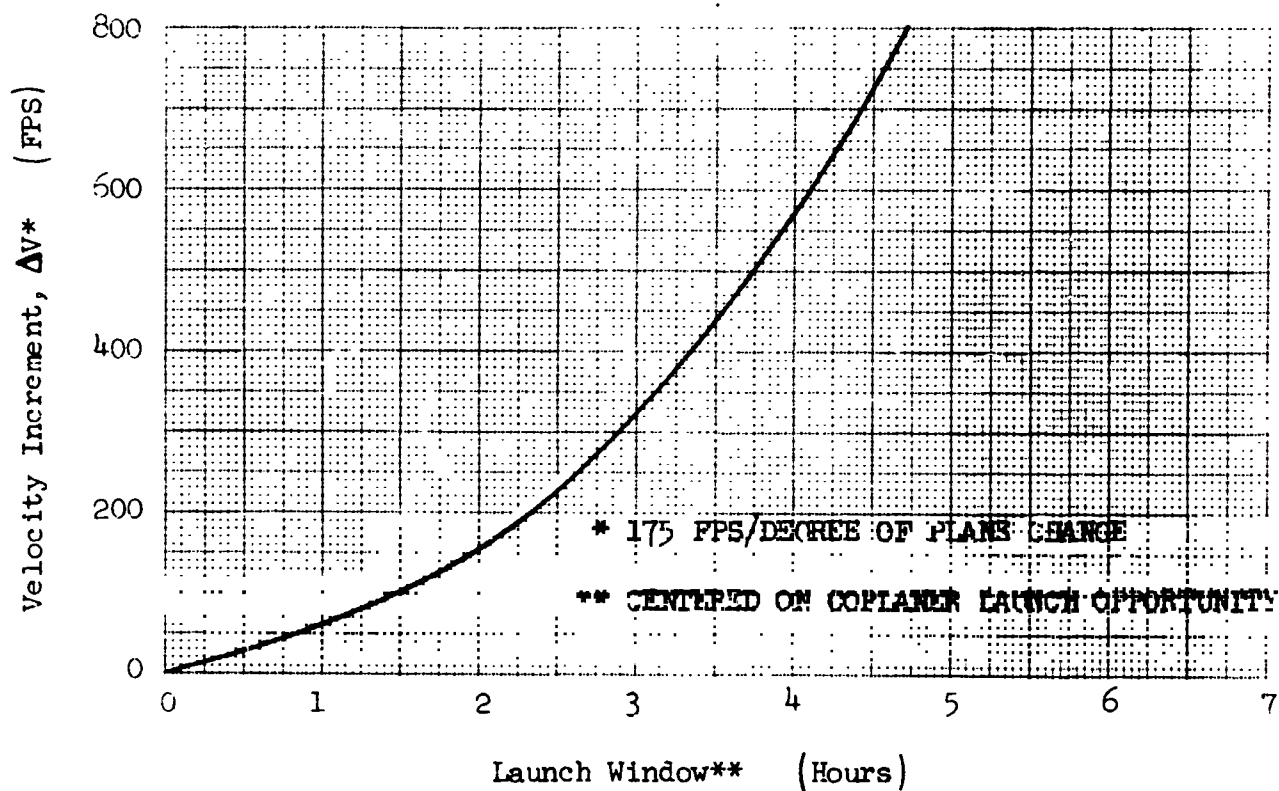


FIGURE 3.4-4: LAUNCH WINDOW  $\Delta V$  REQUIREMENTS

less than 2 fps. Therefore, no problems are anticipated for the light MOT payload and Saturn V combination.

By definition, a satellite in synchronous orbit retraces exactly its ground track once each sidereal day. Once each sidereal day a launch site at 28.5-degree latitude will lie in the plane of a 28.5-degree inclined orbit. The relative positions of the launch site and the synchronous satellite vary uniquely then with a period of one sidereal day. When a rendezvous vehicle is launched coplanar with the MORL orbit (possible only when the launch site lies in the orbit plane), the ascent and rendezvous trajectory is identical to the ascent trajectory of the MORL under errorless operations.

With a launch window it is necessary to launch out of the synchronous-orbit plane. The rendezvous vehicle is launched into a plane that intercepts the MORL orbit plane 90-degrees downrange from the launch site so as to minimize the plane change required for rendezvous. The ascent profile in this plane is similar to the MORL ascent profile complete with coplanar injection into a circular synchronous orbit. The rendezvous vehicle remains in its own circular synchronous orbit until it arrives at the intersection (node) of the two synchronous-orbit planes (MORL and the rendezvous vehicle orbit planes). By properly timing the Hohmann transfer of the rendezvous vehicle, it arrives at the node simultaneously with the MORL. The plane-change-plus-errors terminal maneuver is then performed to complete the rendezvous.

The rendezvous vehicle spends about 8 hours in its own synchronous orbit before rendezvous. During this time, the rendezvous vehicle is tracked and midcourse corrections are made with the multiple restart engine(s) aboard the rendezvous vehicle.

The small variation in timing the Hohmann ascent and the small differences in orbit plane are the only differences in the ascent profiles for the MORL, MOT, and logistics vehicles. For launch windows of several hours or less, the rendezvous vehicle must spend about 8 hours in its own circular synchronous orbit for a total time to rendezvous from launch of 14 to 15 hours.

Salient features of this method of rendezvous are:

- 1) The flight profile of the booster is essentially identical for all of the vehicles (MORL, MOT, and logistics vehicle);
- 2) The performance profile required of the booster complements the present booster definition;
- 3) The terminal rendezvous maneuver is performed by a propulsion system that can be selected specifically for the terminal rendezvous operation;
- 4) Except for error effects, the relative motion between the two rendezvousing vehicles is cyclic so that, if the terminal maneuver is interrupted or delayed, an opportunity for terminal maneuver completion occurs every 12 hours;

- 5) In addition to the propellant required for errors and contingency, the propellant requirements for the terminal maneuver are dependent only on the launch window requirements;
- 6) The closing velocities are low without jeopardizing acquisition.

Alternate candidate ascent and rendezvous trajectories are merely variations in when the plane-change maneuver is performed. For small plane changes ( $< 0.5$  degree), the plane change can be performed by turning during boost. This procedure rapidly becomes costly in terms of payload, however, as the plane change required increases.

A separate plane change in the parking orbit involves maneuvering almost four times as much mass as the proposed procedure and at a  $\Delta V$  rate of 435 fps per degree. Furthermore, such an operation would require two restarts on the S-IVB which entails payload penalties, perhaps several thousand pounds, or else a rendezvous  $\Delta V$  capability aboard the rendezvousing vehicle of about 5000 fps.

A third alternate consists of combining the plane-change maneuver with injection into synchronous orbit. This procedure requires about 20 hours waiting in the parking orbit in order for the MORL to get into favorable position. Wait time in parking orbit is undesirable because liquid hydrogen is lost from the S-IVB stage at a rate of about 600 pounds per hour. If the ascent can be performed over the southern Western Hemisphere (tracking and communication considerations), then the parking-orbit wait could be reduced to about 8 hours. The proposed procedure minimizes the liquid hydrogen boiloff losses by restricting the parking orbit to only about 1.25 hours. Should the synchronous orbit be located at about  $85^\circ W$ , then the parking orbit wait time would be near minimum for this third alternate; but this location of synchronous orbit would put the recovery zone over land masses (western Australia and the Phillipine Islands).

#### 3.4.2 Orbit-Keeping and Stationkeeping

The  $\Delta V$  required for orbit keeping by the MOT and MORL in synchronous orbit is less than 200 fps per year (per vehicle when detached). The  $\Delta V$  required for station-keeping by the MOT and MORL is negligible from the aspect of external disturbances.

A synchronous orbit will change slowly with time as a result of perturbations due to:

- 1) Anomalies in the Earth's gravitational field;
- 2) Gravity forces of the Sun and Moon;
- 3) Solar radiation forces.

The rectification of these perturbations by orbital maneuvers is defined as orbit-keeping. Orbit-keeping of synchronous orbits is performed as necessary to

maintain the same geographic ground track. Stationkeeping is the operation concerned with maintaining the distance between two satellites within specified limits. With perfect control systems, stationkeeping is necessary only if there is a difference in the above perturbative forces on the two satellites. The following brief discussion identifies the effects of the above perturbations and their significance in terms of correction  $\Delta V$ .

3.4.2.1 Perturbations Due to Earth Gravitational Anomalies — The Earth's oblateness and the ellipticity of the Earth's equator are the major sources of synchronous-orbit perturbation due to the Earth's gravitational field. The Earth's oblateness causes the synchronous-orbit plane to rotate westerly about the Earth polar axis at a constant secular rate so that the ground track of the synchronous orbit moves steadily westward geographically. This geographic displacement is readily negated by making the satellite orbit period slightly less than the sidereal period. Except for sensing and control errors, no further orbit adjustment is required to stabilize the ground track with respect to nodal regression (perturbation due to oblateness).

The ellipticity of the Earth's equator also causes the ground track of a synchronous orbit to move longitudinally. But in this case, the movement occurs at a varying rate, either east or west, depending on the longitudinal location of the satellite. This longitudinal movement is the result of the orbital period changing rather than the orbit plane rotating. There are four longitudinal locations where the orbit is stationary, however. Two of the points are stable and two are unstable. The stable points correspond roughly to the minor axis of the equatorial ellipse, and the unstable points are near the major axis.

Analysis of SYNCOM-II data locates one stable stationary point (minor axis) at  $107.3 \pm 2.5^\circ W$  and an unstable stationary point at  $19 \pm 6^\circ W$ .

The ground tracks of satellites established in synchronous orbit at longitudes other than the stable points oscillate longitudinally and symmetrically about the nearest stable point. Under the most unfavorable longitudinal location (45 degrees from the stable point), the  $\Delta V$  required to rectify this perturbation is less than 7 fps per year. The correction maneuver consists of a minute  $\Delta V$  (depending on the longitude drift tolerance) applied tangentially to alter the orbit period in the opposite sense of the perturbation. With the MOT orbit located at the unstable stationary point at  $20^\circ W$ , the  $\Delta V$  required for orbit-keeping is negligible.

3.4.2.2 Perturbations Due to Sun and Moon Gravity Forces — The Sun and Moon resultant gravity force component in the plane of the MORL-MOT synchronous orbit will perturb the orbit insignificantly, i.e., the ground track will oscillate longitudinally only about 0.1 degree. The out-of-plane Sun-Moon gravity component will cause the MORL-MOT orbit plane to regress slowly about an axis that is nearly normal to the ecliptic plane. This perturbation affects the ground track initially as a steady change in the inclination. For an equatorial synchronous orbit, the change in inclination is 0.86 degree per year. For a 28.5-degree

inclined synchronous orbit oriented normal to the galactic plane, a rate of 1 degree per year is assumed to be representative. Rectification of this perturbation is merely a plane-change maneuver performed at an equatorial crossing. The  $\Delta V$  required per year is 175 fps.

3.4.2.3 Perturbation Due to Solar Radiation — The effect of solar radiation on a geocentric orbit is a sinusoidal variation in orbit eccentricity. The period of this variation is 1 year, and the amplitude is directly proportional to the ratio  $A/M$ , where  $A$  is the area of the satellite facing the Sun and  $M$  is the mass of the satellite (because  $A$  will vary somewhat throughout the year, the cycle will not repeat exactly). The values of  $A/M$  for the MOT and MORL are such that solar perturbations are negligible, however. For example, if the MOT is always pointed 90 degrees to the Sun line (worst case) the maximum orbit eccentricity reached from an initially circular orbit is 0.0003. The maximum eccentricity reached by the MORL is about 0.00015. These variations in eccentricity have a negligible effect on the orbit ground track.

3.4.2.4 Stationkeeping — Solar radiation is the only source of orbit perturbation likely to affect the MOT and MORL vehicles sufficiently to require stationkeeping. Using the above variations in orbit eccentricities, the maximum separation between these two vehicles is about 3.4 nautical miles due to the annual variations in eccentricity. To keep the vehicles within 1 nautical mile of each other would require a  $\Delta V$  of 0.25 fps applied no oftener than about 30 days with the possibility of some intervals between corrections being as much as 180 days.

A  $\Delta V$  budget of 200 fps per year per vehicle will cover all orbit-keeping requirements in synchronous orbit. Stationkeeping requirements due to external perturbations will be negligible for the MOT and MORL vehicles.

### 3.4.3 Re-entry

The entry trajectory from synchronous orbit is defined by Douglas in Reference 9. The deorbit  $\Delta V$  is about 5000 fps, the re-entry angle is -7.5 degrees, and the time to entry is about 5 hours. Figure 3.4-1 shows the re-entry zone and recovery zones lifted directly from Reference 9.

The deorbit  $\Delta V$  is supplied by the service module. The  $\Delta V$  capacity of the service module is also sufficient to deorbit a spent logistics vehicle. On attainment of the initial deorbit  $\Delta V$  (5000 fps) sufficient to ensure entry of the logistics vehicle, the CSM separates and perturbs into a slightly different orbit to avoid interference. An additional  $\Delta V$  of 200 fps is budgeted for midcourse corrections by the CSM to ensure achievement of the Apollo entry corridor.

### 3.4.4 Shuttle From Low Earth Orbit

A study of the propulsion requirements for resupply of a MOT in synchronous orbit from a MORL in a low Earth orbit has been conducted. This mode of resupply imposes severe propulsion system requirements due to:

- 1) Potentially large plane change requirements (up to 57 degrees);
- 2) Injection of the supply vehicle into the low-Earth-orbit altitude ( $\Delta V = 7800$  fps for coplanar orbits) on return from the MOT in synchronous orbit.

This mode of resupply is, therefore, not recommended as these propulsion requirements would cause a large payload penalty.

The  $\Delta V$  required to transfer from a 250-nautical-mile circular orbit to a coplanar synchronous orbit is 12,600 fps. The  $\Delta V$  required to return to a coplanar 250-nautical-mile orbit from the synchronous orbit is also 12,600 fps, but the  $\Delta V$  required to return to Earth from synchronous orbit is only 5200 fps. This large difference in  $\Delta V$  between returning to low Earth orbit and returning to the Earth's surface is the  $\Delta V$  required to slow the vehicle to orbital velocity following descent from synchronous-orbit altitude. When returning to Earth, slowdown is achieved by aerodynamic braking (drag) rather than by propulsion.

Because of the Earth's oblateness, the orbit plane of a 250-nautical-mile orbit inclined 28.5 degrees to the equator regresses about the Earth polar axis at a rate of 6.835 degrees per day. A synchronous-orbit plane inclined 28.5 degrees to the equator also regresses but at a rate of less than 5 degrees per year. As a consequence, the low MORL orbit and the synchronous orbit will not be coplanar most of the time. The angle between these planes will cycle from zero to a maximum of 57 degrees and then back to zero in 52.67 days. For routine scheduled resupply operations, this should present no serious problem. But unscheduled resupply or maintenance would be seriously curtailed since the  $\Delta V$  required either to go up to the synchronous orbit or to return to the low Earth orbit varies throughout this period as shown in Figure 3.4-5, reaching a maximum  $\Delta V$  of 16,270 for one way. For example, if an ascent is made 15 days after the coplanar opportunity, the ascent  $\Delta V$  is 15,060. If return to the MORL is then made 5 days later, the  $\Delta V$  to return is 15,860 fps.

Logistically, there is no advantage, but considerable disadvantage, to supporting a MOT in synchronous orbit from a MORL in low Earth orbit. This mode of operation should be considered only if there is an overwhelming reason for not putting a MORL into synchronous orbit.

### 3.5 OPERATIONAL ANALYSIS

The basic telescope configuration for both the synchronous orbit and the low Earth orbit is generally the same. Therefore, the operational analysis pertaining to the orbital functions necessary to accomplish the rendezvous, docking, deployment, initial telescope setup, checkout, and alignment is identical to those described in Section 4.3.1 of Reference 1. The launch vehicle and configuration for injecting the MOT to synchronous orbit, of course, are different and are described in Section 3.1.2 of this document.



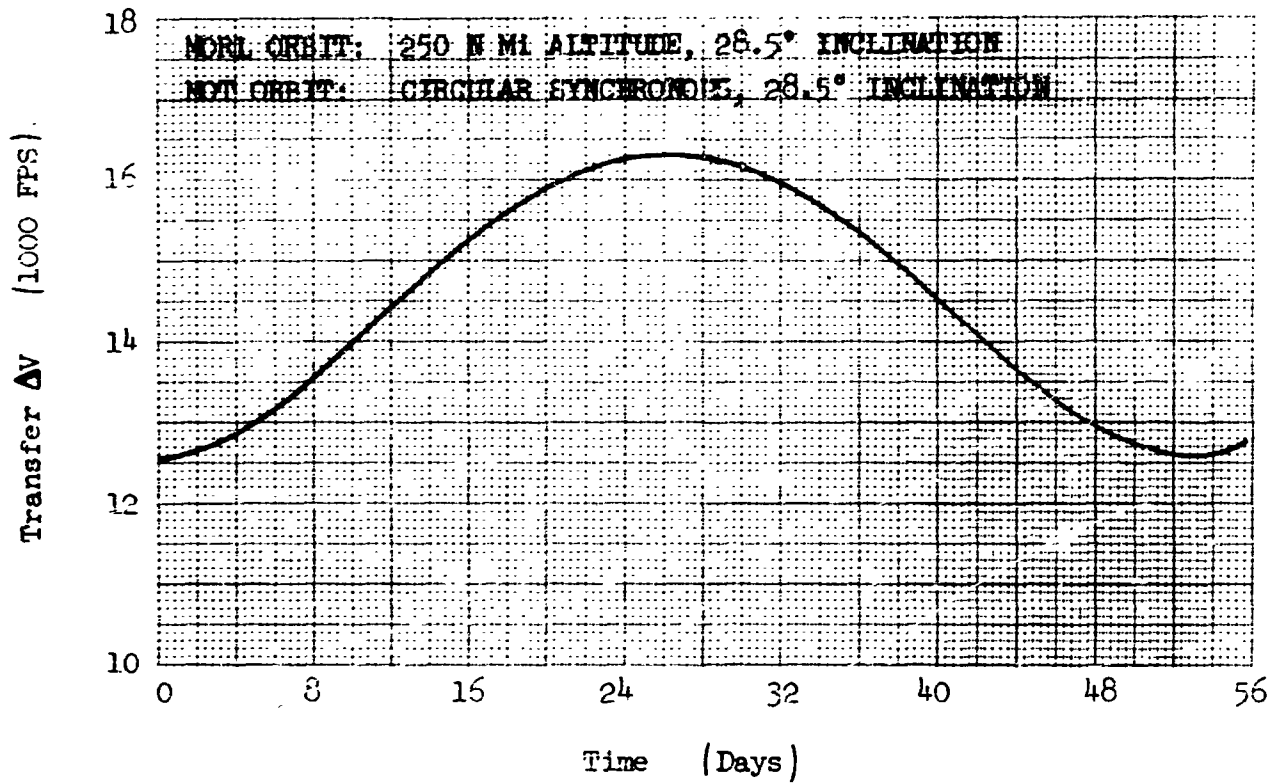


FIGURE 3.4-5:  $\Delta V$  REQUIRED TO TRANSFER BETWEEN MOT AND MORL ORBITS

Maintenance remains an important function in the operation of the MOT. For the synchronous orbit, the same criteria for periodic inspection and maintenance requirements were established as for the low-Earth-orbit case. Although the potential observation time is greatly increased (resulting in longer telescope operation), the optical equipment is largely passive with minimum maintenance effect. Subsystem component operation times are well within the limits of mean time between failures. Those replacement components, such as reaction-control nozzles, are covered within the percentage of scheduled and unscheduled maintenance times allocated for the low-Earth-orbit study.

The operation of the MOT in either soft-gimbal or detached mode is much the same as described in Section 4.3, Reference 1. For the current study, the shuttle travel time between the MORL and MOT was assumed to be time sequenced in parallel with the concluding experiment or observation. The time function allocation for the docking and pressurization sequence of either mode is the same. Therefore, from the MOT normal-operation standpoint, there is relatively little difference between the soft-gimbal and detached modes of operation.

### 3.5.1 Observational Limitations

One primary objective of this study is to determine maximum use of the MOT in a synchronous orbit. Use of the telescope in terms of available or potential observation time is a prime basis for this evaluation. To establish maximum observation time, a study of the orbital mechanics was conducted to determine what occurs during a year's operation and the capabilities for uninterrupted observation, considering constraints imposed by occultations by the Sun, Earth, or Moon. The following discussion identifies the limits of occultation and coverage of the celestial sphere to determine the available observation time per orbit.

The basic assumptions or ground rules used to accomplish this analysis are:

- 1) The orbit is synchronous with an altitude of 19,330 nautical miles at an inclination of 28.5 degrees to the equator.
- 2) The MOT will not be pointed any closer to the solar vector than 90 degrees.
- 3) Astronomical observations will be interrupted when the edge of the Earth's atmosphere or of the Moon comes within the telescope field of view. The Earth is effectively occulting when the outer edge of the Earth's atmosphere enters the acceptance cone of the fine guidance sensor. In this particular problem, it is assumed the fine guidance sensor is offset to the program star. The field of view of the fine guidance sensor is then added to the field of view determined by its offset to determine the MOT field of view.

To permit the Earth (or its atmosphere) to come within the admission cone of the fine guidance sensor would produce a pointing component away from the program star toward the Earth — thus ruining scientific observation.

A similar guidance problem is encountered when the guidance star has relatively bright neighboring stars. The neighboring stars will bias the guidance signal by their stray light impinging on the sensor. The dimmer the guidance star, the smaller the admission angle to maintain a high probability of successful guidance. Spitzer (Reference 61) states that if observations are to be made on stars fainter than 5th magnitude, or on close double stars, a smaller guidance admission angle than 30 arc-minutes is required. It appears conservative then to let the offset guidance sensor have an admission angle of 30 arc-minutes, or a 1-degree field of view.

The offset guidance is assumed to operate over an angular offset of 0.5 degree with respect to the optical axis. This 0.5-degree offset plus the 0.5-degree guidance admission cone makes up the field angle of 1 degree or a total field of 2 degrees.

The effective Earth occultation angle, thus, includes the angular subtend of the Earth, plus the atmosphere, plus the MOT field of view.

To avoid the effects of Aurora Polaris and the thermosphere, the height of the atmosphere is assumed to be 500 nautical miles.

3.5.1.1 Occultation by Earth — Figure 3.5-1 illustrates the effective occultation angle of the Earth as the MOT observes a stellar source. At Position A, the observation is interrupted until Position B is reached; then observation is continued.

For computational purposes, let

$\alpha$  = angle (degrees) through which the MOT travels during the effective occultation

$\theta$  = angle (degrees) subtended by the radius of the Earth plus the thickness of the atmosphere

$\beta$  = the field angle (degrees), which is 1 degree or one-half the field of view

then

$$\alpha = 2(\theta + \beta)$$

where  $\theta$  may be determined by

$$\sin \theta = \frac{R_E + t_A}{A_{MOT} + R_E}$$

where

$R_E$  = radius of the Earth = 3442 nautical miles

$t_A$  = thickness of the atmosphere = 500 nautical miles

$A_{MOT}$  = altitude of MOT = 19,330 nautical miles

Using these values,  $\theta = 9^\circ 58'$  or  $\approx 10$  degrees; therefore,  $\alpha = 22$  degrees.

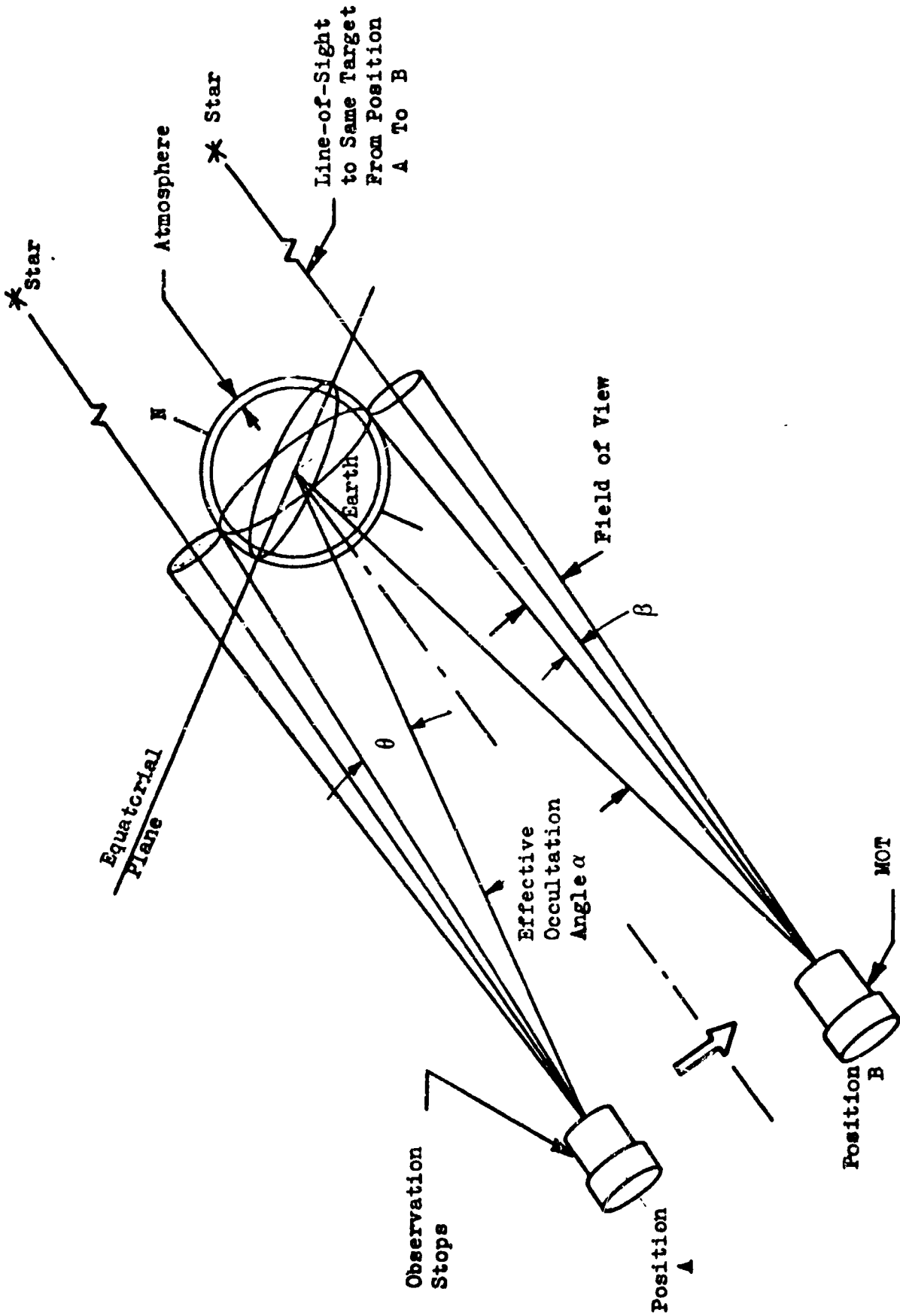


FIGURE 3.5-1: OCCULTATION DUE TO EARTH

The telescope can then view to within 11 degrees of the center of the Earth without interference. Except for minute perturbations due to the Moon, Sun, and the asymmetry of the Earth's gravitational field, the orbit plane of a circular synchronous orbit is fixed in solar space. These minute perturbations are readily cancelled with propulsive maneuvers throughout the MOT mission so that the MOT orbit plane is indeed inertially fixed. This fixed orbit plane then projects onto the celestial sphere as a fixed great circle.

Any point on the celestial sphere within 11 degrees on either side of the MOT orbit plane great circle is subject to occultation or light interference from the Earth once each MOT orbit period (1436 minutes). The duration of occultation or light interference varies from zero at these 11-degree limits to almost 88 minutes for an object in the plane of the MOT orbit. This 22-degree spherical segment in which occultation occurs amounts to 19.1 percent of the total area of the celestial sphere.

A significant factor when considering occultation by the Earth is the time of launch. Figure 3.5-2 illustrates the effect of selecting the launch time 12 hours apart. The MOT in Orbit A is launched in late afternoon where its inclination to the ecliptic plane is 52 degrees. However, a launch 12 hours earlier (or later) would produce an orbital Plane B that is 5 degrees off the ecliptic plane. For planetary observations, Orbit B would not be a choice orbit because of Earth occultation. Orbit A is favored as it would be relatively free of occultation by the Earth except for periods of the equinoxes. On the other hand, for observation of objects or stars within our galaxy, positioning of the 28.5-degree-inclined MOT orbital plane normal to the galactic plane is preferred. This is quite feasible as the galaxy plane is inclined 65 degrees to the equator. This could be accomplished by choosing a launch time somewhere between the 12-hour periods for Orbits A and B. Because of the limited number of planets as compared to the number of stars in the galaxy, the MOT launch time should be approximately 6 hours after the one selected to produce Orbit A.

3.5.1.2 Occultation by the Sun — No direct interference by the Sun is anticipated if the object is 90 degrees or more from the Earth-Sun line. Then, any stellar object can be observed continuously for approximately 6 months per year without direct solar interference. The eccentricity of the Earth's orbit about the Sun prevents the observation interval from being exactly one-half year for all objects.

3.5.1.3 Occultation by the Moon — The part of the celestial sphere that is subject to occultation by the Moon is concentrated near the great circle of the lunar orbit plane. It is estimated that an object can be no closer than 1.25 degrees to the center of the Moon for satisfactory observation by the MOT. Then, if the MOT- and Moon-orbit planes are coplanar, any object within 1.25 degrees of the lunar-MOT plane is subject to occultation. The period of occultation for an object within this 2.5-degree zone varies from 0 to 7.7 hours due to the Moon plus 1.5 hours due to the Earth. Figure 3.5-3 illustrates the geometry and phasing that results in maximum occultation by the Moon when the object being observed is in

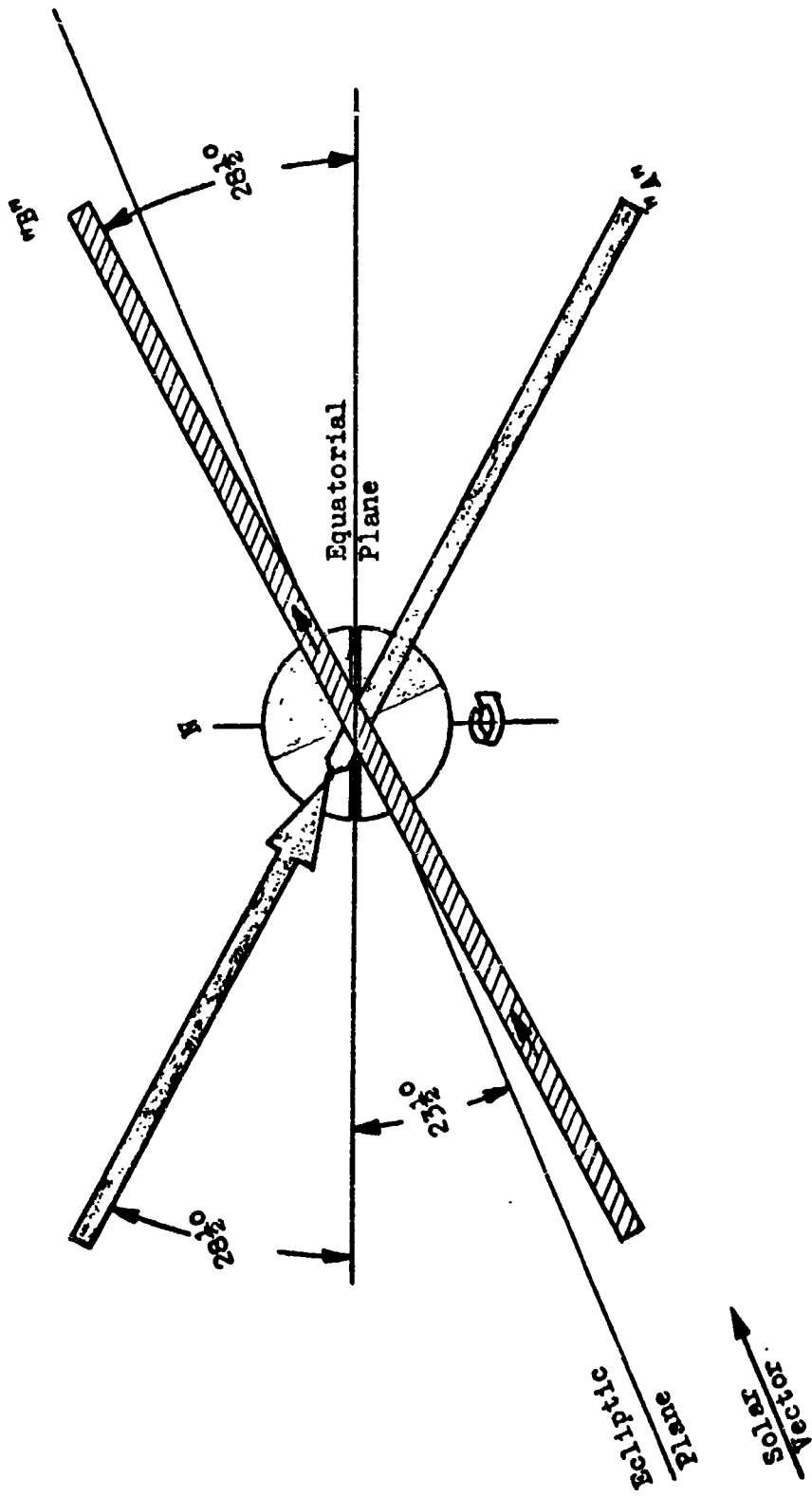


FIGURE 3.5.2 INCLINATION OF MOP ORBIT TO ECLIPTIC PLANE

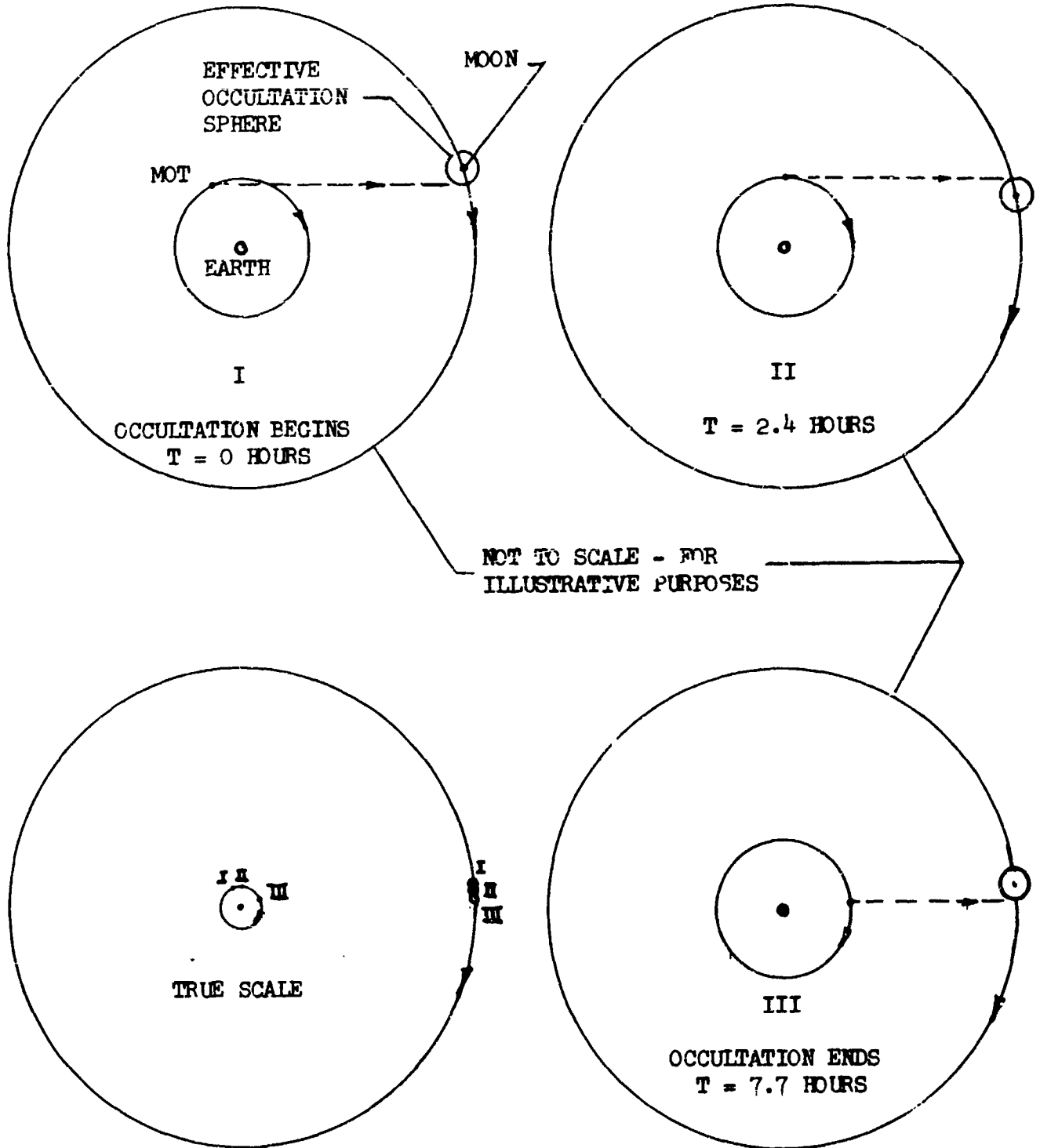


FIGURE 3.5-3 PHASING FOR MAXIMUM OCCULTATION BY MOON

the plane of the MOT and lunar orbits. Occultation of a specific point by the Earth occurs once each MOT-orbit period. Occultation by the Moon occurs once and frequently twice in 24 hours about every 27 days. In reality, the lunar-orbit plane is not fixed in inertial space but rotates about the pole of the ecliptic plane to complete one rotation in 18.6 years. Then the MOT- and lunar-orbit planes are coplanar only momentarily.

Figure 3.5-4 illustrates the effect on occultation of the MOT-orbit plane being inclined to the lunar-orbit plane. It can be visualized that points further and further from the lunar-orbit plane are occulted as the inclination between these orbit planes increases. The locus of occulted points is not a solid segment of the celestial sphere as when the orbits are coplanar, but is a prolate cycloid as shown in Figure 3.5-5. A loop of this trace is completed each sidereal day. When the Moon is in the vicinity of the line of nodes of the MOT- and lunar-orbit planes, the loops are narrow. The loops are fullest when the Moon is 90 degrees from a node. The time required to girdle the celestial sphere is one sidereal lunar month so that 27.4 loops girdle the celestial sphere. The significance of this illustration is that during one sidereal month most of the celestial sphere is free of occultation, even in the vicinity of the lunar-orbit plane. The rotation of the lunar-orbit plane and the synodic period of the MOT and Moon system preclude frequent repetition of an occultation trace.

With the MOT in a 28.5-degree inclined orbit plane, the maximum angle that can exist between the lunar-orbit plane and the MOT-orbit plane is 57.1 degrees. At this limit, points within 6 to 7 degrees on either side of the lunar-orbit plane may be occulted by the Moon, and the maximum occultation interval is 5.5 hours.

The net result is that occultation by the Moon of a specific point may amount to as much as 5 to 8 hours but, in the general case, recurrence is infrequent.

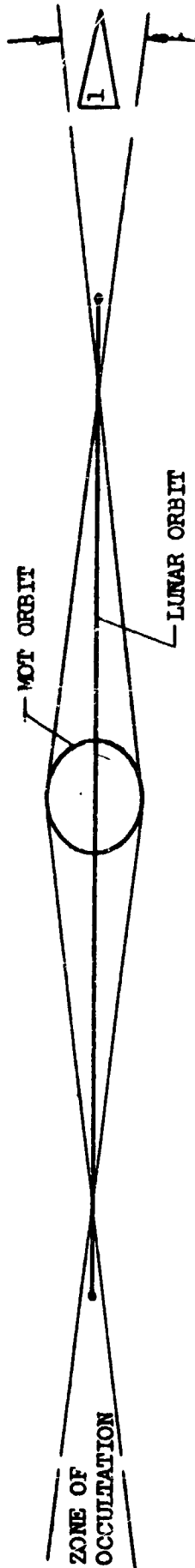
**3.5.1.4 Available Observation Time** — From a synchronous orbit, 80 percent of the celestial sphere can be observed continuously for 6 months of the year free of occultation or interference by the Earth or Sun. The remainder of the celestial sphere (that which is within 11 degrees on each side of the MOT-orbit plane) can be observed for 22.4 hours out of every 23.9 hours for 6 months of the year. Occultation by the Moon can be as long as 5 to 8 hours but in the general case occurs infrequently. With proper target selection, the telescope can be pointed so as to be unaffected by occultation by the Moon or Earth during any one orbit. This situation results in the capability for continuous observation for 24 hours (1436 minutes) per orbit. Therefore, for this study, 24 hours per orbit are assumed available for stellar, galactic, and intergalactic observations and 22.4 hours per orbit for planetary observations.

### 3.5.2 Functional and Timeline Analysis

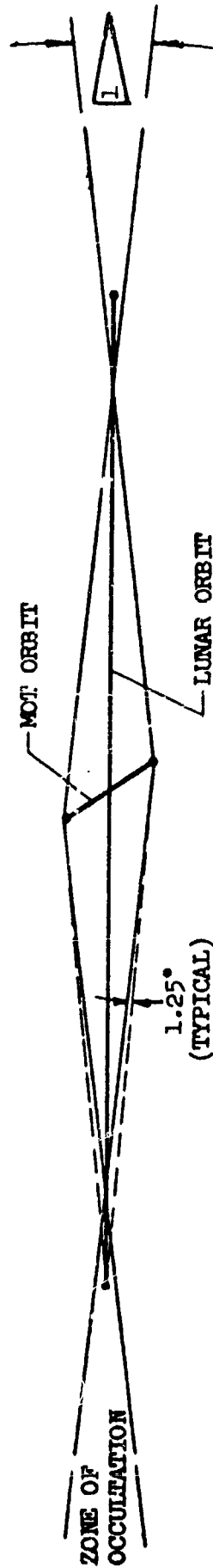
Based on the available or potential observation time from synchronous orbit, a timeline evaluation similar to that accomplished for the low Earth orbit was conducted. A 1-year astronomical program was planned (Figure 3.5-6) to evaluate



When angle between lunar orbit plane and MOT orbit is maximum ( $57.1^\circ$ ), the zone of occultation is about  $13^\circ$  (varies somewhat due to eccentricity of Moon's orbit)

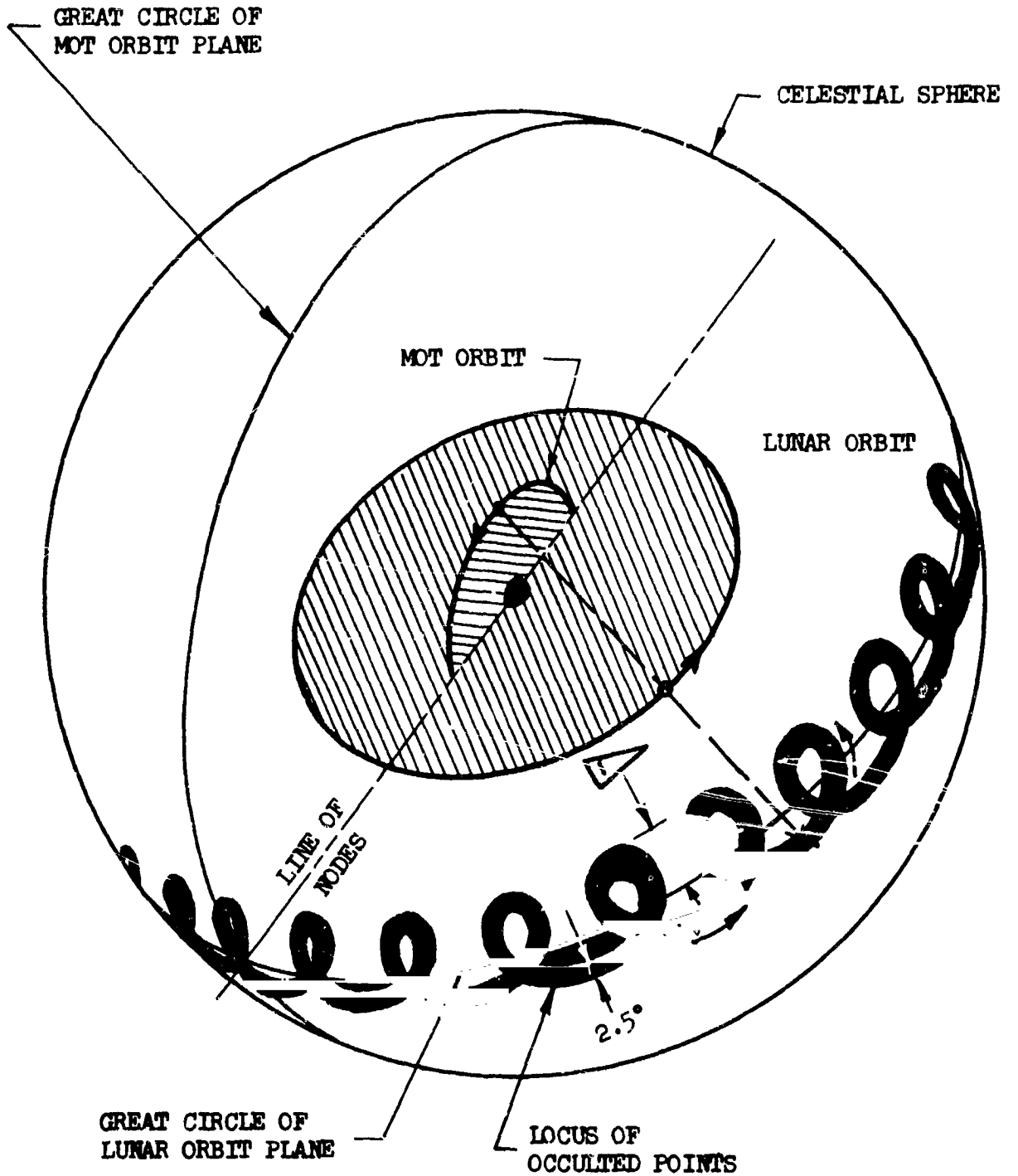


VIEW NORMAL TO LINE OF NODES  
IN PLANE OF LUNAR ORBIT



VIEW ALONG LINE OF NODES

FIGURE 3.5-4 ZONE SUBJECT TO OCCULTATION BY THE MOON



▷ 6.25° - 6.85° WHEN ORBIT PLANES ARE INCLINED 57.1° TO EACH OTHER

FIGURE 3.5-5 OCCULTATION BY THE MOON

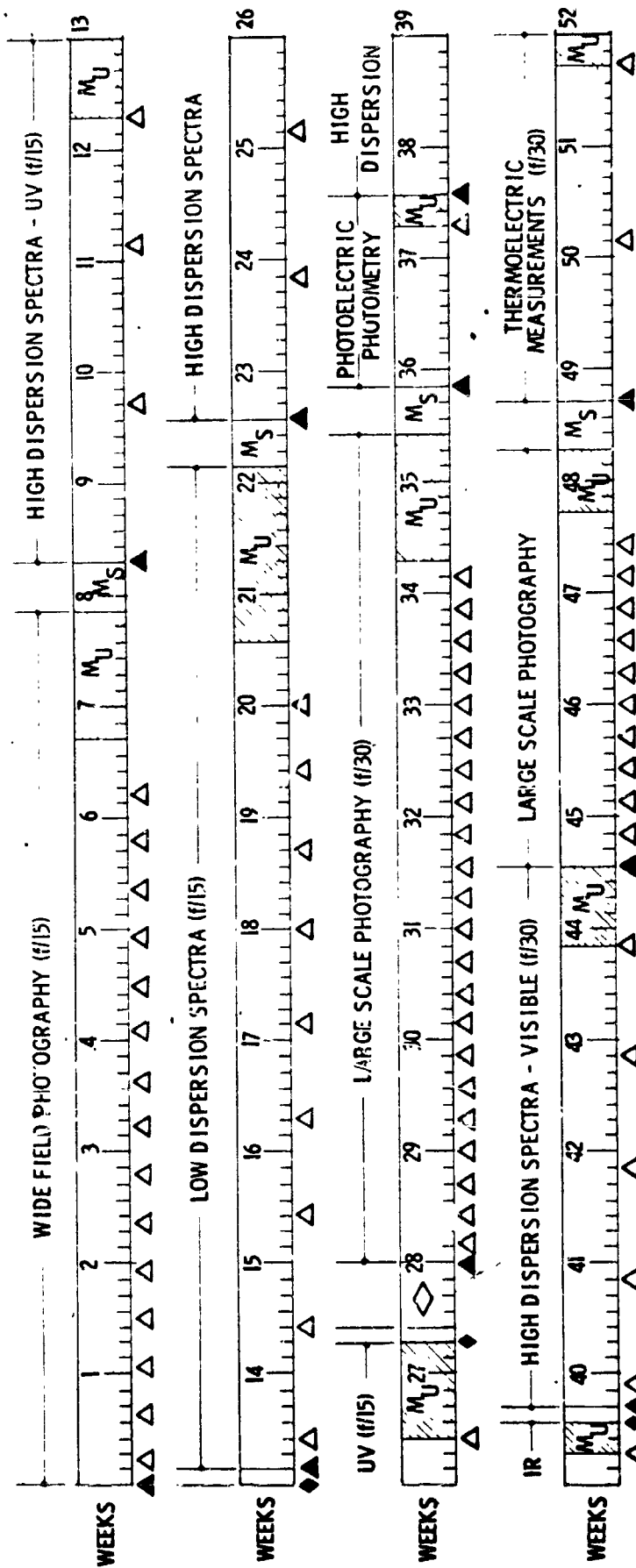


FIGURE 3.5-6 MOT ONE-YEAR ASTRONOMICAL PROGRAM

a typical order for conducting experiments, maintenance, changing of the secondary mirror, trips between MORL and MOT, and crew-rotation or logistics cycles. The time allocated to each experiment is representative of a typical program and associated supporting requirements, but flexible to accommodate varying observation priorities.

Early in the study, the effects of radiation on the sensitive photographic film were examined and determined to have a significant impact on the program. The radiation environment in synchronous orbit, as discussed in Section 4.3, is a limiting factor on both the storage and usage of the film. The film is stored in the MORL biowell to take advantage of increased shielding. Additional shielding around the film storage container is also required. The shielding requirements are based on a 60-day storage time selected as a limit because approximately 53 percent of the time is allocated to experiments that use photographic film. If the film is used immediately following each resupply, the maximum time of exposure to radiation in the space environment is approximately 60 days in each 90-day period. Therefore, the 1-year program schedules photographic observations after each resupply of film (by either a crew-rotation launch or a logistics launch, one of which occurs approximately every 90 days). It is assumed that the film will be developed immediately after being exposed. This immediate processing is desirable to eliminate the film's sensitivity to radiation with resultant loss in image quality.

Magnetic tape used for spectrometry and photoelectric scanning is not affected by radiation, so time in orbit is not restrictive. Therefore, observations using recording tapes are scheduled towards the end of each 90-day period.

Additionally, the program is arranged to allow conducting all f/15 observations before changing the secondary mirrors for f/30 observations. The frequency of trips required between the MORL and MOT, crew-rotation sequence, and the consideration for maintenance are shown in Figure 3.5-6. The same allocations for times to accomplish the various tasks were used as for the low-Earth-orbit study in Section 4.0 of Reference 1.

Large-scale photography of planets was omitted from the prior study, but it is an important consideration in the astronomical program and can result in a significant requirement on the photographic expendables. Of the 18 percent of the time allocated to large-scale photography, 3 percent has been assigned for planetary observations. For astrometric photography of stellar targets, 2- x 2-inch film formats are considered; but, for planetary observations where time-lapse photography may be desired, a cine camera of the 70-millimeter roll type would be added.

Exposure times for planetary observations are relatively short, generally from 1 to 5 seconds. Thus, it is possible to obtain an enormous quantity of photographs within the time allocated for planetary observations. For this study, planetary observations will be conducted intermittently during the two periods scheduled for

large-scale photography in the typical program. For example, approximately 200 exposures per day would be made of the planet Mars at approximately 16 exposures every 2 hours. If each exposure takes 5 seconds, then the time expended is only 1.3 minutes every 2 hours or 13 minutes per day. The next most important planet from the standpoint of obtaining photographic data may well be Jupiter. It is anticipated that approximately 20 intermittent exposures of Jupiter would be taken per day. For Saturn, the exposure time is estimated to be 15 seconds for approximately five photographs per day. Other planets could require an average of 10 seconds of exposure time, five times a day.

Because continuous observation of the planets will not be conducted, frequent re-orientation and stabilization of the MOT to other planets or stellar targets become necessary. The MOT maneuver rate is 4 degrees per minute with an additional 1 minute required to complete target acquisition. Therefore, frequent realignment of the telescope will consume more time than actual observation time. For this study, the time required to reorient and stabilize the MOT for large-scale photography of the planets is included in the 3-percent allocation for this scientific observation.

The summary chart, Figure 3.5-7, indicates the available observation time and number of possible targets for each experiment after deducting the time required for trips and maintenance.

	EFF. f NO.	PERCENT OF TIME	NO. OF DAYS	NUMBER OF TRIPS		AVAILABLE OBSERVATION TIME*	EXPOSURE TIME PER TARGET (AVG)	NUMBER OF EXPOSURES PER TARGET	APPROX. NO. OF TARGETS
				EQUIPMENT SETUP & CHECKOUT	REPLACE FILM				
WIDE FIELD PHOTOGRAPHY	15	13	47	1	15	1075 HRS	2.25 HRS	3	477
LOW DISPERSION SPECTRA	15	14	52	1	9	1213 HRS	17.25 HRS	4	70
SPECTROMETER & SPECTROGRAPH	15	15	55	2	6	1287 HRS	3.75 HRS	1	343
HIGH DISPERSION SPECTRA - UV	15	3	11	1	1	253 HRS	7.5 HRS	1	34
PHOTOELECTRIC PHOTOMETRY	30	15 3 18	66	2	32	1230 HRS 221 HRS	0.75 HRS **	2-4 **	16x0 ---
LARGE SCALE PHOTOGRAPHY									
HIGH DISPERSION SPECTRA VISIBLE	30	8	29	1	5	673 HRS	13.5 HRS	3	50
HIGH DISPERSION SPECTRA - IR	30	3	11	1	1	235 HRS	0.75 HRS	1	313
THERMOELECTRIC MEASUREMENTS	30	4	21	1	2	470 HRS	7.5 HRS	1	63
		80	292	10	71	5657 HRS			
CREW ROTATION (RENEZVOUS, DOCKING, ETC.)		1	3						
Maintenance & Repair Requirements									
SCHEDULED		3	12						
SCIENTIFIC EQUIPMENT		1	4						
CHANGE SECONDARY MIRROR		15	54	15***					
UNCHEDULED		19	70						

- \* POTENTIAL OBSERVATION TIME/ORBIT:  
STELLAR - 24 HOURS  
PLANETARY - 22.4 HOURS
- \*\* EXPOSURE TIME FOR PLANETARY TARGET IS RELATIVELY SHORT, BUT THE NUMBER OF EXPOSURES PER PLANET, SUCH AS P.A. MARS, ARE IN THE ORDER OF THOUSANDS (TIME LAPPED)
- \*\*\* ESTIMATED NUMBER OF TRIPS REQUIRED TO ACCOMPLISH UNSCHEDULED MAINTENANCE

FIGURE 3.5-7 ONE-YEAR ASTRONOMICAL PROGRAM SUMMARY - SYNCHRONOUS ORBIT

NOTES:

- 1 ORBIT - APPROXIMATELY 24 HRS (1436 MINUTES)
- TRIPS TO REPLACE FILM, SLIDES, OR TAPE - 3 HRS
- TRIPS TO SETUP & CHECKOUT EQUIPMENT - 7.5 HRS
- ROUTINE MAINTENANCE

## 4.0 OPERATIONAL AND DESIGN COMPARISONS

## 4.1 THERMAL DISTORTION CONTROL

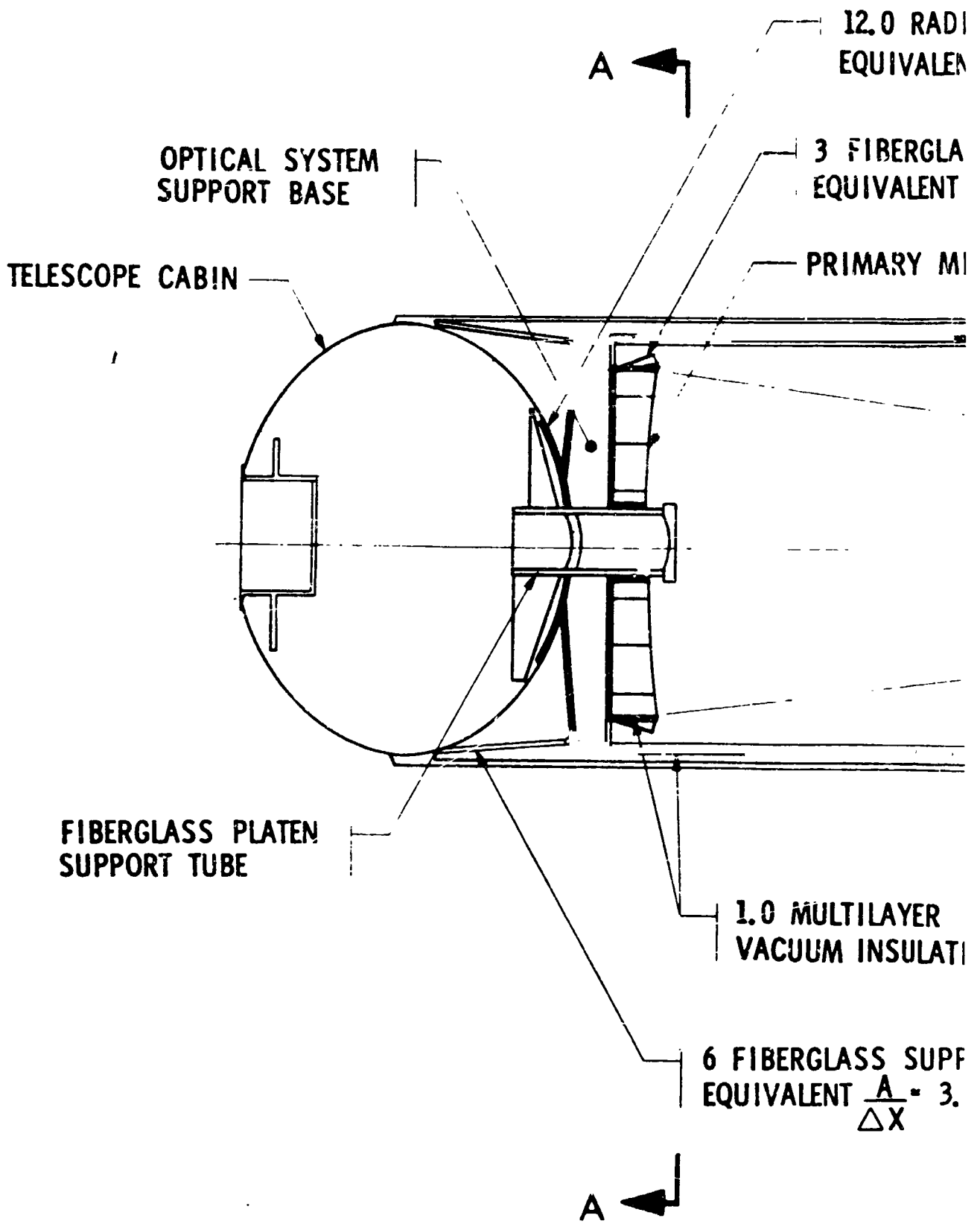
## 4.1.1 Thermal Balance Analysis

Temperature variations in the supporting structure and in the optical elements of the telescope can readily introduce unacceptable distortions in the optical system. A thermal analysis was therefore conducted to determine temperature distributions on the MOT structure and optics. The telescope is assumed launched at summer solstice into a circular synchronous orbit at an inclination of 28.7 degrees so that the Sun vector is incidental to the MOT plane at 5.2 degrees. Variations in thermal environment result from occultation of the telescope by the Earth and from solar-reflected radiation and Earth-emitted radiation entering the optics. Comparisons with temperatures and temperature distributions for low-Earth-orbit (250-nautical-mile) operation (reported in Reference 1) are presented in the following text.

The telescope configuration used in the thermal analysis is shown in Figure 4.1-1 and is identical to that used for the low-altitude thermal studies of Reference 1. This configuration is representative of the final telescope configuration, even though not identical to it. The calculated temperatures and temperature distribution represent either configuration. The mathematical thermal models used in the low-Earth-orbit study were modified to incorporate the thermal environment experienced at synchronous-orbit altitude.

The telescope shell and back of the primary mirror were assumed to be insulated with a 1-inch layer of multilayer vacuum insulation having a nominal conductivity of  $7.0 \times 10^{-5}$  Btu/hr-ft-°R. The primary mirror is supported from the telescope structure with low-conduction fiberglass supports. Further assumptions are:

- 1) Material properties assumed for the thermal analyses are given in Figure 4.1-2;
- 2) Cabin temperature was assumed to be 530°R;
- 3) Telescope attitudes and orbit definition are shown in Figure 4.1-3;
- 4) The solar constant was assumed to be 443 Btu/hr-ft<sup>2</sup>;
- 5) Outer surface coating properties were  $\alpha_{\text{solar}} = 0.2$  and  $\epsilon_{\text{IR}} = 0.9$  (white paint);
- 6) Interior surface coating properties were  $\rho^{\text{diffuse}} = 0.1$  and  $\epsilon_{\text{IR}} = 0.9$  (flat black paint);
- 7) Assumed Earth temperatures were taken from TIROS data;
- 8) The primary mirror is a waffle structure (same construction of the earlier analysis).



95/96  
 1

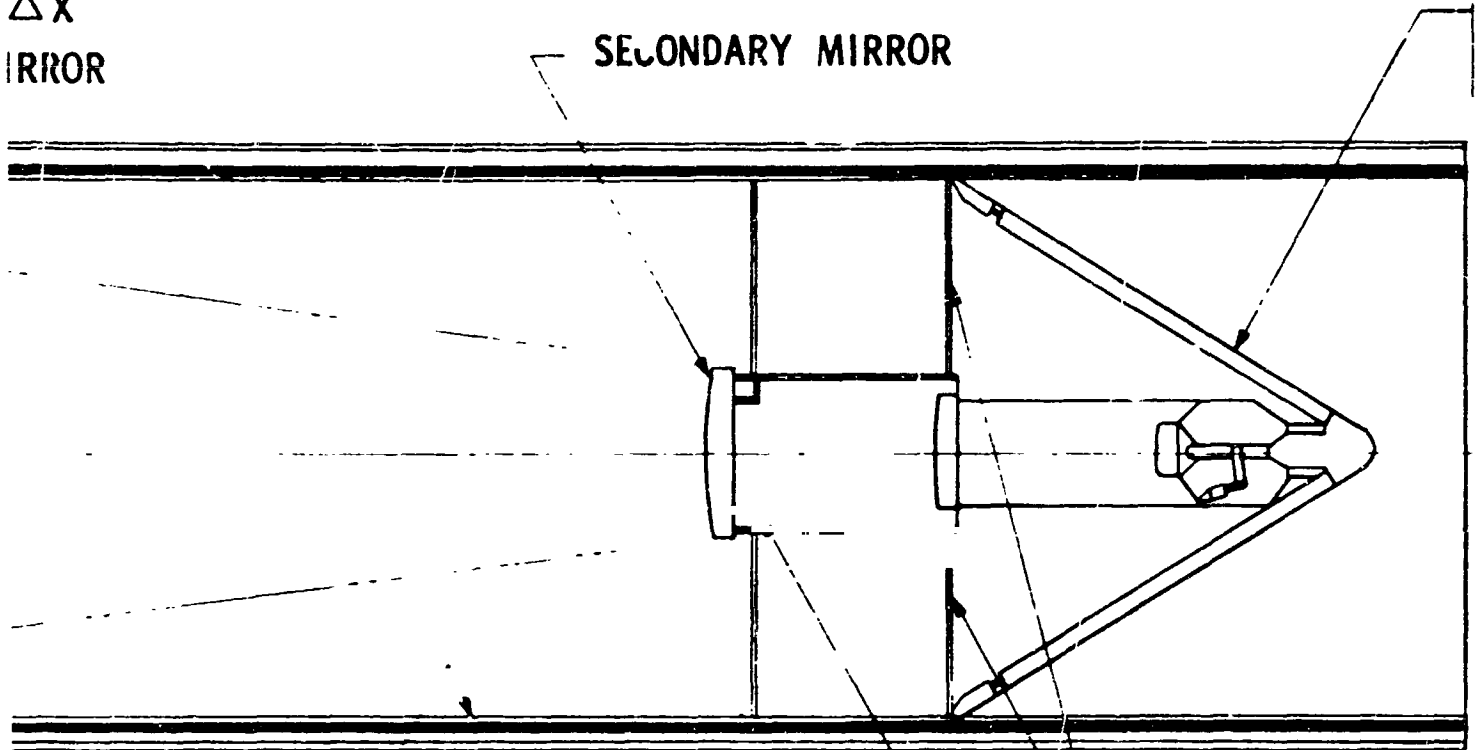


FIBERGLASS COLLAR  
IT  $\frac{A}{\Delta X} = 4.91 \times 10^{-2}$  EACH

SS MIRROR SUPPORTS  
 $\frac{A}{\Delta X} = 4.78 \times 10^{-3}$  EACH

MIRROR

SECONDARY MIRROR



0.50 ALUMINUM HONEYCOMB  
0.010 FACE SHEETS  
4.0 PCF CORE

6 TITANIUM FLE  
EQUIVALENT  $\frac{A}{\Delta X}$

ION

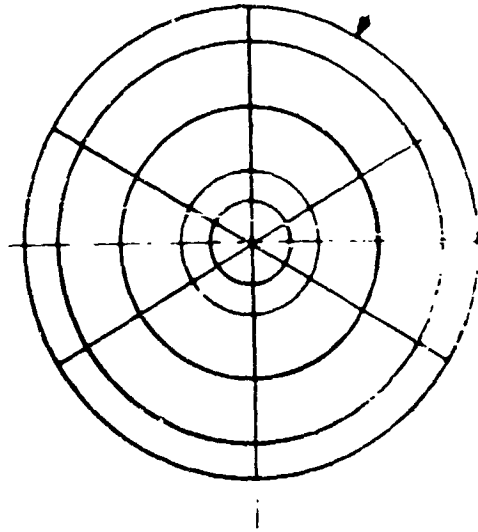
PORT TUBES  
 $05 \times 10^{-3}$  EACH

3 FIBERGLASS M  
EQUIVALENT  $\frac{A}{\Delta X}$

95/96 (2)

3 TITANIUM SUPPORTS  
EQUIVALENT  $\frac{A}{\Delta X} = 2.71 \times 10^{-4}$  EACH

PRIMARY MIRROR



SEC. A-A

STRAPS  
 $2.32 \times 10^{-5}$  EACH

MIRROR SUPPORTS  
 $4.78 \times 10^{-3}$  EACH

FIGURE 4.1-1

**BASELINE CONFIGURATION  
USED IN THERMAL ANALYSIS**

95 & 96



**BLANK PAGE**

<u>Structural Member</u>	<u>Material</u>	<u>Density</u> lb./ft. <sup>3</sup>	<u>Specific Heat *</u> Btu/lb. m <sup>-2</sup> R	<u>Thermal Conductivity*</u> Btu/hr. ft. -°R	<u>Radiative Properties</u>
Telescope Shell	Aluminum 2219-T62	176.	0.204	74.4	Outer $\alpha_s/\epsilon$ IR = 0.2/0.9 Inner $\alpha_s/\epsilon$ IR = 0.9/0.9
Primary Mirror	Beryllium	115.	0.40	96.4	$\rho = 0.96^{**}$ $\epsilon = 0.04$
Secondary Mirror	Fused Silica	137.	0.145	1.02	$\rho = 0.96^{**}$ $\epsilon = 0.04$
Thermal Insulation	Multilayer Aluminum Foil-Dexiglass	12.	0.20	$7.42 \times 10^{-5}$	
Primary Mirror Support	Resin Impregnated Fiberglass	114.	0.30	0.0064	
Secondary Mirror Support	Titanium 6Al4V	276.	0.128	3.62	

\* Nominal value at 460°R

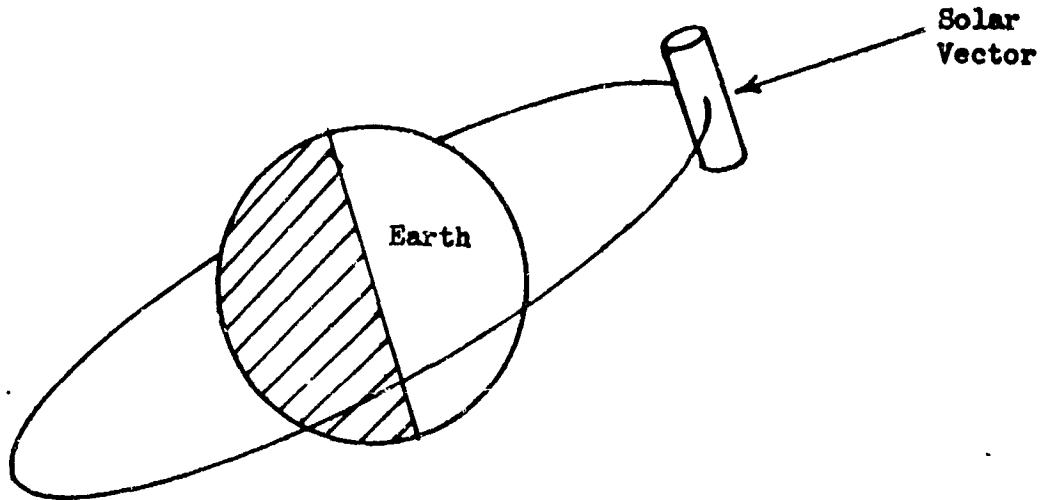
\*\* For the mirror surfaces the assumption was made that  $\rho_s = \rho_{IR}$  and  $\alpha_s = \alpha_{IR}$

Figure 4.1-2: MATERIALS PROPERTIES USED IN THERMAL ANALYSIS

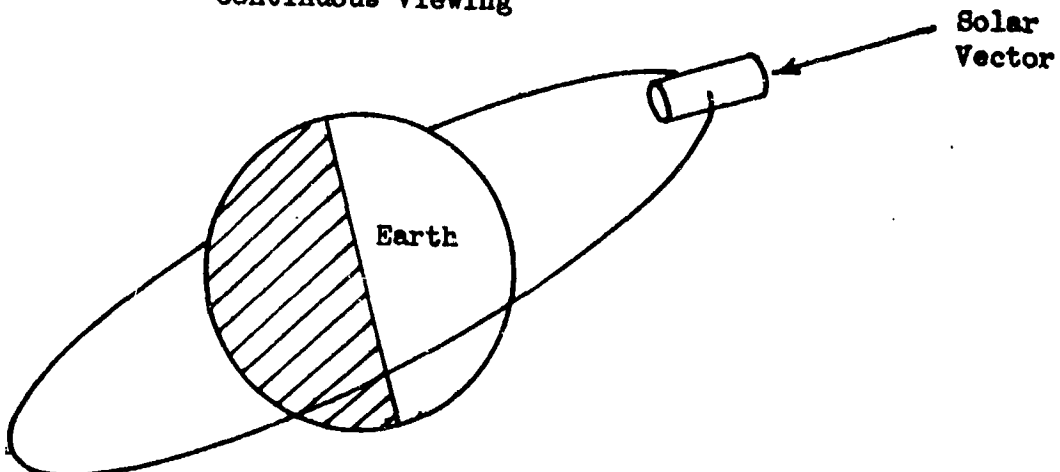
19,330 N M CIRCULAR ORBIT

ORBITAL INCLINATION:  $28.7^\circ$

ANGLE BETWEEN MOT ORBIT PLANE  
AND SUN VECTOR:  $28.7^\circ - 23.5^\circ = 5.2^\circ$



Telescope Axis Perpendicular to  
Solar Vector  
Continuous Viewing



Telescope Axis Parallel to Solar Vector  
Alternate Viewing

MOT THERMAL ANALYSIS ORBIT DEFINITION

FIGURE 4.1-3

Telescope orbit and orientation were selected to obtain maximum variation in its thermal environment at synchronous-orbit altitude. The inclination of the orbit at 28.7 degrees allows the telescope to be occulted by the Earth, creating variations in the thermal environment. The orientation of the telescope parallel to the solar vector allows Earth-reflected solar radiation and Earth-emitted infrared radiation to enter the optics, creating additional variations in the environment. The orientation of the telescope perpendicular to the solar vector eliminates Earth effects; the only variation in thermal environment occurs during occultation.

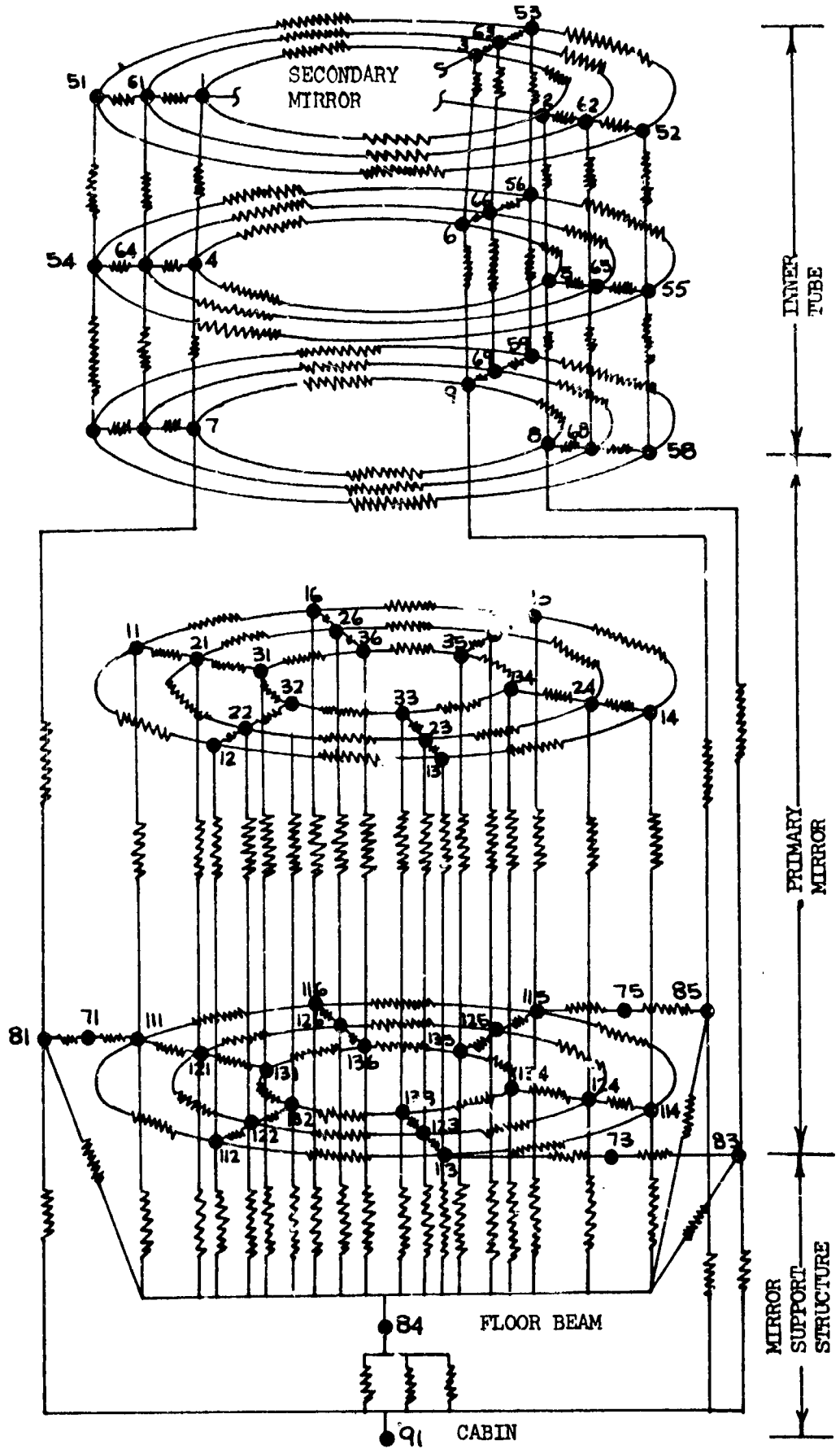
4.1.1.1 Analysis Technique — The thermal balance to the telescope is a function of the incident solar radiation, Earth-emitted infrared radiation, Earth-reflected solar radiation, radiation from the telescope structure to space, internal radiation within the telescope structure, and heat conducted through the telescope structure.

Heating of the telescope due to incident solar, Earth-reflected, and Earth-emitted radiation as functions of orbital position is calculated using the planetary environment computer program. To aid in controlling the thermal environment of the telescope mirrors, direct solar radiation is not allowed to fall on the inner surfaces of the telescope tube. Temperature variations in the telescope structure and in the primary and secondary mirrors are calculated by the Boeing engineering thermal analyzer (BETA) program. Internal reflections resulting from the presence of mirror surfaces and the blocking effect of the secondary mirror structure are considered. The variation in thermal conductivity with temperature of all materials is considered as well as the variation with temperature of the specific heat of beryllium.

The mathematical thermal model of the manned orbital telescope is complex because of the stringent tolerances to which the primary mirror temperature distribution must be restricted to eliminate distortion. A fine nodal mesh was considered necessary to accurately simulate incident radiation from the Earth and Sun, as well as radiation between nodal areas of the telescope structure with other structure and space. Figures 4.1-4 and 4.1-5 show the nodal network and structural thermal conduction paths employed in the analysis. The network is identical to the one used in the low-Earth-orbit analysis of Reference 1.

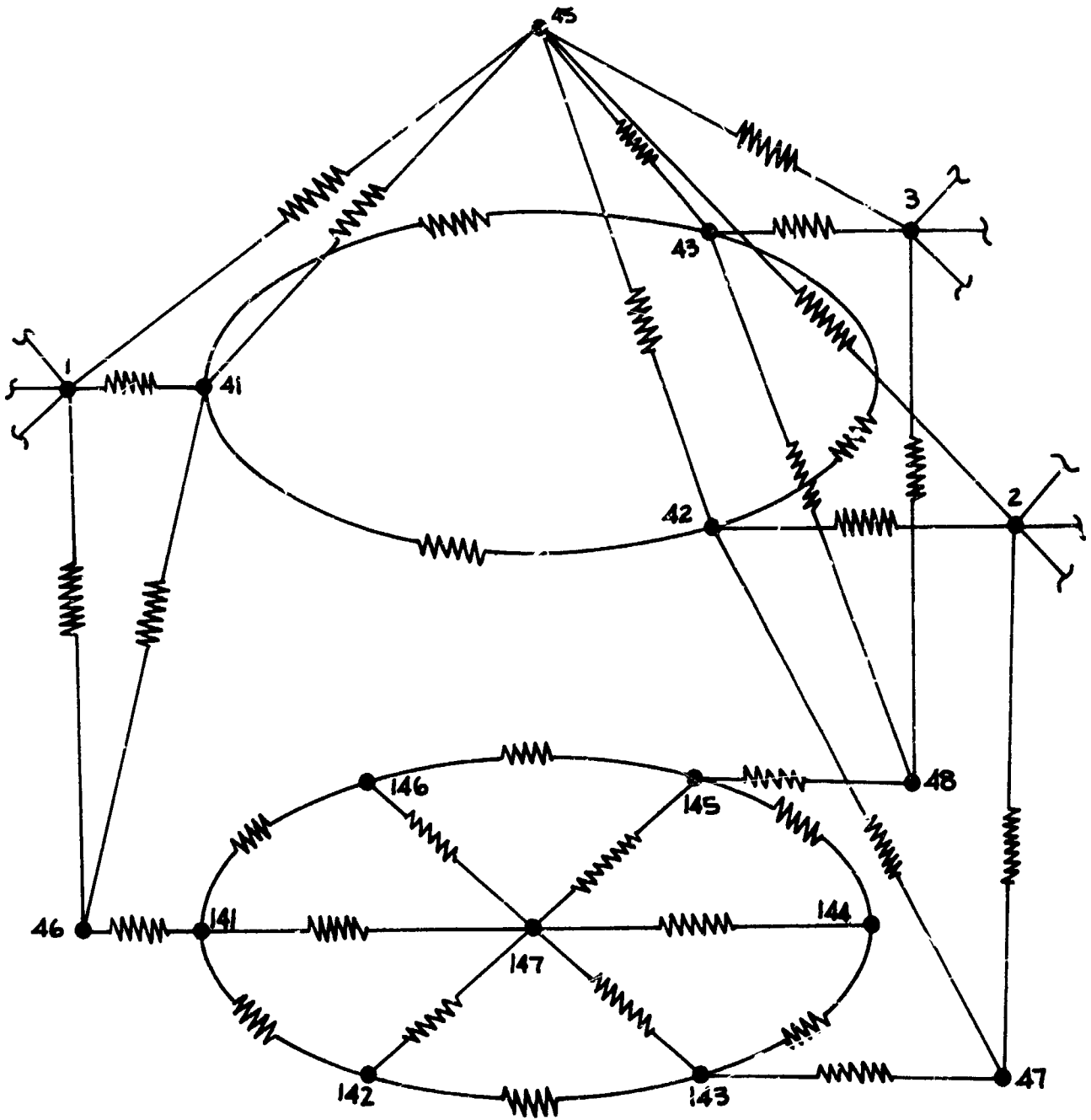
4.1.1.2 Temperature Distributions — Various temperature histories were studied for the two orbit cases.

Transient Temperatures After Launch — The transient-temperature histories of the mirrors and telescope structure after an initial launch temperature of 530°R are shown in Figure 4.1-6. The outer wall temperatures (not shown) reach equilibrium very quickly because the outer wall has a small thermal capacitance and is well insulated from the internal structure. The inner wall temperatures stabilize in approximately 45 hours due to their low thermal capacitance and the effectiveness of the thermal insulation. The primary and secondary mirrors require a much longer time to reach equilibrium temperature due to the insulation of the



PRIMARY MIRROR AND TELESCOPE STRUCTURE THERMAL NETWORK

FIGURE 4.1-4



SECONDARY MIRROR THERMAL NETWORK

FIGURE 4.1-5



Initial Temperature: 530°R  
 Outer Coating:  $\epsilon_s = 0.2$   $\epsilon_{IR} = 0.9$   
 19380 N.M.I. Circular Orbit

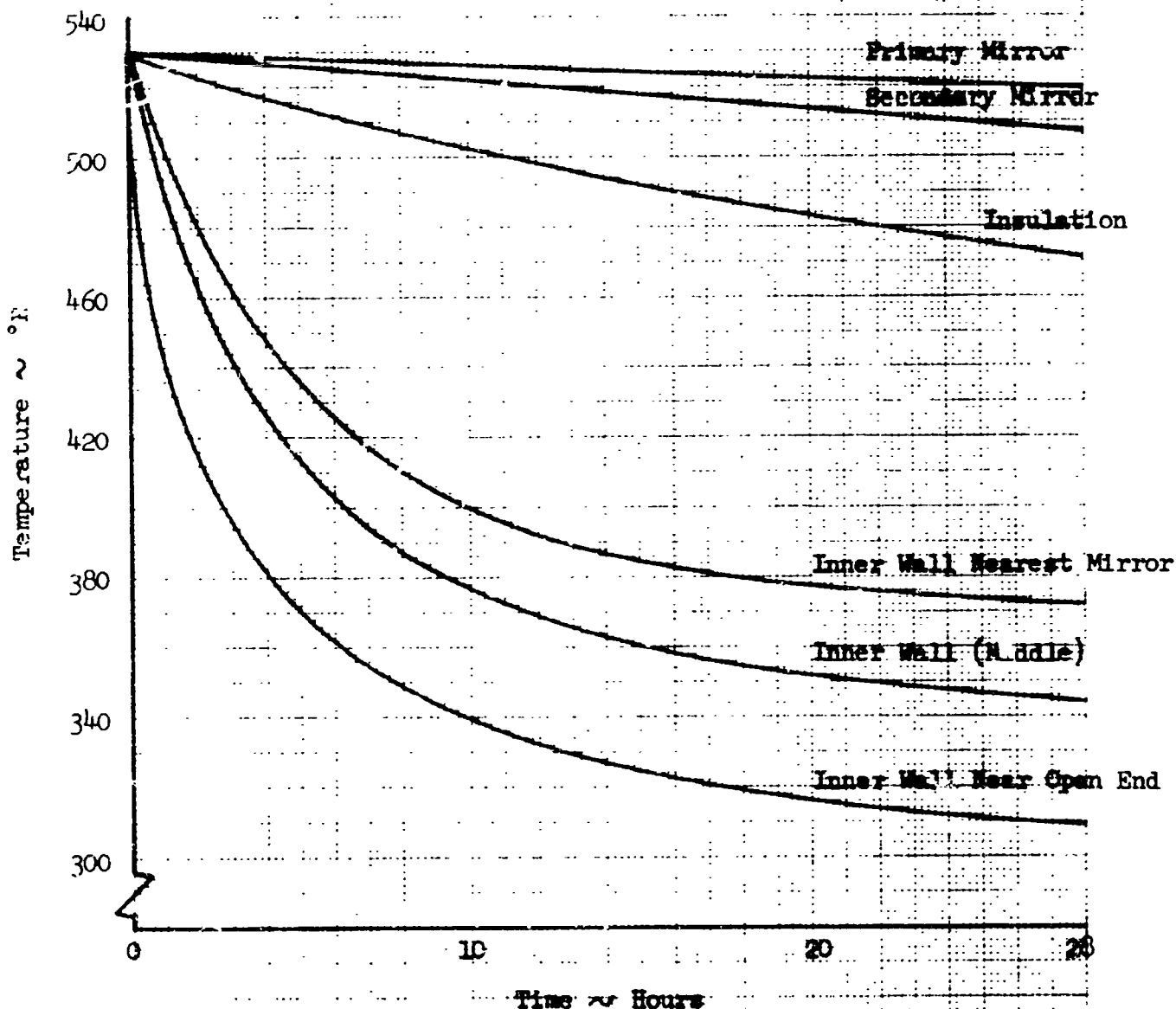


FIGURE 4.1-6 TRANSIENT TEMPERATURES AFTER LAUNCH - TELESCOPE AXIS PARALLEL TO SOLAR VECTOR

optics from the rest of the telescope structure. Even at synchronous-orbit altitude, the equilibrium temperature of the primary mirror is dependent on the telescope attitude and varies from  $335^{\circ}\text{R}$  in the parallel position to  $340^{\circ}\text{R}$  in the perpendicular position. The equilibrium temperature of the secondary mirror is approximately  $35^{\circ}\text{R}$  colder than the primary mirror since it is more isolated from the cabin, the primary source of heat to the telescope optics.

For the low-Earth-orbit case, the maximum primary-mirror temperature variation occurs about 15 hours after launch, with the following temperature differences between adjacent nodes: circumferential,  $0.07^{\circ}\text{R}$ ; radial,  $0.03^{\circ}\text{R}$ ; axial,  $0.13^{\circ}\text{R}$ . The corresponding maximum temperature variations for the synchronous-orbit case occurs about 20 hours after launch. They are: circumferential,  $0.11^{\circ}\text{R}$ ; radial,  $0.03^{\circ}\text{R}$ ; and axial,  $0.17^{\circ}\text{R}$ .

Outer Tube Temperatures — The outer tube temperatures when the telescope axis is perpendicular to the solar vector are shown in Figure 4.1-7. The upper curve represents a 120-degree segment of the outer tube, which is always oriented towards the Sun. The "dip" in the curve is due to the telescope being occulted by the Earth for a period of 1.14 hours. For this orientation, no axial thermal gradients are present. For the low-Earth-orbit case, the maximum and minimum temperatures for this segment of the outer tube wall are  $502^{\circ}\text{R}$  and  $416^{\circ}\text{R}$ , respectively.

For the synchronous-orbit case, the corresponding temperatures are  $502^{\circ}\text{R}$  and  $358^{\circ}\text{R}$ .

The two lower curves of Figure 4.1-7 are the segments of the outer wall that alternately see deep space and Earth. For low Earth orbit, the maximum and minimum temperatures are  $436^{\circ}\text{R}$  and  $300^{\circ}\text{R}$ , respectively. For the synchronous-orbit case, the corresponding temperatures are  $186^{\circ}\text{R}$  and  $134^{\circ}\text{R}$ .

Figure 4.1-8 shows the outer tube temperatures when the telescope axis is parallel to the solar vector. For the low Earth orbit, the maximum and minimum temperatures are  $424^{\circ}\text{R}$  and  $300^{\circ}\text{R}$ , respectively. For the synchronous-orbit case, when all outer wall segments alternately see deep space and Earth, the corresponding temperatures are  $174^{\circ}\text{R}$  and  $110^{\circ}\text{R}$ , respectively.

Except for the segments of the outer tube on which direct solar energy falls, the outer tube is considerably colder in the synchronous-orbit case. This is to be expected since the thermal energy from Earth is substantially reduced at synchronous-orbit altitude and, subsequently, a lower "sink temperature" is experienced by the telescope.

Inner Tube Temperatures — The quasi-steady-state inner tube temperatures for the two telescope attitudes of Figure 4.1-3 are shown in Figure 4.1-9 for the synchronous-orbit case. The axial temperatures of the inner tube range from  $266^{\circ}\text{R}$  at the open end of the telescope to  $333^{\circ}\text{R}$  at the end near the primary mirror.

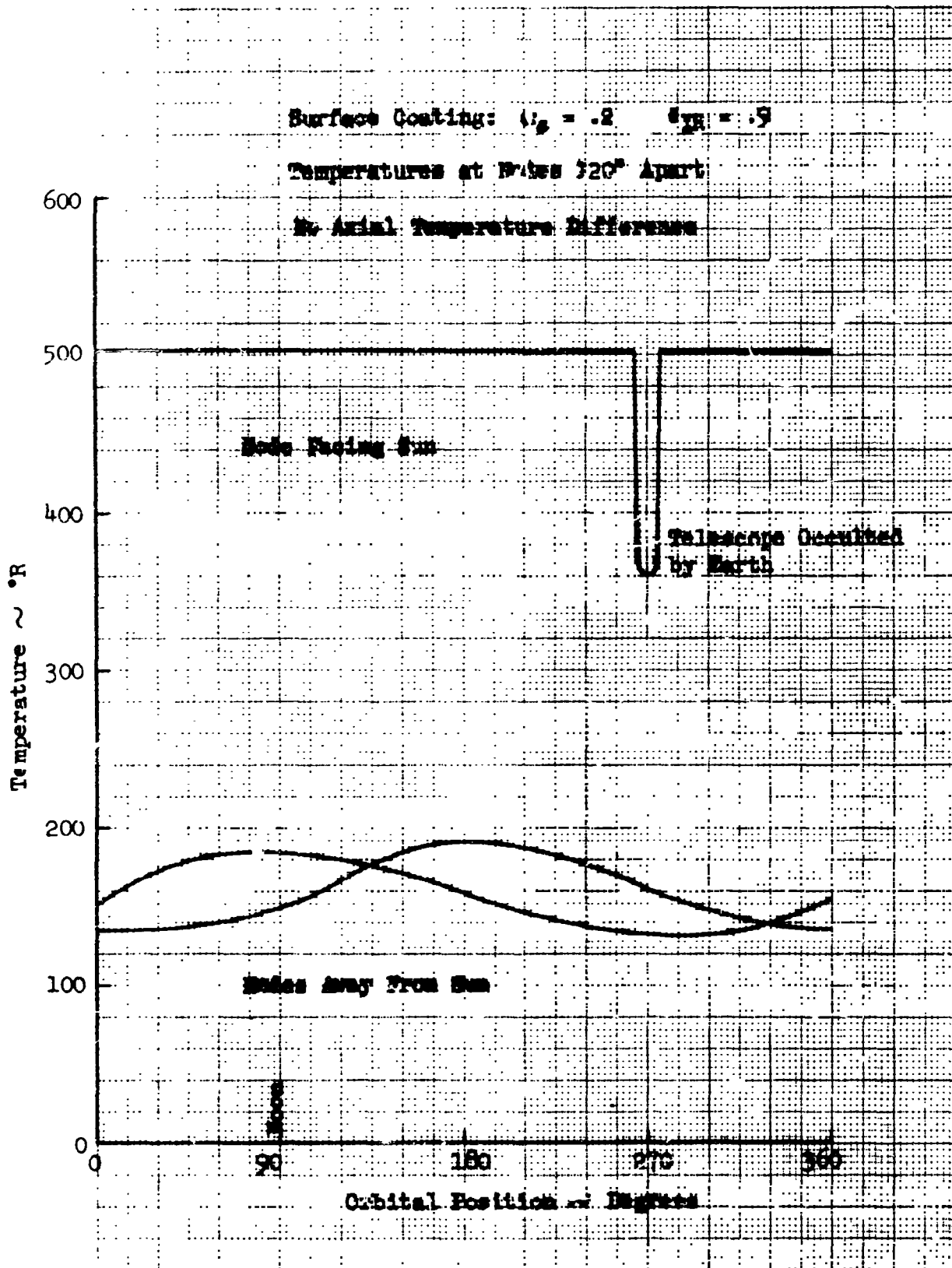
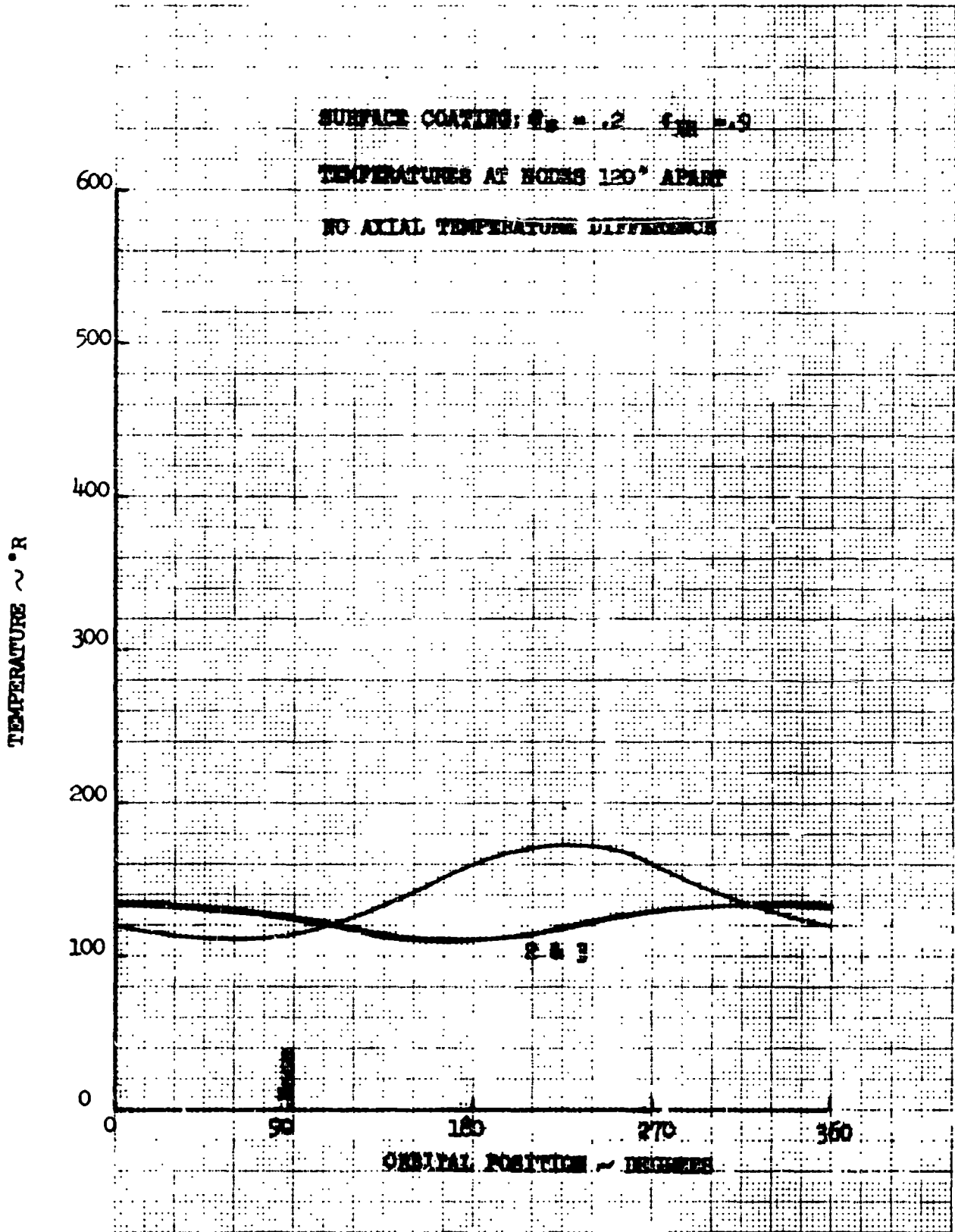


FIGURE 4.1-7 OUTER TUBE TEMPERATURES  
 TELESCOPE AXIS PERPENDICULAR TO SOLAR VECTOR



**FIGURE 4.1-8 OUTER TUBE TEMPERATURES  
TELESCOPE AXIS PARALLEL TO SOLAR VECTOR**

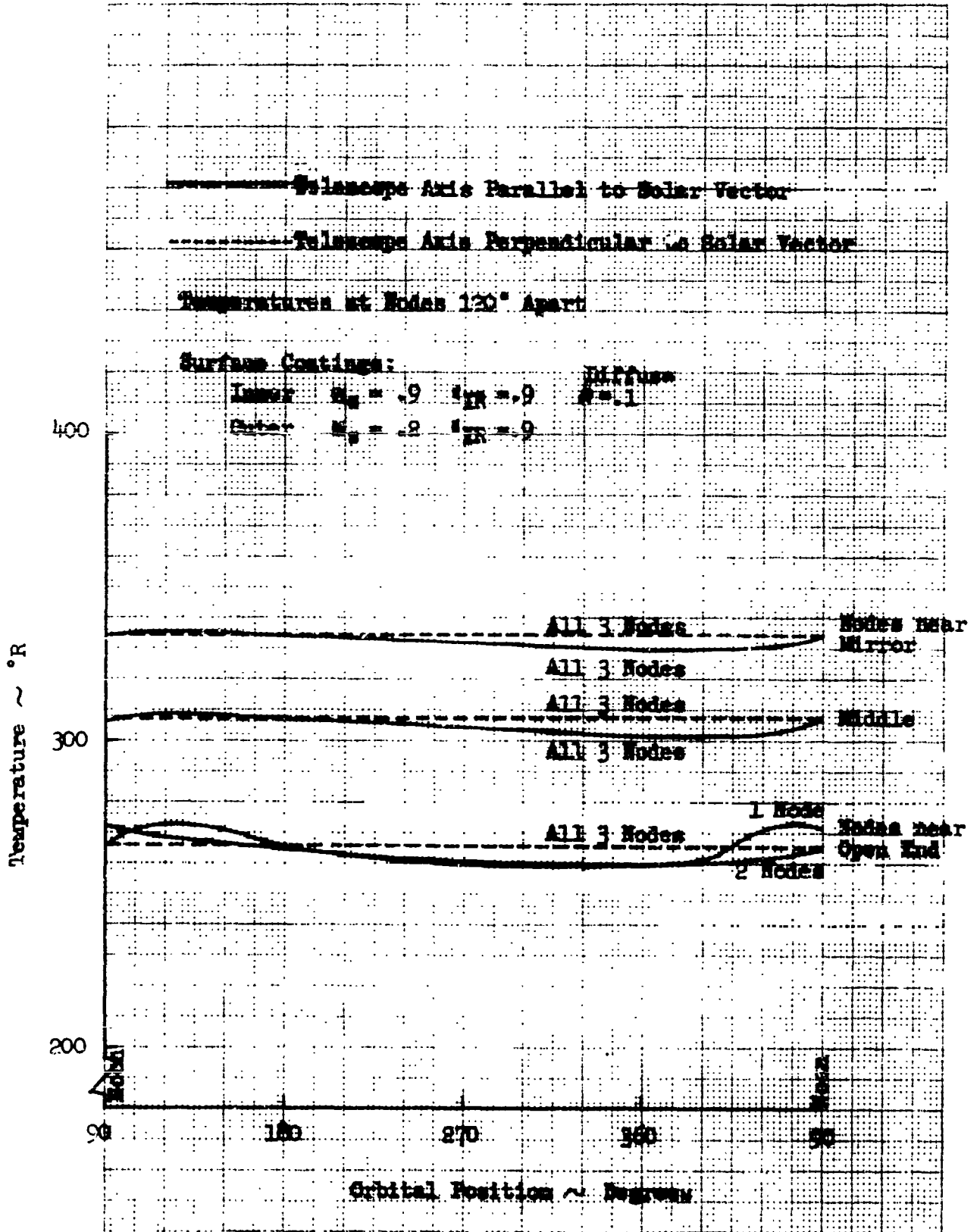


FIGURE 4.1-9 INNER TUBE TEMPERATURES

For the low Earth orbit, the axial temperatures of the inner tube depend more on the telescope attitude. When parallel to the solar vector, the inner tube temperatures range from approximately  $405^{\circ}\text{R}$  at the open end of the telescope to  $436^{\circ}\text{R}$  at the end near the primary mirror. When perpendicular to the solar vector, the inner tube temperatures range from approximately  $370^{\circ}\text{R}$  at the open end of the telescope to  $408^{\circ}\text{R}$  at the end near the primary mirror.

Dependence of the inner tube temperatures on telescope attitude is caused by the difference in thermal environment at each telescope position. When parallel to the solar vector, Earth effects are felt by the inside of the telescope. When perpendicular, the Earth has a minimum effect. Regardless of attitude, the Earth effects are significantly reduced and a nearly isothermal environment is established when the telescope is at synchronous-orbit altitude.

Synchronous- and low-Earth-orbit inner tube temperatures for the nodes nearest the primary mirror are shown in Figure 4.1-10. In the low Earth orbit, the dependence of the inner tube temperatures on telescope attitude can be seen. Differences in the circumferential temperatures occur. In the synchronous orbit, the inner tube temperatures are practically independent of the telescope attitude and the circumferential temperatures do not vary. In addition, the inner tube temperatures are approximately  $100^{\circ}\text{R}$  colder in the synchronous-orbit case because of the reduced effects of Earth-emitted and reflected radiation in synchronous orbit.

**Mirror Temperatures, Quasi-Steady State** — The quasi-steady-state primary and secondary mirror temperatures when the telescope axis is perpendicular to the solar vector (i.e., the telescope views only space) are shown in Figure 4.1-11. The primary mirror circumferential temperature differences between adjacent nodes in both synchronous- and low-Earth-orbit cases are  $0.001^{\circ}\text{R}$  or less due to the nearly isothermal mirror environment when perpendicular to the solar vector.

Temperature differences between adjacent nodes in the secondary mirror are considerably larger due to the lower thermal conductivity of fused silica glass. However, larger temperature differences are tolerable with fused silica glass because of a lower coefficient of expansion.

Quasi-steady-state primary and secondary mirror temperatures when the telescope axis is parallel to the solar vector are shown in Figure 4.1-12. Circumferential temperature differences between adjacent nodes in the primary mirror are  $0.003^{\circ}\text{R}$  or less for the synchronous-orbit case. In the low Earth orbit, the corresponding temperature differences were  $0.008^{\circ}\text{R}$ . Temperature variations in the synchronous-orbit case are less since the primary causes of these variations, Earth effects, are less.

Figure 4.1-13 is a comparison of the maximum and minimum quasi-steady-state mirror temperatures for the synchronous-orbit case and the low Earth orbit with

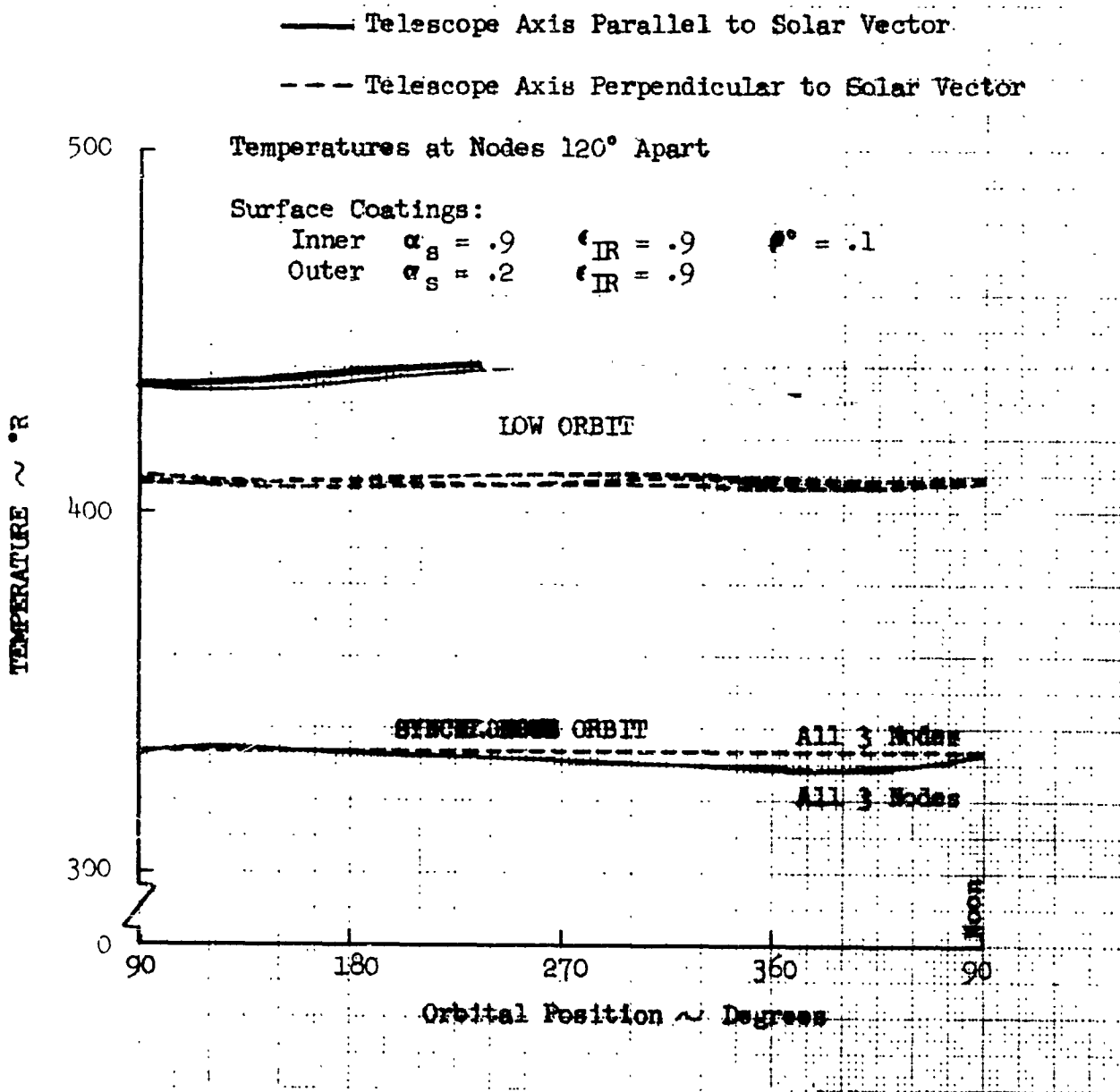


FIGURE 4.1-10 SYNCHRONOUS ORBIT AND LOW ORBIT INNER TUBE TEMPERATURES FOR NODES NEAR PRIMARY MIRROR

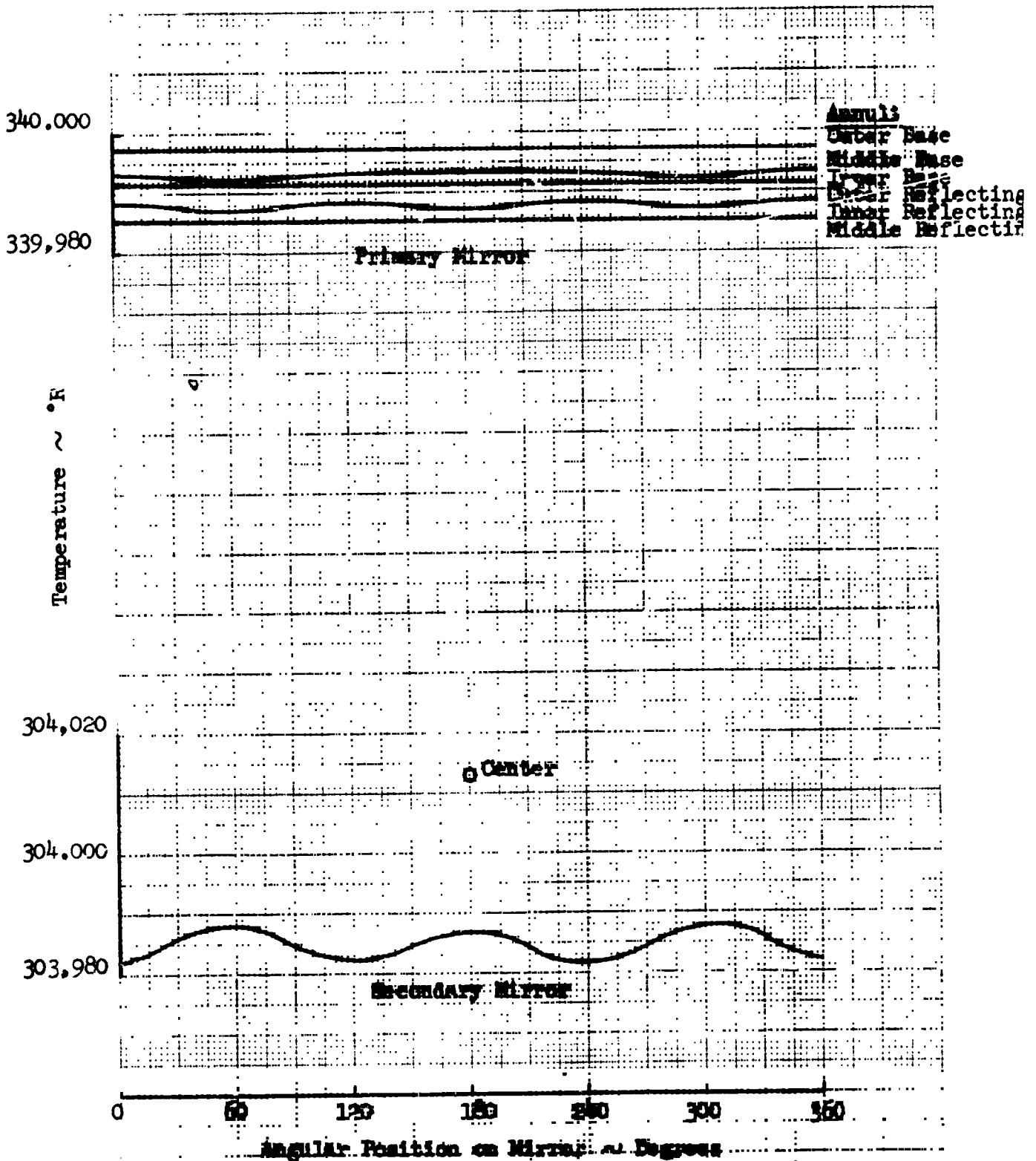


FIGURE 4.1-11 QUASTEADY-STATE MIRROR TEMPERATURES - TELESCOPE AXIS PERPENDICULAR TO THE SOLAR VECTOR



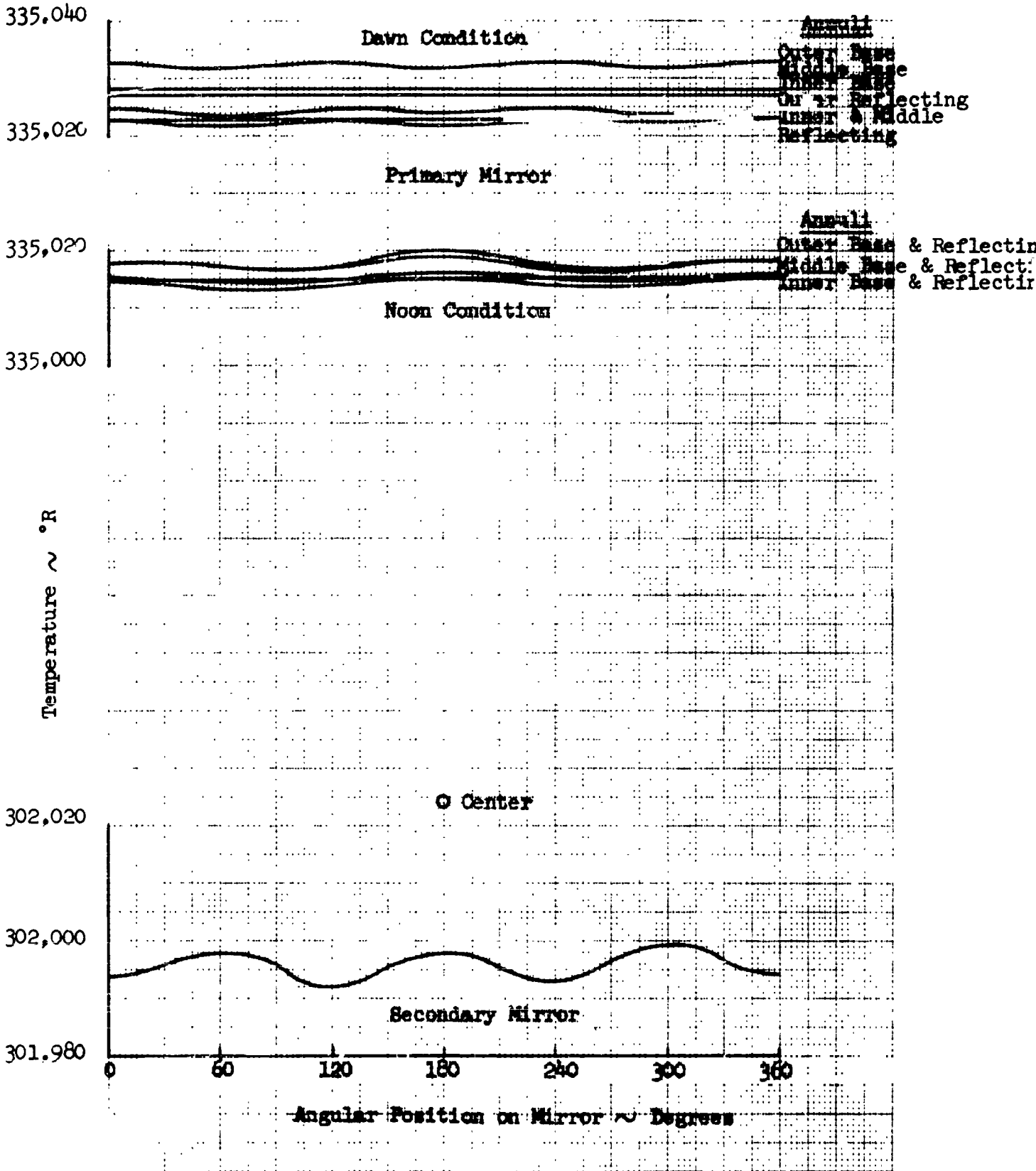


FIGURE 4.1-12 QUASISTEADY-STATE MIRROR TEMPERATURES - TELESCOPE AXIS PARALLEL TO THE SOLAR VECTOR

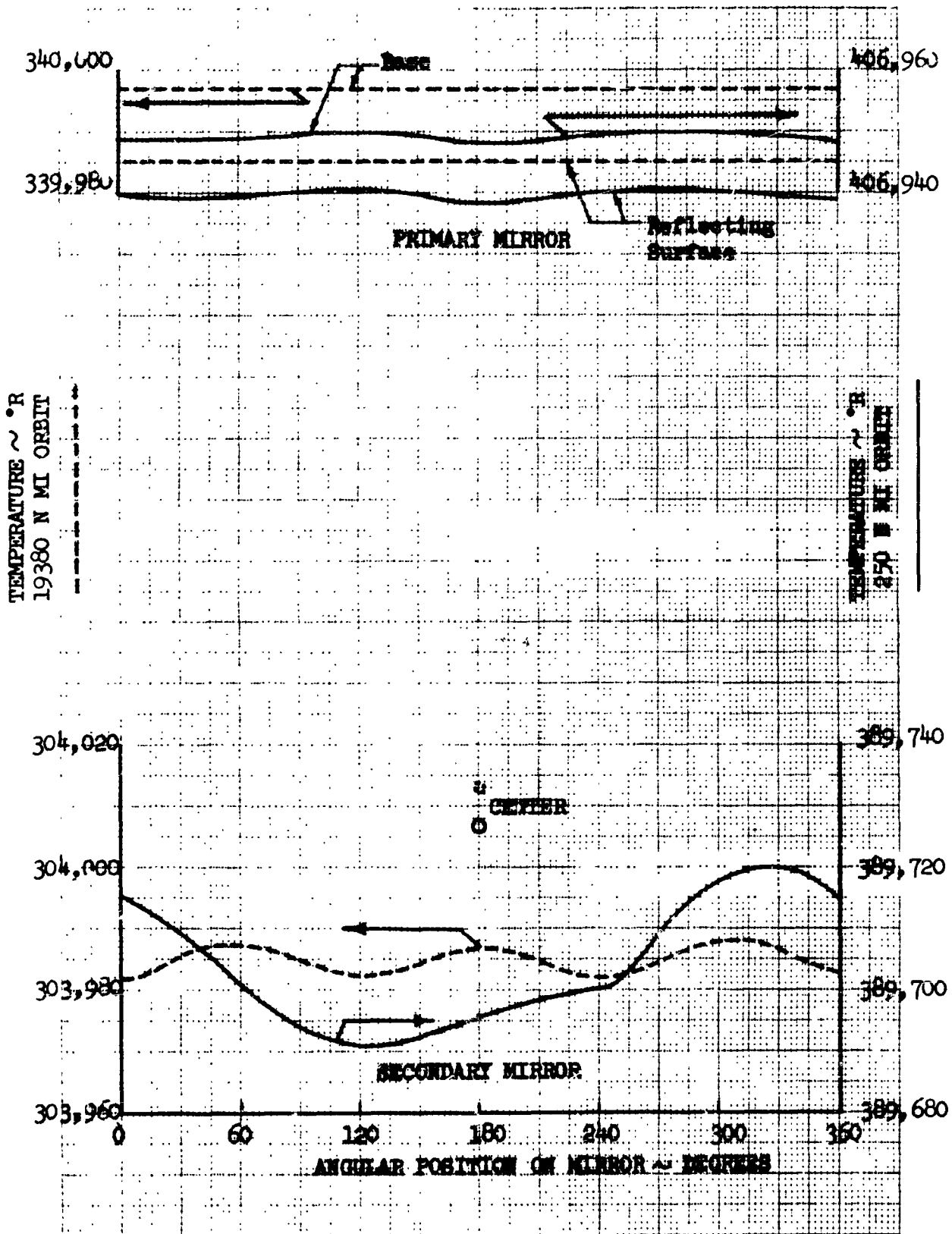


FIGURE 4.1-13 SYNCHRONOUS ORBIT AND LOW ORBIT EXTREME MIRROR TEMPERATURES - TELESCOPE AXIS PERPENDICULAR TO SOLAR VECTOR

the telescope axis perpendicular to the solar vector. The primary mirror equilibrium temperature is  $340^{\circ}\text{R}$  for the synchronous-orbit case,  $67^{\circ}\text{R}$  colder than the low-Earth-orbit equilibrium temperature.

The secondary mirror equilibrium temperature is  $304^{\circ}\text{R}$  for the synchronous-orbit case,  $86^{\circ}\text{R}$  colder than the low-Earth-orbit case. The circumferential temperature differences are greatly reduced from those of the low Earth orbit.

Figure 4.1-14 is a comparison of the maximum and minimum quasi-steady-state mirror temperatures for both the synchronous- and the low-Earth-orbit cases with the telescope axis parallel to the solar vector. The primary mirror equilibrium temperature is  $335^{\circ}\text{R}$  for the synchronous-orbit case,  $102^{\circ}\text{R}$  colder than the low-Earth-orbit equilibrium temperature.

The secondary mirror equilibrium temperature is  $304^{\circ}\text{R}$  for the synchronous-orbit case,  $102^{\circ}\text{R}$  colder than the low earth orbit. The circumferential temperature differences are considerably reduced since the cyclic variations in the thermal environment due to Earth effects are greatly reduced at synchronous orbit, resulting in the mirror being more uniformly heated than in the low Earth orbit.

Cyclic variations in the thermal environment of the telescope have two sources: (1) occultation by the Earth and (2) solar-reflected and Earth-emitted radiation entering the optics. At synchronous-orbit altitude, maximum occultation takes approximately 5 percent of the 24-hour orbit period. At low-Earth-orbit altitude, occultation takes about 38 percent of the 1.445-hour orbit period. At synchronous-orbit altitude, the radiation from Earth enters the optics of the telescope for approximately 3 percent of the 24-hour orbit period; at low Earth orbit, radiation from Earth enters the telescope for approximately 38 percent of the 1.445-hour orbit period. Therefore, for the low-Earth-orbit case, the thermal environment of the telescope is changing over approximately 76 percent ( $\approx 1.1$  hours) of the 1.445-hour orbit period. At synchronous-orbit altitude, the thermal environment of the telescope is changing over approximately 8 percent ( $\approx 1.92$  hours) of the 24-hour orbit period. In addition, the radiation view factors between the telescope optics and Earth are reduced at synchronous-orbit altitude. For these reasons, the cyclic variations in the thermal environment of the telescope have a minimal effect on the telescope at synchronous-orbit altitude.

Mirror Temperatures, Attitude Change — Mirror temperature variations that occur during transient operation are shown in Figures 4.1-15 and 4.1-16. To determine the transient temperature gradients, the telescope structure and mirrors are first permitted to reach equilibrium temperature with the telescope axis parallel to the solar vector so that the primary mirror views space and, occasionally, Earth. From Figure 4.1-12, the equilibrium primary and secondary mirror temperatures for the synchronous orbit are  $335^{\circ}\text{R}$  and  $302^{\circ}\text{R}$ , respectively. The telescope attitude is then rotated 90 degrees so that the telescope axis is perpendicular to solar vector and the telescope continuously views space. The new mirror

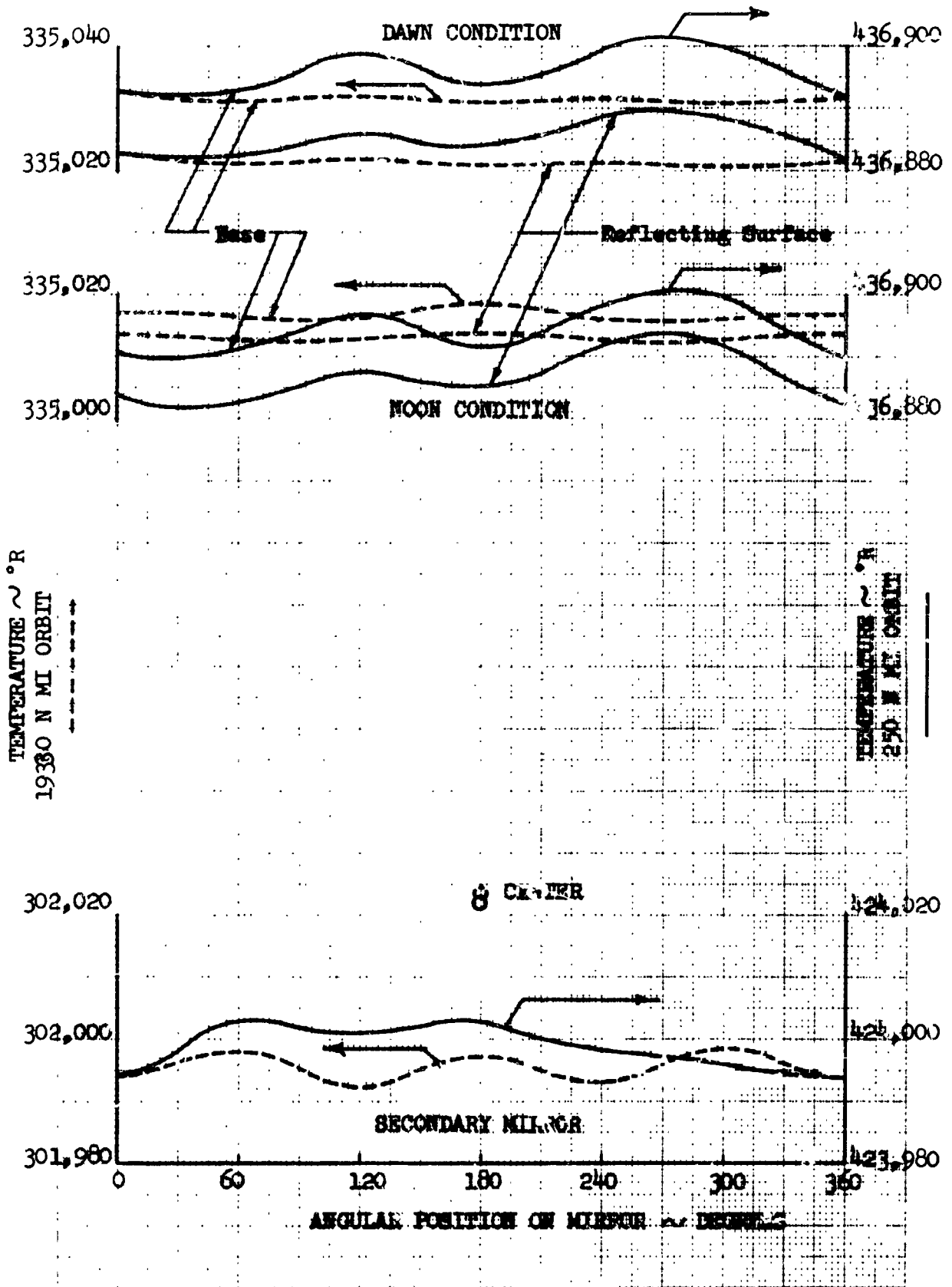


FIGURE 4.1-14 SYNCHRONOUS ORBIT AND LOW ORBIT EXTREME MIRROR TEMPERATURES - TELESCOPE AXIS PARALLEL TO THE SOLAR VECTOR

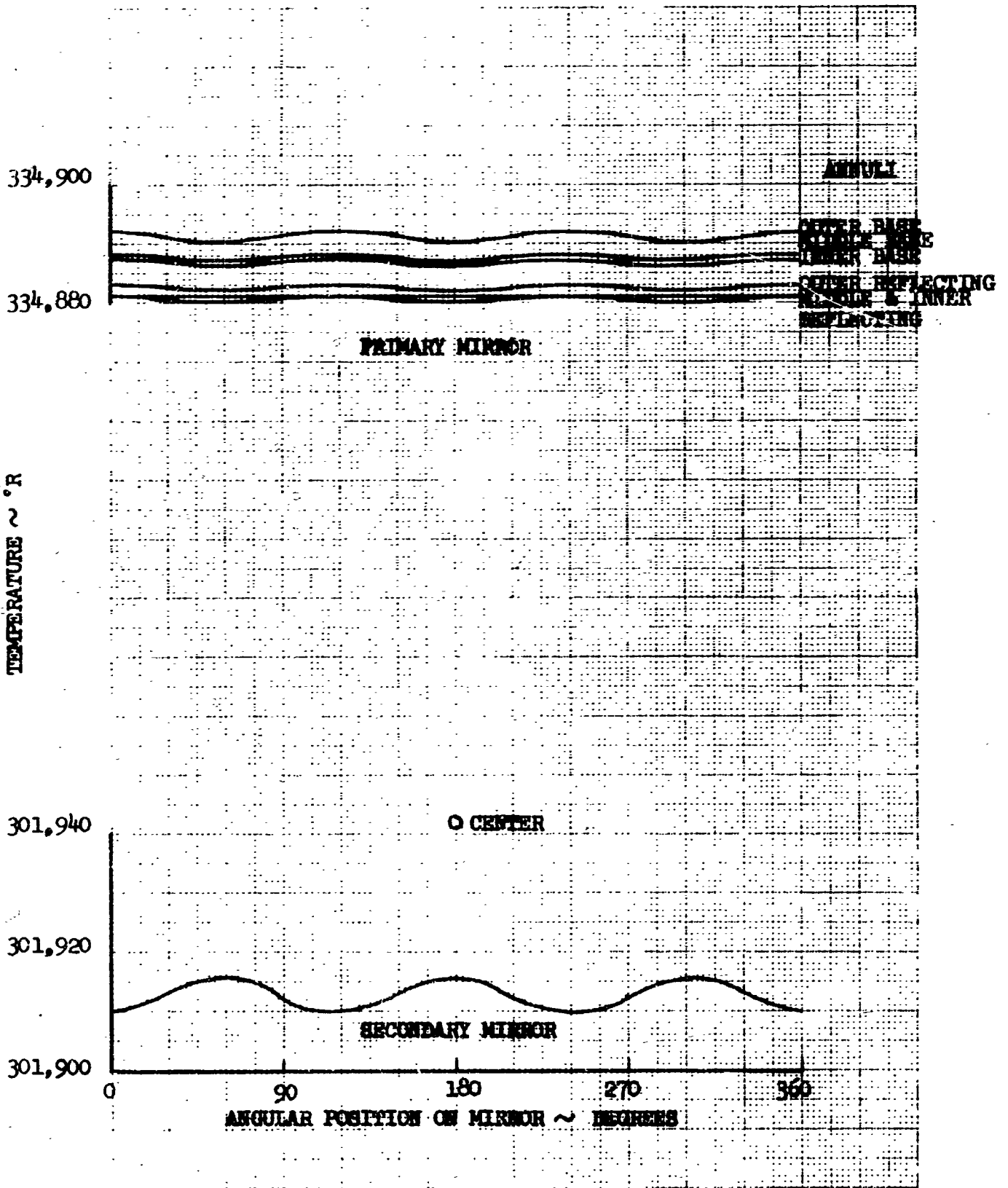


FIGURE 4.1-15 TRANSIENT MIRROR TEMPERATURES 20 HOURS AFTER CHANGING ATTITUDE FROM PARALLEL TO PERPENDICULAR TO THE SOLAR VECTOR

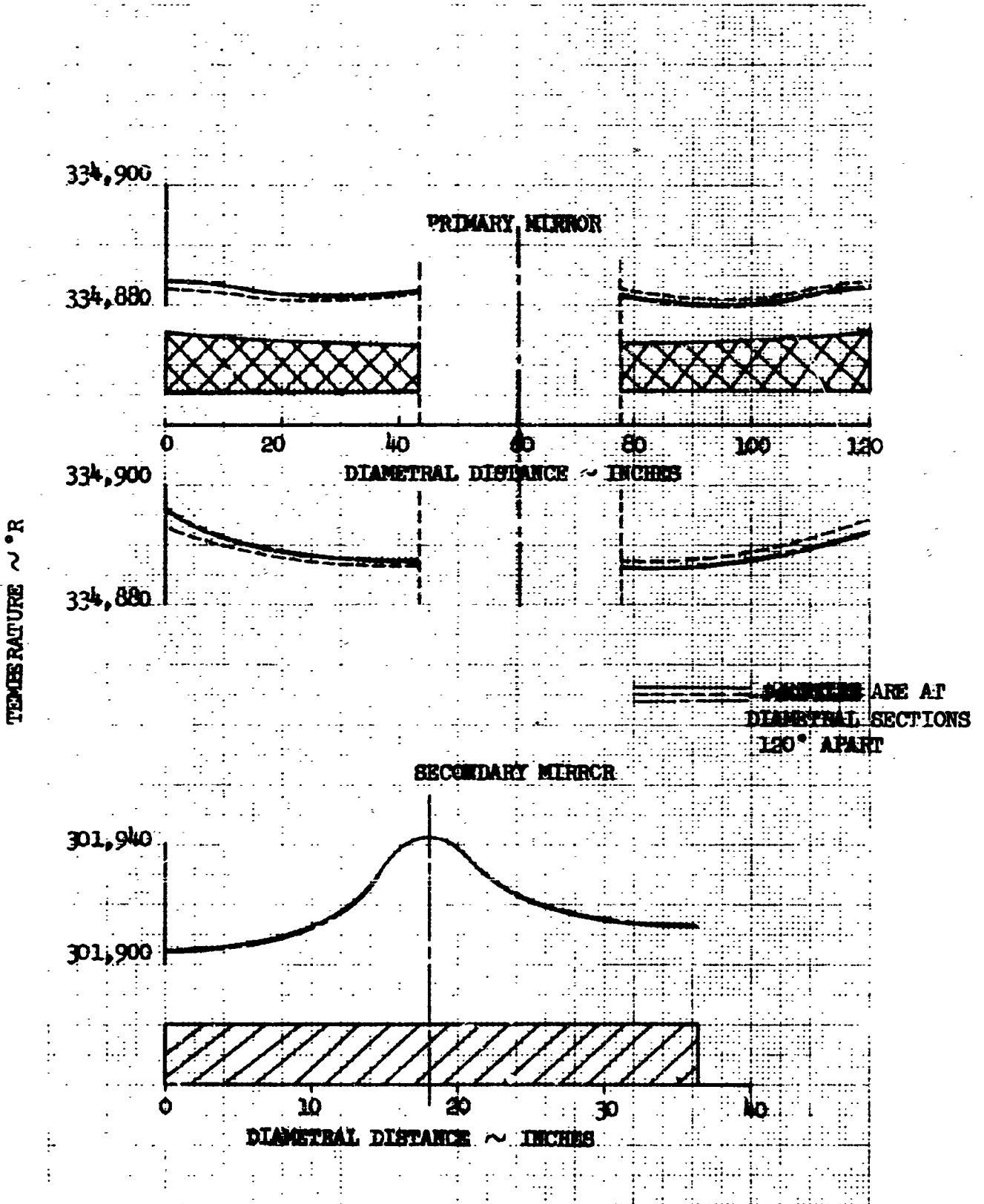


FIGURE 4.1-16 RADIAL TEMPERATURE PROFILES  
 TRANSIENT CONDITION 20 HOURS AFTER  
 CHANGING TELESCOPE ATTITUDE FROM  
 PARALLEL TO PERPENDICULAR TO SOLAR VECTOR

equilibrium temperatures for this position of the telescope are  $340^{\circ}\text{R}$  and  $304^{\circ}\text{R}$ , from Figure 4.1-13.

Figure 4.1-15 shows circumferential temperature variations. The greatest circumferential variation on the primary mirror for the synchronous-orbit case is  $0.002^{\circ}\text{R}$ . For the low-Earth-orbit case, the circumferential variation is  $0.015^{\circ}\text{R}$ .

Figure 4.1-16 shows radial temperature variations. The largest radial variation on the primary mirror for the synchronous-orbit case is  $0.001^{\circ}\text{R}$ . For the low-Earth-orbit case, the radial variation is  $0.011^{\circ}\text{R}$ . Maximum temperature variations occur approximately 20 hours after reorientation of the telescope.

Instead of increasing in temperature as might be expected, the primary mirror initially cools. This initial cooling is reasonable, though, since the equilibrium temperatures of the inner tube are dependent on a small amount of Earth radiation entering the telescope. By removing the Earth radiation that occurs at the noon position in orbit, Figure 4.1-9, the inner tube wall temperatures decrease and, since the primary mirror is coupled by conductors to the inner tube, its temperature likewise decreases. The temperature of the primary mirror continues to decrease until the effect of the solar heating of the outer tube is felt by the inner tube. Then the primary mirror temperature will start to approach  $340^{\circ}\text{R}$ , its equilibrium temperature when perpendicular to the solar vector.

**4.1.1.3 Conclusions** — Thermal control of the primary and secondary optical geometry by passive means appears to be feasible for operation at the telescope attitudes studied. Temperature differences experienced by the optics in the low-Earth-orbit case are considerably reduced by the nearly isothermal environment found at synchronous-orbit altitude. The temperature variations presented in this analysis are clearly dependent on the ability to manufacture a telescope structure having the previously defined insulation and support thermal conductance properties. The effective thermal insulation of the primary mirror from the floor beam and use of low conductive attachments to the inner telescope tube structure are of prime importance for preventing the occurrence of excessive temperature variations in the mirrors.

The Earth shade and doors that were recommended for the low-Earth-orbit operation to reduce the Earth heating effects were not included in this analysis. The results show that the temperature variations are less without the doors and Earth shade, than at low-Earth-orbit altitude with the doors and shade.

The recommended surface coatings of the low-Earth-orbit analysis were used for this analysis and appear to be quite satisfactory for the telescope attitudes studied.

#### 4.1.2 Thermal Distortions

**4.1.2.1 Primary Mirror** — Thermal distortions of the primary mirror were computed with the aid of a digital program for performing structural analyses. The

structural idealization used for this analysis, along with identification of nodes and structural elements, are shown in Figures 4.1-17 and 4.1-18. The structural elements are quadrilateral plates joined at the nodes.

Temperatures are given in Figures 4.1-19, 4.1-20, and 4.1-21, and interpolated to provide a temperature input for each node. The cases analyzed include: (1) perpendicular to solar vector, (2) parallel to solar vector at dawn, and (3) parallel to solar vector at noon. It was assumed in the analysis that the mirror had been figured to  $f/4$  at  $-54.9^\circ\text{F}$ .

Distortions of the mirror reflecting surface are shown in Figures 4.1-22, 4.1-23, and 4.1-24. A least-square paraboloid was fitted to the data and an RMS error computed. This paraboloid is described by the equation:

$$z = a r^2 + b x + c$$

where  $a$ ,  $b$ , and  $c$  are the coefficients to be determined by the method of least squares.

The RMS deviations are:

<u>Telescope Orientation</u>	<u>RMS Deviations</u>
Perpendicular to solar vector	$0.592(10^{-7})$
Parallel to solar vector — dawn	$0.871(10^{-7})$
Parallel to solar vector — noon	$0.529(10^{-7})$

or approximately  $\lambda/330$ ,  $\lambda/225$ , and  $\lambda/375$ , respectively.

Overall thermal deformation of the mirror in synchronous orbit is larger than for the low-Earth-orbit case of Reference 1 because of the difference of approximately 125 degrees between the mirror fabrication temperature and the low operating temperature in synchronous orbit. This change in bulk temperature has a small effect on mirror capability, as shown by the RMS deviation values above, but results in a decrease in the mirror focal length. The change in focal length caused by a bulk change in temperature for a mirror computed at  $70^\circ\text{F}$  is shown in Figure 4.1-25. The method suggested by Dr. Bolser to circumvent this large change in focal length is to check the mirror figure on the ground at the anticipated operating temperature and attain correct figure at this condition. This technique would virtually eliminate any large change in the back focus location.

4.1.2.2 — Secondary Mirror-Support Tube — An examination of the temperatures in the support tube will show that the secondary mirrors can be held within tolerances by the baseline configuration.

4.1.2.3 Conclusions — It can be concluded that the thermal distortion of the mirror optics can be kept within acceptable tolerances on all counts.



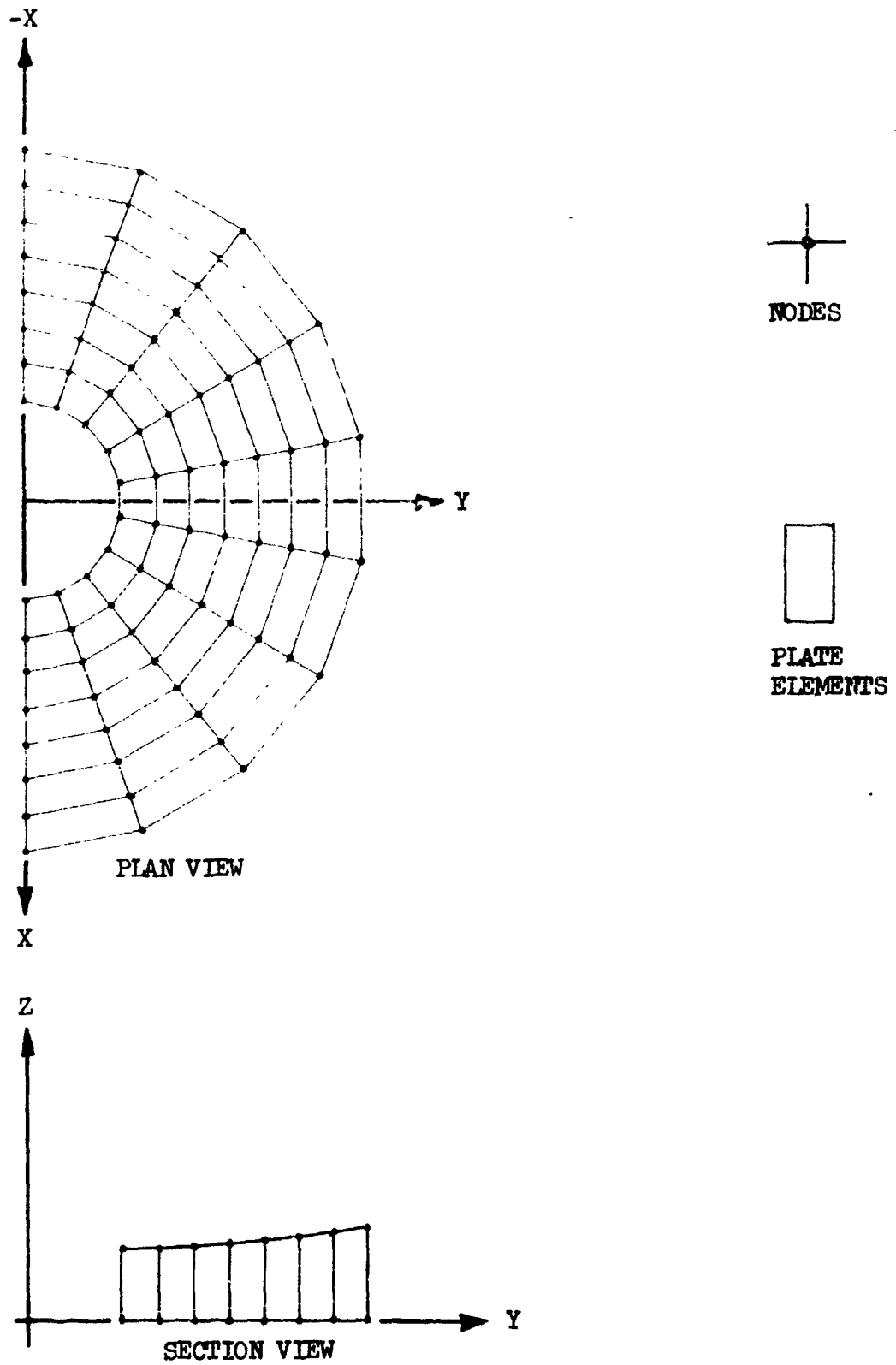


FIGURE h.1-17 PRIMARY MIRROR THERMAL DISTORTION IDEALIZATION

- Even Numbered Nodes on Upper Surface
- Odd Numbered Nodes on Lower Surface
- Nodes Sequenced Consecutively Lower to Upper Along Radial Ribs
- Z Axis - X-Y Plane in Right Hand Coordinate System

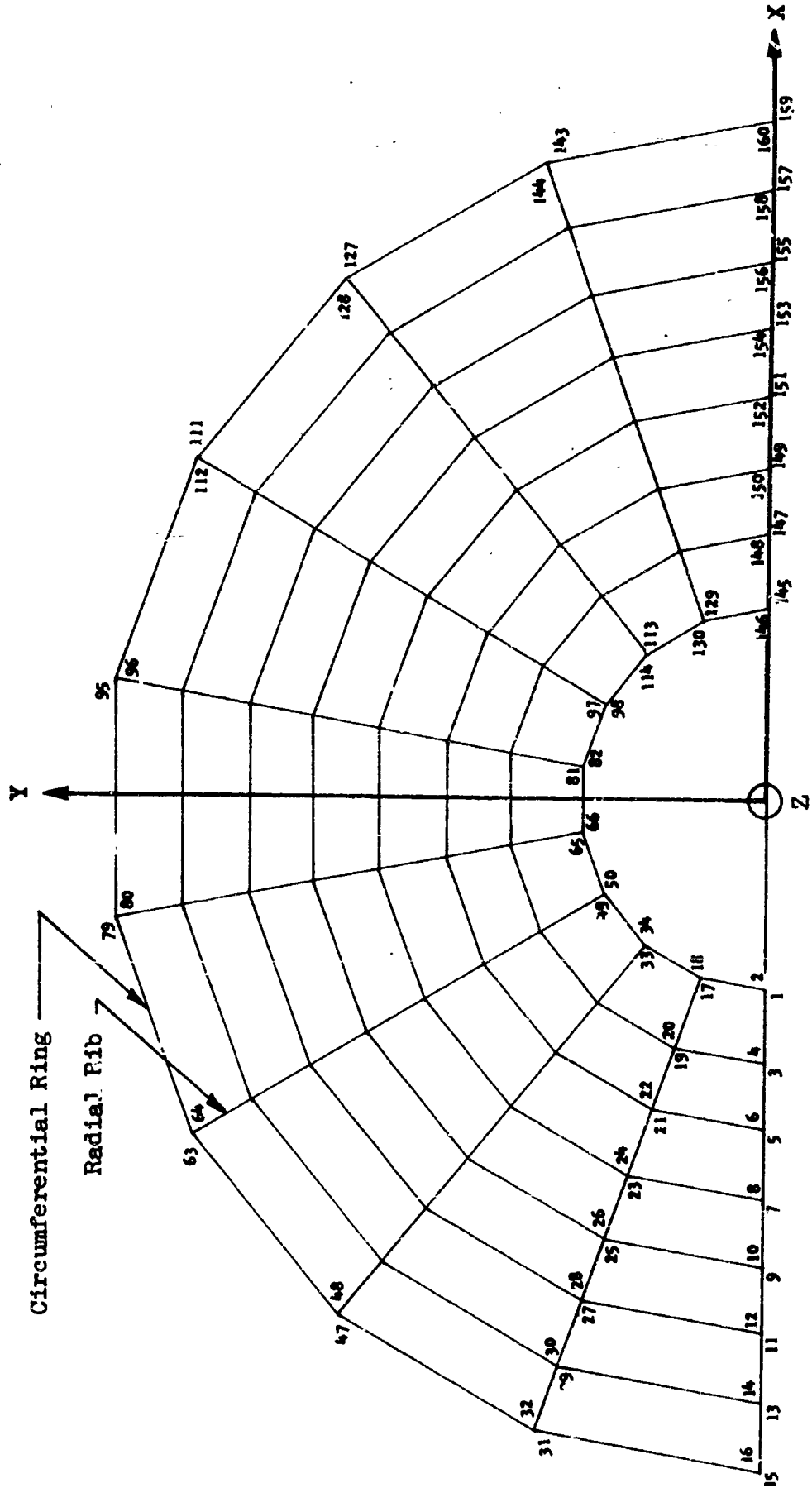


FIGURE 4.1-18 THERMAL DISTORTION NODE & ELEMENT DIAGRAM FOR PRIMARY MIRROR

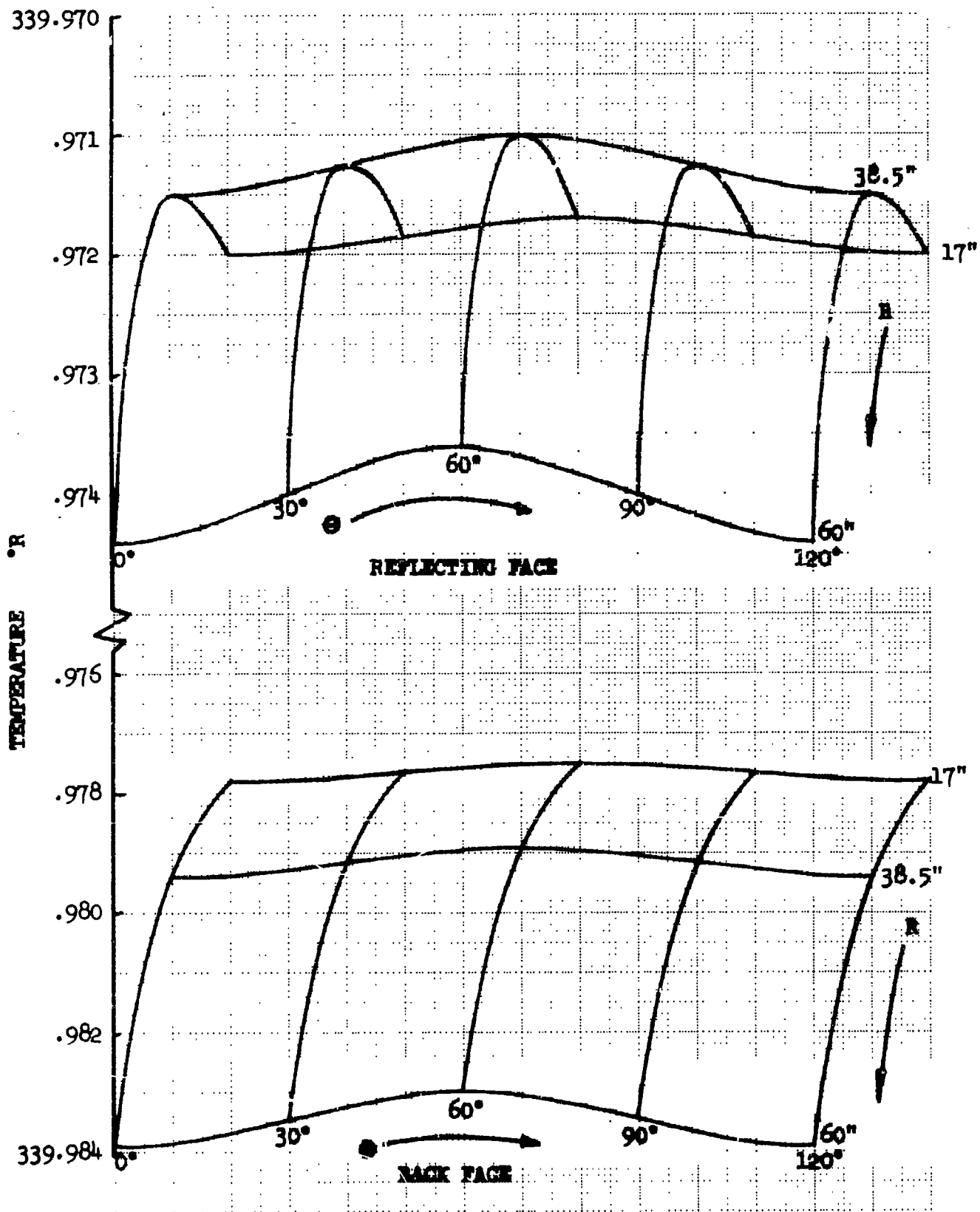


FIGURE 4.1-19 MIRROR TEMPERATURE DISTRIBUTION SYNCHRONOUS ORBIT - TELESCOPE AXIS PERPENDICULAR TO SOLAR VECTOR

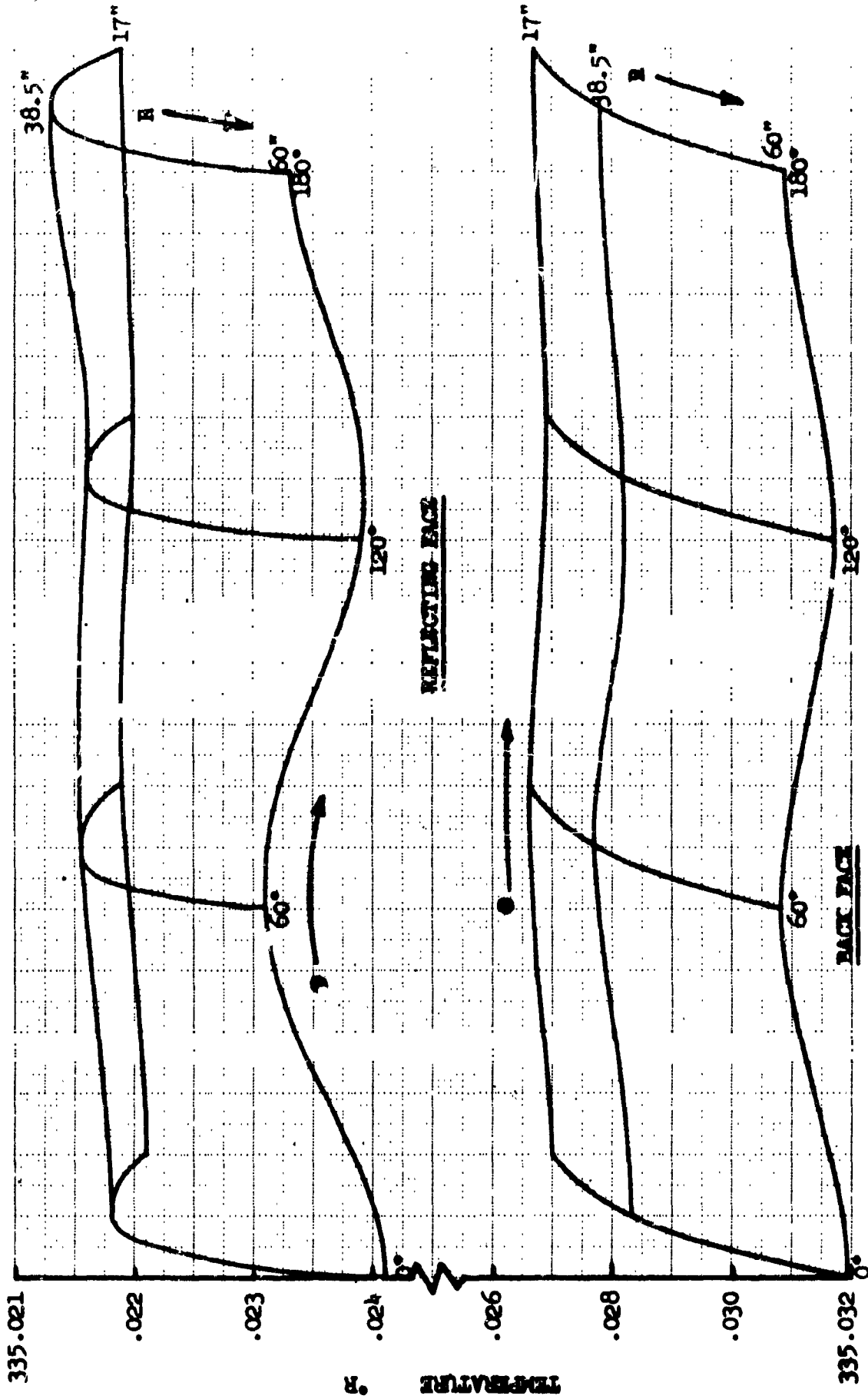


FIGURE 4.1-20 MIRROR TEMPERATURE DISTRIBUTION STRUCTURE ORBIT - TELESCOPE AXIS PARALLEL TO SOLAR VECTOR-DRAWN CONDITION

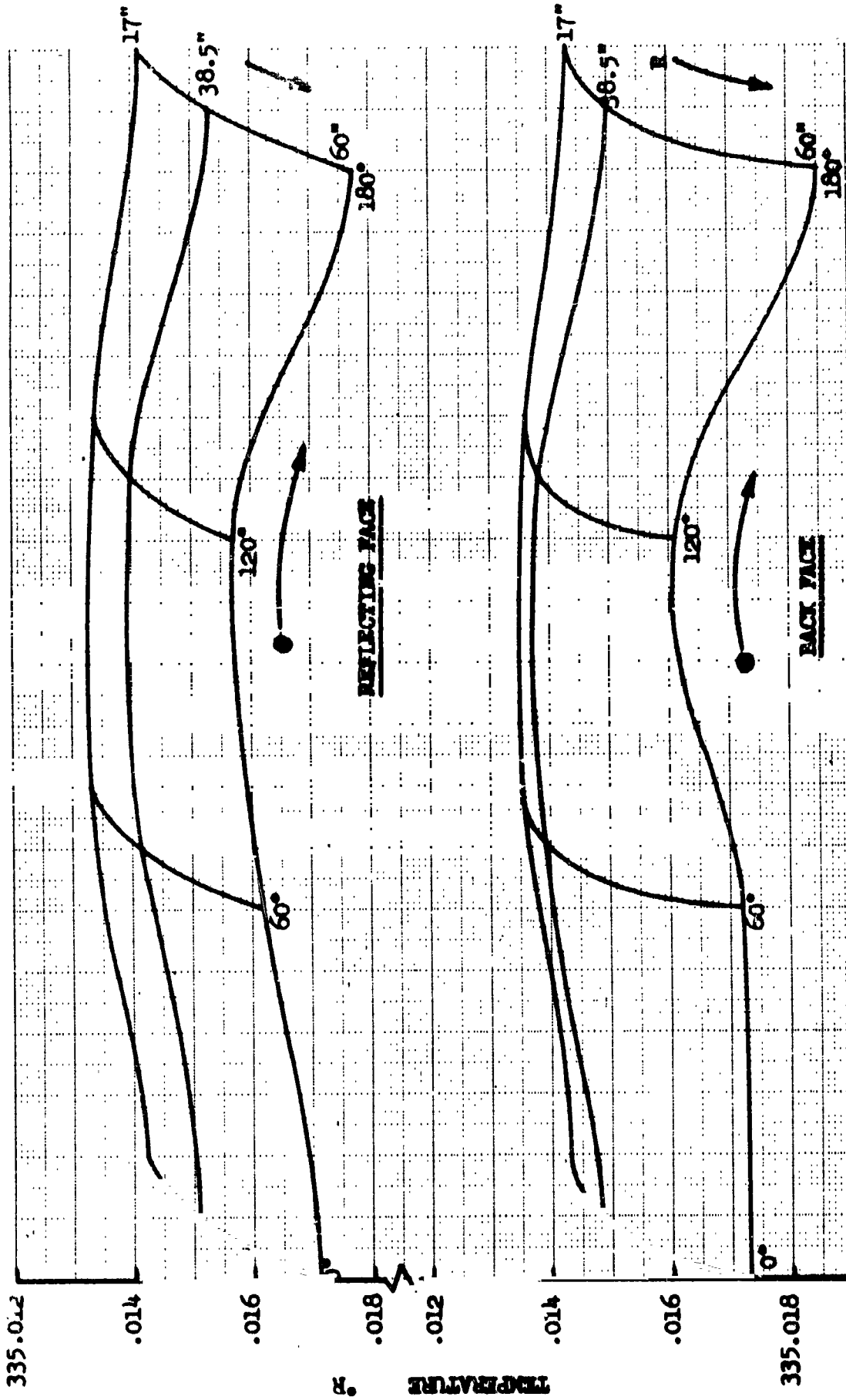


FIGURE 4.1-21 MIRROR TEMPERATURE DISTRIBUTION SYNCHRONOUS ORBIT - TELESCOPE AXIS PARALLEL TO SOLAR VECTOR-BOOM CONDITION

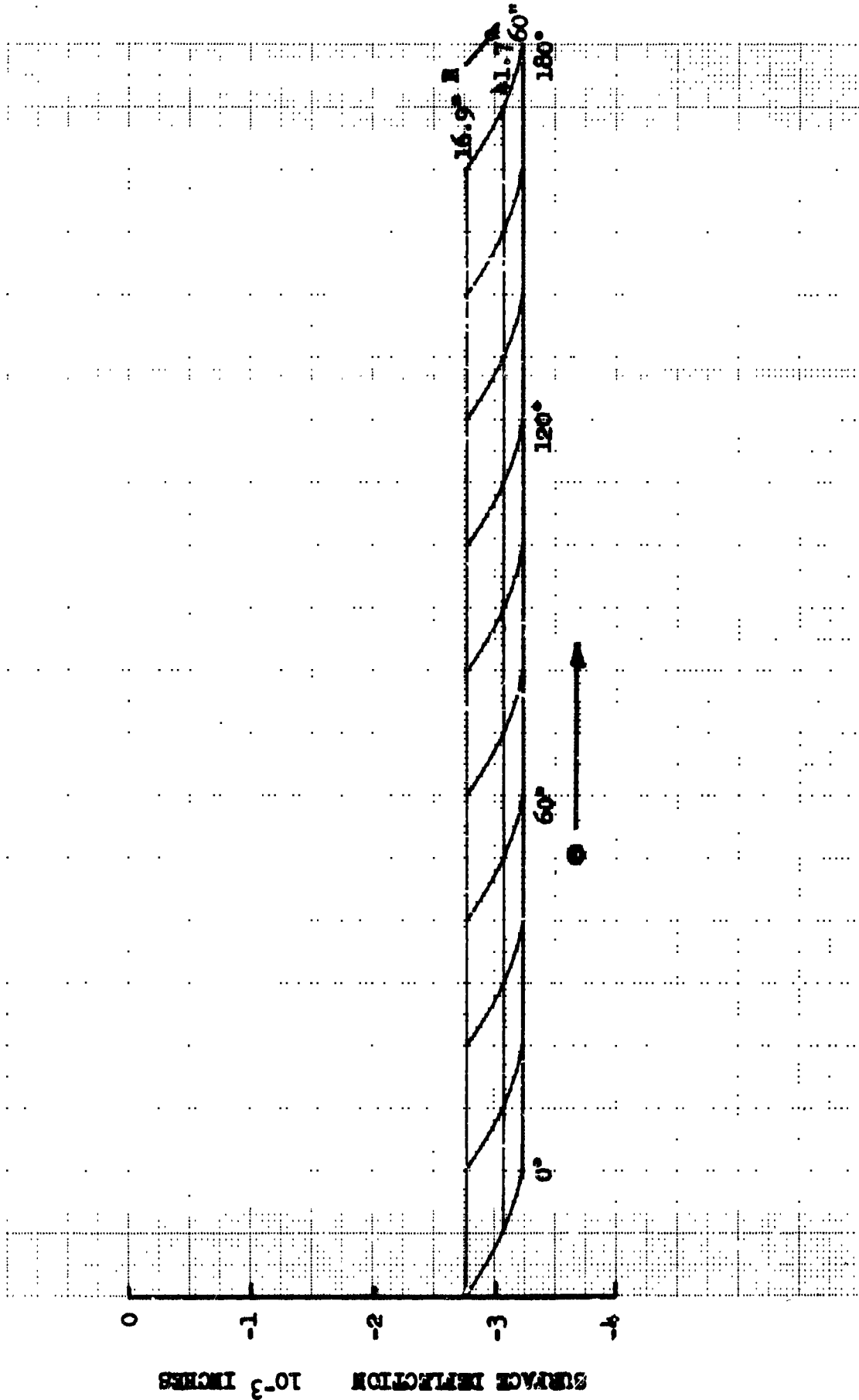


FIGURE 4.1-22 MINOR THERMAL DISTORTIONS SYNCHRONOUS ORBIT - TELESCOPE AXIS PERPENDICULAR TO SOLAR VECTOR

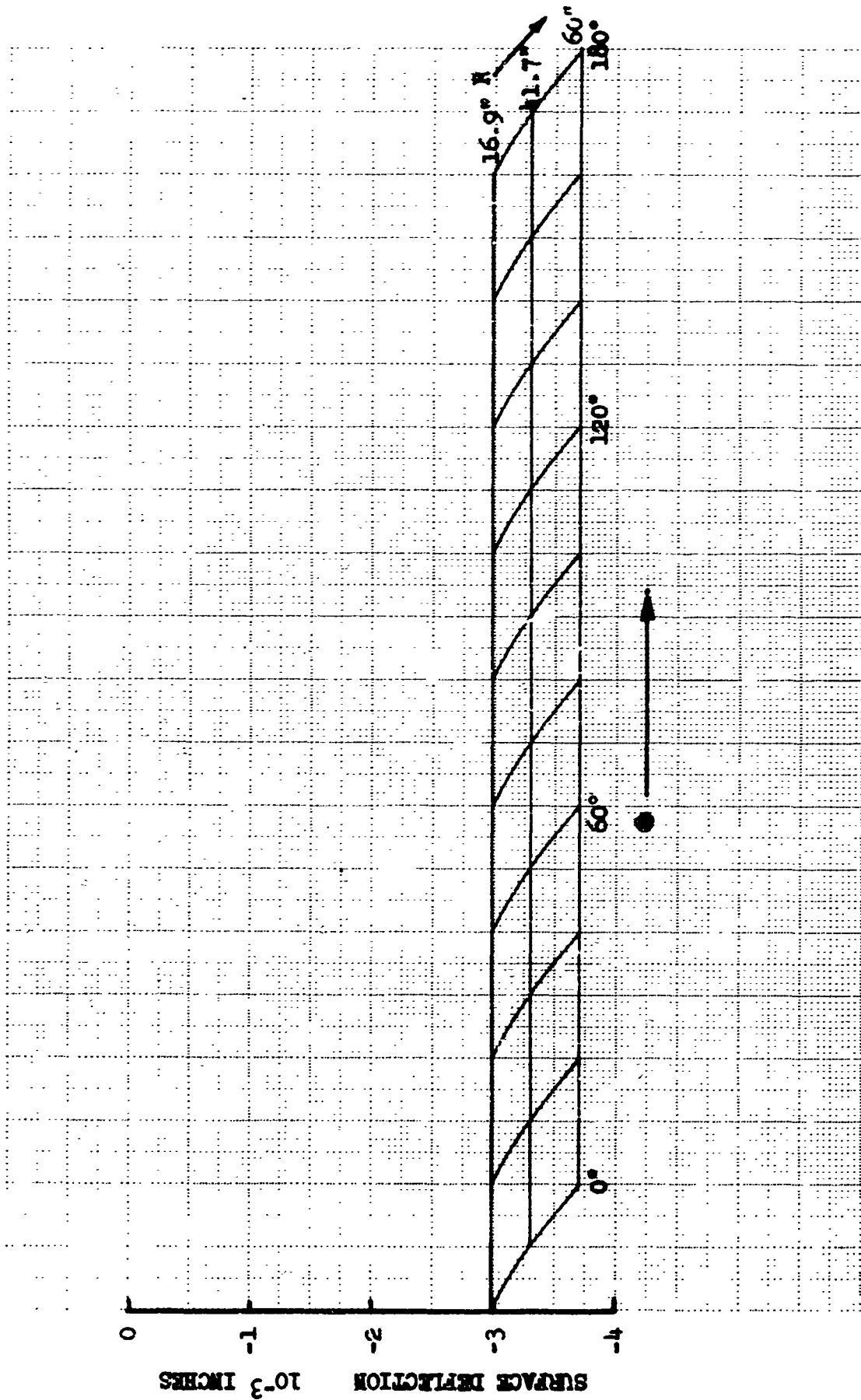


FIGURE 4.1.1-23 MIRROR THERMAL DISTORTIONS SYNCHRONOUS ORBIT -  
TELESCOPE AXIS PARALLEL TO SOLAR VECTOR-DAWN CONDITION

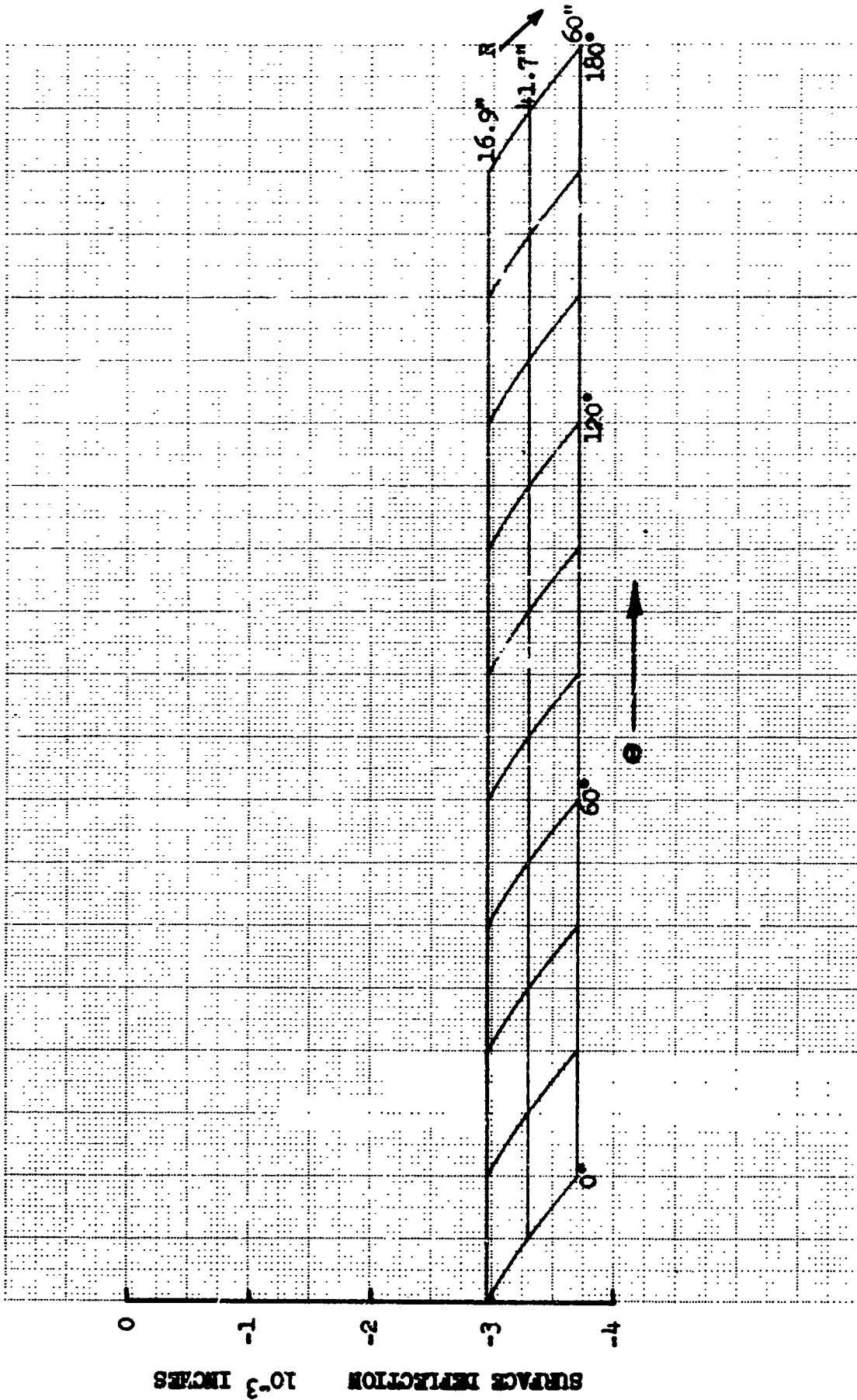


FIGURE 4.1.1-24 MIRROR THERMAL DISTORTIONS SYNCHRONOUS ORBIT - TELESCOPE AXIS PARALLEL TO SOLAR VECTOR-MOON CONDITION



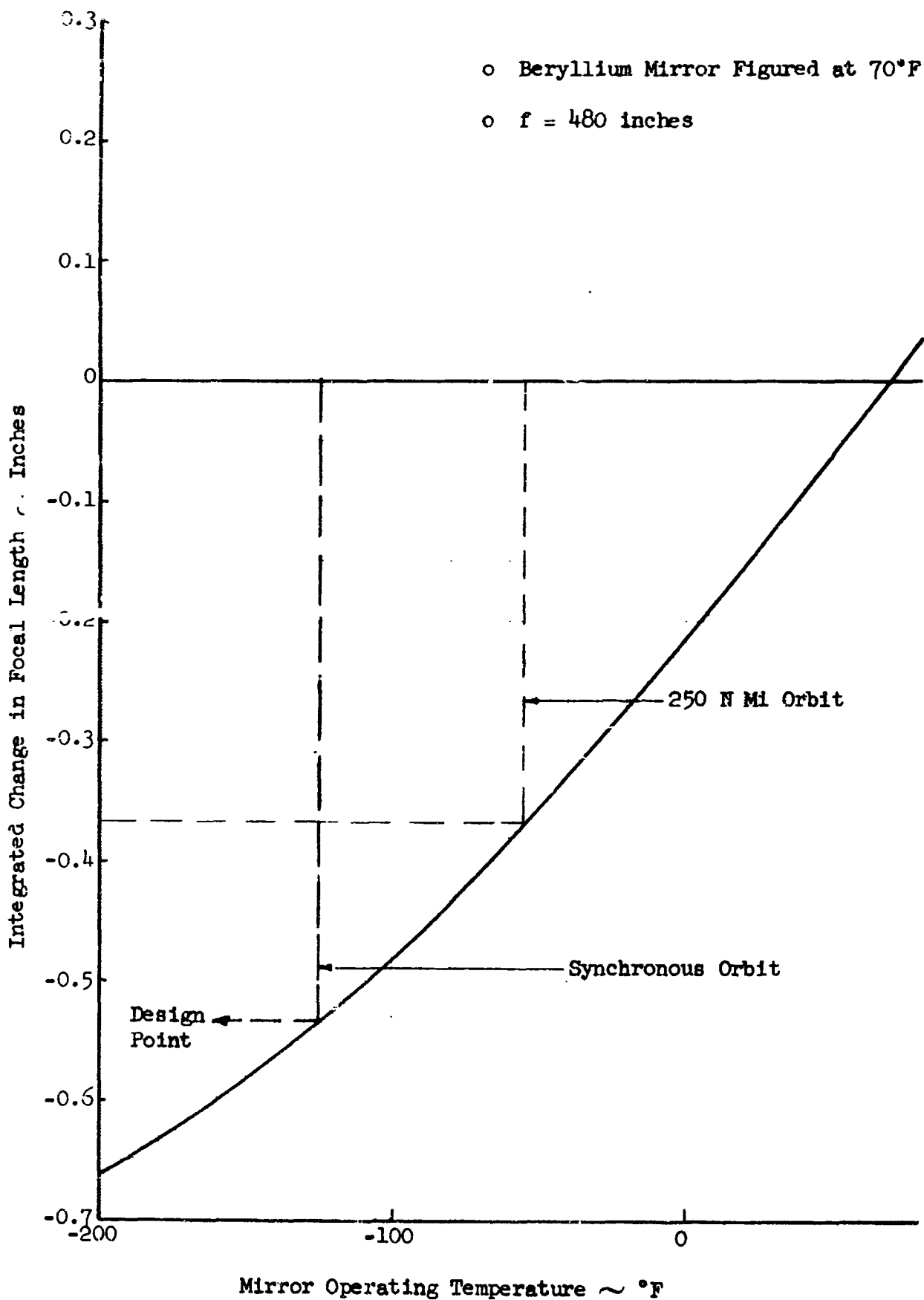


FIGURE 4.1-25 FOCAL LENGTH CHANGE WITH OPERATING TEMPERATURE

## 4.2 ATTITUDE CONTROL

### 4.2.1 Summary and Technical Approach

The attitude-control study was oriented towards satisfying two major objectives: (1) analyze the feasibility of providing adequate attitude control for the synchronous orbit MOT and (2) compare synchronous and low-Earth-orbit operation and the detached- and soft-gimbal-mode configurations. Differences in attitude-control requirements between low-Earth-orbit and synchronous-orbit operations were found to be minimal. The study was then concentrated on the following two tasks:

- Synchronous-Orbit Disturbance Analysis
- Soft-Gimbal-Mode Analysis

Predominant disturbances in synchronous orbit are due to gravity gradient and solar pressure. These two sources require a telescope momentum-storage requirement of 180 ft-lb-sec for one orbit, which ensures that desaturation will not be required during an observation. The corresponding momentum-storage requirement for the low Earth orbit is 355 ft-lb-sec; thus, the two systems are of comparable size.

Simulation of the MOT-MORL combination in the soft-gimbal mode showed that:

- 1) The MOT and MORL ACS's remain stable;
- 2) The MORL control system provides damping for one of the linear degrees of freedom between the MOT and MORL;
- 3) The MORL crew disturbances are attenuated by a factor of 30,000; however, even this level of disturbance can induce excessive MOT pointing errors by interaction with the gimbal friction within the control moment gyros (CMG's);
- 4) The use of a high-frequency MOT ACS with high-frequency CMG's makes the errors quite small.

From an attitude-control viewpoint, there is little difference between operation at low-Earth- or synchronous-orbit altitudes. A slight advantage is accrued in the synchronous orbit due to lower disturbances (lower momentum CMG's), less background light to affect the optical sensors (possibly less sensor noise), and shorter times per observation (relaxed long-term drift requirements). The detached mode remains the more advantageous from the standpoint of ability to maintain the required  $\pm 0.01$ -arc-second pointing stability; however, this accuracy can also be attained with the soft-gimbal configuration.

### 4.2.2 System Description

4.2.2.1 Requirements — The MOT ACS must provide stabilization during the final phase of rendezvous, docking, and stationkeeping with the MORL, as well

as subsequently providing adequate control accuracy to satisfy the scientific experiments.

The Saturn IV-B provides attitude control up to and including injection into synchronous orbit. The MOT attitude-control computer is then activated to command midcourse corrections and the plane-change maneuvers. The MOT ACS is used to complete the rendezvous with the MORL. Latter phases of this rendezvous and the docking are accomplished by the MORL crew commanding MOT motions. This control authority assigned to the MOT is based on results of a Boeing-conducted docking simulation that included the crew in the maneuvering vehicle. However, since the low control authorities found acceptable result in low physiological feedbacks to the crew, it is anticipated that the docking task can be performed equally proficiently by the MORL crew

The most critical control requirement is to provide adequate pointing of the telescope's optical line of sight to meet the experiment requirements. This pointing requirement is identical for both the low-Earth- and synchronous-orbit altitudes, but the total elapsed time to accomplish an observation is different. In the low-Earth-orbit case, some of the longer experiments require multiple-orbit exposures and, consequently, target reacquisition. In the synchronous-orbit altitude, the observation times anticipated are all less than the orbit period; thus, reacquisition requirements are removed and the total time required to perform a given experiment is reduced. Figure 4.2-1 summarizes the accuracy and stability requirements per Reference 1. The highest pointing stability required is  $\pm 0.01$  arc-second ( $2\sigma$ ) during the photographic experiments, while the highest pointing accuracy required is  $\pm 0.01$  arc-second during high-dispersion spectroscopy experiments. Here pointing accuracy is defined as the deviation between the desired pointing and the long-term average of the pointing actually achieved. The pointing stability is defined as the amplitude of the pointing excursions around the long-term average position.

4.2.2.2 Selected Configuration — To keep the system as simple as possible, only single-level vehicle torquers were considered. Techniques such as servoed optics or other dual-level torquing systems may well prove advantageous; however, results with the present system continue to look very encouraging. The selected torquer is a control moment gyro (CMG); its selection being due primarily to its extremely high linearity and response, and secondarily to the size, weight, and power advantages it offers. Like any momentum storage device, the CMG is limited in the amount of angular momentum that it can store and, thus, reaction control jets (RCJ's) must be provided to desaturate or remove the stored angular momentum from the CMG. Previous studies have shown that CMG's cannot be desaturated by the RCJ's without inducing appreciable system errors, thus, the CMG's must have sufficient momentum-storage capability to overcome external disturbances for the longest continuous viewing period required. An analysis of the disturbance environment for the synchronous-orbit MOT indicates Y- and Z-axis momentum-storage requirements of 48 and 180 ft-lb<sub>f</sub>-sec, respectively, for a 24-hour period. This requirement is essentially applicable to either the detached

## INITIAL RENDEZVOUS

Pitch, Roll, Yaw	±0.5 degree
------------------	-------------

## SUN ACQUISITION

Pitch and Yaw	±0.25 degree
Pitch, Yaw, and Roll Rate	±0.09 degree/sec
Acquisition Time	6 minutes

## ORBIT AND STATIONKEEPING

Pitch, Roll, Yaw	±0.5 degree
------------------	-------------

## DOCKING—MOT TO MORL

Pitch, Roll, Yaw	Manual control
Control Authority	0.1 ft/sec <sup>2</sup> —1.0 deg/sec <sup>2</sup>
Maximum Frequency	14 per year

## STAR ACQUISITION

Coarse Pointing—Pitch, Yaw, Roll	±3 arc minutes
Initial Star Acquisition Time	15 minutes
Reorientation in Coarse Mode	5 degrees in 2 minutes, 90 degrees in 30 minutes
Intermediate Pointing	±2 arc seconds

## FINE POINTING

## ON AXIS—MOT optical axis coincident with fine error sensor null axis

Pitch	±0.03 arc second
Yaw	±0.15 arc second
Roll	±3 arc minutes
Star Magnitude	10th magnitude or brighter
Maximum duration	24 hours pointing

## OFF AXIS—MOT optical axis has angular offset from fine pointing sensor null axis

Absolute Pointing	
Pitch, Yaw	±0.2 arc second
Roll	±30 arc seconds
Stability and Repeatability	
Pitch, Yaw	±0.01 arc second
Roll	±0.2 arc second
Star Magnitude	+11 to +13
Maximum Duration	24 hours

Figure 4.2-1: ATTITUDE-CONTROL REQUIREMENTS

or soft-gimbal mode. The CMG's for both the Y and Z axes are sized at 200 ft-lb<sub>f</sub>-sec, thus permitting maneuver rates of up to 4 degrees per minute. (By way of comparison, the Y and Z axes required 600 ft-lb<sub>f</sub>-sec CMG's in the low Earth orbit for control over a 40-minute interval.) Because of lower disturbances and inertias about the X axis, a 60-ft-lb<sub>f</sub>-sec storage capability is adequate.

The synchronous-orbit altitude CMG configuration is the same as that for the low Earth orbit and consists of three twin-rotor, one-degree-of-freedom CMG's, as shown in Figure 4.2-2. This CMG configuration has the advantage of possessing minimum interaxis cross coupling.

To cover the total range of angular measurements required (130 million to one) requires several sensors. Figure 4.2-3 shows how these sensors are used in the attitude-control system. During orbit-plane-change, rendezvous, and docking maneuvers, the gyro reference is used to command the CMG's, which in turn torque the telescope. During this operation, the CMG's require frequent desaturation by the RCJ's.

Attitude control for scientific experiments is initiated by first acquiring the Sun with the Sun sensors and then performing a slow roll around the Sun LOS to permit the coarse-mode star trackers to determine the celestial orientation of the telescope. Control is then switched to these star trackers, which in conjunction with the digital computer continually maintain a knowledge of the MOT's orientation. The coarse star trackers command the CMG's through the digital computer. The other guidance loops operate in a completely analog fashion to avert loss in resolution due to quantization. Once a desired target has been selected by the MORL crew, the coarse star trackers provide command signals to maneuver the telescope to the selected orientation. An intermediate sensor then acquires a guide star (which may or may not be the target star), and control is transferred to this sensor to stabilize the telescope at a point that lies within the range of the fine pointing sensors. There are two fine pointing sensors: an on-axis sensor for high-dispersion stellar spectrometry and an off-axis sensor for all other experiments. With this configuration, the ACS size, weight, power, and resupply requirements are as shown in Figure 4.2-4. The total system weight is 1130 lb<sub>f</sub>, of which some 60 percent must be replaced every year. Although these calculations are made using existing reliability data (and as such are pessimistic), they do emphasize the strong requirement for manned operation of the telescope.

4.2.2.3 CMG Characteristics — The CMG's rotate through complementary angles as shown in Figure 4.2-2 to transfer momentum into the vehicle. One way of constraining the equal and opposite gimbal angles is by the use of gear coupling. Reference 1, however, has shown that one important limitation on system performance is due to friction of the CMG gimbals. Because both the friction and backlash of gearing are objectionable, an alternate constraint mechanism studied at Boeing involves the use of "power tape wheels." Construction and tests of such CMG's have shown that they are ideally suited for high-precision attitude control. One such CMG is shown in Figure 4.2-5. The

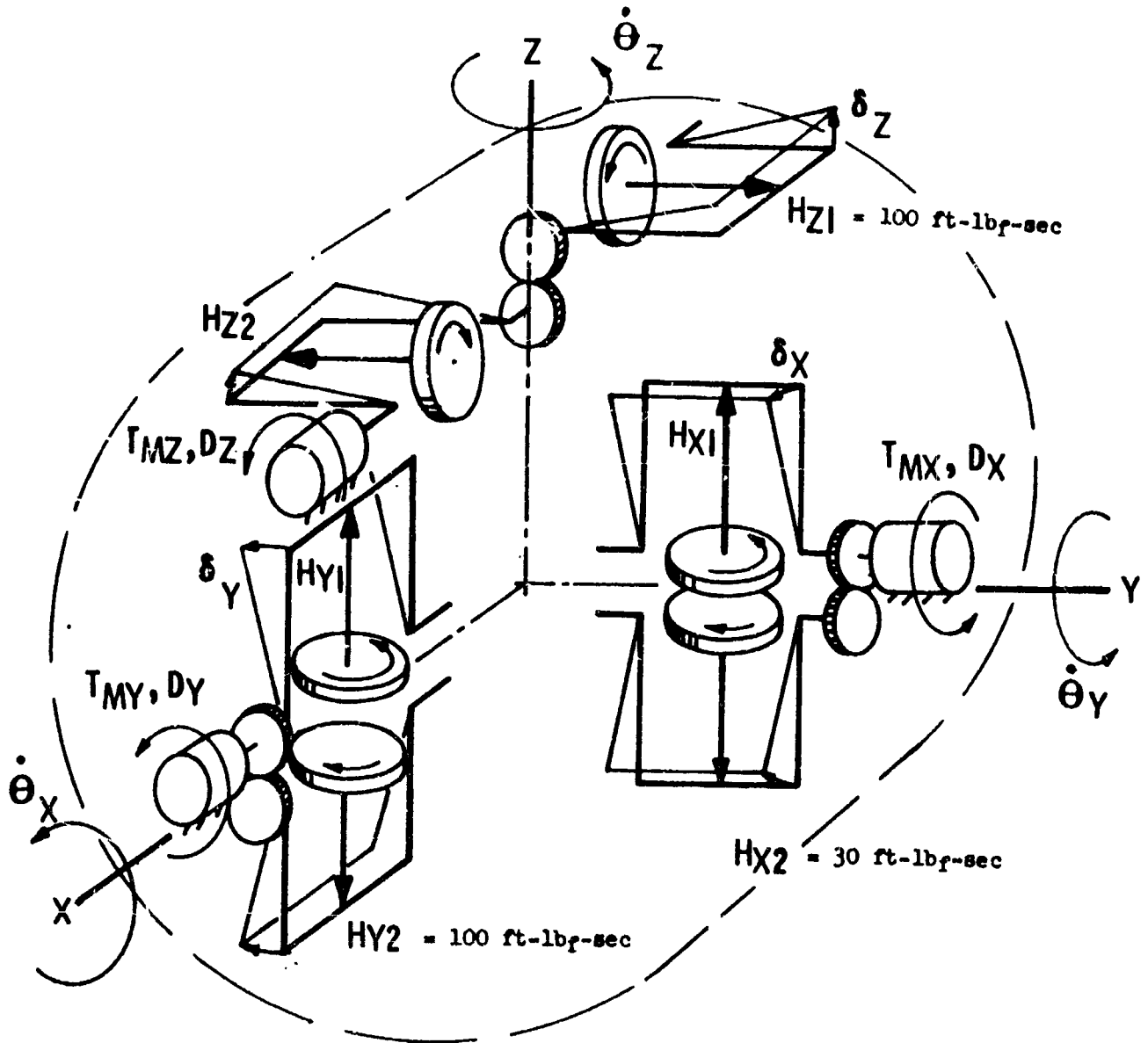


FIGURE 4.2-2  
CMG CONFIGURATION

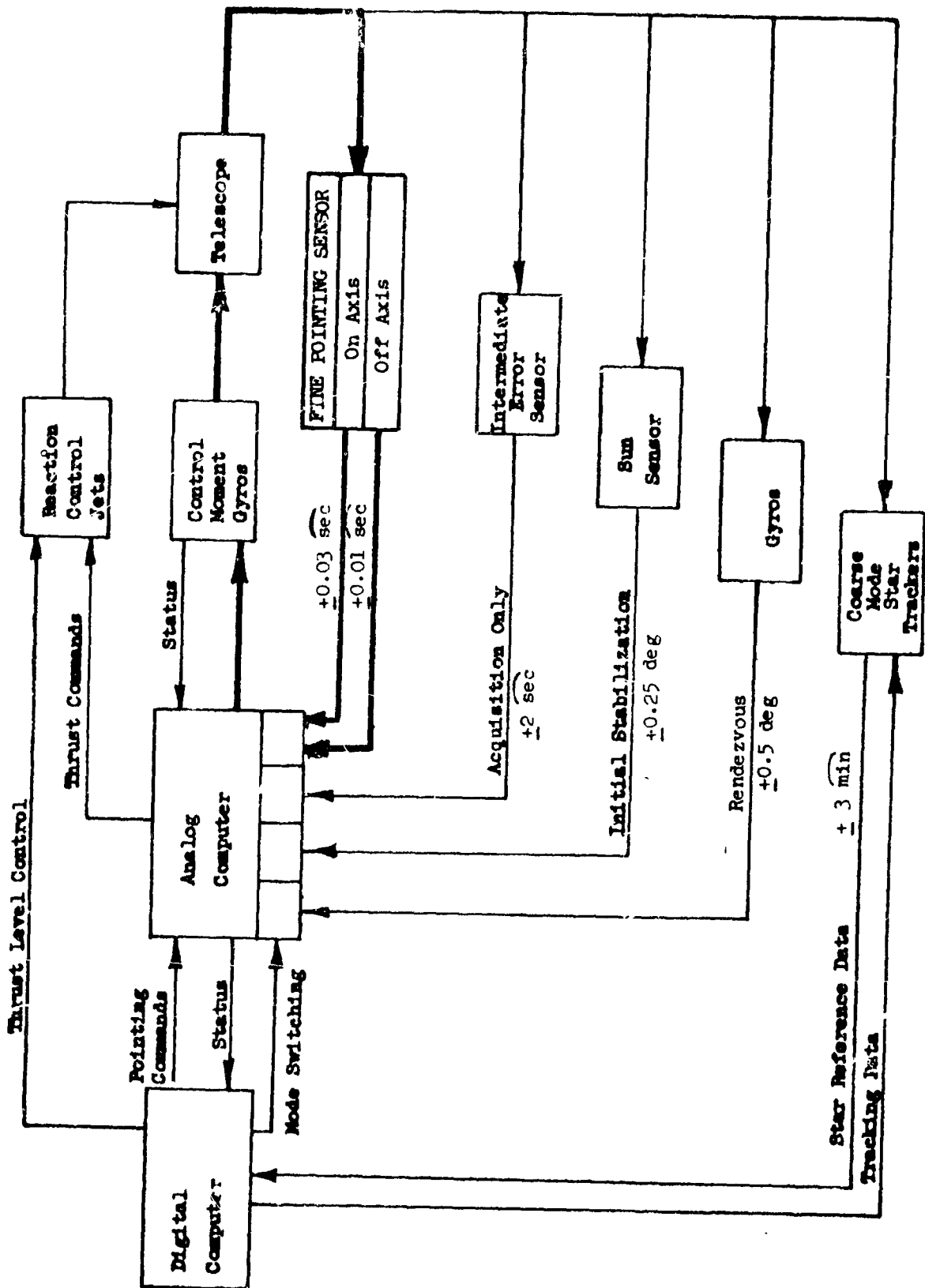


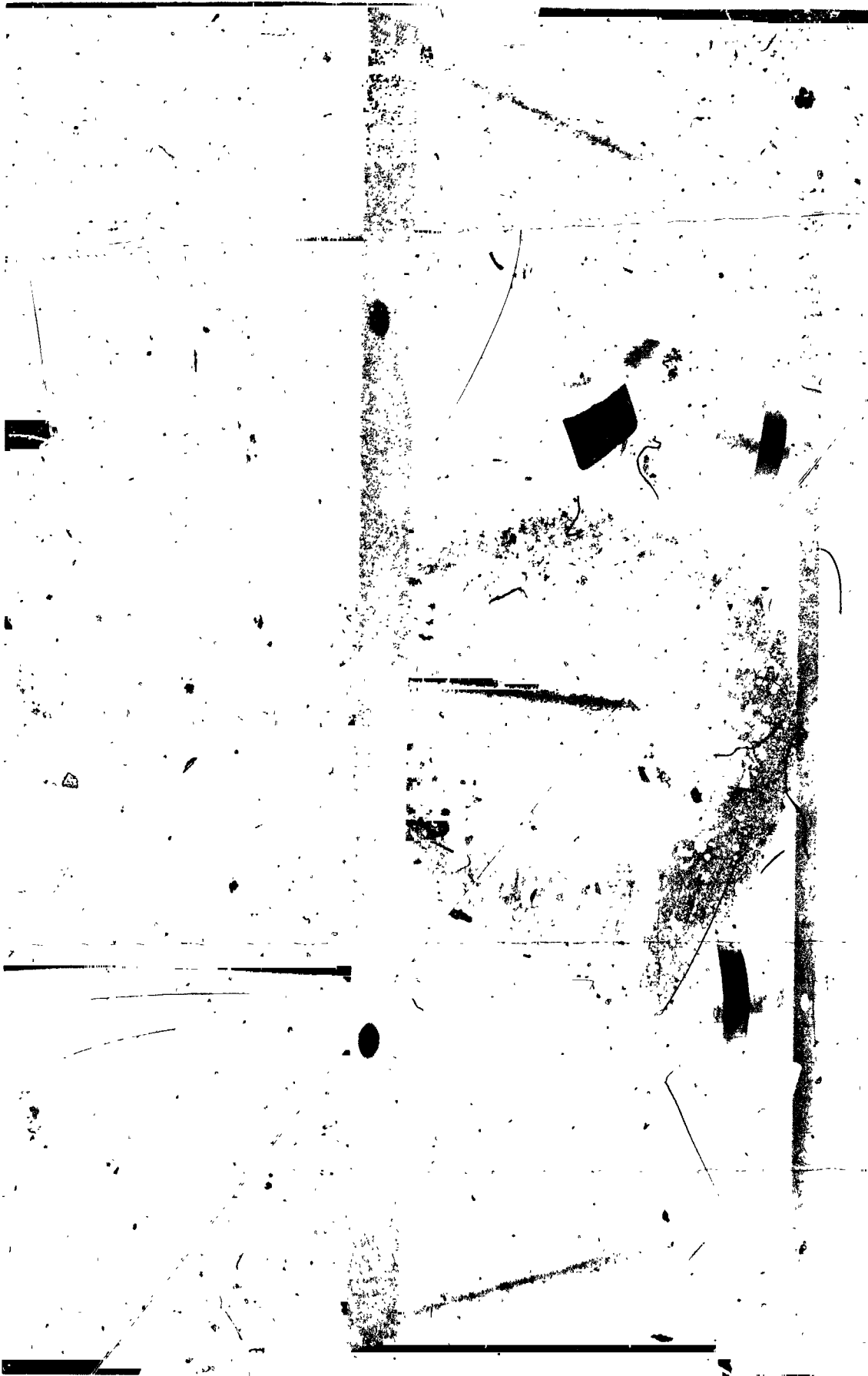
FIGURE 4.2-3  
ATTITUDE CONTROL FUNCTIONAL DIAGRAM

<u>Components</u>	<u>Number Required</u>	<u>Total Spares (No./Year)</u>	<u>Size (Ft<sup>3</sup>/Each)</u>	<u>Weight (Lbf/Each)</u>	<u>Average Power (Watts/Each)</u>
<b>SENSORS</b>					
Sun Sensors	1	0	0.01	3.3	---
Gyro Package	1	1	0.15	16	---
Star Trackers	5	5	1.7	24	1.8
Intermediate Pointing	1	1	2.8	50	15
Fine Pointing					
On Axis	1	0.25	0.12	20	10
Off Axis	1	0.15	0.5	40	10
<b>ELECTRONICS</b>					
Digital Computer	1	0.2	5.3	290	90
Star Tracker	5	1	0.9	27.5	12
Analog Computer	1	0.2	1.0	50	26
CMG Electronics	1	1	1.8	45	15
Sensor Gyro Electronics	1	0.2	0.2	5	12
<b>CMG's</b>					
X Axis	1	1	1.2	54	11
Y Axis	1	1	1.8	90	16
Z Axis	1	1	1.8	90	16
<b>REACTION CONTROL SYSTEM</b>					
	1	1	0.7	120	0.5
<b>Total</b>					<b>290</b>
		716*	30.4	1130	

\*Converted to lb/year

Figure 4.2-4: ATTITUDE-CONTROL PHYSICAL CHARACTERISTICS





**FIGURE 4.2-5**  
**1. DEGREE OF FREEDOM CMG**

White bands are the tape wheels. The rotors are inside the gimbaled black housings. The tape wheels solve the synchronization problem and permit use of a single-gimbal servo. This servo is formed by feeding the gimbal rate as measured by a brushless direct-current tachometer through amplifiers to a brushless direct-current torque motor. By using an active-gimbal servo, high-response CMG's can be used; these help reduce effects of gimbal friction. The gimbal-torque-motor torque capacity is selected to provide torque sufficient for vehicle maneuvering with the CMG. The gimbal inertias are estimated at  $H/2000$  per Reference 1. The estimated gimbal frictions are based on the same Barden A540T3 ball bearings used in Reference 30 (1.5/16-inch outside diameter, 450 lb<sub>f</sub> max load). The CMG specifications are shown in Figure 4.2-6.

FIGURE 4.2-6: CMG SPECIFICATIONS\*

<u>Quantity</u>	<u>Symbol</u>	<u>Dimensions</u>	<u>X Axis</u>	<u>Y and Z Axis</u>
Momentum	2H	ft-lb <sub>f</sub> -sec	60.0	200.0
Gimbal Inertia	2J <sub>G</sub>	in-oz <sub>f</sub> -sec <sup>2</sup>	5.8	19.2
Gimbal Friction	T <sub>f</sub>	in-oz <sub>f</sub>	0.03	0.05
Torque Capacity	T <sub>C</sub>	in-oz <sub>f</sub>	20.0	30.0
Weight		lb <sub>f</sub>	54.0	90.0
Power		watts	11.0	16.0
Steps - Soft		degrees	+60.0	-60.0
Hard		degrees	+65.0	+65.0

\*All values for twin rotor pair

4.2.2.4 Reaction-Control System — The synchronous-orbit-altitude reaction-control system is identical to that of the low-Earth-orbit configuration except for the amount of propellant required. There are 16 reaction-control jets (four clusters of four engines) located 15 feet fore and aft of the center of gravity. Each engine can be modulated in thrust between 4 and 40 lb<sub>f</sub>. The lower levels are used during CMG desaturations (1.4-second pulse); the higher thrust levels are used to obtain adequate control authorities for docking. The characteristics of this system are summarized in Figure 4.2-7.

	<u>Detached MOT</u>	<u>Soft-Gimbal MOT</u>
<u>Reaction Control Jets</u>	4-40 lb <sub>f</sub>	4-40 lb <sub>f</sub>
Thrust	4-40 lb <sub>f</sub>	4-40 lb <sub>f</sub>
Number Required	16	16
Weight	2.5 lb ea.	2.5 lb ea.
I <sub>sp</sub>	300	300
Lever Arms - Pitch	15 ft	15 ft
Lever Arm - Roll	7 ft	7 ft
<u>Tankage and Plumbing</u>		
Number of Tanks	2	2
Total Weight	139 lb	80 lb
<u>Propellant</u>		
CMG Desaturation	5 lb/year	5 lb/year
Cancel Initial Separation Rates	5 lb	5 lb
Docking (35 lb ea)	245 lb/6 months	35 lb (Initial docking)
RCS Rendezvous (12 lb ea)	84 lb/6 months	12 lb

FIGURE 4.2-7: REACTION CONTROL SYSTEM CHARACTERISTICS

4.2.2.5 Sensor Characteristics — The sensor concepts generally follow those of the low-Earth-orbit.

For the coarse mode, four star trackers ring the telescope in the vicinity of the primary mirror; a fifth tracker is mounted along the telescope optical axis in front of the secondary mirrors. Each star tracker is of the OAO type with a 45 degree square field of view capable of tracking stars brighter than +2 magnitude. With this array of star trackers, approximately 83 percent of the celestial sphere is covered; this is adequate to provide reference for any celestial orientation.

The intermediate-level star tracker is again mounted in front of the secondary mirror. It may be either a gimballed beam splitter photomultiplier or an image tube. Of the two, the latter offers several operational advantages in that it has a higher linear range (easier acquisition) and it presents a continuous display of the telescope field-of-view that would be available for use by the MORL crew in selection of targets. It has drawbacks, however, because of its size, weight, power, and complexity (Reference 30). The final choice between these two sensors will require a detailed design evaluation.

There are two fine pointing sensors: one on-axis sensor integral with the high-dispersion spectrograph to satisfy its accuracy requirement and one off-axis sensor on a movable base to satisfy requirements for the other experiments. Although sensor requirements have not been examined in detail to determine if a single off-axis sensor is adequate, the basic requirements are similar enough to make this probable. The fine-pointing sensors consist of beam-splitter type photomultiplier sensors, as shown in Figure 4.2-8. Light collected by the telescope is focused at a mechanical beam splitter where it is divided four ways; the four reflections then impinge on separate photomultiplier tubes. Reference 30 has shown that the basic performance of the fine error sensors are noise limited. Four potential sources of such noise in this type sensor are discussed below.

**Signal Current Noise** — An optical signal can be thought of as the arrival of discrete photons and, as such, are subject to fluctuations or noise. For high-intensity optical signals, these fluctuations are swamped out by the average value of the signal and produce large signal-to-noise ratios. The signal current is the predominant noise source in the MOT fine-pointing sensors.

**Dark Current Noise** — The photocathode of a phototube normally emits electrons when thermally excited. For the fine-pointing sensors, this noise source is appreciable only at much higher magnitude stars (i. e. , +18).

**Load Resistor Johnson Noise** — This source is negligible for the MOT application. Its value can be reduced by increasing the load resistance. Calculations indicate that practical resistance values are seven orders of magnitude above where this noise source becomes appreciable.

**Electronics Preamplifier Noise** — This noise source is also normally negligible due to the extremely high gain available in photomultiplier tubes (current amplifications of  $10^7$ ) reduce the purely electronic amplification required. There are indications, however, that the electron multiplication in the photomultiplier is not completely noiseless, since it decreases the signal-to-noise ratio by  $G/1+G$ , where  $G$  is the gain per dynode stage. Typical photomultipliers have a gain of 3 to 4 per stage, so the contribution of this additional noise is nominal.

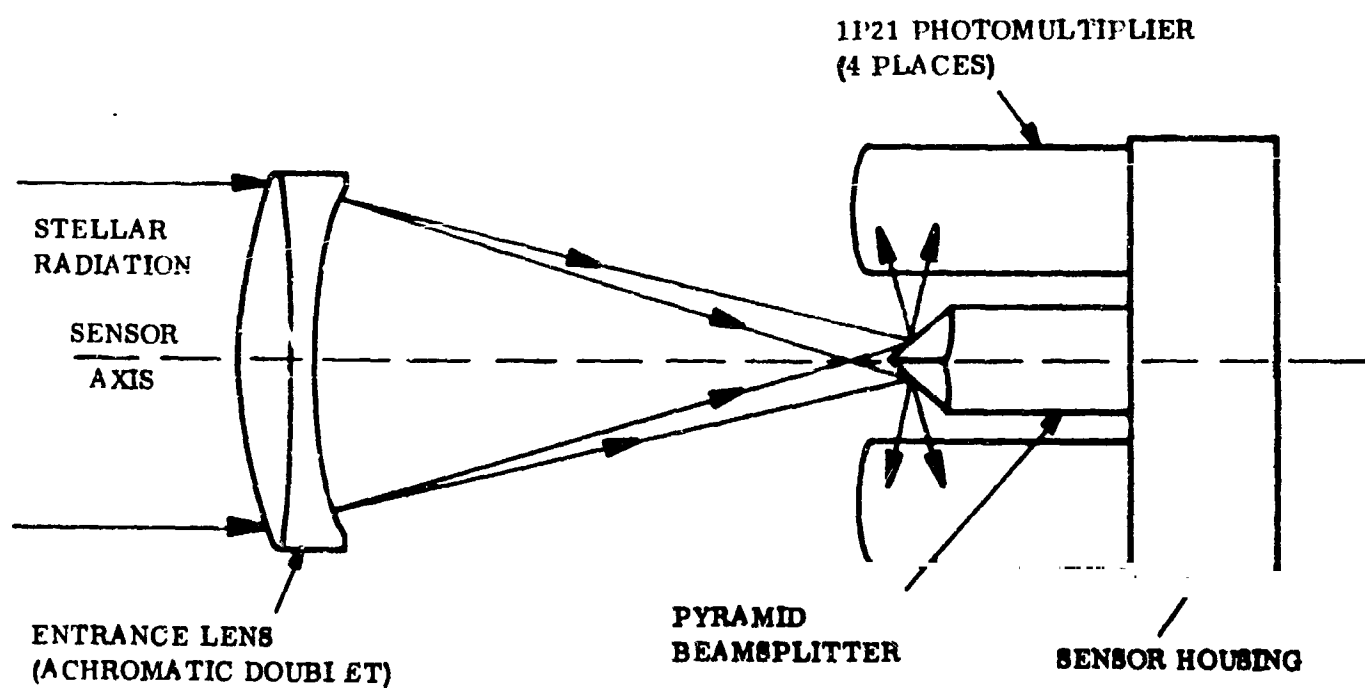


FIGURE 4.2-8

BEAMSPLITTER PHOTOMULTIPLIER FINE POINTING SENSOR

Considering these noise sources, the detector signal-to-noise ratio (S/N) can be expressed as:

$$S/N = \left[ \frac{R \lambda P \lambda}{2 \Delta f \left(1 + \frac{id}{i}\right) \left(1 + \frac{1}{G}\right)} \right]^{1/2} \quad (4.2-1)$$

where  $P\lambda$  = photomultiplier quantum efficiency

$R\lambda$  = photon arrival rate (photons/second)

$\Delta f$  = detector bandwidth, cps

$id$  = photomultiplier dark current noise

$i$  = photomultiplier signal current

$G$  = gain per dynode stage

For  $id \ll i$ , and  $G \gg 1$ , it is seen that the sensor S/N varies with the input signal. At a given input signal level, the only detector parameter available for improving the S/N is the quantum efficiency. For a typical state-of-the-art detector, Figure 4.2-9 shows the pertinent parameters. These parameters can be used to derive the quantum efficiency of the photomultiplier as a function of wavelength as shown in Figure 4.2-10. Also shown is the spectral distribution of a 10th-magnitude Class-A<sub>0</sub> star (using the entire MOT collecting aperture) and the product of the quantum efficiency with this incident energy.

#### Parameters

Spectral response	S-20
Number of stages	14
Photocathode material	K-Na-Cs-Sb
Photocathode diameter	1.68 inches
Maximum cathode sensitivity*	0.064 amps/watt
Anode sensitivity*	$1.4 \times 10^6$ amps/watt
Current amplification*	$2 \times 10^7 = 3.24/\text{stage}$
Equivalent noise input (25°C)*	$7.5 \times 10^{-13}$ lumen = $1.75 \times 10^{-15}$ watts
Window material	Corning lime glass

\*At 2400V anode-to-cathode voltage, unequally distributed.

Figure 4.2-9: RCA 7265 PHOTOMULTIPLIER TUBE

If this product is integrated over the wavelength, approximately 7 percent of the incident photons are converted to electrons by the photoemissive surface. Restricting the discussion to a single axis, since the photomultiplier noise in white, the

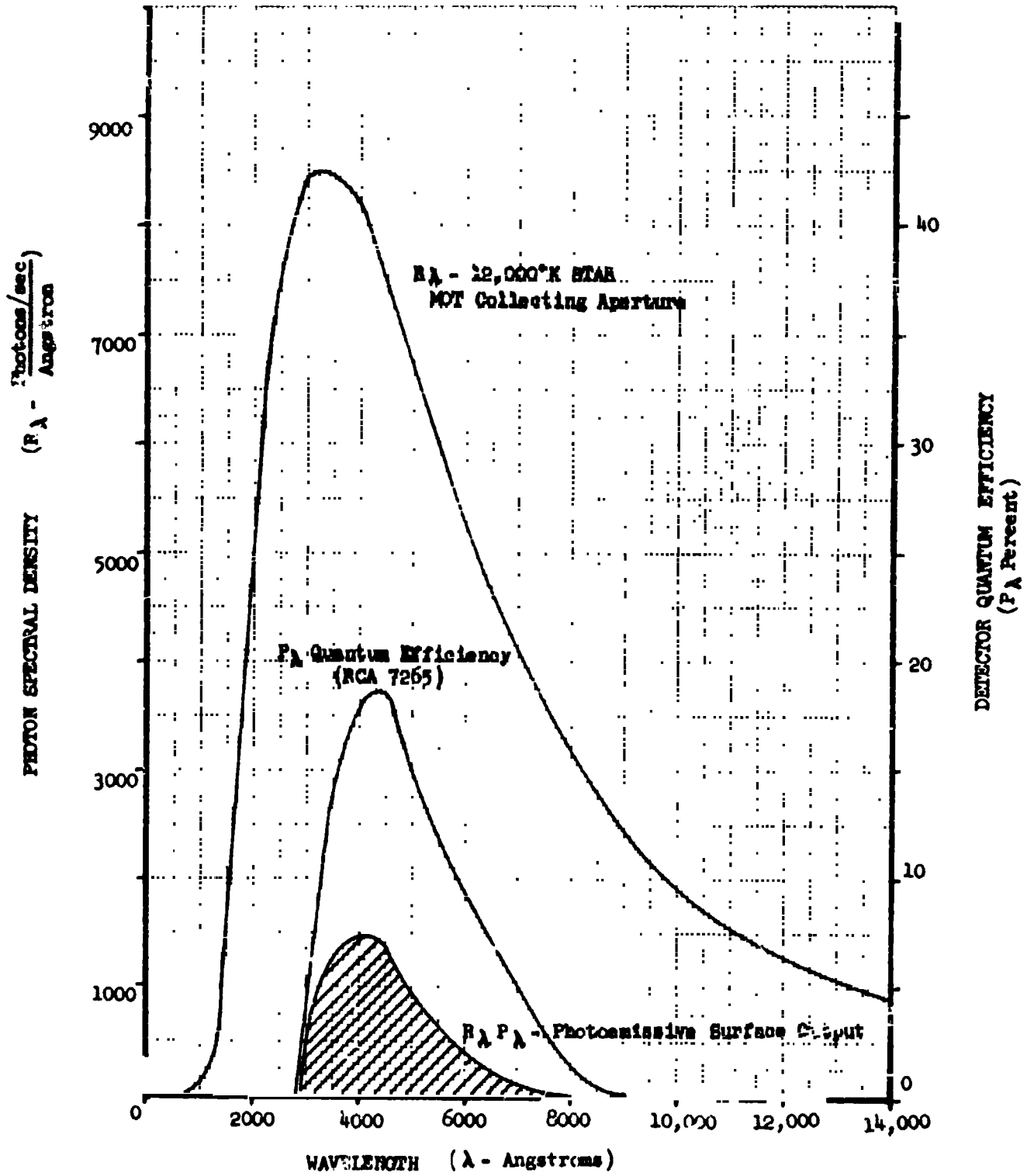


FIGURE 4.2-10  
DETECTOR SPECTRAL CHARACTERISTICS

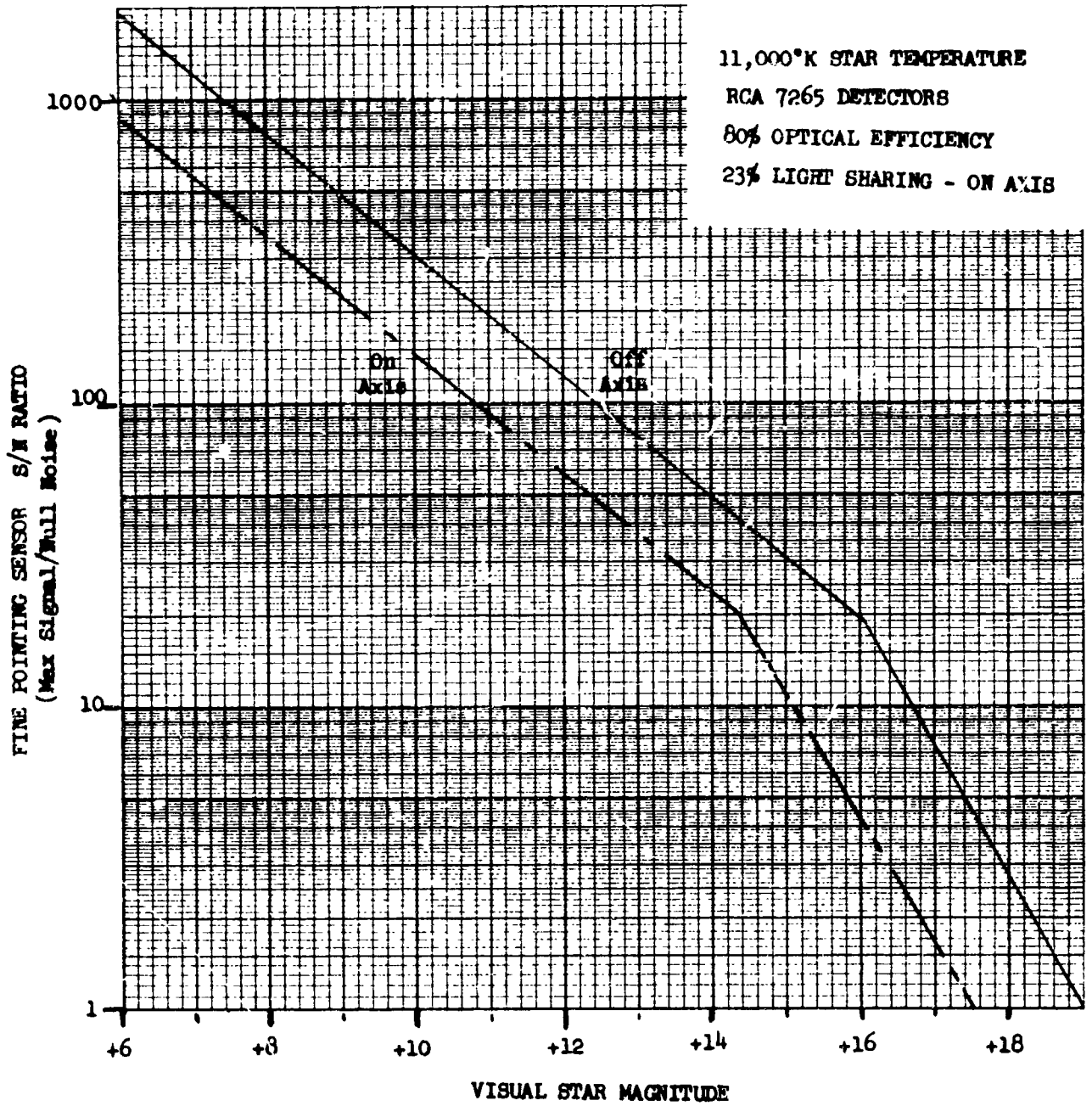
noise at null will be uncorrelated and additive; but, the signals will subtract exactly. The sensor S/N at null will then be zero, and the noise will correspond to twice that of a detector receiving one-quarter of the light. At saturation, the signal will correspond to one detector receiving one-half the light. Because the null noise measured in arc-seconds is the quantity of interest and the sensor linear range must be tailored to achieve it, the maximum signal-to-null noise ratio is the major quantity of interest. Using the spectrums of Figure 4.2-10 and Equation 4.2-1, the sensor S/N can be plotted versus star magnitude as shown in Figure 4.2-11. The difference between the on- and off-axis sensors is due to the 23-percent light sharing for on axis, while the off-axis sensors use the entire collecting aperture. For the on-axis sensor, linear ranges down to  $\pm 0.05$  second are feasible and sensor noises down to 0.000357 second are possible with 10<sup>th</sup> magnitude stars. Since the system stability required is  $\pm 0.03$  second (at 10<sup>th</sup> magnitude), the on-axis sensor is felt to be within present state of the art. For the off-axis sensor, the minimum linear range is governed by how well the Ritchey-Chretien system can correct for off-axis aberrations. The present design anticipates a  $\pm 15$ -minute corrected field of view, and that the maximum aberrations (at the edge of the field) will be less than 0.5 arc-second. From the star-population charts of Reference 30, on the average there will exist at least one 12.5 magnitude star in this field of view, giving a sensor S/N of 100. With the 0.25-arc-second linear range, this S/N corresponds to a sensor noise of 0.0025 arc-second, which may be excessive for the 0.01-arc-second system stabilization required. There are several possible ways in which this could be improved.

- Use of a larger field of view so that higher-magnitude guide stars could be used
- Better correction of the main optics
- Use of lower-bandwidth systems (and, thus, sensors)

For example, using a 1-radian-per-second system (1 cps sensor), the corresponding sensor noise would be 0.000791 arc-second, which is acceptable. (0.001 arc-second was initially allocated to sensor noise.)

It must be remembered, that the sensor characteristics used are for an off-the-shelf detector and that improvements in detectors, as well as methods of minimizing the effects of sensor noise, will be developed. These calculations also assume that the collecting optics can be made sufficiently efficient and that the detector drifts from thermal and aging effects are not excessive. Because the main optics are used for light collecting and only one additional refracting element is anticipated, the collection efficiency should easily exceed 80 percent. Since the drift need be only compatible with the S/N, tolerances up to 1 percent per day are permissible. Further investigation is warranted to ensure that these requirements are not excessive.





FINE POINTING SENSOR S/N RATIO  
FIGURE 4.2-11

### 4.2.3 Analyses

This section describes analyses of the synchronous-orbit disturbance environment and the soft-gimbal mode. The former was accomplished to determine the effects of orbit altitude on the MOT ACS problem, while the latter was accomplished to further the attitude-control comparison of the soft-gimbal and detached MOT.

**4.2.3.1 External Disturbance Summary** — From the study of the synchronous-orbit external disturbances, it was determined that solar pressure predominates; the gravity gradient is the only other appreciable source. In the low Earth orbit, the gravity gradient predominated with aerodynamic torques being the only other appreciable source. Figure 4.2-12 shows a comparison of the low-Earth- and synchronous-orbit disturbance environment. The synchronous-orbit disturbance torques are down by two orders of magnitude. The disturbance momentums would be likewise down on a per time basis; however, the numbers shown are felt to represent a more valid comparison. For the low Earth orbit, the Earth can cause disruption of the experiment every half orbit, so the CMG's could be de-saturated at that time.

	<u>Low Earth Orbit Detached MOT</u>	<u>Synchronous Orbit Detached MOT</u>
Torque (X axis)	$2.3 \times 10^{-3}$ ft-lb <sub>f</sub>	$9.1 \times 10^{-5}$ ft-lb <sub>f</sub>
Torque (Y axis)	0.22 ft-lb <sub>f</sub>	0.0011 ft-lb <sub>f</sub>
Torque (Z axis)	0.22 ft-lb <sub>f</sub>	0.0026 ft-lb <sub>f</sub>
Momentum (X axis)	3.85 ft-lb <sub>f</sub> -sec/half orbit	7.3 ft-lb <sub>f</sub> -sec/orbit
Momentum (Y axis)	353 ft-lb <sub>f</sub> -sec/half orbit	47.6 ft-lb <sub>f</sub> -sec/orbit
Momentum (Z axis)	350 ft-lb <sub>f</sub> -sec/half orbit	180 ft-lb <sub>f</sub> -sec/orbit

Figure 4.2-12: DISTURBANCE COMPARISON

In the synchronous orbit, observations can be continuous, and it is reasonable to expect the CMG's to store the disturbances for the maximum observation time; in this way, requirement for reacquisition is eliminated. Since low-dispersion spectroscopy experiments average 17 hours, the CMG's for the synchronous orbit were sized to provide continuous control for a full orbit. This sizing is also consistent with the CMG momentum required for telescope maneuvering.

The only other important disturbance source is that due to micrometeorites. The impact of a meteorite of appreciable size with the telescope can induce excessive pointing errors. The analysis indicates that the probability of such an event is quite low. It is less than 0.003 per observation period. Also, since the event is of such a short duration, its effect on the anticipated experiments is fairly negligible.

4.2.3.2 Orbital Geometry and Configurations — Due to the solar panels being gimballed around a single axis (the Z axis), the MOT has a preferred roll orientation. Figure 4.2-13 depicts and defines the orbital geometry of this situation. It is seen that retaining the Z axis in a plane perpendicular to the Sun LOS satisfies the solar-panel pointing requirements (with the solar-panel gimbal degree of freedom), while freedom in Euler angles  $\theta$  and  $\phi$  allows the telescope to observe in any direction. For the solar pressure disturbances, only  $\phi$  is of interest since the disturbances are expressed in respect to MOT body axes.

Figures 4.2-14 and 4.2-15 list the parameters used in generating the disturbance calculations. The synchronous-orbit configuration is based on data presented in Section 3.3.

The low-Earth-orbit configuration based on data given to General Electric during the previous MOT study was analyzed to permit a direct comparison of disturbances for the low-Earth- and synchronous-orbit altitude MOT's.

The following sections present results of the analyses of the external disturbances for the synchronous orbit.

4.2.3.3 Solar Pressure — The electromagnetic radiation from the Sun is a primary source of angular disturbance to the vehicle. From quantum theory, this radiation energy can be converted to an equivalent pressure. To form the true torque, this pressure must be integrated over the entire vehicle, taking into account shaded areas, type of reflection and absorption, etc. This leads to a very complex analysis; thus a simplification is normally made to approximate the vehicle by flat plates with given center-of-pressure (cp) to center-of-mass (cm) displacements and uniform reflection properties. For the inertially oriented vehicle, the resulting torques are steady state and the momentum accumulation is proportional to time. From Reference 32, this radiation pressure can be expressed as:

$$P = \frac{S}{c} \cos \phi \left[ \cos\left(\phi + \frac{2}{3}\right) + \rho (1 - A) \cos\left(\phi - \frac{2}{3}\right) \right]$$

$$\tau = \frac{S}{c} \cos \phi \sin \phi \left[ 1 - \rho (1 - B) \right]$$

where  $P$  = solar pressure normal to surface

$\tau$  = solar pressure parallel to surface (shear)

$\frac{S}{c}$  = solar radiation constant =  $9 \times 10^{-8}$  lb<sub>f</sub>/ft<sup>2</sup>

$\phi$  = angle between solar LOS and normal to surface

$\rho$  = surface reflectivity

A, B = type of reflectance (equal to 1 for diffuse reflectance)

Note:  $\bar{K}$  is perpendicular to the solar LOS and is parallel to the ecliptic plane

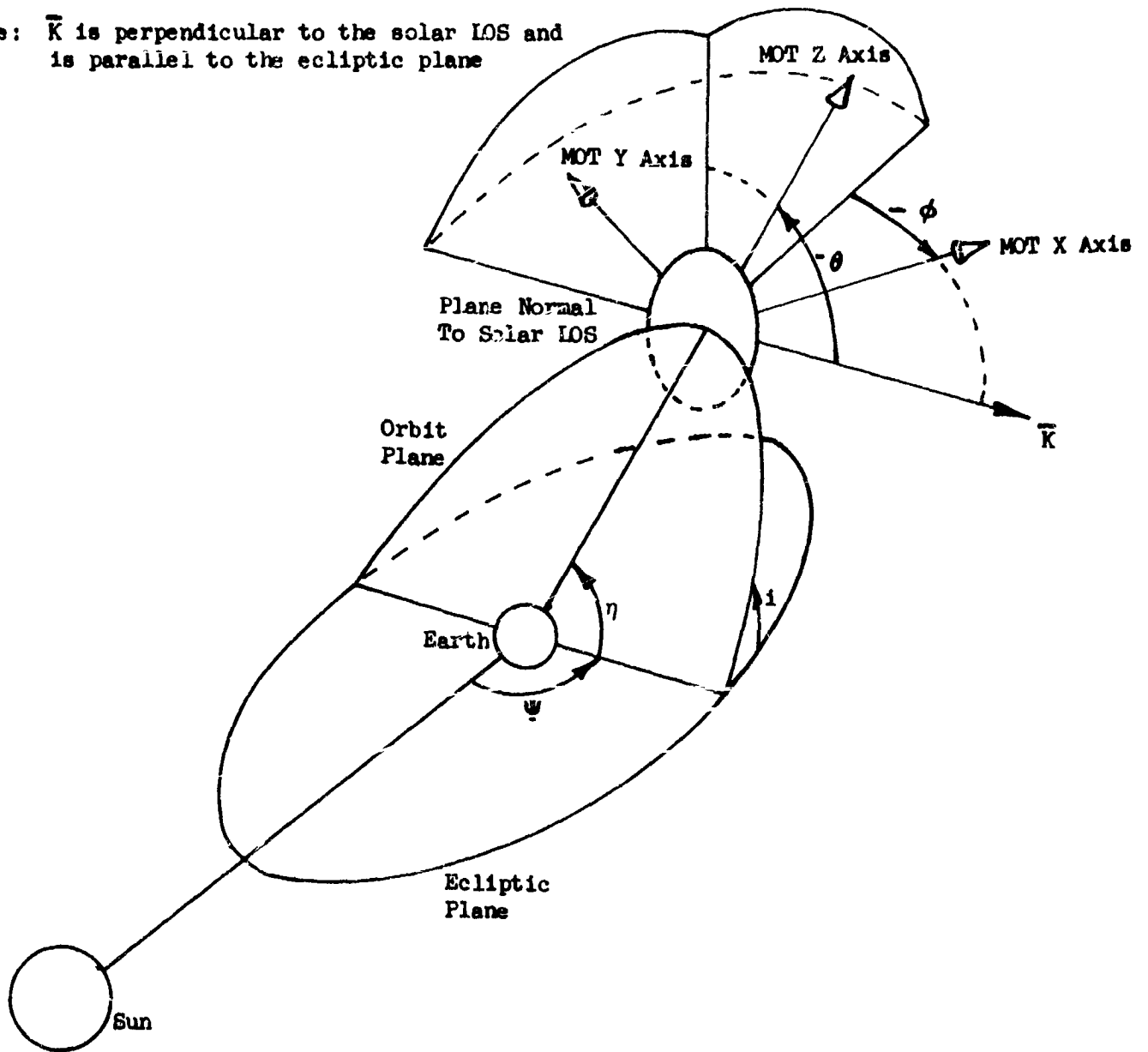
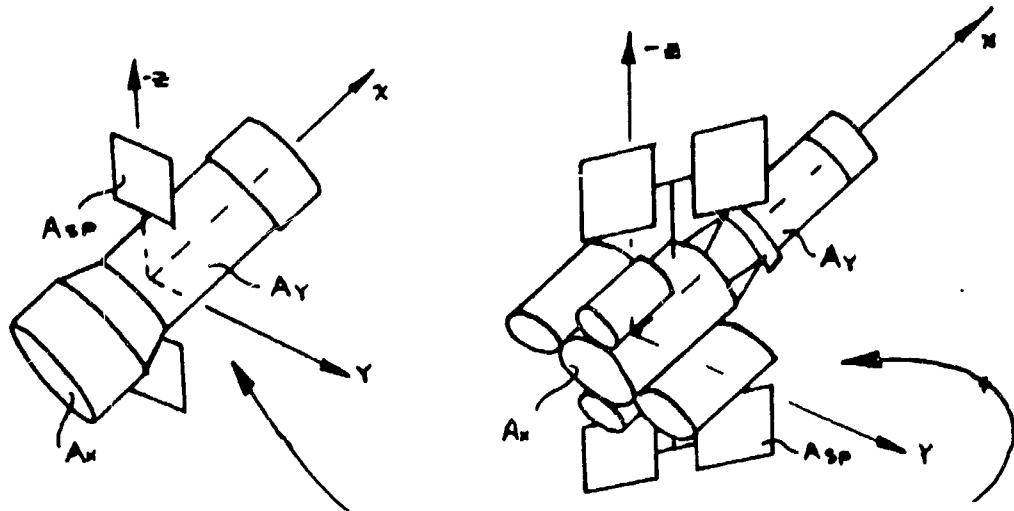


FIGURE 4.2-13

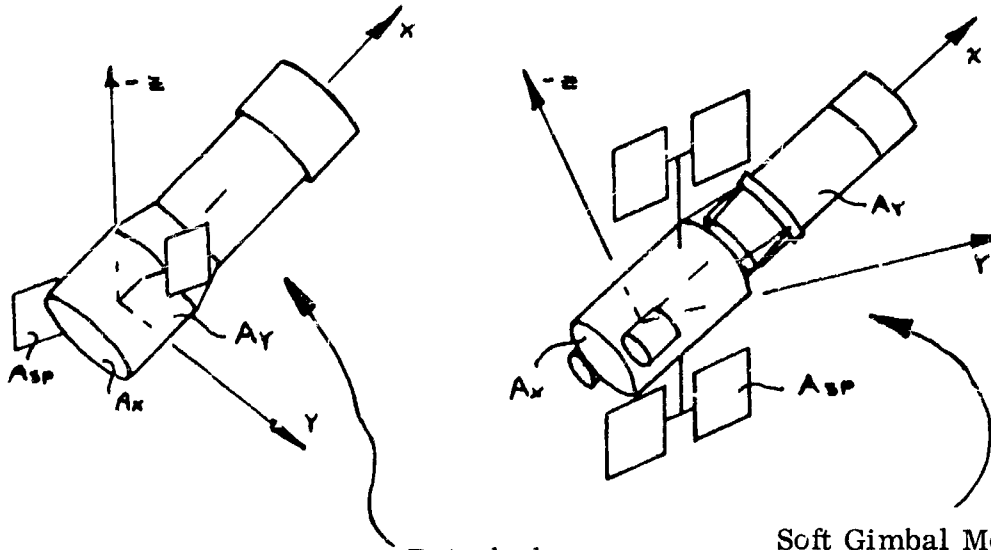
ORBIT AND ORIENTATION GEOMETRY



Parameters and Dimensions	Detached MOT	Soft Gimbal Mode	
		MOT	MOT-MORL
Inertia — Ft Lb <sub>f</sub> Sec <sup>2</sup>			
Ix	25,100	21,100	991,960
Iy	165,000	157,600	1,796,890
Iz	163,200	156,800	2,212,840
Projected Areas — Ft <sup>2</sup>			
Ax	180	---	886
Ay	810	810	2,000
Asp	220	0	1,720
CP-CM Offset — Ft			
Lxx	-16.4	---	-20.7
Lxy	±0.5	---	±2.7
Lxz	±0.5	---	±2.7
Lyx	+12.5	+13.3	+16.4
Lyy	+4.5	+4.5	+5.7
Lyz	+0.5	±0.5	±2.7
Lpx	±0.1	---	+17.7
Lpy	±0.5	---	+2.7
Lpz	±0.5	---	±2.7

Solar pressure based on 19,330-nautical-mile orbit at 45-degree ecliptic inclination.

Figure 4.2-14: SYNCHRONOUS-ORBIT-ALTITUDE CONFIGURATION PARAMETERS



<u>Parameters and Dimensions</u>	<u>Detached</u>	<u>Soft Gimbal Mode</u>	
	<u>MOT</u>	<u>MOT</u>	<u>MOT-MORL</u>
Inertia -- Ft Lb <sub>f</sub> Sec <sup>2</sup>			
Ix	22,000	22,000	382,000
Iy	133,400	133,400	2,110,000
Iz	132,700	132,700	1,940,000
Area -- Ft <sup>2</sup>			
Ax	125	0	370
Av	570	570	1,700
Asp	222	0	1,700
CP-CM Offset -- Ft			
Lxx	-15.5	---	-19.3
Lxy	±0.5	---	±2.7
Lxz	±0.5	---	±2.7
Lyx	+12.3	+12.3	+15.6
Lyy	+4.5	+4.5	+5.7
Lyz	±0.5	±0.5	±2.7
Lpx	±0.1	---	+10.7
Lpy	±0.5	---	±2.7
Lpz	±0.5	---	±2.7

Figure 4.2-15: LOW-EARTH-ORBIT CONFIGURATION PARAMETERS

For calculating solar torques, the vehicle may be approximated by the surfaces shown in Figure 4.2-16. Solar torques arise only from three surfaces shown because the Z surface must remain parallel to the solar line of sight due to solar-panel orientation requirements. The torques from the surfaces are evaluated in the following paragraphs.

Antioptic End of Telescope (Ax) — From the previous study, a flat white paint with a diffuse reflectivity of 0.2 was assumed. The force on Ax is:

$$\bar{F}_X = \left[ Ax \frac{S}{c} \cos \varphi \quad \cos\left(\varphi + \frac{2}{3}\right) \right] \bar{i} - \left[ Ax \frac{S}{c} \cos \varphi \sin \varphi \right] \bar{j}$$

The radius from the telescope cm to the surface cp is:

$$\bar{r}_X = l_{XX} \bar{i} + l_{XY} \bar{j} + l_{XZ} \bar{k}$$

and the torque is:

$$\bar{T}_X = \bar{r}_X \times \bar{F}_X$$

$$\begin{aligned} \bar{T}_X = & \left[ \frac{Ax l_{XZ} S}{c} \cos \varphi \sin \varphi \right] \bar{i} + \left[ \frac{Ax l_{XZ} S}{c} \left( \cos^2 \varphi + \frac{2}{3} \cos \varphi \right) \right] \bar{j} \\ & + \left[ - \frac{Ax l_{XY} S}{c} \left( \cos^2 \varphi + \frac{2}{3} \cos \varphi \right) - \frac{Ax l_{XX} S}{c} \cos \varphi \sin \varphi \right] \bar{k} \end{aligned}$$

Solar Panel — The solar panel will always be facing the Sun, thus, the normal pressure can be resolved as:

$$\bar{F}_{SP} = \left[ \frac{5}{3} A_{SP} \frac{S}{c} \cos \varphi \right] \bar{i} - \left[ \frac{5}{3} A_{SP} \frac{S}{c} \sin \varphi \right] \bar{j}$$

$$\bar{r}_{SP} = l_{PX} \bar{i} + l_{PY} \bar{j} + l_{PZ} \bar{k}$$

$$\begin{aligned} \bar{T}_{SP} = \bar{r}_{SP} \times \bar{F}_{SP} = & \left[ \frac{5}{3} \frac{A_{SP} l_{PZ} S}{c} \sin \varphi \right] \bar{i} + \left[ \frac{5}{3} \frac{A_{SP} l_{PZ} S}{c} \cos \varphi \right] \bar{j} \\ & - \left[ \frac{5}{3} \frac{A_{SP} l_{PX} S}{c} \sin \varphi + \frac{5}{3} \frac{A_{SP} l_{PY} S}{c} \cos \varphi \right] \bar{k} \end{aligned}$$

Transverse Surface (Ay) — Care must be taken because different sides receive the incident radiation depending on the sign of  $\varphi$  (shielding effect). Treating the two transverse surfaces separately, the torques on the +y surface (+ $\varphi$ ) can be expressed as:

$$\begin{aligned} F_{Y+} = & \left[ \frac{Ay S}{c} \cos\left(\frac{\pi}{2} - \varphi\right) \sin\left(\frac{\pi}{2} - \varphi\right) \right] \bar{i} + \left[ - \frac{Ay S}{c} \cos\left(\frac{\pi}{2} - \varphi\right) \left( \frac{2}{3} \right. \right. \\ & \left. \left. + \cos\left(\frac{\pi}{2} - \varphi\right) \right) \right] \bar{j} \end{aligned}$$

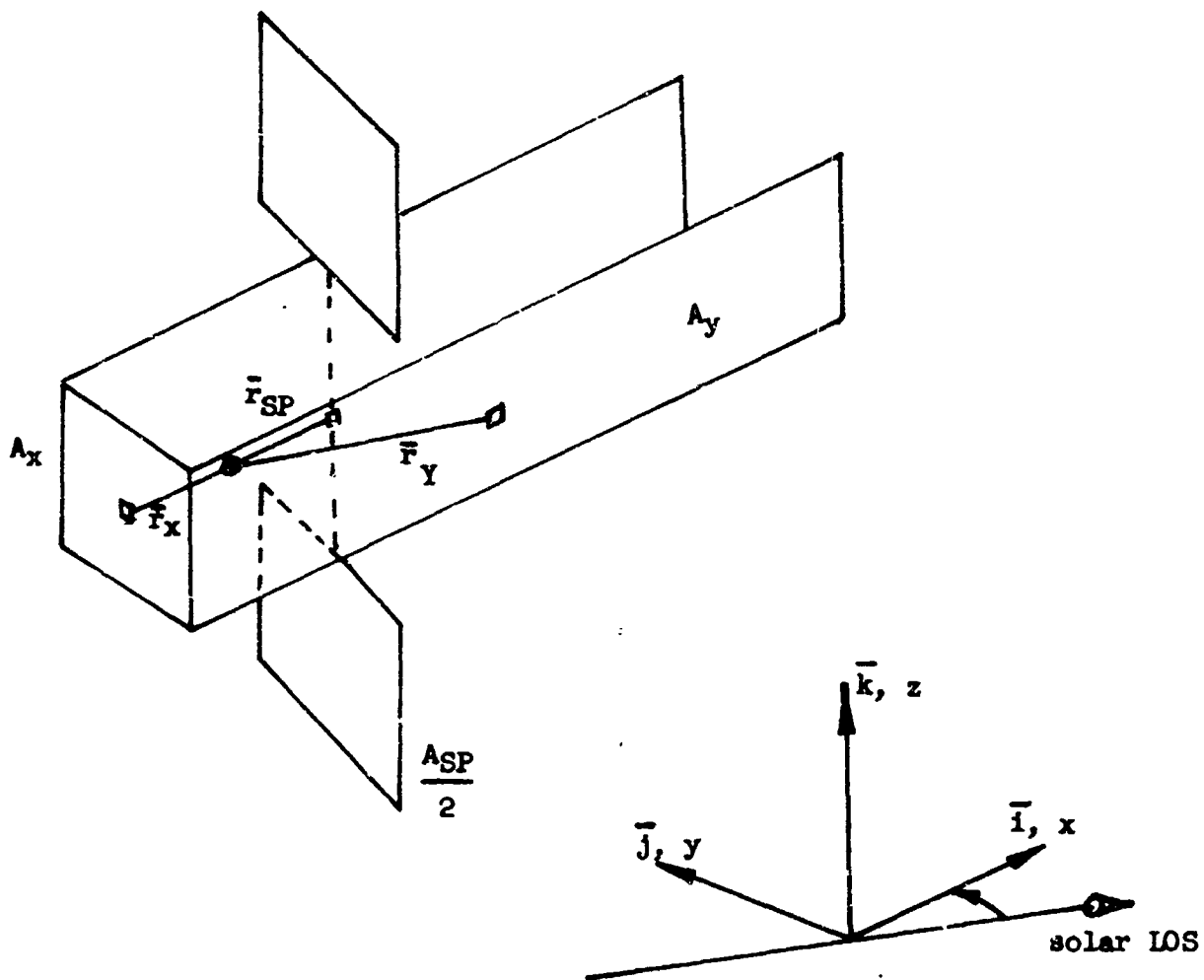


FIGURE 4.2-16  
VEHICLE MODEL FOR SOLAR TORQUES



which can be simplified to:

$$\bar{F}_{y+} = \left[ \frac{A_y S}{c} \sin \varphi \cos \varphi \right] \bar{i} - \left[ \frac{A_y S}{c} \sin \varphi \sin\left(\varphi + \frac{2}{3}\right) \right] \bar{j}$$

$$\bar{r}_{y+} = l_{yx} \bar{i} + l_{yy} \bar{j} + l_{yz} \bar{k}$$

$$\bar{T}_{y+} = \bar{r}_{y+} \times \bar{F}_{y+}$$

$$\begin{aligned} \bar{T}_{y+} = & \left[ \frac{A_y l_{yz} S}{c} \sin \varphi \sin\left(\varphi + \frac{2}{3}\right) \right] \bar{i} + \left[ \frac{A_y l_{yz} S}{c} \sin \varphi \cos \varphi \right] \bar{j} \\ & - \left[ \frac{A_y l_{yy} S}{c} \sin \varphi \cos \varphi + \frac{A_y l_{yx} S}{c} \sin \varphi \sin\left(\varphi + \frac{2}{3}\right) \right] \bar{k} \end{aligned}$$

For  $\pi > \varphi > 0$ .

Similarly, for the -y surface ( $-\varphi$ ):

$$\bar{F}_{y-} = \left[ \frac{A_y S}{c} \cos\left(\frac{\pi}{2} + \varphi\right) \sin\left(\frac{\pi}{2} + \varphi\right) \right] \bar{i} + \left[ \frac{A_y S}{c} \cos\left(\frac{\pi}{2} + \varphi\right) \cos\left(\frac{\pi}{2} + \varphi - \frac{2}{3}\right) \right] \bar{j}$$

which can be simplified to:

$$\bar{F}_{y-} = - \left[ \frac{A_y S}{c} \sin \varphi \cos \varphi \right] \bar{i} - \left[ \frac{A_y S}{c} \sin \varphi \left( - \sin \varphi + \frac{2}{3} \right) \right] \bar{j}$$

$$\bar{r}_{y-} = l_{yx} \bar{i} - l_{yy} \bar{j} + l_{yz} \bar{k}$$

$$\bar{T}_{y-} = \bar{r}_{y-} \times \bar{F}_{y-}$$

$$\begin{aligned} \bar{T}_{y-} = & \left[ \frac{A_y l_{yz} S}{c} \sin \varphi \left( - \sin \varphi + \frac{2}{3} \right) \right] \bar{i} - \left[ \frac{A_y l_{yz} S}{c} \sin \varphi \cos \varphi \right] \bar{j} \\ & - \left[ \frac{A_y l_{yy} S}{c} \sin \varphi \cos \varphi + \frac{A_y l_{yx} S}{c} \sin \varphi \left( - \sin \varphi + \frac{2}{3} \right) \right] \bar{k} \end{aligned}$$

For  $0 > \varphi > -\pi$ .

Combining these two surfaces into a single equation gives:

$$\bar{T}_y = \left[ \frac{A_y I_{yz} S}{c} \sin \varphi \sin\left(|\varphi| + \frac{2}{3}\right) \right] \bar{i} + \left[ \frac{A_y I_{yz} S}{c} \sin |\varphi| \cos \varphi \right] \bar{j} \\ - \left[ \frac{A_y I_{yy} S}{c} \sin \varphi \cos \varphi + \frac{A_y I_{yx} S}{c} \sin \varphi \sin\left(|\varphi| + \frac{2}{3}\right) \right] \bar{k}$$

The equations can thus be combined to obtain total solar pressure torque:

$$T_x = \frac{A_x I_{xz} S}{c} \cos \varphi \sin \varphi + \frac{5 A_{sp} I_{pz} S}{3c} \sin \varphi \\ - \frac{A_y I_{yz} S}{c} \sin \varphi \sin\left(|\varphi| + \frac{2}{3}\right) \\ T_y = \frac{A_x I_{xz} S}{c} \cos \varphi \left(\cos \varphi + \frac{2}{3}\right) + \frac{5 A_{sp} I_{pz} S}{c} \cos \varphi \\ + \frac{A_y I_{yz} S}{c} \cos \varphi \sin |\varphi| \\ T_z = - \frac{A_x I_{xy} S}{c} \left(\cos^2 \varphi + \frac{2}{3} \cos \varphi\right) - \frac{A_x I_{xx} S}{c} \cos \varphi \sin \varphi \\ - \frac{5 A_{sp} I_{px} S}{3c} \sin \varphi - \frac{5 A_{sp} I_{py} S}{3c} \cos \varphi \\ - \frac{A_y I_{yy} S}{c} \sin \varphi \cos \varphi - \frac{A_y I_{yx} S}{c} \sin \varphi \sin\left(|\varphi| + \frac{2}{3}\right)$$

When the configuration parameters from Figure 4.2-14 and 4.2-15 are substituted into these equations, the values shown in Figure 4.2-17 result. Here, the MORL requirements are obtained by subtracting the soft-gimbal MOT requirements from those for the combined vehicles.

**4.2.3.4 Gravity Gradient** — Because the orbit radius varies throughout a satellite, integration of the gravitational attraction force over the body leads to a torque term that, for circular orbits, is expressed by:

$$\begin{bmatrix} L_x \\ L_y \\ L_z \end{bmatrix} = \frac{3 \omega^2}{2} \begin{bmatrix} (I_y - I_z) (\bar{j} \cdot \bar{K}) (\bar{k} \cdot \bar{K}) \\ (I_z - I_x) (\bar{i} \cdot \bar{K}) (\bar{k} \cdot \bar{K}) \\ (I_x - I_y) (\bar{i} \cdot \bar{K}) (\bar{j} \cdot \bar{K}) \end{bmatrix}$$

Low-Earth-Orbit Configuration (in Synchronous Orbit)      Synchronous-Orbit Configuration

	Detached		Soft Gimbal		Detached		Soft Gimbal	
	<u>MOT</u>	<u>MORL</u>	<u>MOT</u>	<u>MORL</u>	<u>MOT</u>	<u>MORL</u>	<u>MOT</u>	<u>MORL</u>
Tx <sup>(1)</sup>	5.9 x 10 <sup>-5</sup>	4.3 x 10 <sup>-5</sup>	1.3 x 10 <sup>-3</sup>	1.3 x 10 <sup>-3</sup>	7.7 x 10 <sup>-5</sup>	6.1 x 10 <sup>-5</sup>	1.4 x 10 <sup>-3</sup>	
Ty <sup>(1)</sup>	2.7 x 10 <sup>-5</sup>	1.3 x 10 <sup>-5</sup>	7.7 x 10 <sup>-4</sup>	7.7 x 10 <sup>-4</sup>	3.8 x 10 <sup>-5</sup>	1.8 x 10 <sup>-5</sup>	9.3 x 10 <sup>-4</sup>	
Tz <sup>(1)</sup>	1.0 x 10 <sup>-3</sup>	1.0 x 10 <sup>-3</sup>	5.6 x 10 <sup>-3</sup>	5.6 x 10 <sup>-3</sup>	1.5 x 10 <sup>-3</sup>	1.6 x 10 <sup>-3</sup>	7.8 x 10 <sup>-3</sup>	
Hx <sup>(2)(3)</sup>	5.15	3.7	116	116	6.7	5.3	123	
Hy <sup>(2)(4)</sup>	2.35	1.1	66.4	66.4	3.3	1.6	80	
H <sub>z</sub> <sup>(2)(3)</sup>	91	91	489	489	132	141	678	

- (1) Ft Lb<sub>f</sub>
- (2) Ft Lb<sub>f</sub> Sec/Orbit
- (3) Hx and Hz evaluated at  $\Phi = \pi/2$
- (4) Hz evaluated at  $\Phi = \pi/4$

Figure 4.2-17: SOLAR-PRESSURE DISTURBANCES

where

- $L_x, L_y, L_z$  = body components of torque  
 $\omega$  = orbital rate  
 $I_x, I_y, I_z$  = vehicle principal moments of inertia  
 $\bar{i}, \bar{j}, \bar{k}$  = body fixed-coordinate system  
 $\bar{K}$  = unit vector along local vertical

This situation may be visualized as the  $\bar{K}$  vector rotating in the inertial  $\bar{i}, \bar{j}, \bar{k}$  coordinate system at the orbital rate. The maximum torque for each axis occurs when  $\bar{K}$  rotates in the plane formed by the other two axes of the  $\bar{i}, \bar{j}, \bar{k}$  coordinate system, and at a time when it is at a 45-degree angle to both. The extremum torques for the synchronous orbit thus become:

$$L_{xm} = \frac{1.59 \times 10^{-8}}{2} (I_y - I_z) \cos 2\omega t$$

$$L_{ym} = \frac{1.59 \times 10^{-8}}{2} (I_z - I_x) \cos 2\omega t$$

$$L_{zm} = \frac{1.59 \times 10^{-8}}{2} (I_x - I_y) \cos 2\omega t$$

These torques are zero averaging; they oscillate at twice orbital frequency.

It is also of interest to determine the long-term accumulation of momentum. The worst case occurs when the local vertical rotates in a plane that bisects two axes and includes the third, the torque about this latter axis becomes:

$$L = \frac{3\omega^2}{2} (\Delta I) \cos^2 \omega t$$

Integrating to determine the maximum momentum accumulated gives:

$$H_{GG} = \frac{3\omega^2}{2} \Delta I \int_0^T \cos^2 \omega t dt$$

$$= \frac{3\omega^2}{4} \Delta I \left[ T + \frac{1}{2\omega} \sin 2\omega T \right]$$

For a complete orbit, this reduces to:

$$H_{GG}/ORBIT = \frac{1.59 \times 10^{-8}}{4} (\Delta I) T$$

where T is the orbit period, and  $\Delta I$  is the difference between the moments of inertia of the other two body axes.

To determine the disturbance momentum applied to the telescope, its inertias are used directly in the equations above. For the MORL, however, the inertias of the combined MORL and MOT are used, and then the disturbances from the MOT, treated as a separate body, are subtracted. The amplitudes of the gravity gradient torques and momentums thus become as shown in Figure 4.2-18.

4.2.3.5 Micrometeorites — Disturbances from micrometeorites are probably the least well defined of all the disturbance sources. This is due to the lack of knowledge of the micrometeorite flux density and the corresponding velocity distribution. Figure 4.2-19 shows a composite of the current estimates of the meteoroid flux density. It is observed that the spread in these estimates is over four orders of magnitude, which lends little confidence to the accuracy of final results. In spite of this uncertainty, the calculations of micrometeorite disturbances are useful for gross estimation of their importance. As shown by Curve 1 of Figure 4.2-19, the micrometeorite flux density varies with the particle mass according to:

$$F = m^{-4/3} \times 10^{-14.4}$$

where

$F$  = micrometeorite flux density-particles/meter<sup>2</sup> - sec

$m$  = micrometeorite mass - gm<sub>m</sub>

This flux density can be converted to an equivalent pressure by integration as below:

$$P = \int_m \frac{F m V_p}{g_e} dm$$

Where  $V_p$  is the micrometeorite mean velocity, assumed 22 km/sec (Reference 34). This expression can be integrated yielding an equivalent micrometeoroid pressure of:

$$P = - \frac{4 V_p}{10^{10.4} g_e} = 7.3 \times 10^{-11} \text{ lb}_f/\text{ft}^2$$

Again, when compared with the secular solar pressure of  $9 \times 10^{-8} \text{ lb}_f/\text{ft}^2$ , the micrometeorite average disturbances are negligible. An appreciable effect remains, however, and that concerns the probability of a single impact inducing appreciable vehicle errors.

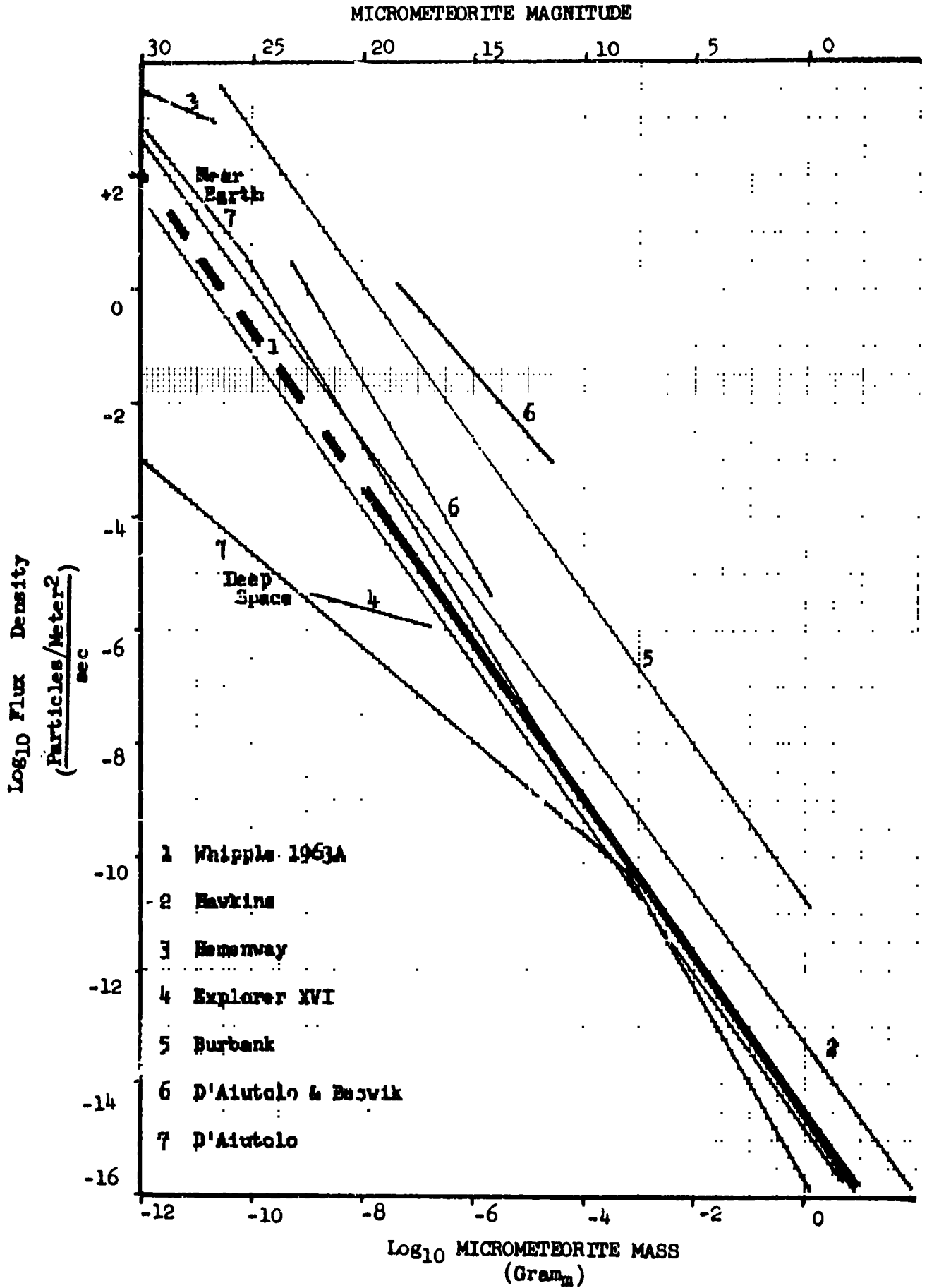
Using the total area and a 20-hour observation, the meteorite flux density can be proportioned to the number of impacts per observation. Using the vehicle inertia and mean cp-cm displacement, the micrometeorite mass can be proportioned to an induced vehicle rate.

	Low-Earth-Orbit Configuration (In Synchronous Orbit)		Synchronous-Orbit Configuration	
	<u>Detached</u> <u>MOT</u>	<u>Soft Gimbal</u> <u>MOT</u> <u>MORL</u>	<u>Detached</u> <u>MOT</u>	<u>Soft Gimbal</u> <u>MOT</u> <u>MORL</u>
T <sub>x</sub> <sup>(1)</sup>	5.5 x 10 <sup>-6</sup>	5.5 x 10 <sup>-6</sup> 0.0013	1.4 x 10 <sup>-5</sup>	6.3 x 10 <sup>-6</sup> 3.3 x 10 <sup>-3</sup>
T <sub>y</sub> <sup>(1)</sup>	8.8 x 10 <sup>-4</sup>	8.8 x 10 <sup>-4</sup> 0.011	1.1 x 10 <sup>-3</sup>	1.1 x 10 <sup>-3</sup> 8.7 x 10 <sup>-3</sup>
T <sub>z</sub> <sup>(1)</sup>	8.9 x 10 <sup>-4</sup>	8.9 x 10 <sup>-4</sup> 0.013	1.11 x 10 <sup>-3</sup>	1.4 x 10 <sup>-3</sup> 5.0 x 10 <sup>-3</sup>
H <sub>x</sub> <sup>(2)</sup>	0.24	0.24      58.3	0.62	0.27      143
H <sub>y</sub> <sup>(2)</sup>	38.2	38.2      500	47.6	46.5      373
H <sub>z</sub> <sup>(2)</sup>	38.4	38.4      556	48.1	47      230

(1) Ft Lb<sub>f</sub>

(2) Ft Lb<sub>f</sub> Sec

Figure 4.2-18: GRAVITY GRADIENT DISTURBANCES



Doing so for the detached telescope, the results are shown in Figure 4.2-20. Using the results of the initial servoelastic study, Page 162 of Reference 30, a 0.21-arc-second overshoot is shown for an initial rate error of 0.2 arc-second per second. Assuming this same correspondence at 0.01 arc-second, the corresponding probabilities are in the neighborhood of 0.003 per observation, which would indicate a negligible effect. Probability of the disturbance causing loss of acquisition (5 arc-seconds) can be seen to be negligibly small. The probability that multiple impacts could induce appreciable pointing errors has been neglected due to the extreme time coincidence required. An interesting conclusion can be drawn by again referring to Curve 7 of Figure 4.2-19. This shows a large difference in the micrometeorite flux density between that at low Earth orbit and that in deep space. Although the magnitude of this effect is somewhat controversial, its existence is corroborated by the Earth dust belts and satellite test data, such as that from Pioneer I and Mariner II. To induce a rate of 0.01 arc-second per second however, a micrometeorite mass of  $10^{-4}$  gram or greater is required, and in this area the currently hypothesized differences between low-Earth- and synchronous-orbit altitude flux densities are lost in the uncertainties of the data.

Another effect is that of periodic micrometeorite showers, during which the flux densities can increase by a factor of 20. These effects are predictable and in general not excessive, so they have been neglected in the above calculations.

4.2.3.6 Aerodynamic Torques — Aerodynamic torques at synchronous-orbit altitude are completely negligible. Reference 33 gives the average electron concentration of the upper ionosphere (5.6 Earth radii) at 70 electrons per  $\text{cm}^3$ . Because proton density is equal to the electron density at the altitude, this concentration corresponds to a dynamic pressure of  $2.6 \times 10^{-12}$   $\text{lb}_f/\text{ft}^2$ . This value is roughly four orders of magnitude less than the secular solar pressure, so the aerodynamic disturbances are neglected.

4.2.3.7 Magnetic Torques — No source of significant disturbance arises from reaction against the Earth's magnetic field, if the vehicle is not designed with a permanent magnetic dipole. Since no inherent requirement for a magnetic dipole is known, magnetic torques are neglected as a source of disturbance; however, it remains an outside possibility for use in desaturating the CMG's. This would provide continuous desaturation and permit use of very small CMG's. Initial calculations indicate the power consumption would be prohibitive (roughly 1.3 kilowatts); however, the use of superconducting coils and configuration control could alleviate this situation.

4.2.3.8 Solar Corpuscular Radiation — Corpuscular radiation — high-speed protons and other charged particles — has a flux density that varies appreciably (dependant partly on solar flares) but an average value has been estimated at  $10^{-23}$   $\text{gm}_m/\text{cm}^3$  at a mean velocity of 300 km/sec (Reference 36). This value corresponds to an equivalent dynamic pressure of  $9 \times 10^{-12}$   $\text{lb}_f/\text{ft}^2$ . Again, when compared to the pressure from electromagnetic radiation, this dynamic pressure is considered negligible.



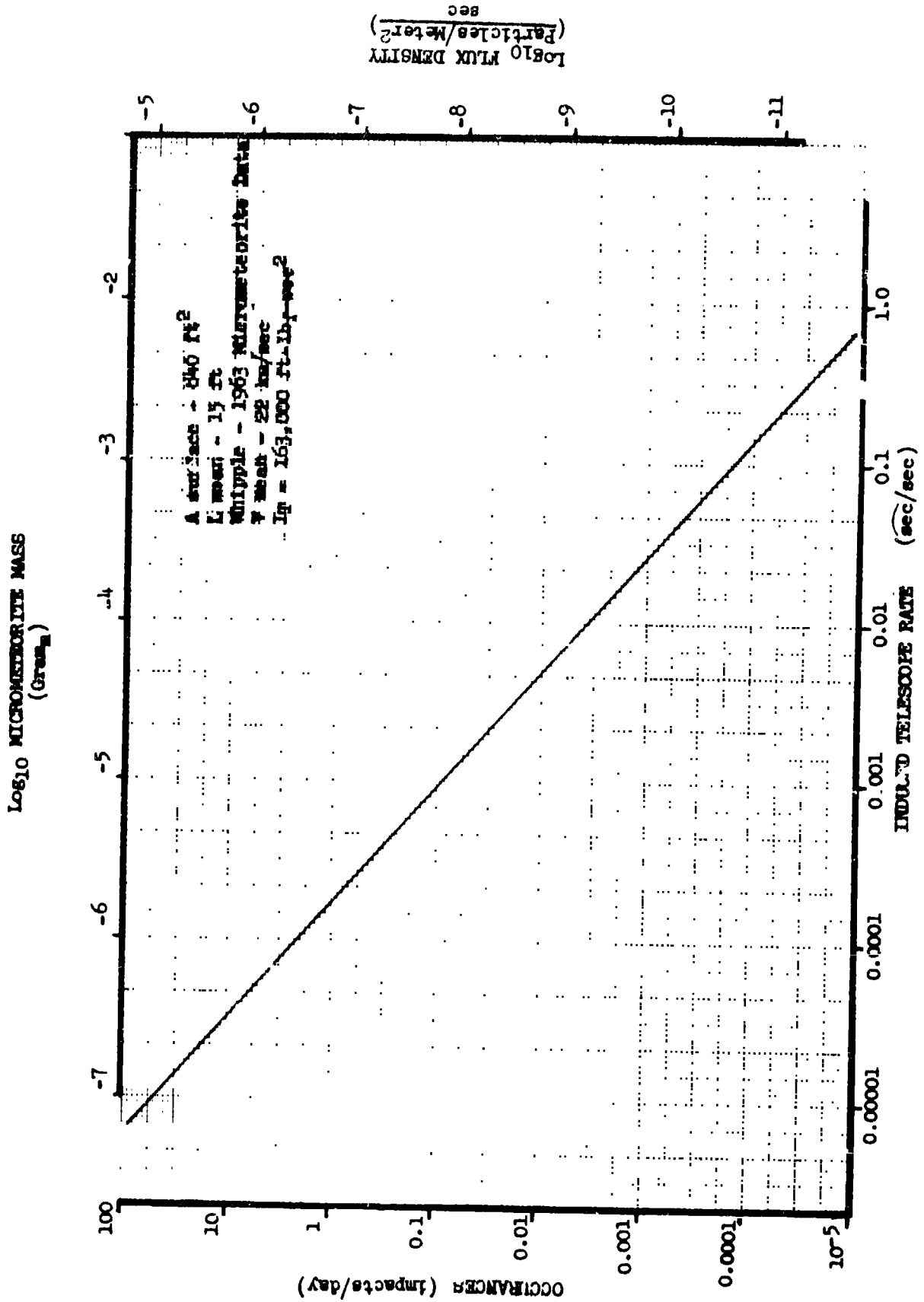


FIGURE 4.2-20  
MICROMETEORITE DISTURBANCES

4.2.3.9 Soft-Gimbal Disturbances — Analysis of the soft-gimbal suspension indicates that the MORL exerts a torque of 0.0332 ft-lb<sub>f</sub> for every degree of misalignment between the MOT and MORL. The MORL attitude-control system is accurate only to ±0.5 degree, the largest errors are due to the attitude references. The maximum soft-gimbal torque could thus be as large as 0.0316 ft-lb<sub>f</sub>, if this torque is assumed to be an undirectional maximum, MOT CMG's of 2700 ft-lb<sub>f</sub>-sec/orbit capacity would be required. This size is unwarranted; the requirement can be eliminated by updating the MORL reference system from the MOT CMG's to prevent their saturation. This technique would also permit the CMG's to be much smaller than the selected 200-ft-lb<sub>f</sub>-sec capacity, if the CMG gimbal friction makes this desirable.

4.2.3.10 Total Disturbance Environment — The preceding analyses can be used to determine the total disturbances that the attitude-control system must overcome. These analyses indicate that the only significant sources are due to solar pressure and gravity gradient. While an exact solution to determine the maximum disturbance of the combination involves solution of rather complex transcendental equations, some useful conclusions can be derived by observing the quasi worst-case condition shown in Figure 4.2-21 (symbols per Figure 4.2-13).

	$\psi$ <u>Radians</u>	$\theta$ <u>Radians</u>	$\phi$ <u>Radians</u>	<u>Combination</u>
X Axis	$\pi/2$	0	$\pi/2$	Additive
Y Axis	0	0	$\pi/2$	G.G Alone
Z Axis	$\pi/2$	$\pi/2$	$\pi/2$	Additive

i = 45° INCLINED ORBIT

Figure 4.2-21: MAXIMUM DISTURBANCE ORIENTATIONS

It is seen that the X- and Z-axis maximum disturbances combine directly at the orientations shown. No such orientation was found for the Y axis but the gravity gradient predominates; it is thus considered to be of little significance. Maximum disturbance torques and momentum storage requirements for the various configurations are given in Figure 4.2-22.

Figure 4.2-23 shows a typical history of the total-disturbance environment for the Z axis. These disturbances are based on the worst-case orbital-ecliptic inclination of 45 degrees. Other inclinations can give considerably smaller disturbance levels. Other changes, such as relocation of the solar panels, can also minimize these disturbances.

4.2.3.11 Soft-Gimbal Analysis — The soft-gimbal mode was conceived as a result of the attitude-control-panel discussions (MOT low-Earth-orbit midterm) concerning the stationkeeping problem in the "floating socket" mode. Because of the timing, it was not possible to study the soft-gimbal mode in the same depth

Low-Earth-Orbit Configuration (In Synchronous Orbit)      Synchronous-Orbit Configuration

	Detached		Soft Gimbal		Detached		Soft Gimbal	
	<u>MOT</u>	<u>MORL</u>	<u>MOT</u>	<u>MORL</u>	<u>MOT</u>	<u>MORL</u>	<u>MOT</u>	<u>MORL</u>
Tx <sup>(1)</sup>	6.5 x 10 <sup>-5</sup>	4.8 x 10 <sup>-5</sup>	4.8 x 10 <sup>-5</sup>	2.6 x 10 <sup>-3</sup>	9.1 x 10 <sup>-5</sup>	6.7 x 10 <sup>-5</sup>	6.7 x 10 <sup>-5</sup>	4.7 x 10 <sup>-3</sup>
Ty <sup>(1)</sup>	8.8 x 10 <sup>-4</sup>	8.8 x 10 <sup>-4</sup>	8.8 x 10 <sup>-4</sup>	1.1 x 10 <sup>-2</sup>	1.1 x 10 <sup>-3</sup>	1.1 x 10 <sup>-3</sup>	1.1 x 10 <sup>-3</sup>	8.7 x 10 <sup>-3</sup>
Tz <sup>(1)</sup>	1.9 x 10 <sup>-3</sup>	1.9 x 10 <sup>-3</sup>	1.9 x 10 <sup>-3</sup>	1.9 x 10 <sup>-2</sup>	2.6 x 10 <sup>-3</sup>	3.0 x 10 <sup>-3</sup>	3.0 x 10 <sup>-3</sup>	1.3 x 10 <sup>-2</sup>
Hx <sup>(2)</sup>	5.4	3.9 *	3.9 *	174	7.3	5.6 *	5.6 *	266
Hy <sup>(2)</sup>	38.2	38.2*	38.2*	500	47.6	46.5*	46.5*	373
H <sub>z</sub> <sup>(2)</sup>	129	129 *	129 *	1045	180	188 *	188 *	908

(1) Ft Lb<sub>f</sub>

(2) Ft Lb<sub>f</sub> Sec/Orbit

\* Not including spring torques on MOT in soft-gimbal mode

Figure 4.2-22: TOTAL SYNCHRONOUS ORBIT DISTURBANCE ENVIRONMENT\*

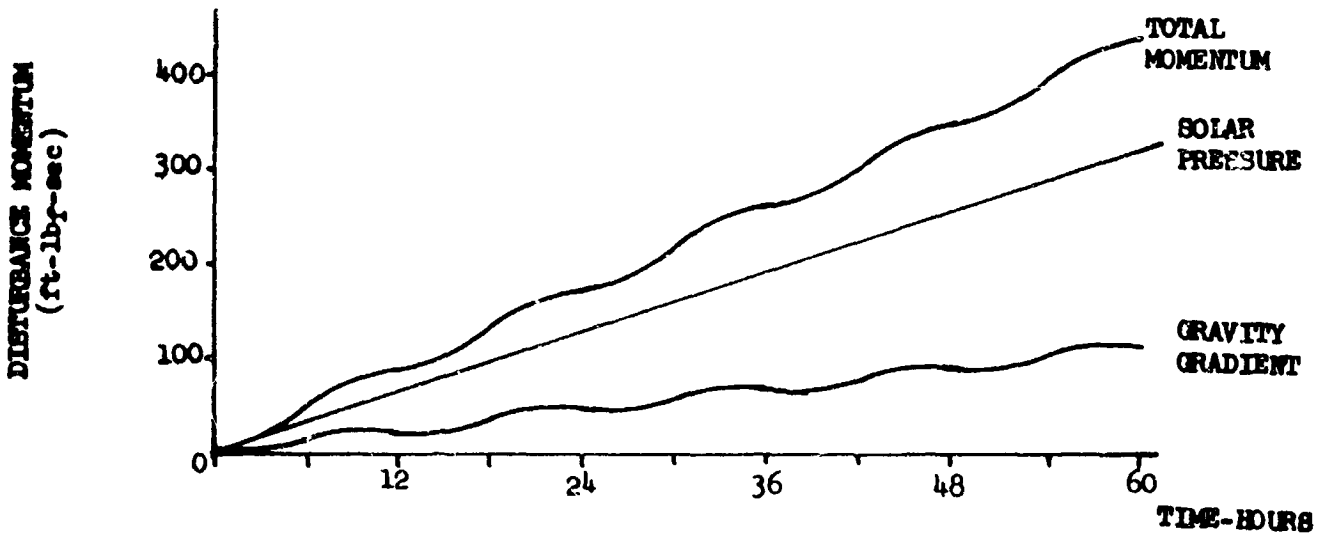
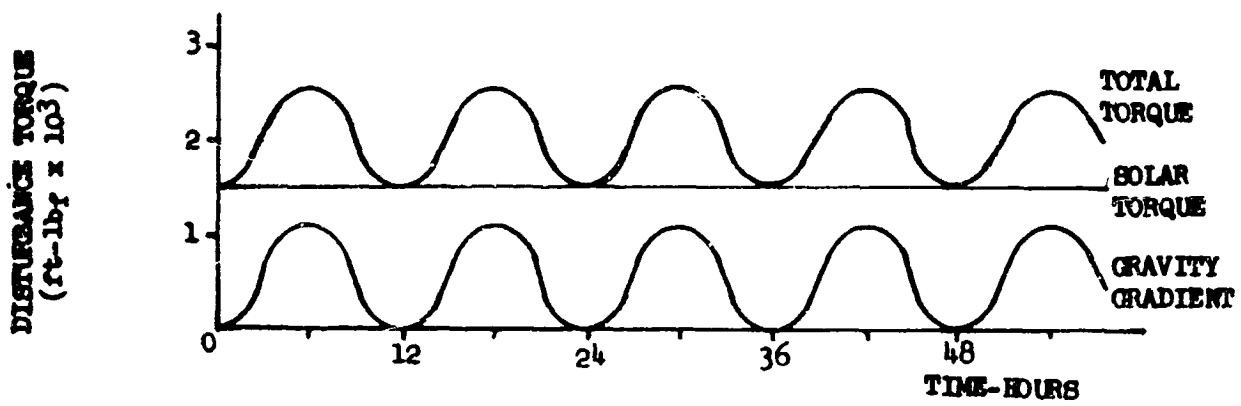


FIGURE 4.2-23  
EXTERNAL DISTURBANCE TIME HISTORIES

as that of the detached mode. Consequently, questions remained at the conclusion of the low-Earth-orbit study as to whether the coupled MORL and MOT attitude-control systems remained stable and if stable, what effect this coupling might have on the ACS pointing performance. The soft-gimbal mode thus received much more attention in this study, thereby permitting a more valid comparison of the soft-gimbal and detached modes. Equations of motion of the system are derived below; these equations were programmed in an analog computer simulation. Figure 4.2-24 shows a sketch of the dynamic model and quantities used to derive these equations. The spring geometry considered consisted of three sets of two springs equally spaced between the MORL and the MOT gimbal, which, in turn, was assumed massless and frictionless. The motion was restricted to be coplanar only in order to accomplish the task within the study contract constraints. Forces and torques acting on the MORL and MOT are derived by assuming relative displacements across the geometric orientations of the spring sets; from geometry these displacements can be related to the system independent variables as below.

$$\begin{aligned}
 dZ_1 &= Z_m - Z_T + l_m \varphi_m - l_t \theta_T \\
 dZ_2 &= Z_m - Z_T + l_m \varphi_m - l_t \theta_T \\
 dX_1 &= X_m - X_T + r_m \varphi_m + r_T \theta_T \\
 dX_2 &= X_m - X_T + \frac{r_m}{2} \varphi_m - \frac{r_T}{2} \theta_T
 \end{aligned}
 \tag{1}$$

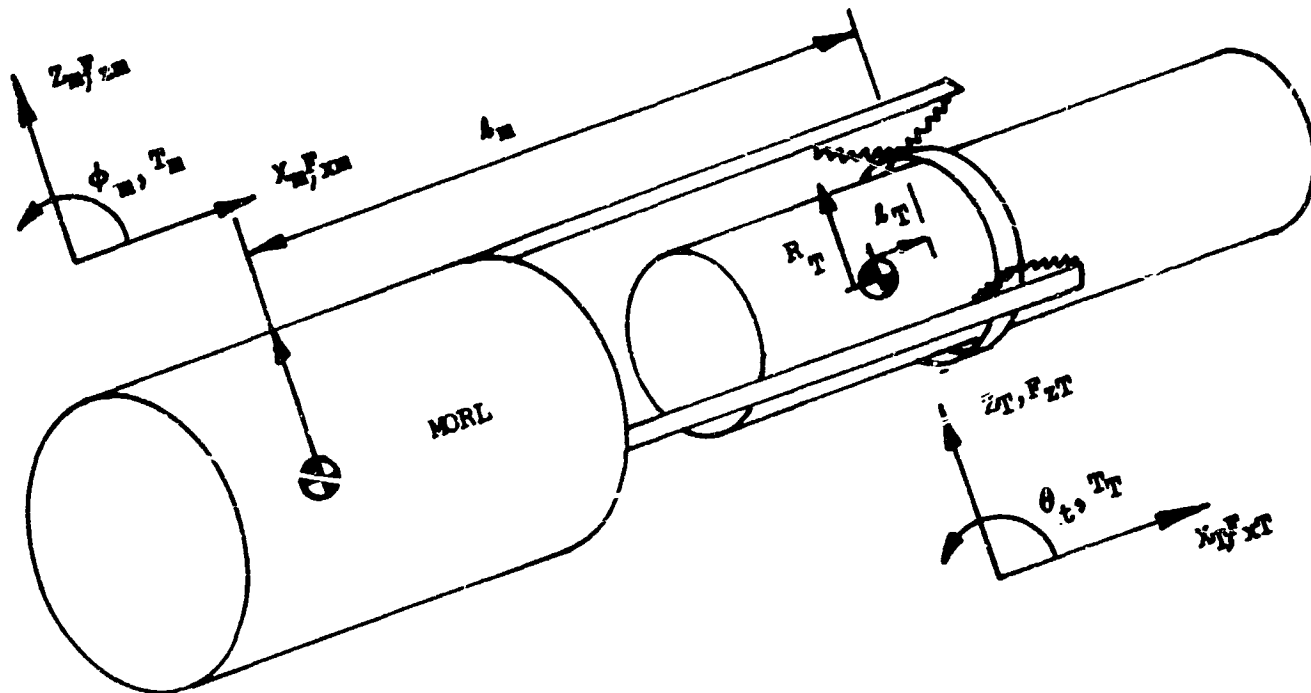
To obtain the forces, the springs were defined in equivalent X- and Z-axis spring constants as below, realizing that due to symmetry, the second and third spring sets will be identical.

$$\begin{aligned}
 KX_1 &= 2 K \cos^2 \theta_0 \\
 KZ_1 &= 2 K \sin^2 \theta_0 \\
 KX_2 &= 2 K \cos^2 \theta_0 \\
 KZ_2 &= 2 K \sin^2 \theta_0 \sin^2 30^\circ
 \end{aligned}
 \tag{2}$$

The forces and torques can thus be expressed as:

$$\begin{aligned}
 F_{xm} &= -F_{xT} = +F_{xm_1} + 2 F_{xm_2} \\
 &= KX_1 dX_1 + 2 KX_2 dX_2 \\
 F_{zm} &= -F_{zT} = F_{zm_1} + 2 F_{zm_2} \\
 &= KZ_1 dZ_1 + 2 KZ_2 dZ_2
 \end{aligned}
 \tag{3}$$

SPRING SUSPENSION



SPRING GEOMETRY

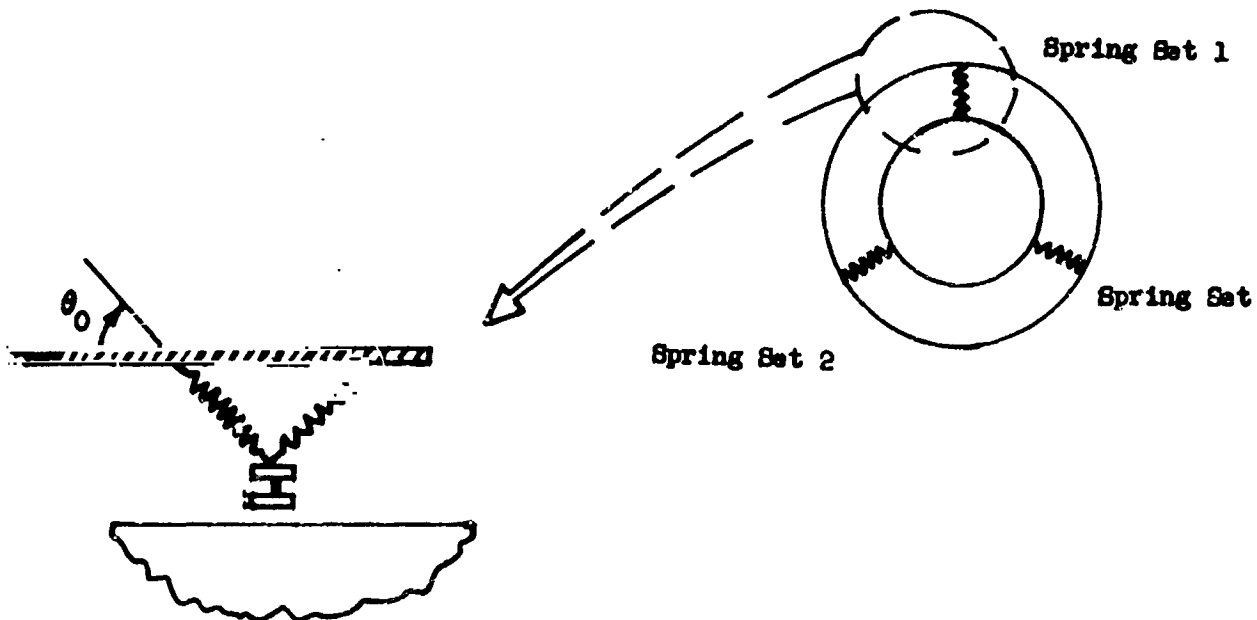


FIGURE 4.2-24  
SOFT GIMBAL MODE

$$T_m = F_{zm_1} l_m - F_{xm_1} r_m + 2 F_{xm_2} \frac{r_m}{2} + 2 F_{zm_2} l_m$$

$$= F_{zT} l_T$$

Substituting the deflections from Equations (1) and the equivalent spring constants from Equations (2) into the forces and torques (Equations (3)) and simplifying, the coupling becomes:

$$F_{xm} = -6K \cos^2 \theta_0 (X_m - X_T)$$

$$F_{zm} = -2K \sin^2 \theta_0 (1 + 2 \sin^2 30^\circ) [Z_m - Z_T + l_m \theta_m - l_T \theta_T]$$

$$T_m = -2K \sin^2 \theta_0 (1 + 2 \sin^2 30^\circ) l_m [Z_m - Z_T + l_m \theta_m - l_T \theta_T]$$

$$+ 2K \cos^2 \theta_0 \left[ 3 \frac{r_T r_m}{2} \theta_T - 3 \frac{r_m^2}{2} \theta_m \right]$$

$$T_T = 2K \sin^2 \theta_0 (1 + 2 \sin^2 30^\circ) l_T [Z_m - Z_T + l_m \theta_m - l_T \theta_T]$$

The linear X-axis oscillations are not coupled to the other variables; thus, it will not enter the stability question and was neglected from further analysis. The equations then become as expressed in Equation (4), where the spring couplings are defined and evaluated in Equation (5). These equations are expressed in block diagram form in Figure 4.2-25, which reflects the concern as to whether or not the vehicles retained their stability. This analysis is only a preliminary effort; the full system is strongly coupled in eleven degrees of freedom.

$$\begin{bmatrix} F_{zm} \\ T_m \\ T_T \end{bmatrix} = \begin{bmatrix} -K_Z & -K_{Z\phi} & K_{Z\theta} \\ -K_{\phi Z} & -K_{\phi\phi} & K_{\phi\theta} \\ K_{\theta Z} & K_{\theta\phi} & -K_{\theta\theta} \end{bmatrix} \begin{bmatrix} \Delta Z \\ \phi_m \\ \theta_T \end{bmatrix} \quad (4)$$





$$\begin{aligned}
\Delta Z &= Z_m - Z_T \\
K_Z &= +2K \sin^2 \theta_0 (1 + 2 \sin^2 30^\circ) \\
K_{Z\phi} &= +2K \sin^2 \theta_0 (1 + 2 \sin^2 30^\circ) l_m \\
K_{Z\theta} &= +2K \sin^2 \theta_0 (1 + 2 \sin^2 30^\circ) l_T \\
K_{\phi Z} &= +2K \sin^2 \theta_0 (1 + 2 \sin^2 30^\circ) l_m \\
K_{\phi\phi} &= +2K \sin^2 \theta_0 (1 + 2 \sin^2 30^\circ) l_m^2 \\
&\quad + 3K \cos^2 \theta_0 r_m^2 \\
K_{\phi\theta} &= +2K \sin^2 \theta_0 (1 + 2 \sin^2 30^\circ) l_T \\
&\quad + 3K \cos^2 \theta_0 r_m r_T \\
K_{\theta Z} &= +2K \sin^2 \theta_0 (1 + 2 \sin^2 30^\circ) l_T \\
K_{\theta\phi} &= +2K \sin^2 \theta_0 (1 + 2 \sin^2 30^\circ) l_m l_T \\
K_{\theta\theta} &= +2K \sin^2 \theta_0 (1 + 2 \sin^2 30^\circ) l_T^2
\end{aligned} \tag{5}$$

For the following set of values based on the synchronous-orbit configuration, the coupling terms become:

$$K = 0.0424 \text{ lb}_f/\text{in}$$

$$l_T = 1 \text{ in.}$$

$$l_m = 42.8 \text{ ft.}$$

$$\theta_0 = 54.7 \text{ deg.}$$

$$r_m = 8.15 \text{ ft.}$$

$$r_T = 7.13 \text{ ft.}$$

$$K_Z = 0.0846 \text{ lb}_f/\text{in}$$

$$K_{Z\phi} = 0.76 \text{ lb}_f/\text{deg}$$

$$K_{Z\theta} = 4.1 \times 10^{-7} \text{ lb}_f/\widehat{\text{sec}}$$

$$K_{\theta Z} = 0.00706 \text{ ft lb}_f/\text{in}$$

$$K_{\theta \omega} = 0.0632 \text{ ft lb}_f/\text{deg}$$

$$K_{\theta \theta} = 3.42 \times 10^{-8} \text{ ft lb}_f/\widehat{\text{sec}}$$

$$K_{\omega Z} = 3.62 \text{ ft lb}_f/\text{in}$$

$$K_{\omega \omega} = 33.1 \text{ ft lb}_f/\text{deg}$$

$$K_{\omega \theta} = 1.62 \times 10^{-4} \text{ ft lb}_f/\widehat{\text{sec}}$$

#### 4.2.4 System Synthesis and Performance

This section presents a synthesis of the three attitude-control systems used in the analog simulation. The first system is a 10-rad-per-second MOT loop, second is a 1-rad-per-second MOT loop, and the third is the MORL attitude-control system. Using the analog simulation of these control loops, the stability of the ACS for the soft-gimbal mode was examined.

4.2.4.1 10-Rad-Per-Second Attitude-Control System — Figure 4.2-26 shows a block diagram of this system, which is identical to that used in the low-Earth-orbit study. The CMG was equipped with a passive gimbal damper that resulted in a 4.2-rad-per-second first-order CMG transfer function. The compensation network consisted of a 7.4-to-1 double lag-lead network to achieve a very high gain and a 13.3-to-1 double lead-lag network to achieve the damping needed near crossover. In addition, a notch filter consisting of a complex pole zero pair was used to stabilize the amplitude resonance that occurs at the 53.7-rad-per-second first structural mode frequency.

Bode diagrams for this loop are shown in Figure 4.2-27, and some sample time histories are shown in Figure 4.2-28. Although this is a conditionally stable system, its transient response is quite satisfactory. Trace A of Figure 4.2-28 shows the step response without the vehicle flexibility or notch filter; Trace B shows the corresponding response with both in the loop. Even with the notch filter, the structural and flexibility effects are excited. This condition illustrates that structural flexibility strongly influences the practicability of a 10-rad-per-second control loop. It also demonstrates one advantage of lower frequency outer loops because structural coupling is not as important.

It was found in the previous study that the CMG gimbal friction induced a system limit cycle; indeed, this was the reason the initial 1-rad-per-second MOT-ACS was resynthesized to a 10-rad-per-second system. Trace A of Figure 4.2-29 shows this limit cycle with the passive CMG. If an active gimbal rate loop is closed around the CMG, the effects of this friction can be reduced to that shown in Trace B. This data was taken with a 4.2-rad-per-second first-order filter driving a 15-cps CMG. In this way, the overall loop dynamics were nearly preserved. The effect is to enclose the friction in a very tight inner loop, thereby potentially relaxing response requirements on the outer loop.

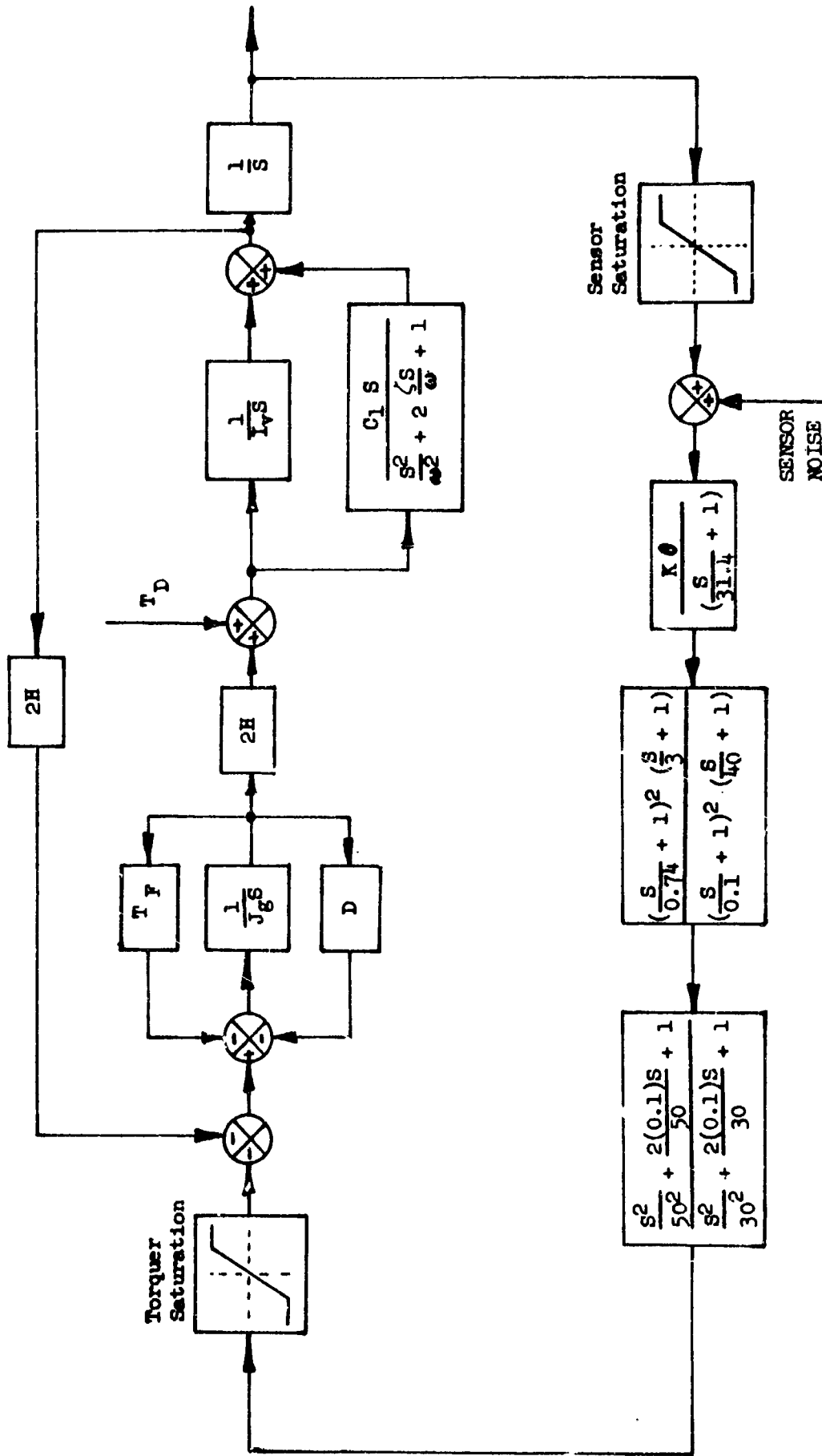


FIGURE 4.2-26  
MOT ACS BLOCK DIAGRAM - 10 RAD/SEC

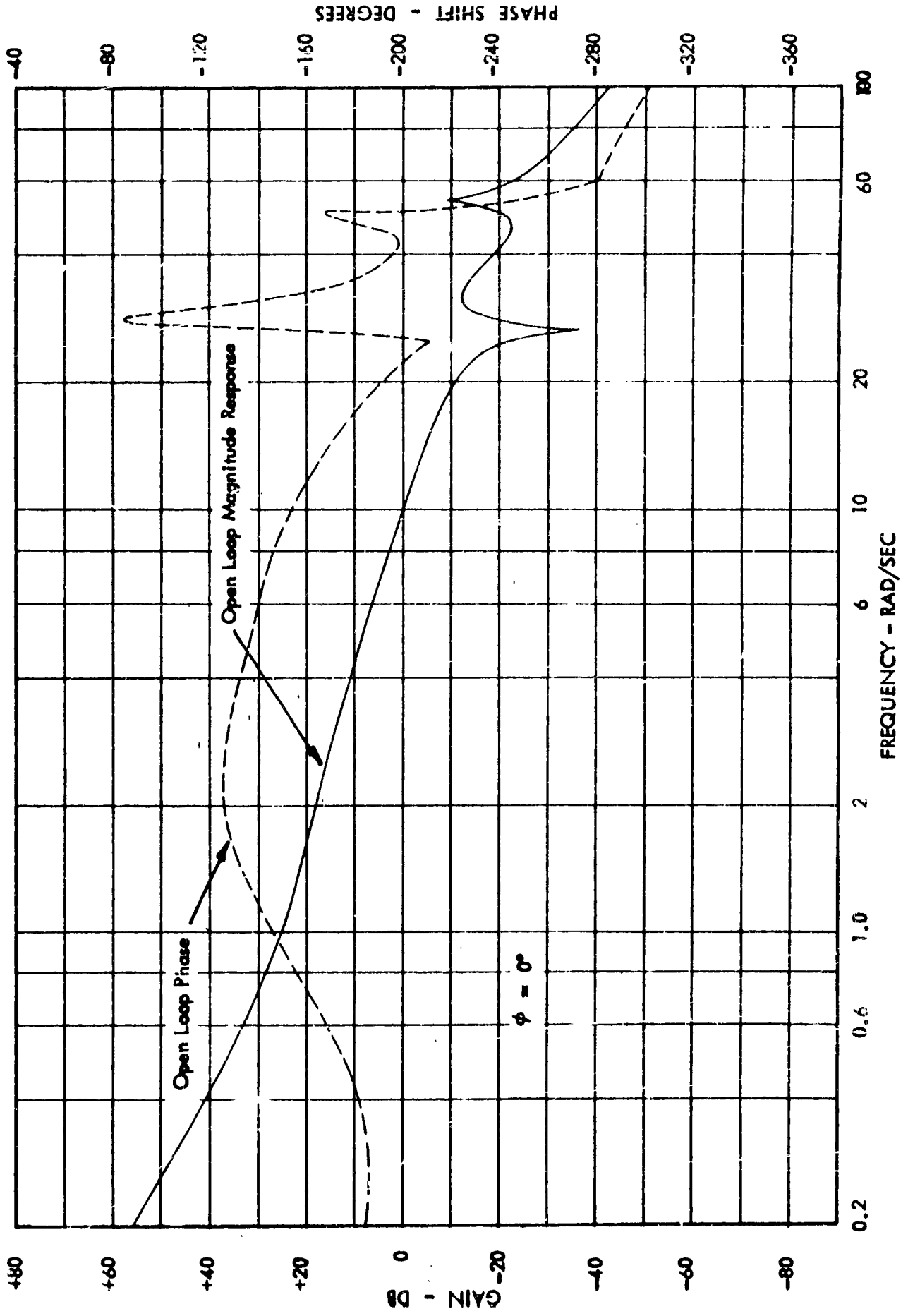
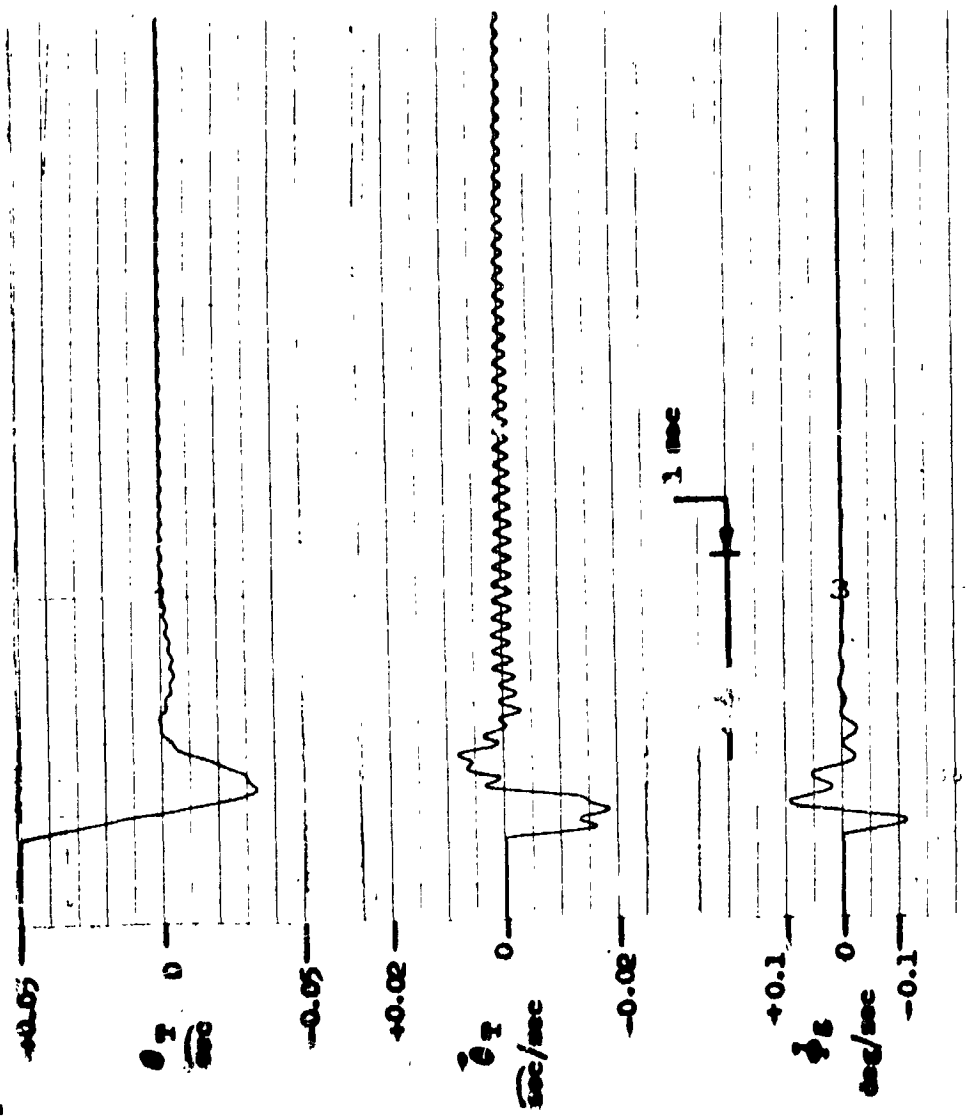


FIGURE 4.2-2  
NOT ACS BLOCK DIAGRAM - 10 RAD/SEC

20 MILIION  
PASSIVE CIR



B) VIB STRUCTURAL FREQUENCY

A) WEDGE STRUCTURAL FREQUENCY

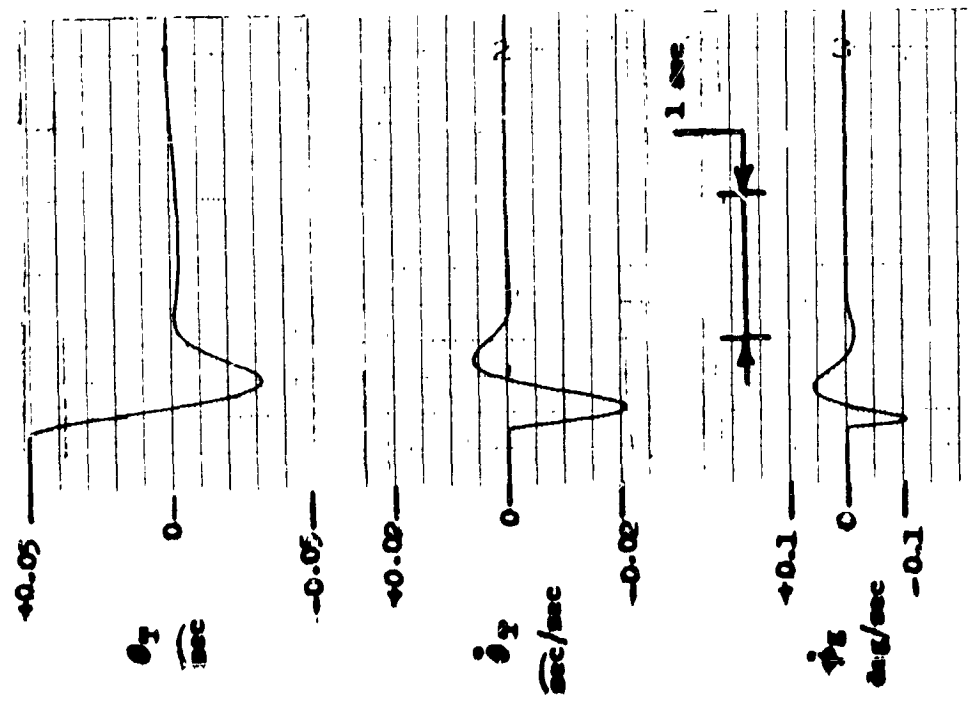
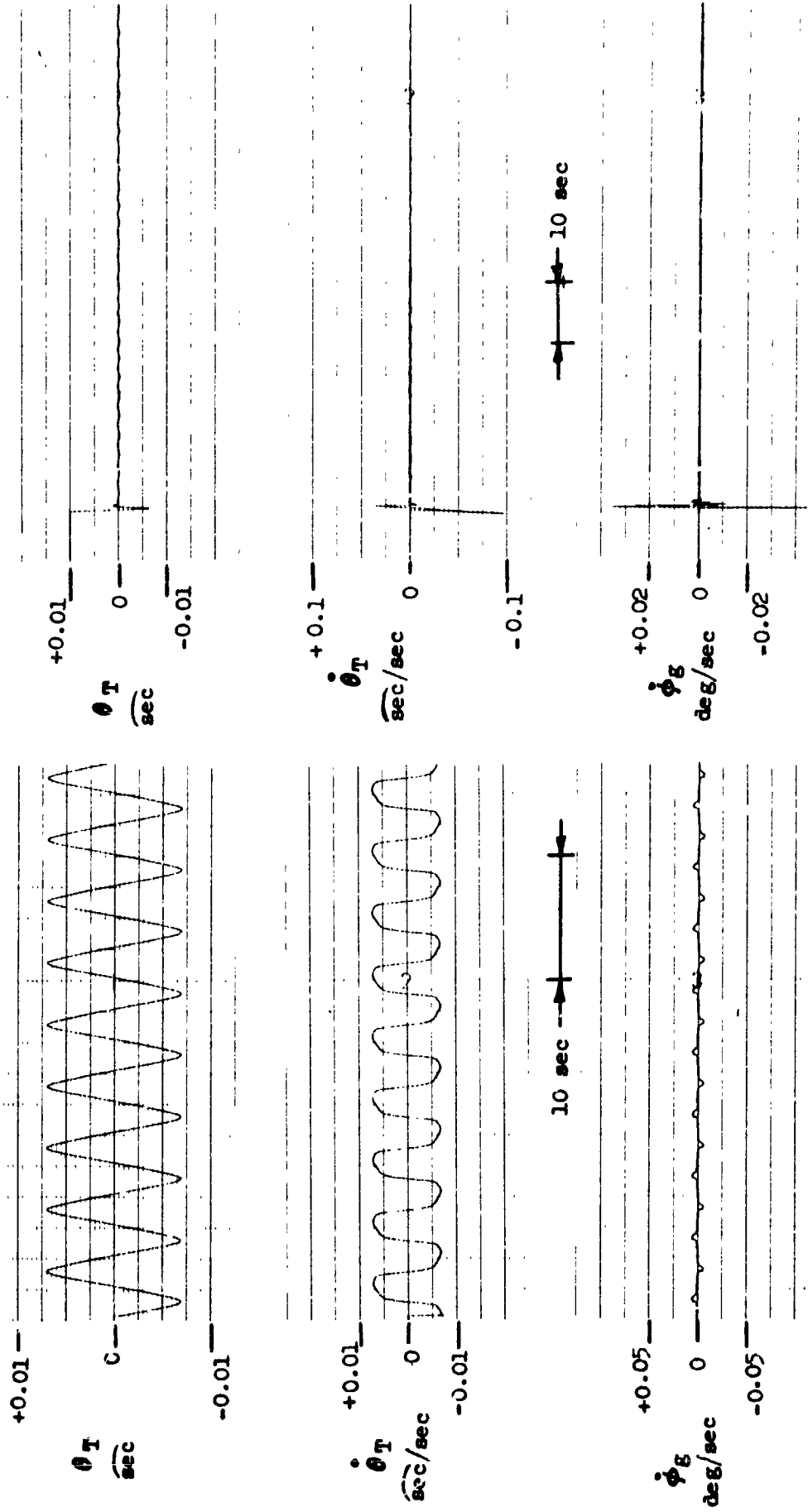


FIGURE 4-2-28  
TRANSIENT RESPONSES - 10 RAD/SEC



B) ACTIVE CMG (15 CPS)  
0.05 IN OZ FRICTION

A) PASSIVE CMG  
0.05 IN OZ FRICTION

FIGURE 4.2-23  
ACTIVE-PASSIVE CMG'S - 10 RAD/SEC

4.2.4.2 1-Rad-Per-Second Attitude-Control System — The block diagram for this loop is shown in Figure 4.2-30. Differences between this and the previous loop include the use of an active CMG, the elimination of a notch filter, and the use of a single lead-lag (differentiator) network because CMG dynamics occur above the crossover frequency. Bode diagrams for this loop are shown in Figure 4.2-31, and its transient response is shown in Figure 4.2-32 both with and without gimbal friction. While the gain of this loop is significantly less than that of the previous loop, the inverse stiffness is still extremely large — 332 ft-lb<sub>f</sub> per arc second. The low-frequency external disturbances and corrections required for velocity aberrations thus induce negligible pointing errors —  $8 \times 10^{-8}$  and  $3 \times 10^{-11}$  arc second, respectively.

4.2.4.3 Detached Mode Performance — The two previously described systems were simulated on an analog computer. Figures 4.2-33 through 4.2-35 show the computer diagrams of this simulation (the diagrams also include the soft-gimbal simulation discussed in the following sections). Sensitivity of the loops to sensor noise was determined using this simulation. Figure 4.2-36 shows some typical time histories of the results. The results for the 10-rad-per-second loop are shown in Figure 4.2-37. Small amounts of noise are beneficial for the passive CMG in that it breaks the CMG gimbal friction. Use of the active CMG results in a considerable performance improvement in the absence of sensor noise. This improvement occurs because the active CMG prevents a system limit cycle by enclosing the gimbal friction in a tight gimbal servo loop. It is seen, however, that a sensor-noise level as low as 0.003 arc second can again induce this limit cycle. At higher values of sensor noise, the limit cycle is again broken, and the performance of the two systems would eventually be expected to approach each other. Differences between the two active-CMG curves at different friction levels is attributed to errors in estimating the maximum pointing errors, rather than an increase in performance with higher gimbal friction.

Time histories for the 1-rad-per-second loop when subjected to sensor noise are shown in Figure 4.2-38. Results of these (and other) tests are shown in Figure 4.2-39. The sensor noise again induces a limit cycle, the amplitude of which is significantly higher than that of the 10-rad-per-second loop. However, the 1-rad-per-second loop exhibits better performance in the presence of higher sensor-noise levels. The lower loop frequency also permits the use of lower-frequency sensors. This decrease in sensor noise is shown in Figure 4.2-40 for the 0.5- and 5-cps off-axis fine-pointing sensors. Using these sensor characteristics, the results of Figures 4.2-37 and 4.2-39 can be plotted with respect to star magnitude (Figure 4.2-41). The curve for the 1-rad-per-second system is somewhat in error since a 5-cps sensor was used for the data of Figure 4.2-39; however, the difference is not expected to be large except at higher noise levels. This curve indicates that the pointing performance requirements can be maintained for stars with magnitudes greater than  $\pm 14$ . Within the  $\pm 15$ -minute telescope field of view, at least one star of 12.5 magnitude or brighter will exist, so the present concept is considered feasible.

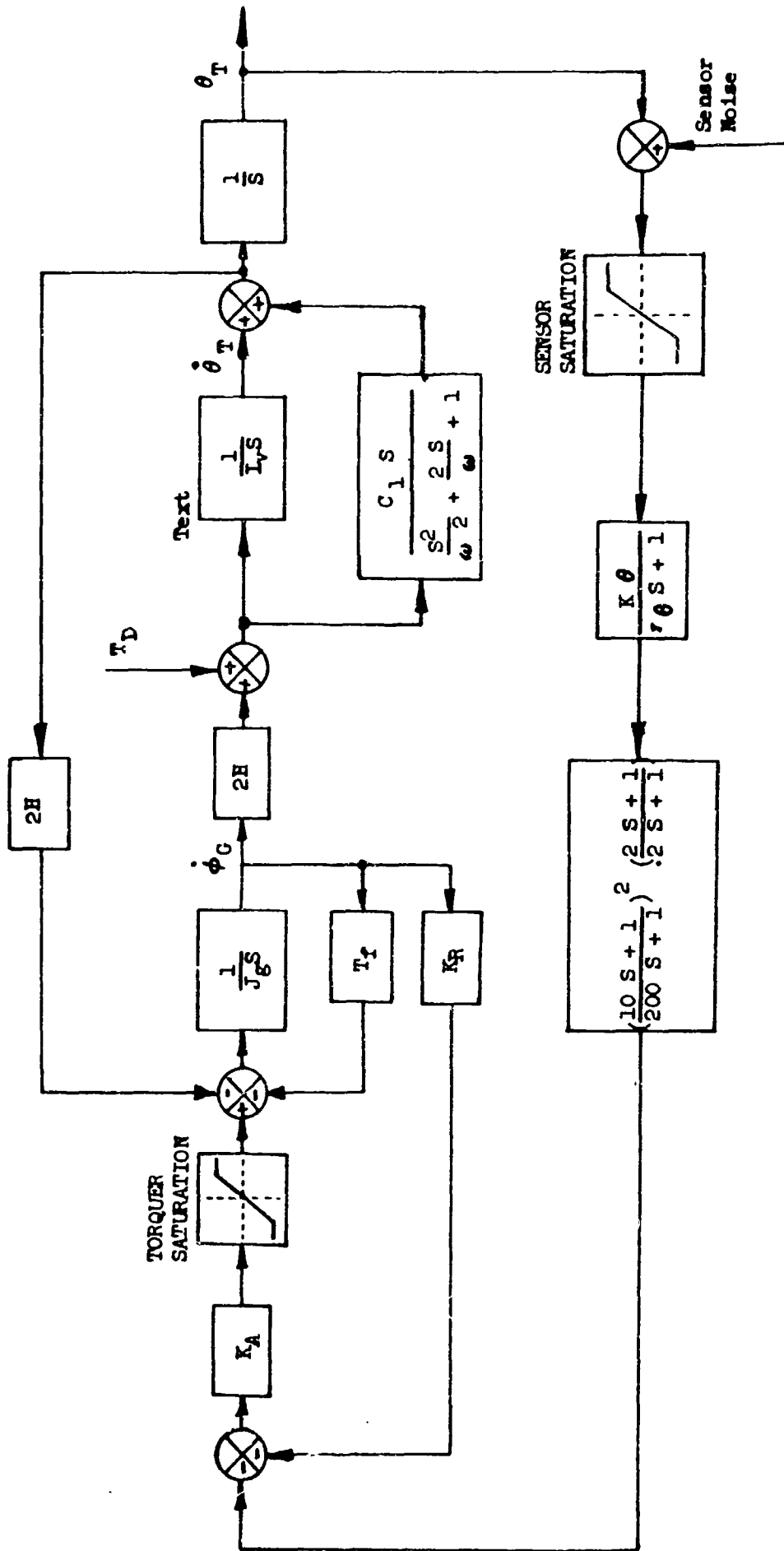


FIGURE 4.2-30  
MOT ACS BLOCK DIAGRAM - 1 RAD/SEC



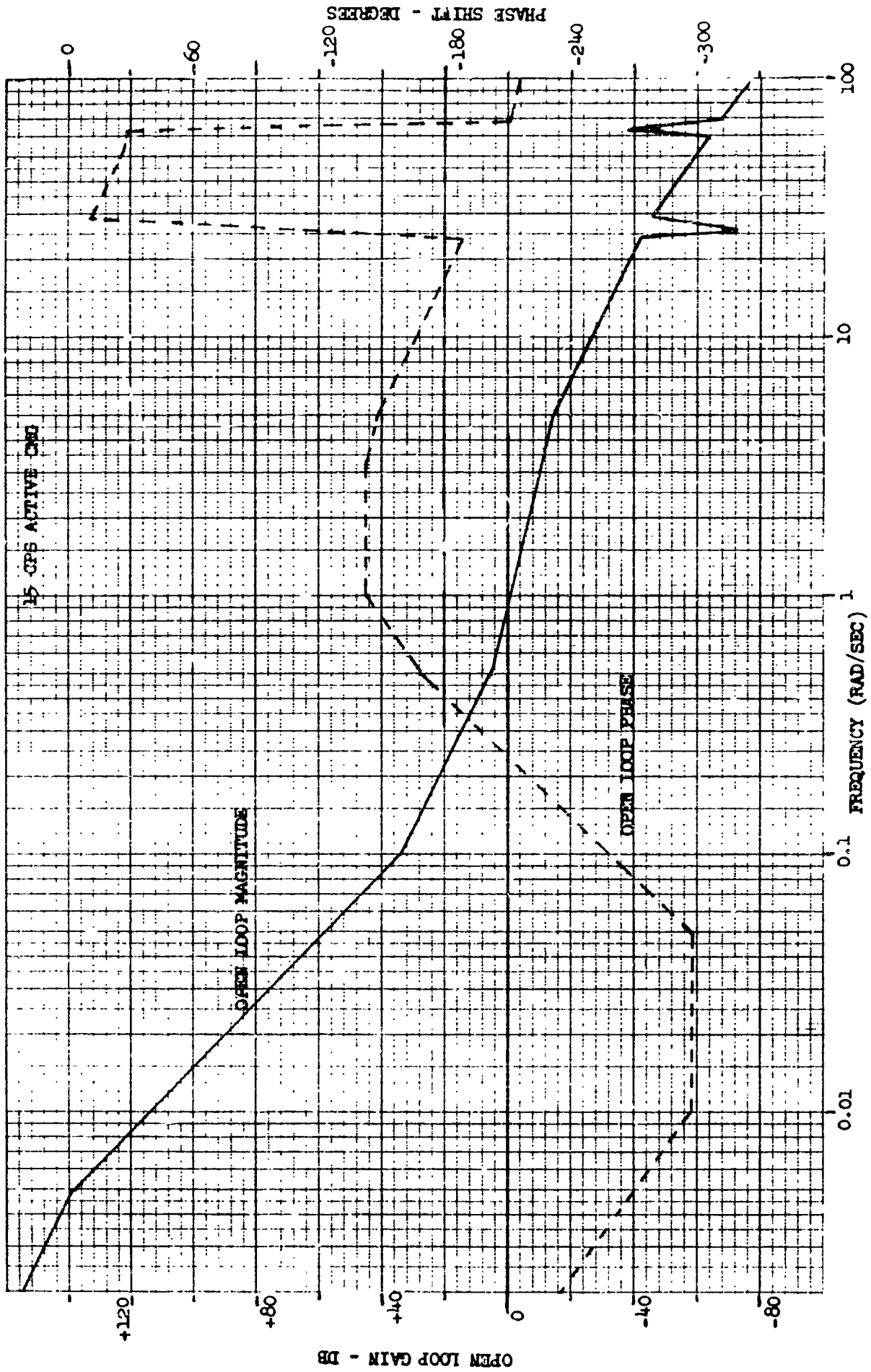
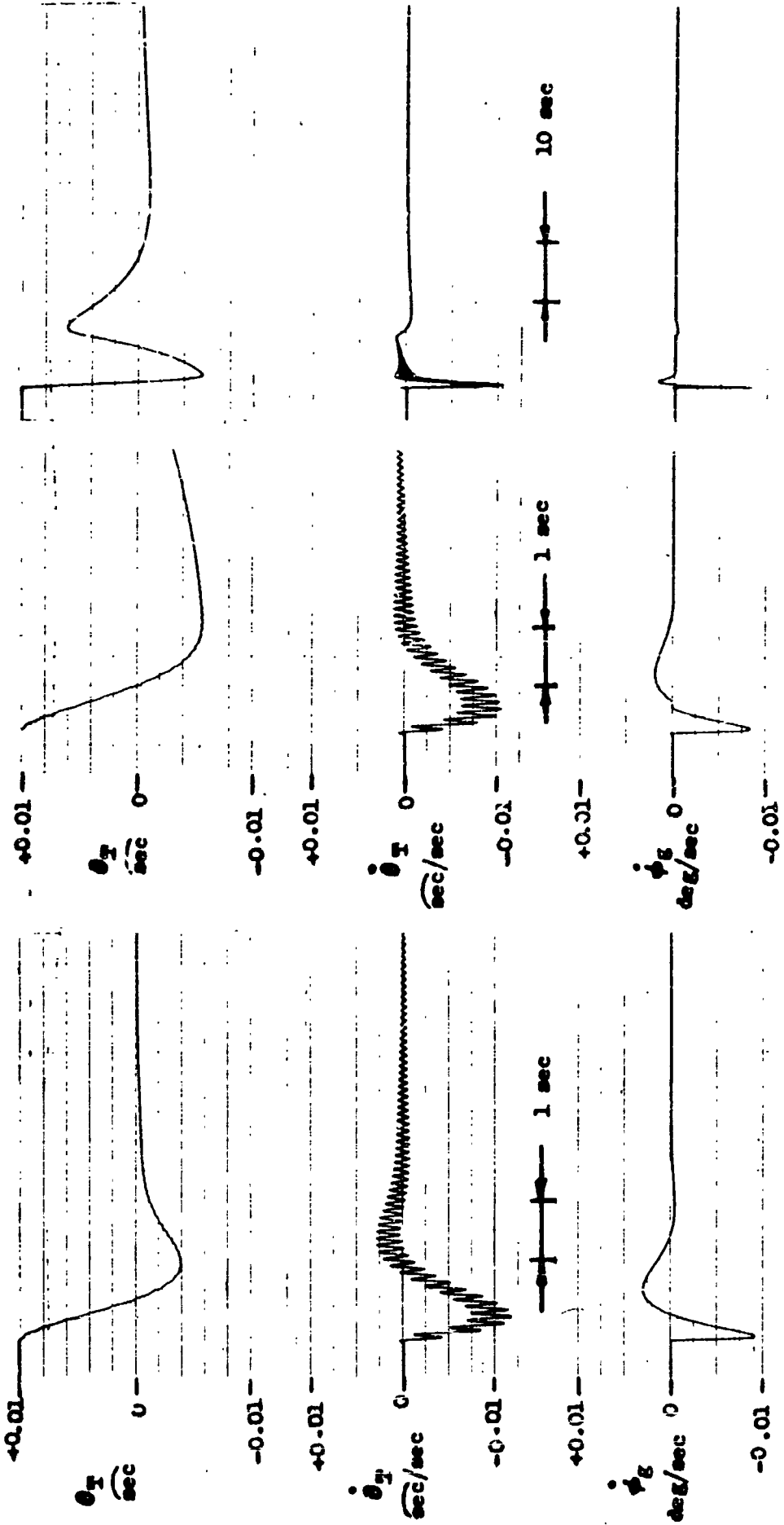


FIGURE 4.2-31  
MOT ACS BODE DIAGRAM - 1 RAD/SEC



A) NO FRICTION  
15 CPS CMG

B) 0.025 IN OZ GYRAL FRICTION  
15 CPS CMG

FIGURE 4.2-32  
TRANSIENT RESPONSE - 1 RAD/SEC

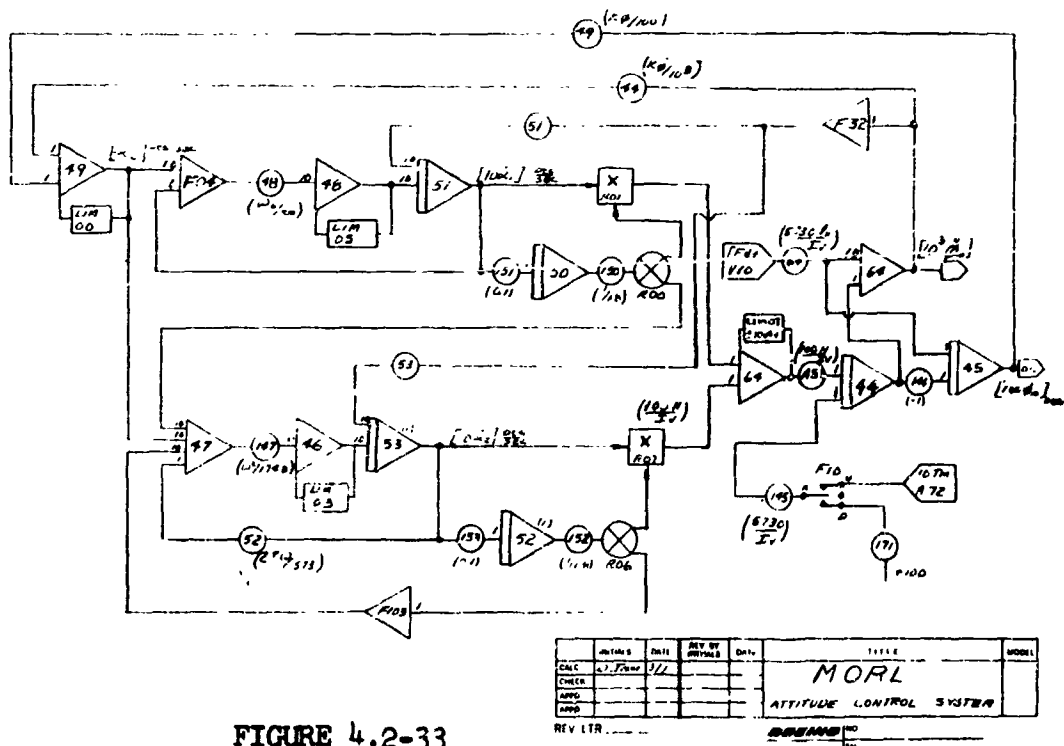
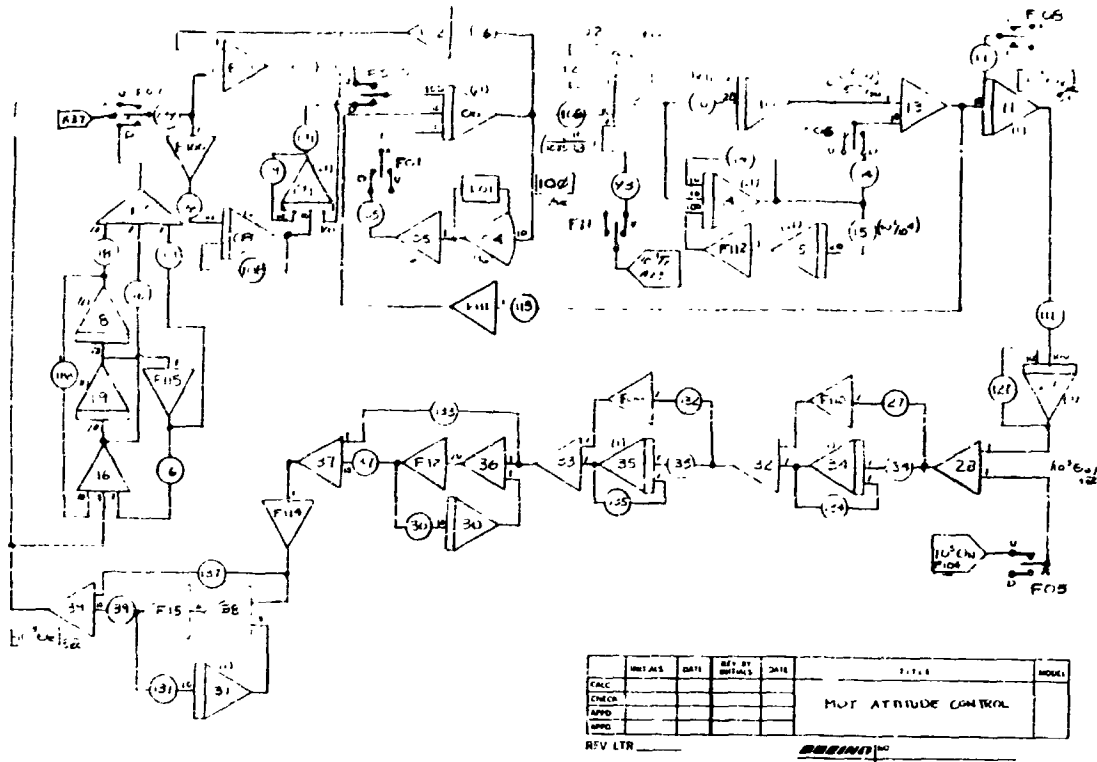


FIGURE 4.2-33  
ANALOG COMPUTER DIAGRAMS

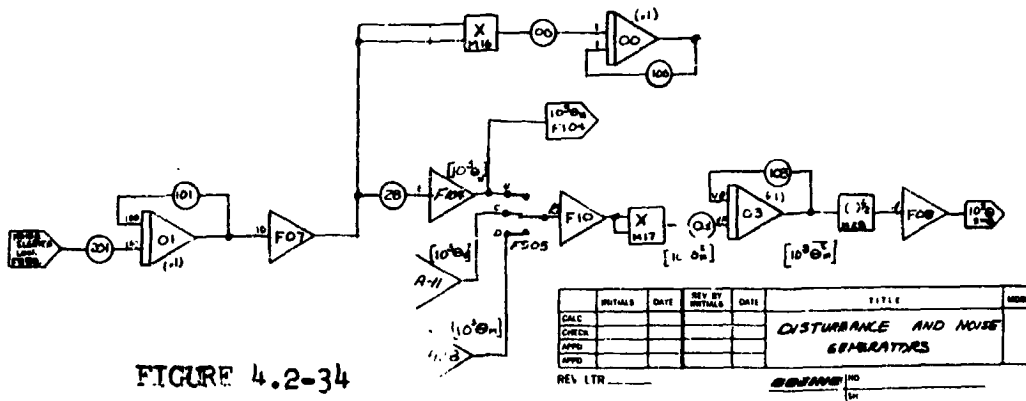
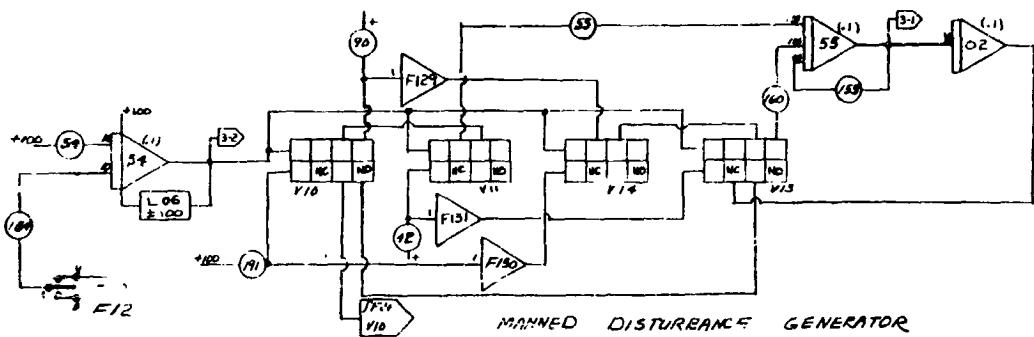
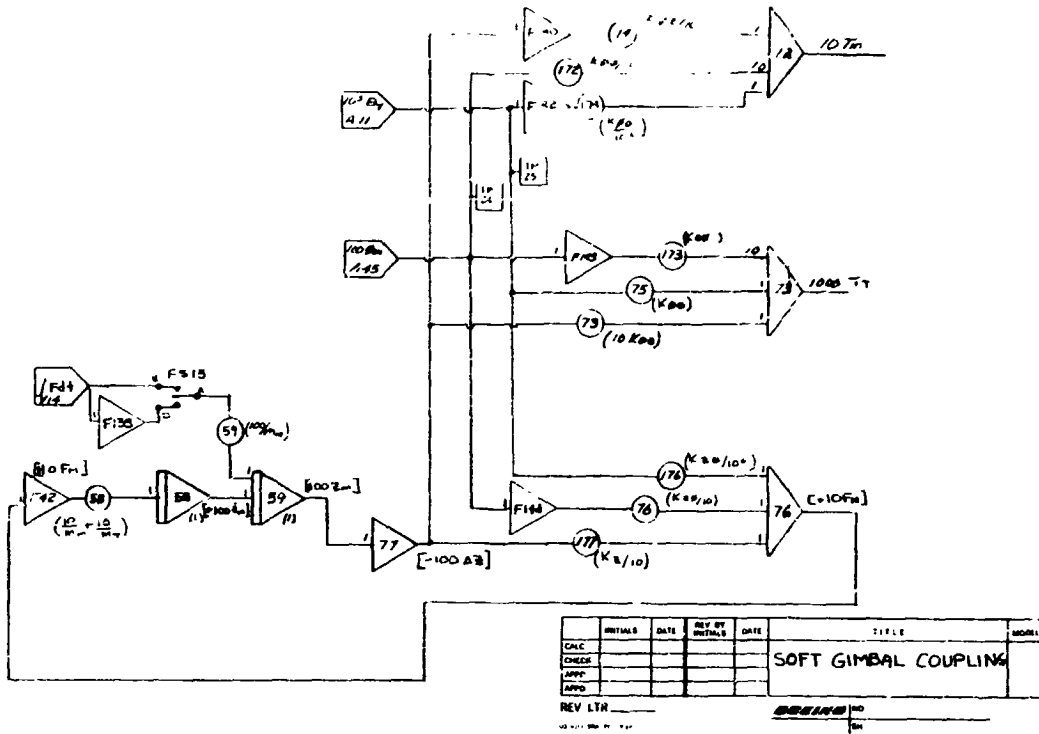
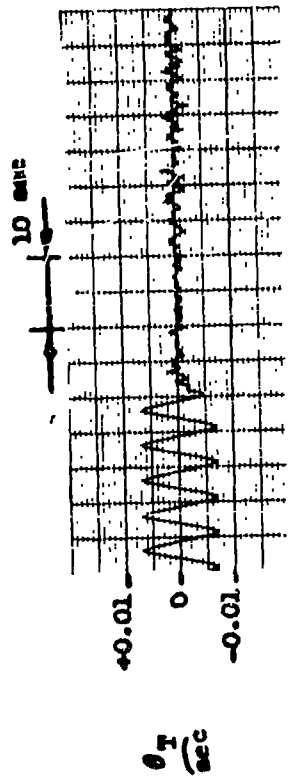


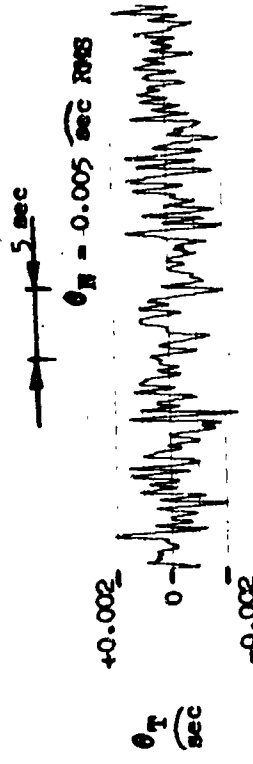
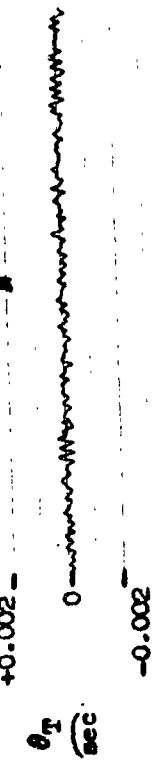
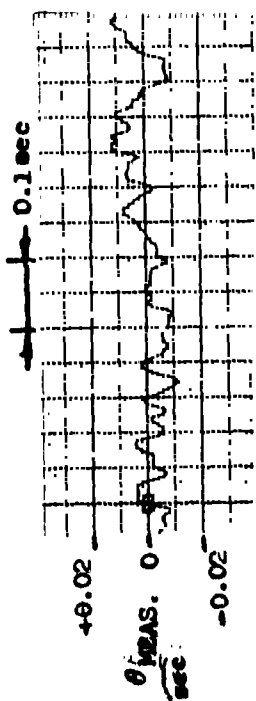
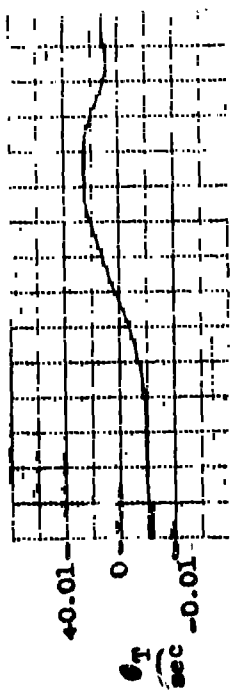
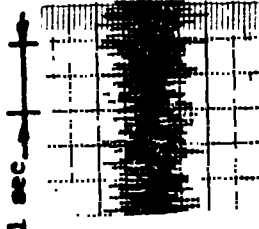
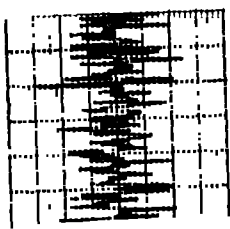
FIGURE 4.2-34  
ANALOG COMPUTER DIAGRAMS

Pot	Value	Pot	Value	Pot	Value	Pot	Value	Pot	Value	Pot	Value	Pot	Value
S000	+0100	S036	+0000	S072	+0000	S108	+0420	S144	+1000	S180	+0000	S216	+0000
S001	+0000	S037	+1232	S073	+0707	S109	+6319	S145	-0094	S181	-0000	S217	+0000
S002	+0000	S038	+0000	S074	+3620	S110	+0000	S146	+0000	S182	+0000	S218	+0000
S003	+1000	S039	+1233	S075	+0000	S111	+3140	S147	+9010	S183	+0000	S219	+0000
S004	-0000	S040	+0000	S076	+0760	S112	+0000	S148	+0000	S184	+0000	S220	+0000
S005	+4400	S041	+0000	S077	+0000	S113	+0000	S149	+0000	S185	+0000	S221	+0000
S006	+1405	S042	+3750	S078	+0000	S114	+5192	S150	+5500	S186	+0000	S222	+0000
S007	+0001	S043	+0000	S079	+0000	S115	+0000	S151	+1000	S187	+0000	S223	+0000
S008	+0421	S044	+1240	S080	-0000	S116	+3600	S152	+5500	S188	+0000	S224	+0000
S009	+9896	S045	+0905	S081	+0000	S117	+0000	S153	+1000	S189	+0000	S225	+0000
S010	+6320	S046	+0000	S082	+0000	S118	+9000	S154	+1001	S190	+0000	S226	+0000
S011	+0500	S047	+0000	S083	+0000	S119	+0000	S155	+9895	S191	+6250	S227	+0000
S012	+0220	S048	+3139	S084	-0000	S120	+0000	S156	+0000	S192	+0000	S228	+0000
S013	+0000	S049	+0283	S085	+0000	S121	+0000	S157	+0000	S193	+0000	S229	+0000
S014	+1100	S050	+0000	S086	+0000	S122	+0000	S158	+0000	S194	+0000	S230	+0000
S015	+2880	S051	+5501	S087	+0000	S123	+0000	S159	+0001	S195	+0000	S231	+0000
S016	+6001	S052	+3066	S088	+0000	S124	-0000	S160	+9175	S196	+0000	S232	+0000
S017	+3600	S053	+5500	S089	+0000	S125	+0000	S161	+0000	S197	+0000	S233	+0000
S018	+9000	S054	+0500	S090	+0600	S126	+0000	S162	+0000	S198	+0000	S234	+0000
S019	+0001	S055	+9898	S091	+0000	S127	+3140	S163	+0000	S199	+0000	S235	+0000
S020	+0000	S056	+0000	S092	+0000	S128	+0000	S164	+0000	S200	+0020	S236	+0000
S021	+0000	S057	+0000	S093	+0101	S129	+0000	S165	+0000	S201	-0000	S237	+0000
S022	+0000	S058	+2072	S094	+0000	S130	+0000	S166	+0000	S202	+0003	S238	+0000
S023	+0100	S059	+3120	S095	+0000	S131	+4000	S167	+0000	S203	+0004	S239	+0000
S024	+0000	S060	+0000	S096	+0000	S132	+1350	S168	+0000	S204	+0293	S240	+0000
S025	+0000	S061	+0000	S097	+0000	S133	+9899	S169	+0000	S205	+0000	S241	+0000
S026	+0000	S062	+0000	S098	+0000	S134	+1001	S170	+0000	S206	+0003	S242	+0000
S027	+1350	S063	+0000	S099	+0000	S135	+1000	S171	+5000	S207	+0003	S243	+0000
S028	+0665	S064	+1882	S100	+0100	S136	+0000	S172	+3310	S244	+0000	S245	+0000
S029	+0000	S065	+0000	S101	+3141	S137	+9899	S173	+0633	S246	+0000	S247	+0000
S030	+3999	S066	+0000	S102	+0000	S138	+0000	S174	+0000	S248	+0000	S249	+0000
S031	+0000	S067	+0000	S103	+1001	S139	+3928	S175	+0000	S250	+0000	S251	+0000
S032	+0000	S068	+0000	S104	+0000	S140	+0001	S176	+0000	S252	+0000	S253	+0000
S033	-0000	S069	+0000	S105	+1496	S141	+0000	S177	+0085	S254	+0000	S255	+0000
S034	+0865	S070	+0000	S106	+3490	S142	+0000	S178	+0000	S256	+0000	S257	+0000
S035	+0865	S071	+0000	S107	+0299	S143	+0000	S179	+0000	S258	+0000	S259	+0000
										LIM00	+8 volts		
										LIM01	±10 volts		
										LIM02	±10 volts		
										LIM03	±87.5 volts		
										LIM05	±87.5 volts		
										LIM06	±100 volts		
										LIM07	±100 volts		

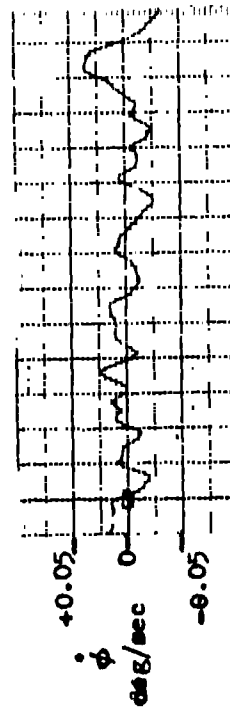
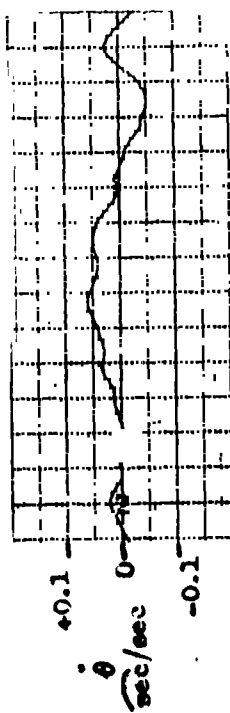
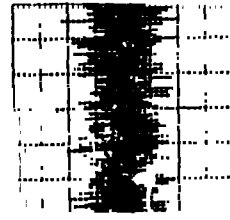
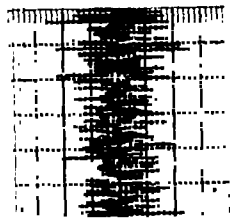
Figure 4.2-35: ANALOG SIMULATION POT SETTINGS



PASSIVE CMG  
0.05 IN OZ FRICTION  
 $\theta_N = 0.001 \text{ sec RMS}$



15 CFS CMG  
0.05 IN OZ FRICTION



PASSIVE CMG  
0.05 IN OZ FRICTION  
 $\theta_N = 0.005 \text{ sec RMS}$

FIGURE 4.2-36  
TIME HISTORIES - 10 RAD/SEC WITH SENSOR NOISE

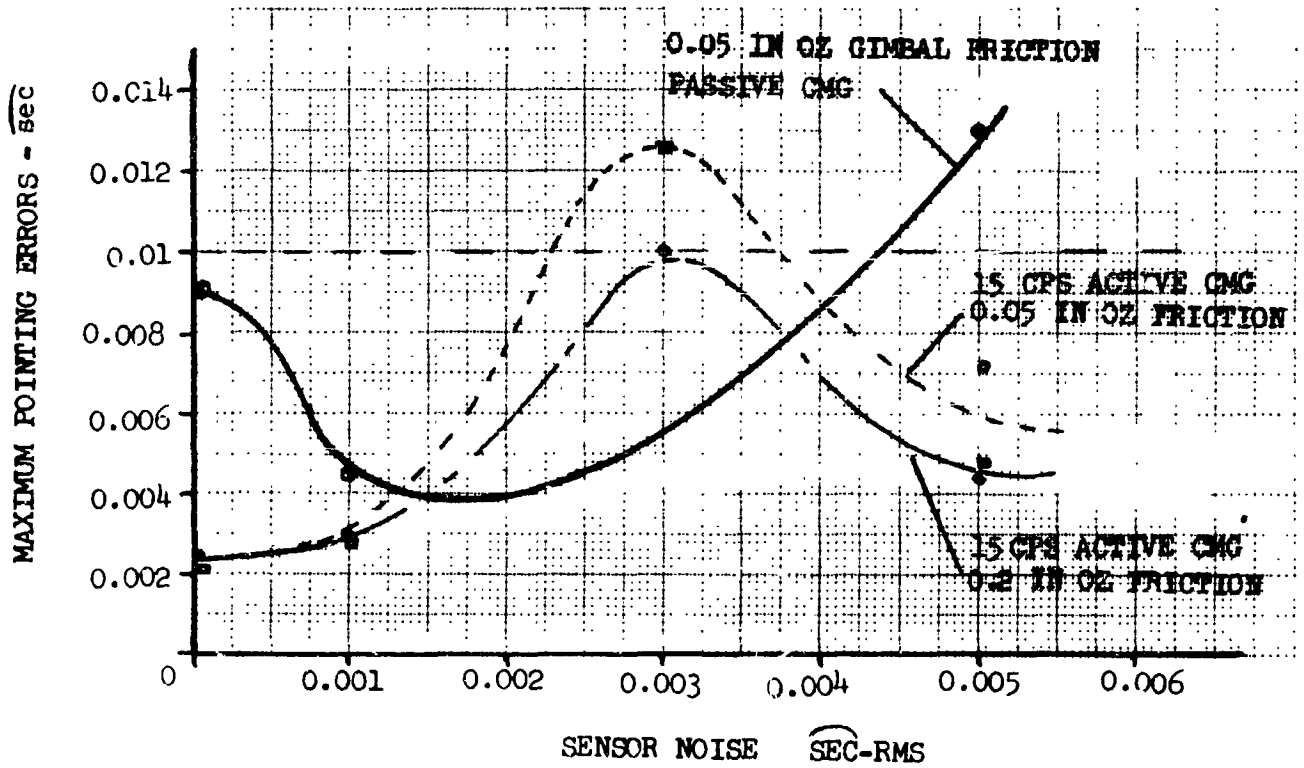


FIGURE 4.2-37  
 POINTING ERRORS - 10 RAD/SEC WITH SENSOR NOISE

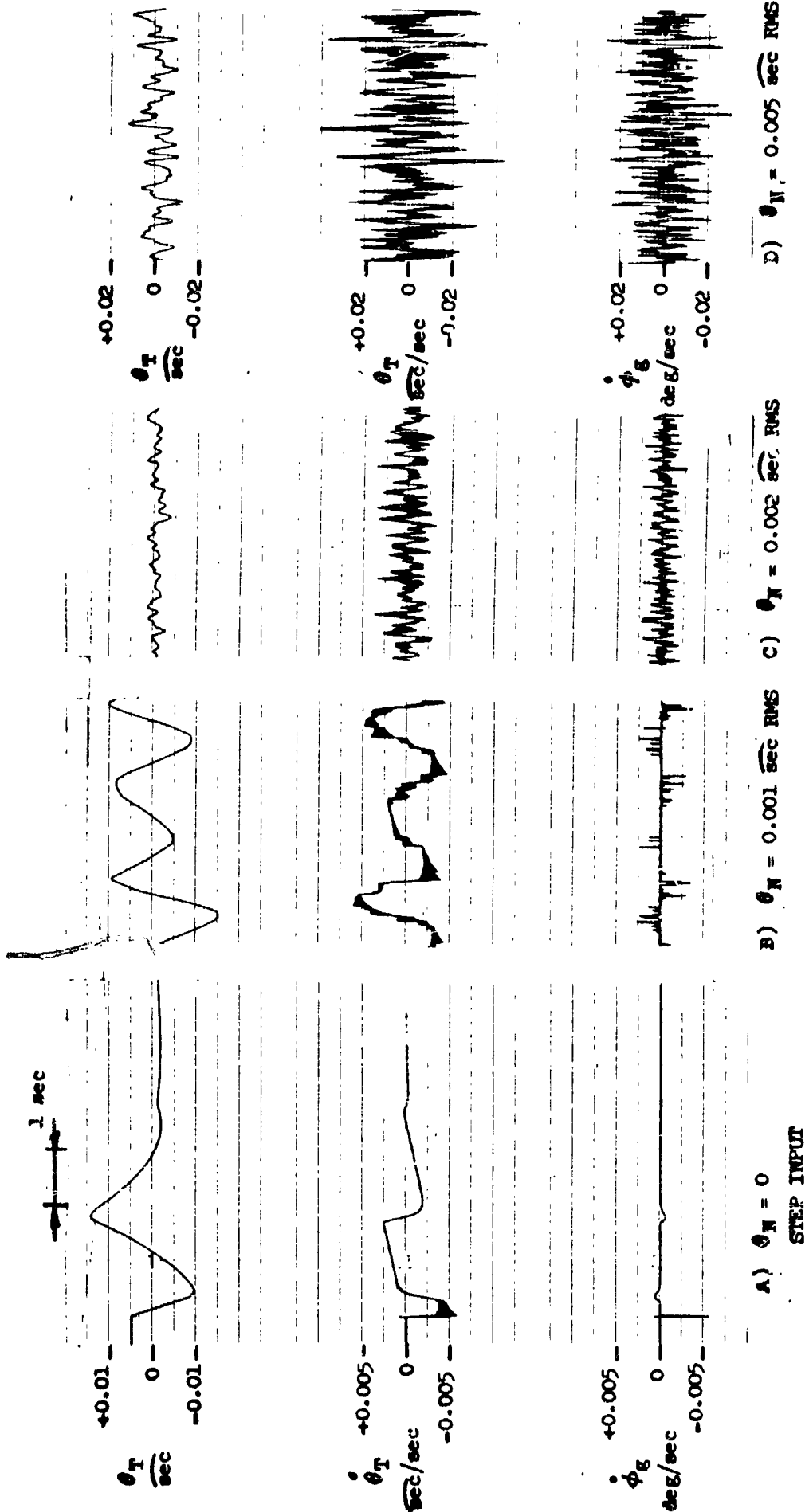


FIGURE 4.2-36

TIME HISTORIES - 1 RAD/SEC WITH SENSOR NOISE



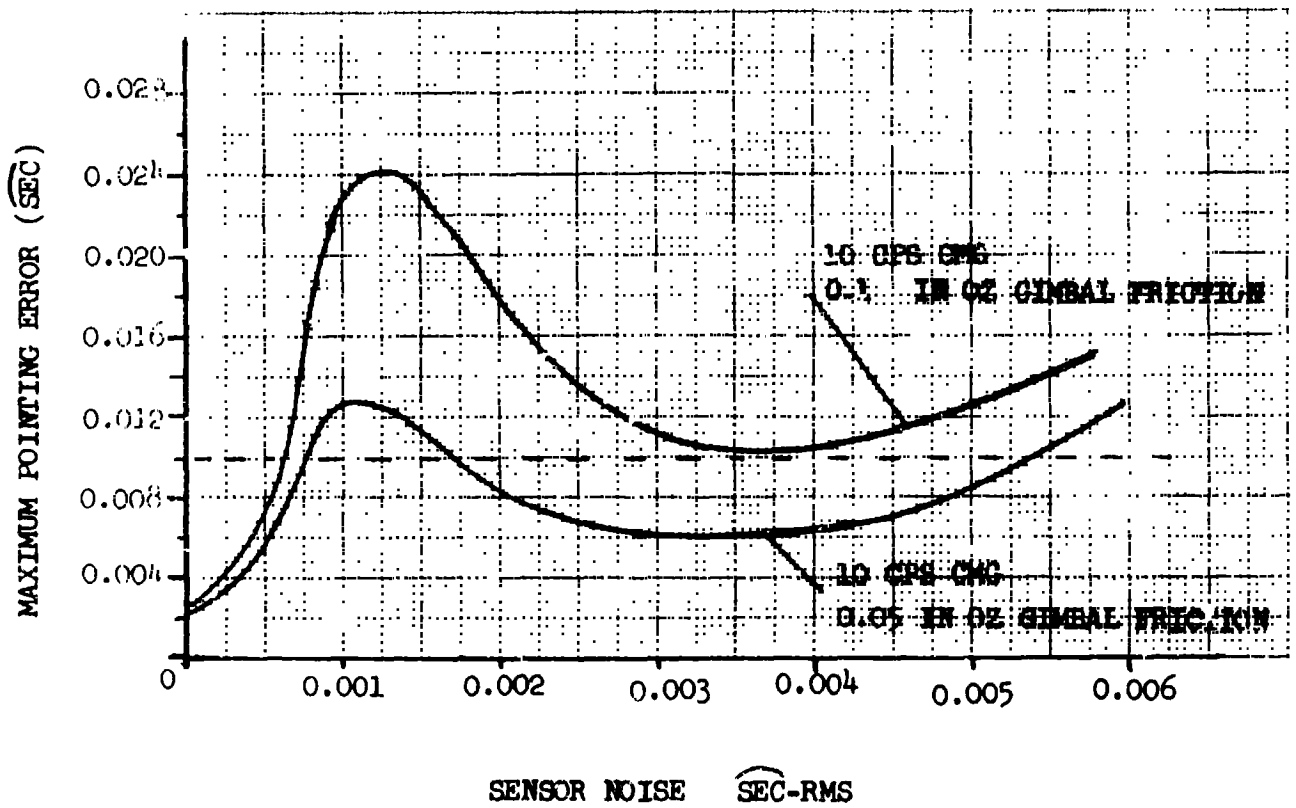


FIGURE 4.2-39  
 POINTING ERRORS - 1 RAD/SEC WITH SENSOR NOISE

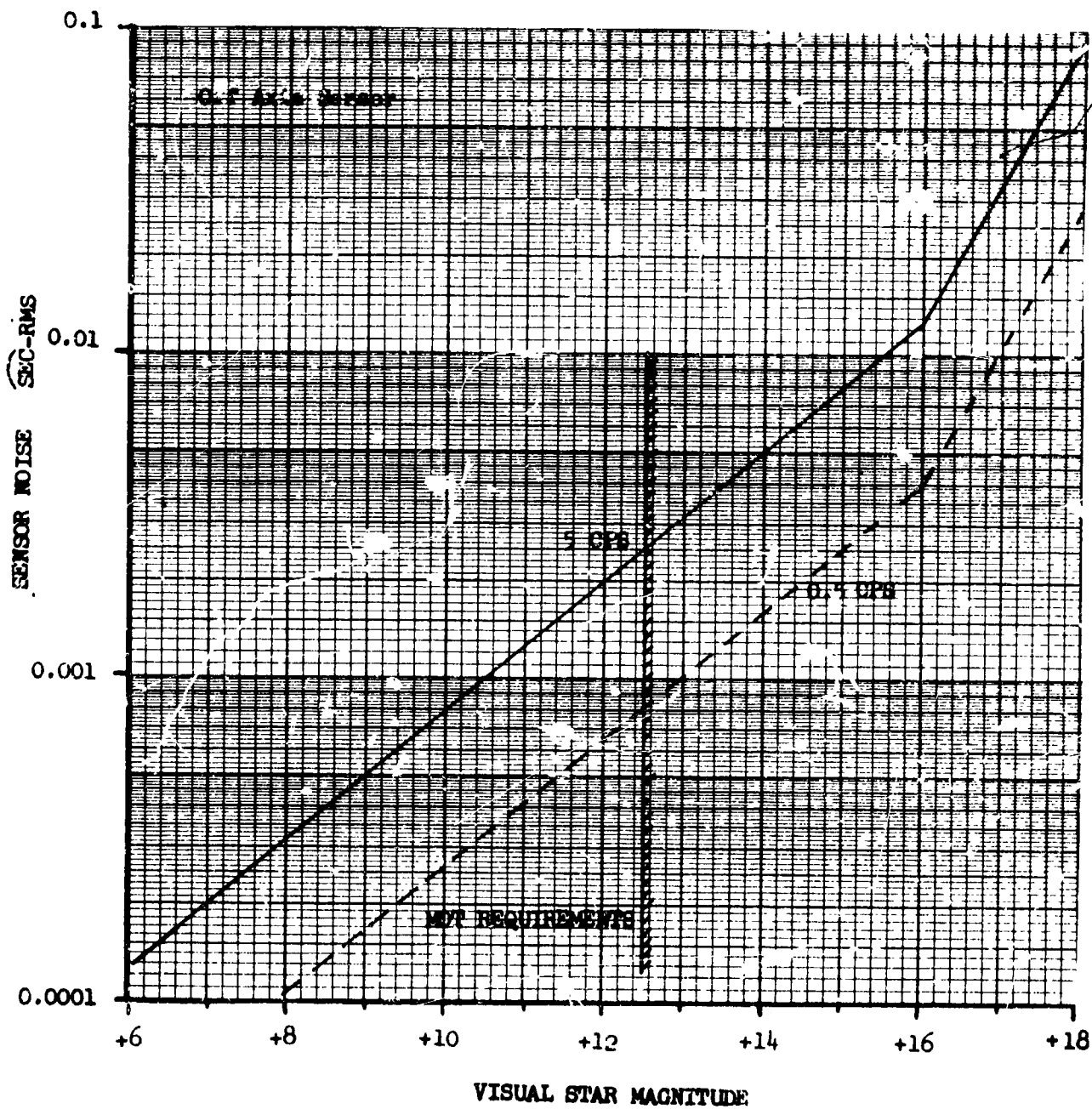


FIGURE 4.2-40  
 SENSOR NOISE VS STAR MAGNITUDE

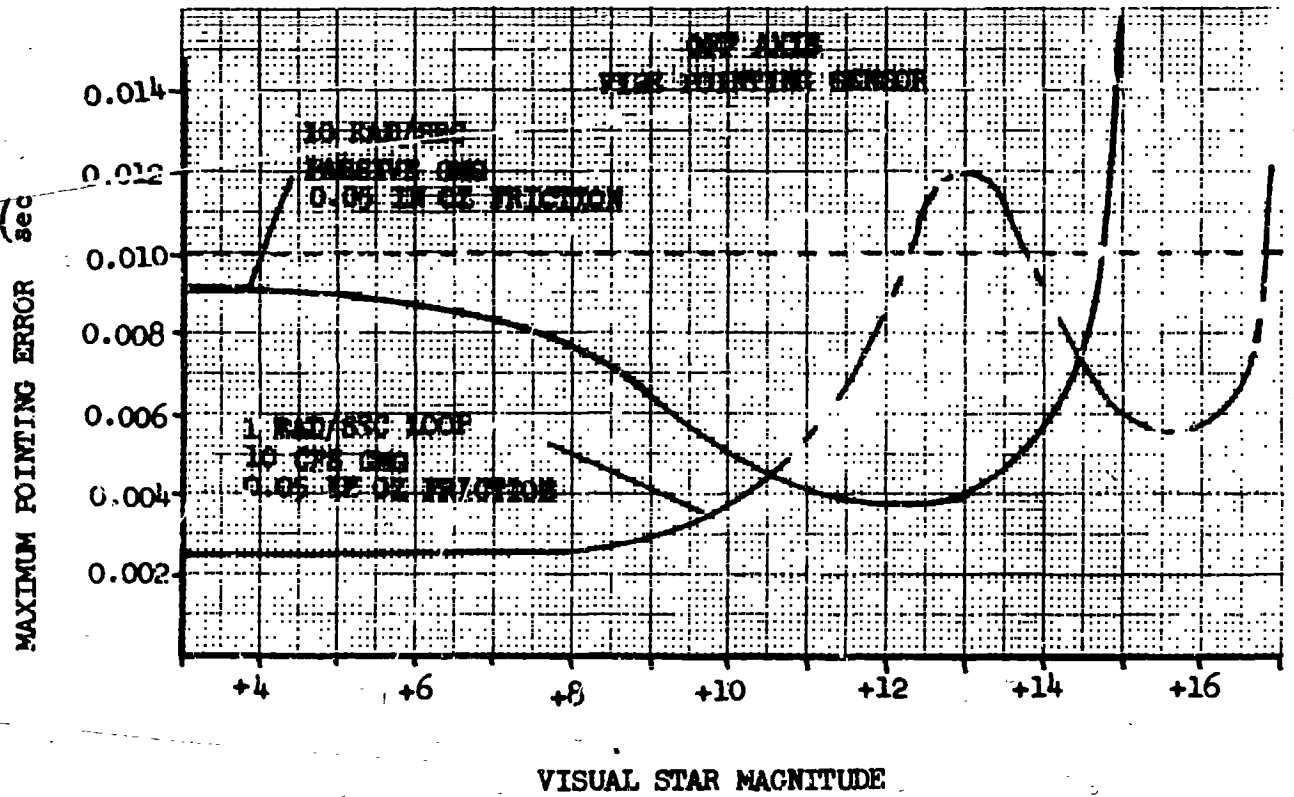


FIGURE 4.2-41  
POINTING ERRORS VS STAR MAGNITUDE

4.2.4.4 MORL Attitude-Control System -- Per Reference 16, the MORL also uses a CMG control system. The total CMG configuration consists of a twin-rotor two-degree-of-freedom CMG (Y- and Z-axis control) and a twin-rotor one-degree-of-freedom CMG (X-axis control). The Y axis was used in the simulation, for which the inner gimbal axis of the CMG's are used for control. The block diagram of the entire control loop is shown in Figure 4.2-42. The first CMG has a 5-cps first-order-response gimbal-rate servo; the second CMG is slaved to the first with a 2-cps position loop. The gimbal-torque-motor limits were set at 5 ft-lb<sub>f</sub>. The CMG's receive their commands through gyro sensors that measure vehicle position and rate. The gains of these sensors (as were the other parameters except the MORL inertias) were set at the values recommended from the MORL studies. The values used for these parameters are shown in Figure 4.2-43.

$$\begin{aligned}
 K\omega &= \dot{\alpha} / \dot{\phi}_m = 2.83 \frac{\text{rad/sec}}{\text{rad/sec}} \\
 K\omega &= \dot{\alpha} / \dot{\phi}_m = 124 \frac{\text{rad/sec}}{\text{rad/sec}} \\
 I_v &= 609,000 \text{ ft-lb}_f\text{-sec}^2 \\
 H &= 550 \text{ ft-lb}_f\text{-sec/rotor} \\
 J_G &= 1 \text{ ft-lb}_f\text{-sec}^2
 \end{aligned}$$

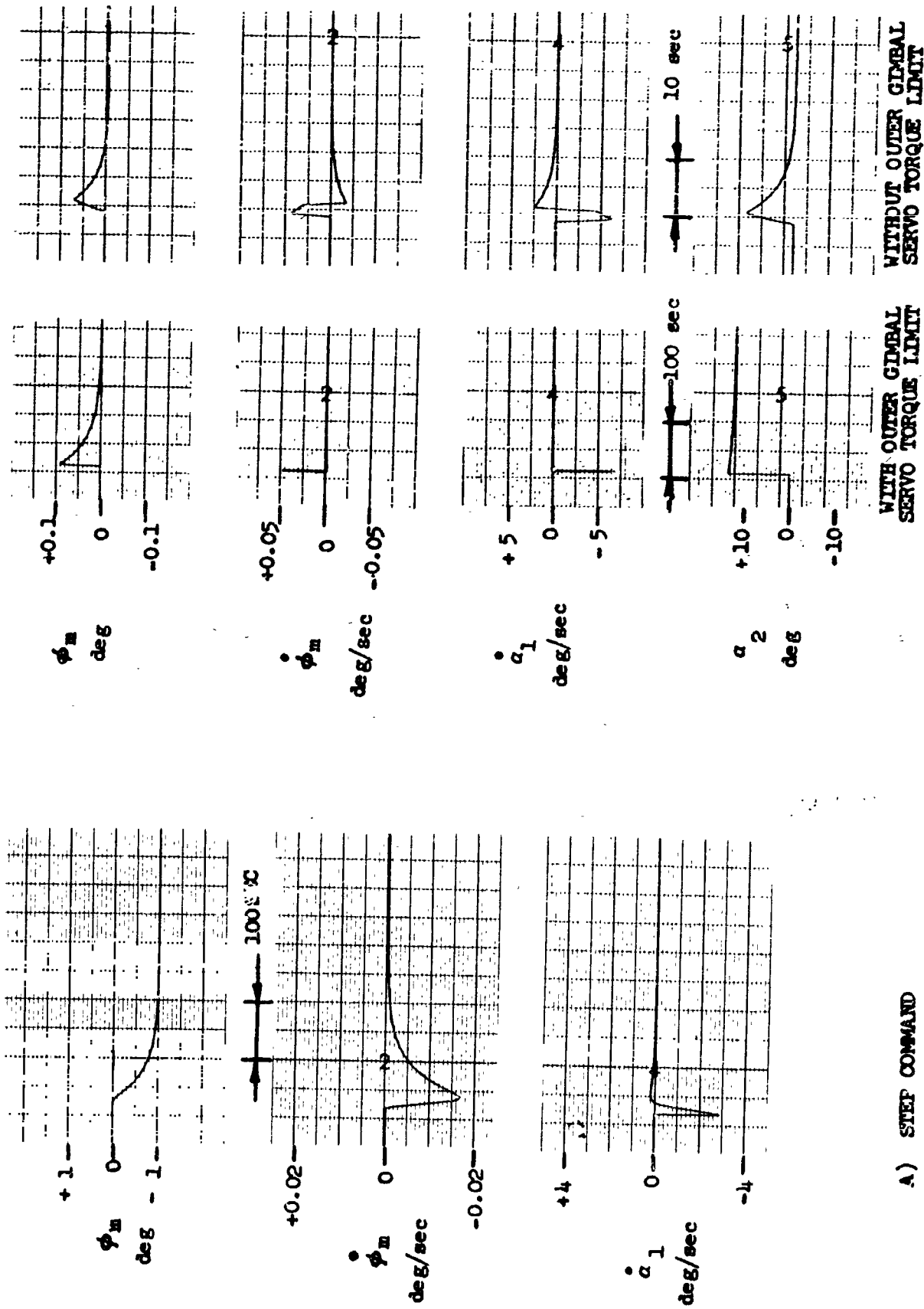
Figure 4.2-43: MORL ACS PARAMETERS

These parameters combine to give a second-order transfer function for the MORL control system. This system exhibits a natural frequency of 0.072 rad per second and a damping ratio of 1.56. The transient response of MORL is shown in Figure 4.2-44. The first trace shows step response; the second shows response to a manned disturbance. This manned disturbance was equivalent to a 6-slug man accelerating to 5 feet per second in 0.5 second at a 20-foot lever arm (as defined in Reference 30). This disturbance induces 0.07-degree error into the MORL; the worst case predicted by the MORL studies is 0.12 degree. The second traces also show the effects of a torque limit on the outer gimbal servo. The inner gimbal control torques must be transmitted through this servo; thus, torque limiting induces appreciable response changes. The torque limit cannot be accurately represented on a coplanar simulation, so all other runs assume perfect outer-gimbal servos.

4.2.4.5 Soft-Gimbal Mode Performance -- In an attempt to determine the stability and performance of the soft-gimbal mode, an analog simulation of the MORL and MOT attitude-control systems and the coupling between them was performed. This was only a partial analysis, and it is considered useful to present sufficient details about the simulation so that its limitations can be assessed.

The simulation of the MOT ACS corresponded to that previously discussed and shown in Figures 4.2-26 and 4.2-30. Effects of gimbal friction and sensor noise were included. The MORL control system corresponded to the one in Figure 4.2-42; the only nonlinearities included were the gain loss relative to CMG gimbal





A) STEP COMMAND

B) CREW DISTURBANCE

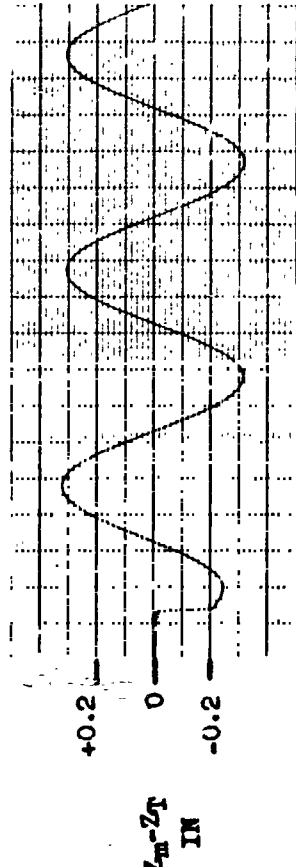
FIGURE 4.2-44  
MORL TRANSIENT RESPONSE

angle and the saturation of the CMG torque motor. The coupling from the soft gimbal corresponded to Equation (4) (Section 4.2.3.11).

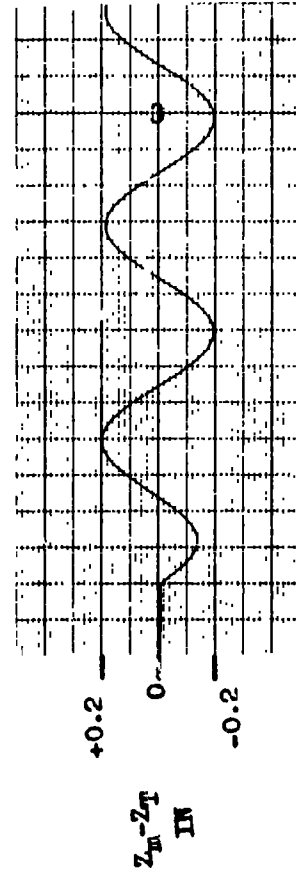
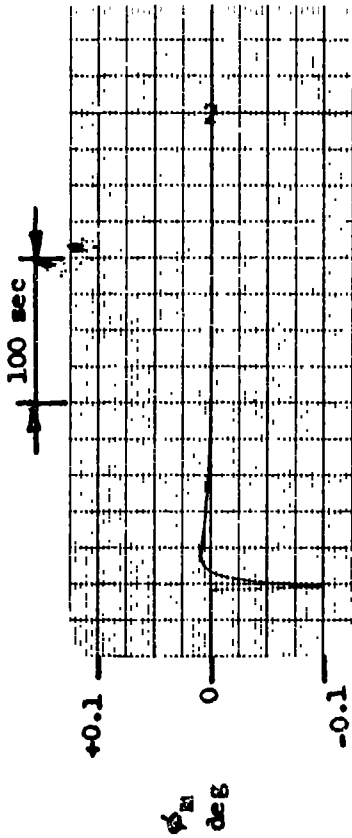
The three degrees of freedom simulated were the MORL and MOT angular orientations and their relative Z-axis displacements. Assuming that the MORL receives no torque from the soft-gimbal suspension, the result of a MORL crew disturbance on the variables of interest is shown in Figure 4.2-45. Trace A shows the case for an angular disturbance only; Trace B shows the case for a combined angular and linear disturbance. It is seen that the low-frequency linear oscillations persist as would be expected because the two large masses are connected through a very weak spring. If the coupling torques are added to the MORL and MOT, however, the linear oscillations are rapidly damped as shown in Figure 4.2-46. The conclusion, therefore, was that the angular degrees of freedom are indeed stable, and the MORL attitude-control system was damping a linear degree of freedom. Since this result was totally unexpected, a linearized analysis of the situation was performed, neglecting the MOT angular degree of freedom. With this assumption, the soft-gimbal block diagram can be simplified as shown in Figure 4.2-47. The root locus of this system is shown in Figure 4.2-48, where it is seen that the analysis predicts a 0.14 damped, 0.006 cps second-order response, which agrees quite satisfactorily with the computer results. The analysis points out how fortuitous was the choice of system parameters. Had a higher MORL control frequency been chosen, the linear oscillations would remain undamped; however, for any reasonable choice of parameters, the system is never unstable. It must be remembered, however, that the X-axis oscillations are uncoupled and, as such, oscillations will persist ad infinitum. Over a long term, MORL crew motions could build these oscillations up to an appreciable level, and some method must be found for damping this degree of freedom. Some suggested techniques include:

- 1) Designing the spring suspension such that all degrees of freedom are strongly coupled;
- 2) Use of soft-gimbal springs with appreciable amounts of hysteresis damping;
- 3) Mounting the soft-gimbal structure in a damper so that the suspension would look like a series spring damper.

With the soft-gimbal stability ensured, the study progressed to the MOT pointing errors as a result of MORL crew disturbances. Several cases were studied. Sample time histories are shown in Figure 4.2-49. It was found that MOT pointing errors were appreciably increased by the presence of MOT CMG gimbal friction. Results of these tests are shown in Figure 4.2-50 for the 1-rad-per-second system. The use of a high-frequency CMG and high-frequency control loops is very beneficial in reducing pointing errors in the soft-gimbal mode. The level of these errors is rather exorbitant, however, when allocations are made for other error sources. This area requires further study as evidenced by the traces in Figure 4.2-49, where it is seen that the 10-rad-per-second system remains essentially unaffected by soft-gimbal disturbances. However, the



B) 1200 FT LB<sub>f</sub> ANGULAR DISTURBANCE  
60 LB<sub>f</sub> LINEAR DISTURBANCE



A) 1200 FT LB<sub>f</sub> ANGULAR DISTURBANCE

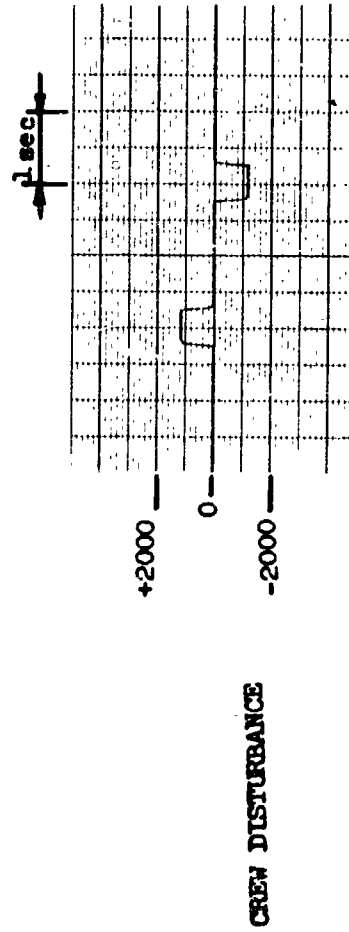
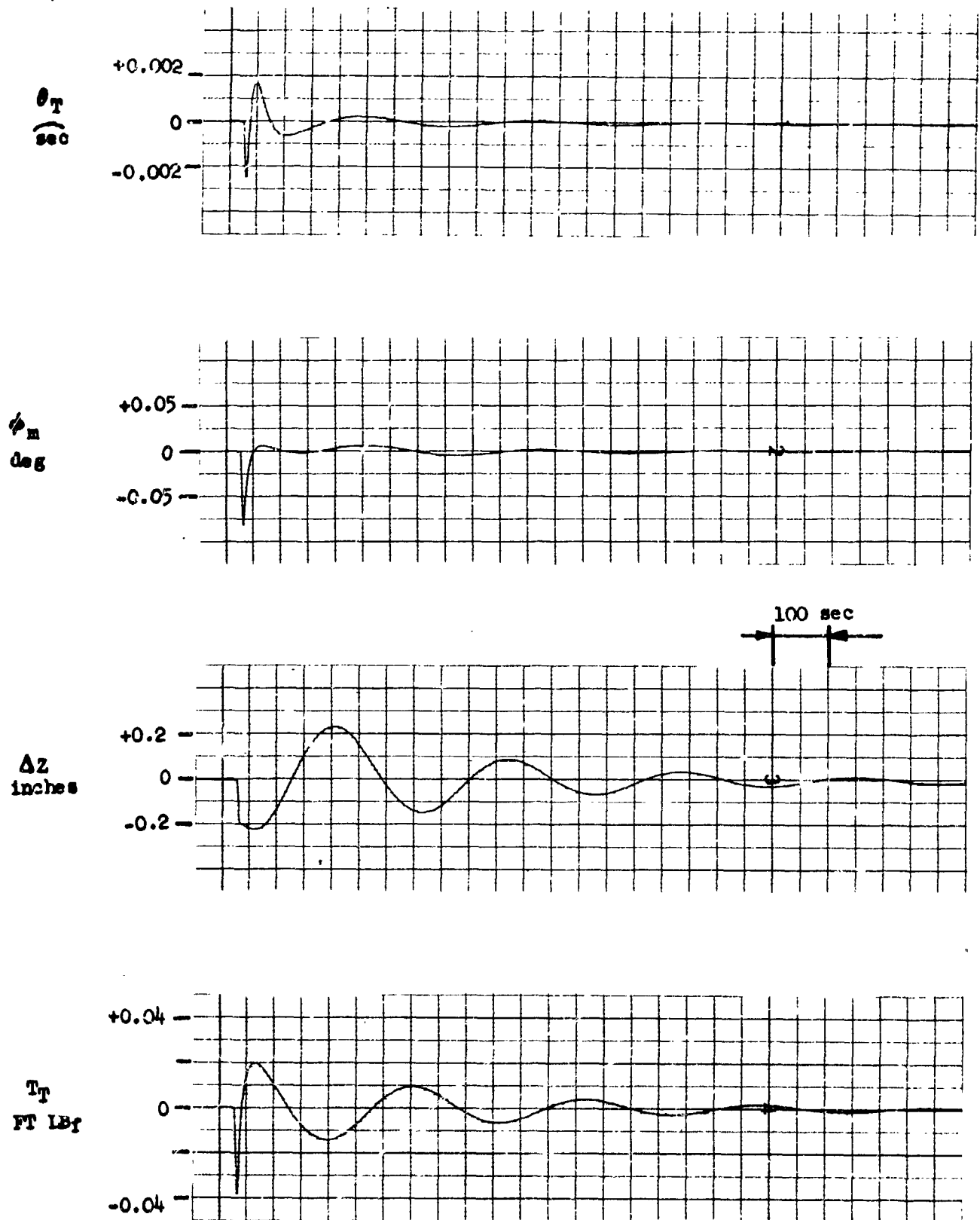


FIGURE 4.2-45  
MORL CREW DISTURBANCE - UNCOUPLED





1 RAD/SEC LOOP  
 5 CPS ACTIVE CMG  
 NO CMG GIMBAL FRICTION

FIGURE 4.2-46  
 MORL CREW DISTURBANCE - COUPLED

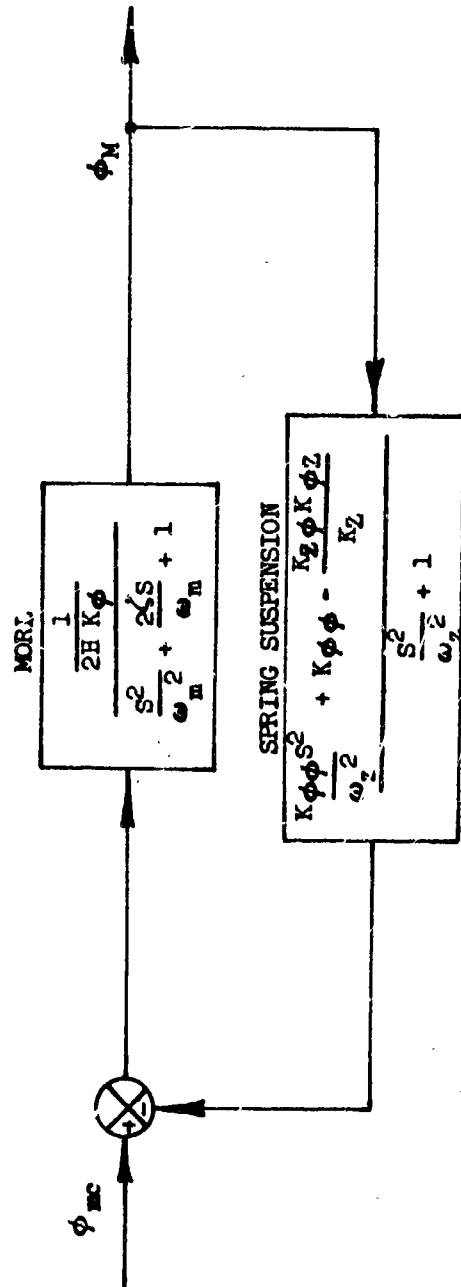
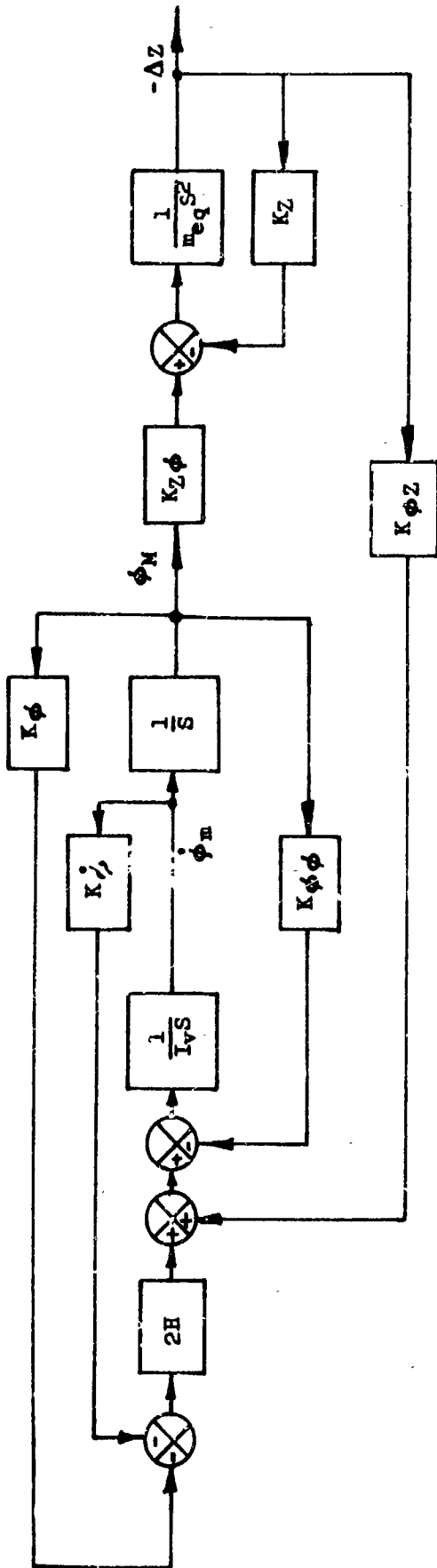


FIGURE 4.2-47  
SIMPLIFIED SOFT GIMBAL BLOCK DIAGRAM

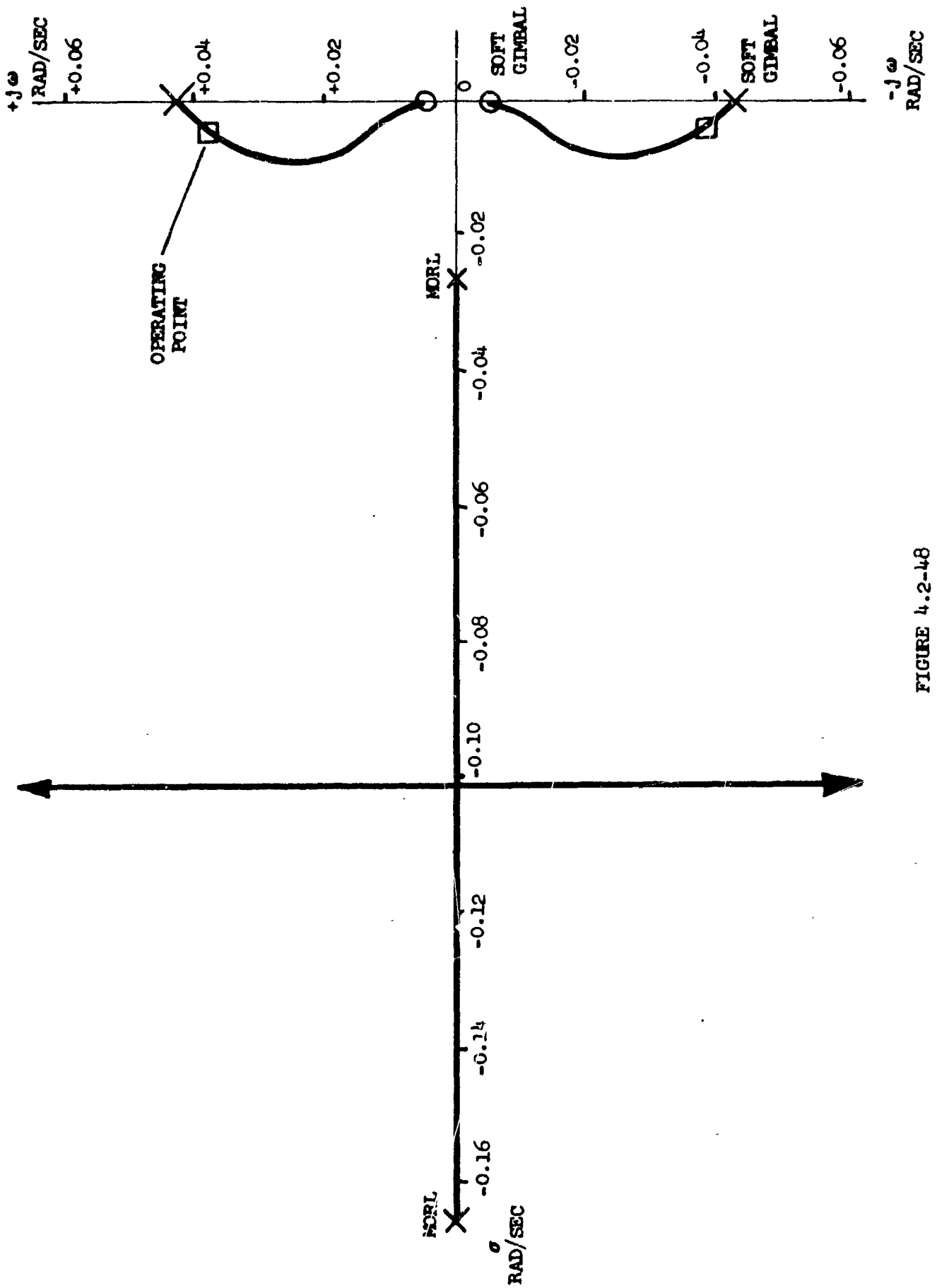


FIGURE 4.2-48  
ROOT LOCUS - SOFT GIMBAL MODE

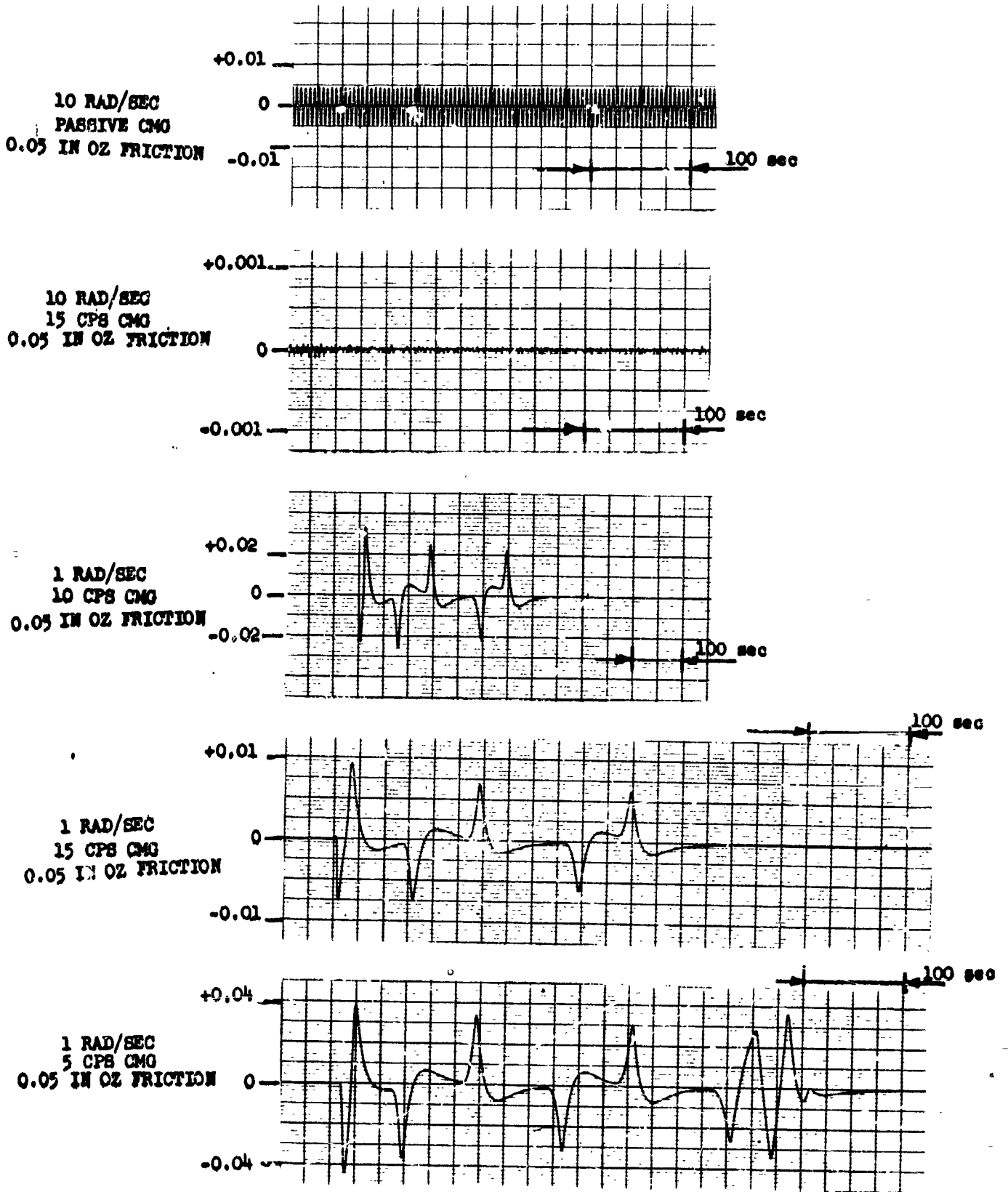


FIGURE 4.2-4g  
TIME HISTORIES - SOFT GIMBAL MODE

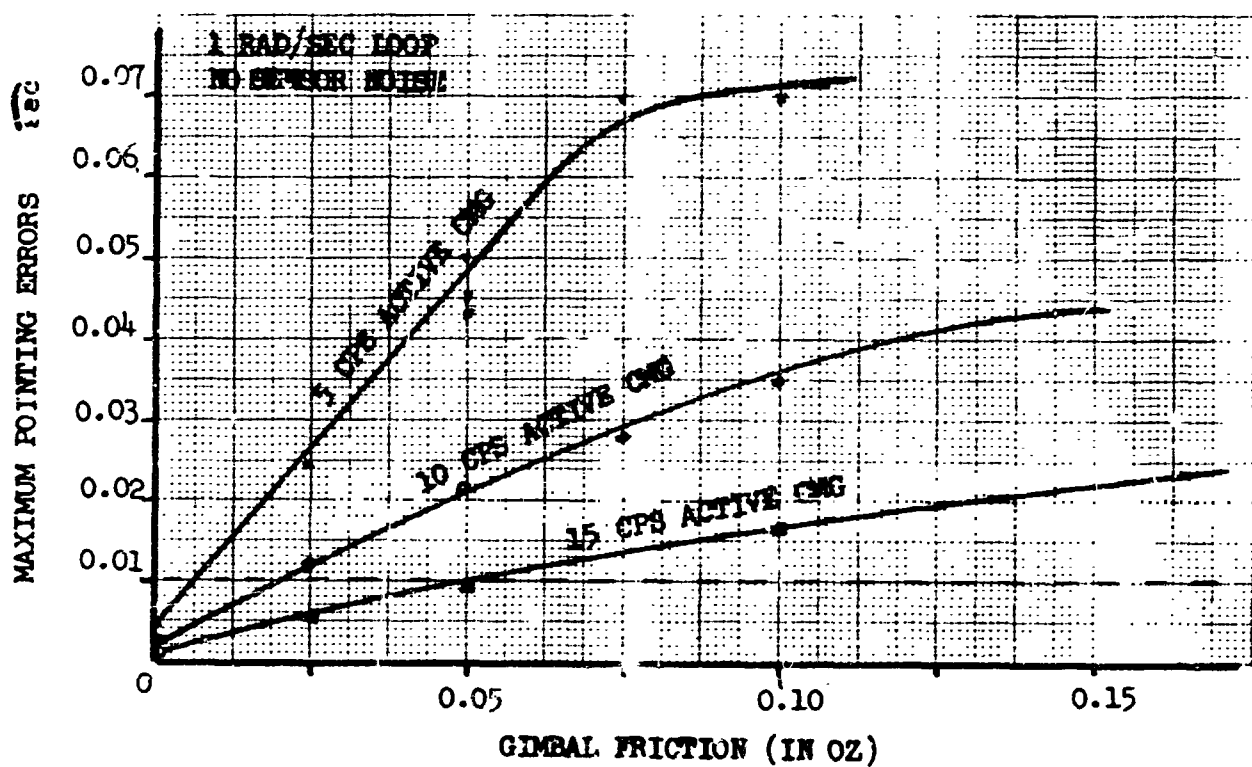


FIGURE 4.2-50  
POINTING ERRORS - SOFT GIMBAL MODE

10-rad-per-second system has a disadvantage due to the noise and structural flexibility problems it introduces. It may thus be concluded that the soft-gimbal control problem will be significantly more difficult than with the detached mode, although present results indicate that pointing requirements can be met.

#### 4.2.5 Conclusions and Recommendations

This section summarizes effects of orbit altitude and configuration on the attitude-control problem; further study of some critical attitude-control problem areas is recommended.

4.2.5.1 Orbit Altitude Comparison — Orbit altitude does not affect the ACS pointing requirements; but, it can affect the performance of the ACS components. Four such effects are summarized below.

- 1) The external disturbance torques at synchronous-orbit altitude are two orders of magnitude less than those in a low Earth orbit. At low altitudes, these external disturbances were beneficial; they were of sufficient magnitude to smooth out the limit cycle induced by CMG gimbal friction. Because these torques were cyclic, however, the system required the ability to work in the absence of these disturbances. At synchronous-orbit altitude, the disturbances are not of sufficient magnitude to accomplish smoothing. Thus, external disturbance effects are negligible as they neither hurt or help the system performance.
- 2) In the synchronous orbit, continuous exposures are possible; the CMG is then required to store the external disturbances for periods of 24 hours instead of for the 40 minutes required in low Earth orbit. Even though the external disturbance torques are greatly reduced, the momentums thus differ only by a factor of two. The synchronous orbit thus has a slight advantage; however, it is not appreciable with the system concepts now under study.
- 3) The higher orbit altitude has less background radiation, that is, a "darker sky." This effect is not appreciable because the extremely small field of view of the fine pointing sensors (twenty millionths of a square degree) does not permit the background noise to become appreciable with respect to the signal from the guide star.
- 4) In synchronous orbit, a single observation will be accomplished in half the time for that of the low Earth orbit. Since the ACS must maintain its null within a given tolerance for the total experiment time, the synchronous orbit will allow twice the rate of null shift as is allowable in the low Earth orbit. This null shift can arise from such sources as component aging and thermal induced drift. This effect is not expected to be acute due to the extremely narrow linear range ( $\pm 0.1$  arc-second) of the fine pointing sensors; however, past history indicates that it is an effect that warrants consideration.

Summarizing, the degree of difficulty of the attitude-control problem is not particularly sensitive to the orbit altitude; however, the synchronous-orbit altitude looks slightly advantageous.

4.2.5.2 Operational Mode Comparison — The attitude-control problem is quite sensitive to the telescope's mode of operation due to the effects of manned disturbances. In the detached mode, a 1-rad-per-second control loop is favored because:

- 1) The design of the control loop is considered significantly more conservative than higher response systems;
- 2) The low-response loop minimizes the effects of structural flexibility;
- 3) Low-response sensors are permissible, thereby decreasing the sensor noise.

It was found, however, that even small amounts of noise could interact with the CMG gimbal friction to induce system limit cycles. Although such errors could be maintained within requirements by using high-frequency CMG's the performance margin is very small. It is expected that further study into this interaction will develop techniques by which to minimize it; thus, the low-frequency loop with high-frequency active CMG's remains the most promising approach for the detached mode.

In the soft-gimbal mode, there is an additional source of error due to crew disturbances. This source exists in spite of the remarkable ability of the soft gimbal to attenuate the 1200-ft-lb<sub>f</sub>-crew disturbances to the 0.04 ft-lb<sub>f</sub> disturbance level applied to the telescope. Even these small disturbances, however, cause momentary MOT pointing errors in excess of requirements unless high-frequency CMG's are employed in high-frequency control loops. While these techniques indicate that the pointing specifications can be achieved, they lead to a less conservative design. The following considerations illustrate this point.

- 1) The use of very-high-frequency CMG's increases the possibility of noise inherent in the CMG gimbal servos.
- 2) The high-frequency loop implies high-frequency sensors that exhibit high noise levels.
- 3) The high-frequency loop increases the amount of coupling with the telescope structural flexibility.

Summarizing, the detached mode is favorable from the standpoint of minimizing the attitude-control problem; however, both configurations are feasible. The advantage of the detached mode lies in the absence of crew disturbances.

4.2.5.3 Recommendations — Although the studies have indicated that the attitude control of the MOT is feasible, the magnitude of the task (0.01 arc-second is equivalent to viewing a human hair from a distance of 1 mile) requires further study. Below are some areas where this need is most acutely felt.

Breadboard Studies of Control Hardware — These studies are required to verify the analytical results, as well as to point out at an early date those problem areas that are only uncovered by hardware simulation. A program orientated towards

the laboratory demonstration of the required pointing accuracy on an air bearing simulator is both practical and imperative.

**System Synthesis Studies** — The studies to date have only begun to uncover the problem areas and the techniques necessary to solve these problems. For example in the detached mode, methods minimizing the errors due to CMG gimbal friction and sensor noise are required.

**Thermally-Induced Structural and Electronic Instability** — Changes in the thermal environment can produce both structural bending and electronic null shifts. The importance of these effects is not well known, but is fairly amenable to determine from an analytic study.

**System Synthesis Studies** — The studies to date have only begun to uncover the problem areas and the techniques necessary to solve these problems. For example, in the detached mode, methods to minimize the errors due to CMG gimbal friction and sensor noise are required. The soft-gimbal analysis presented here has barely scratched the surface of that required. Simulation of the full 11-degrees-of-freedom problem, including the soft-gimbal suspension bearing friction and control system nonlinearities and noise, is required for an adequate assessment of the ACS performance to be expected in this mode.

**Acquisition Problem** — The ACS sensor problem on MOT is overcome by using multiple sensors and a very-narrow-linear-range fine sensor. Such procedures lead to inefficient acquisition, particularly since the optical signal is differentiated to achieve system damping.

**Image Motion Compensation** — When viewing planetary objects, the telescope must obtain its reference from nearby stars and perform slewing to compensate for the planetary motion. Techniques for accomplishing this function need study.

**Roll Axis Control** — A fairly high level of roll axis stability is required for several of the observational programs. By "a fairly high level" is meant potentially as stable as 0.2 second of arc. The problem arises from the fact that a star tracker for roll attitude control should nominally be directed at right angles to the telescope axis. It is expected that the thermal/structural stability of the spacecraft structure would be the major problem in achieving this stability.



### 4.3 RADIATION AND MICROMETEOROID PROTECTION

In both the synchronous-orbit and 250-nautical-mile-orbit missions, the radiation environment constitutes a significant hazard. Shielding is successful in protecting man but is only partially successful in the protection of film. An impractical amount of shielding is needed to eliminate fogging completely. The results point up the need for some other means of protecting the film, such as making it less radiation sensitive or reducing the time of storage within a radiation environment.

The micrometeoroid environment is somewhat more severe in synchronous orbit but has negligible effects on MOT operations, as discussed in Section 4.3.5.

#### 4.3.1 Radiation Environment

The ionizing radiation that the MOT will encounter is classified as trapped or untrapped according to whether or not the particles are significantly trapped by the geomagnetic field. Trapped particles consist of protons and electrons. Untrapped particles are galactic cosmic rays and solar-event particles.

Galactic cosmic rays are predominantly very-high-energy protons with a small percentage of higher Z particles. Due to their high energy, these particles are impervious to any reasonable shielding.

Solar-event particles are most likely to be encountered during the years around solar maximum when the Sun is most active. Solar events can be predicted a month or more before the event by observation of activity on the Sun; but, these predictions are uncertain due to a lack of understanding of the causes of events. However, a few hours warning is provided by the solar flare that precedes arrival at Earth of the main body of solar event particles. Solar events have durations from 30 hours to 6 days, but approximately 3 days is typical. Most of the radiation is encountered 6 to 30 hours after the flare.

The fluence,  $J$ , of the solar-event particles for an event may be expressed as an exponential rigidity spectrum. That is:

$$J (> P) = J_0 e^{-P/P_0} \quad (1)$$

where  $P = \sqrt{E^2 + 1876E}$  is the proton's rigidity (momentum/charge) and  $E$  is the proton's energy in mev. The average  $P_0$  during the 6 years around the last solar maximum (1956 to 1961) was 100 Mv.

The fluxes and spectra of both the trapped and untrapped radiation are strong functions of position. Therefore, environments at both high and low orbits will be treated separately.

4.3.1.1 Radiation Environment at Synchronous-Orbit Altitude — The environment at synchronous-orbit altitudes is somewhat uncertain due to its large fluctuation with time. In this study, dose rates are not critical, but the integrated dose is. Thus, conservative time averages are used where applicable.

Trapped Radiation — The flux of trapped electrons varies over a large range dependent on local time and geomagnetic disturbances; therefore, a time average over several months is used. The spectra of both the protons and electrons are quite steep (i. e., predominantly low-energy particles). The flux of electrons above 40 kev is  $5 \times 10^7/\text{cm}^2/\text{sec}$  while the flux above 500 kev is only  $4 \times 10^4/\text{cm}^2/\text{sec}$ . Two  $\text{g}/\text{cm}^2$  of Al (0.292-inch) is sufficient to stop the electrons. The resulting Bremsstrahlung gives a dose rate of  $2.6 \times 10^{-2}$  rads per day or about 10 rads per year.

Similarly, the flux of protons above 10 kev is approximately  $3 \times 10^8/\text{cm}^2/\text{sec}$  and is less than  $50/\text{cm}^2/\text{sec}$  above 4 mev. The protons are stopped by a few  $\text{mg}/\text{cm}^2$  of material so that their dose contribution is negligible except for surface effects. In considering damage to optical surfaces and thermal coatings, energies of a few kev must be considered. The low-energy protons are important because they stop very near the surface and deposit all of their energy there. Extrapolating the proton flux to zero energy yields a value of approximately  $6 \times 10^8/\text{cm}^2/\text{sec}$  above zero mev.

Untrapped Radiation — The flux of galactic cosmic rays is small enough that it does not constitute a significant hazard to the men in the MOT mission. However, since the film is so much more sensitive to radiation than man, the galactic cosmic ray dose must be considered in detail.

The galactic cosmic ray intensity has been found to vary by approximately a factor of two with the solar cycle. At solar maximum, the dose is approximately 5 rads per year and at solar minimum, approximately 12 rads per year. This difference is due to an increase in the solar magnetic field near the Earth when the Sun is active. The increased field prevents lower-energy particles from reaching the Earth. Thus, the change in flux is due primarily to a change in spectra. At solar maximum the spectrum is harder, and shielding ( $\sim 50 \text{ g}/\text{cm}^2$ ) increases the dose because of the secondaries produced. A shield of  $50 \text{ g}/\text{cm}^2$  will increase the dose by approximately 15 percent. On the other hand, shielding will decrease the dose at solar minimum because the spectrum is softer. During this period,  $50 \text{ g}/\text{cm}^2$  will decrease the dose by approximately 50 percent. Both the time variation and shielding effects have been incorporated into this study.

The solar event particles constitute a significant hazard to both film and man. Since long-range predictions of events are not possible, a probabilistic approach is commonly used. In determining adequate shielding for men in the MORL, Douglas used the probabilities of encountering one or more large events. However, the great sensitivity of film to radiation necessitates the consideration of all the events. The resultant shielding curves are shown in Figure 4.3-1 for two probability levels. The curves depict

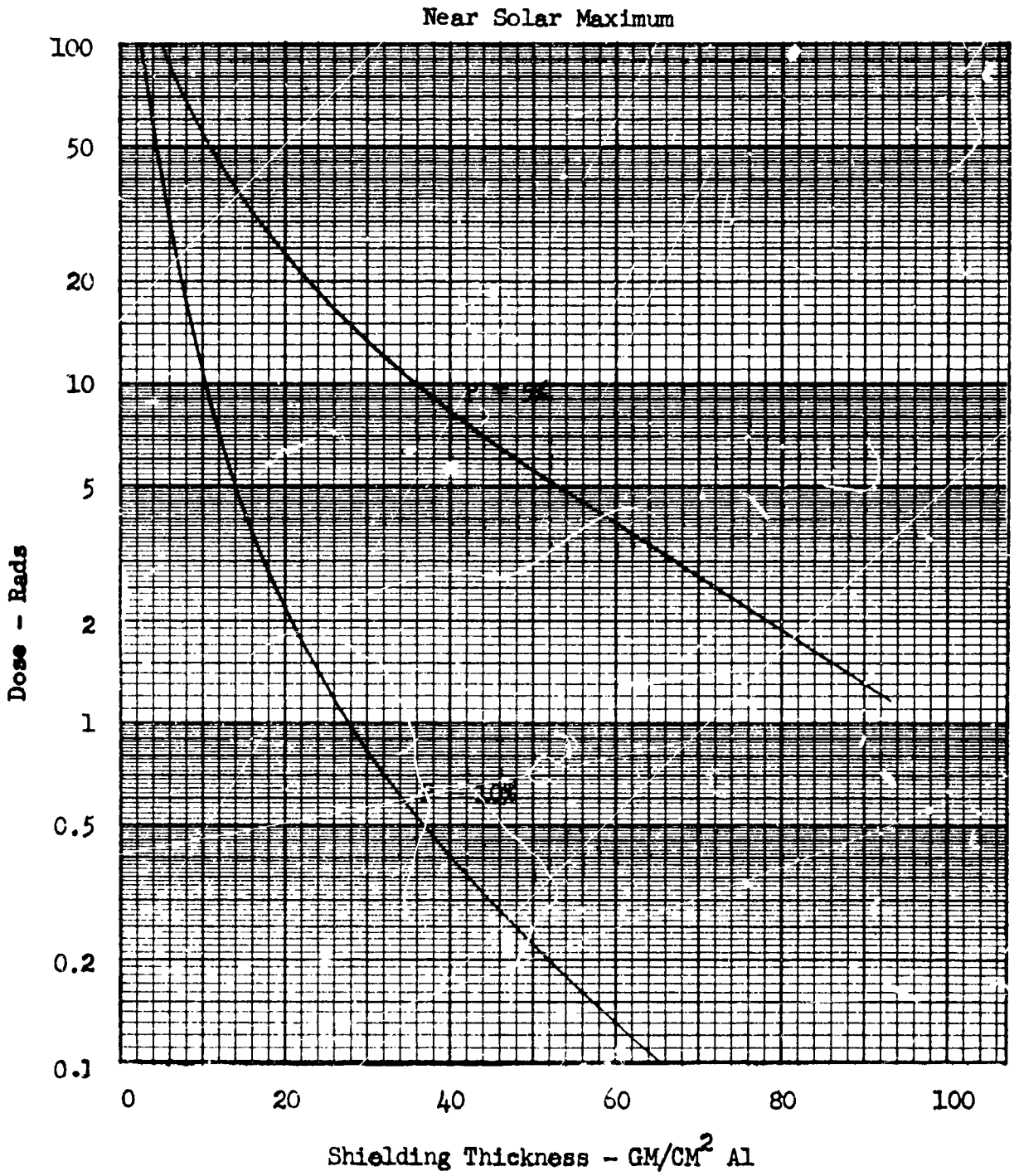


FIGURE 4.3-1 DOSE IN 60 DAYS - SYNCHRONOUS ORBIT

the dose inside a uniform aluminum sphere at constant probability of receiving that dose or greater in a 60-day period. (The 60-day period is the maximum time that unexposed film will be stored.) The study was based on the 6 years (1956-1961) surrounding the last solar maximum.

During solar minimum, the smaller events are less likely to occur than during solar maximum. However, there have not been enough large events to correlate them with the solar cycle. For this study, one-fourth the average yearly fluence for the 6 years around solar maximum was used as the expected yearly fluence during solar minimum. Using a characteristic rigidity,  $P_G$ , of 100 Mv., the shielding curves in Figure 4.3-2 were generated. This figure also includes the shielding curve for galactic cosmic rays at solar minimum.

Besides the radiation encountered at synchronous-orbit altitudes, the dose received in the transfer orbit must also be considered. The transfer studied for the MOT avoided the intense inner belt. The predicted doses for man and film are 0.4 rad or less and 0.25 rad or less, respectively. The dose to man is negligible. The dose to film is taken as 0.25 rad and incorporated in the fogging estimates.

4.3.1.2 Radiation Environment at Low-Earth-Orbit Altitude — The geomagnetic field prevents all but the highest-energy untrapped particles from reaching the 250-nautical-mile orbit at low latitudes. Most high-energy particles are galactic cosmic rays, which contribute a dose of approximately 0.003 rad/day independent of shielding. The solar event particle contribution is negligible.

The trapped protons and electrons constitute the largest hazard at low altitudes. These fluxes are encountered over the South Atlantic for 10 to 20 minutes during six or seven consecutive orbits per day.

The trapped electron flux is due primarily to the Starfish experiment in July 1962. The penetrating electrons from this experiment are decaying, and the flux is estimated to return to natural background between 1970 and 1972. The natural background is expected to be soft with very few electrons penetrating 2 g/cm<sup>2</sup> of aluminum. The Bremsstrahlung dose rate behind 2 g/cm<sup>2</sup> is expected to be  $3.7 \times 10^{-3}$  rads per day.

The trapped proton flux is the primary hazard due to its intensity and spectral hardness. The proton flux is from the high-energy proton (HEP) map compiled by Dr. James Vette from pre-1963 data. The proton shielding curve for the low-Earth-orbit mission is shown in Figure 4.3-3.

The proton flux at low altitudes varies with the solar cycle. When the Sun is active, the Earth's atmosphere expands due to heating and scatters the lower-energy trapped particles. Thus, the flux is higher around solar minimum; the HEP map

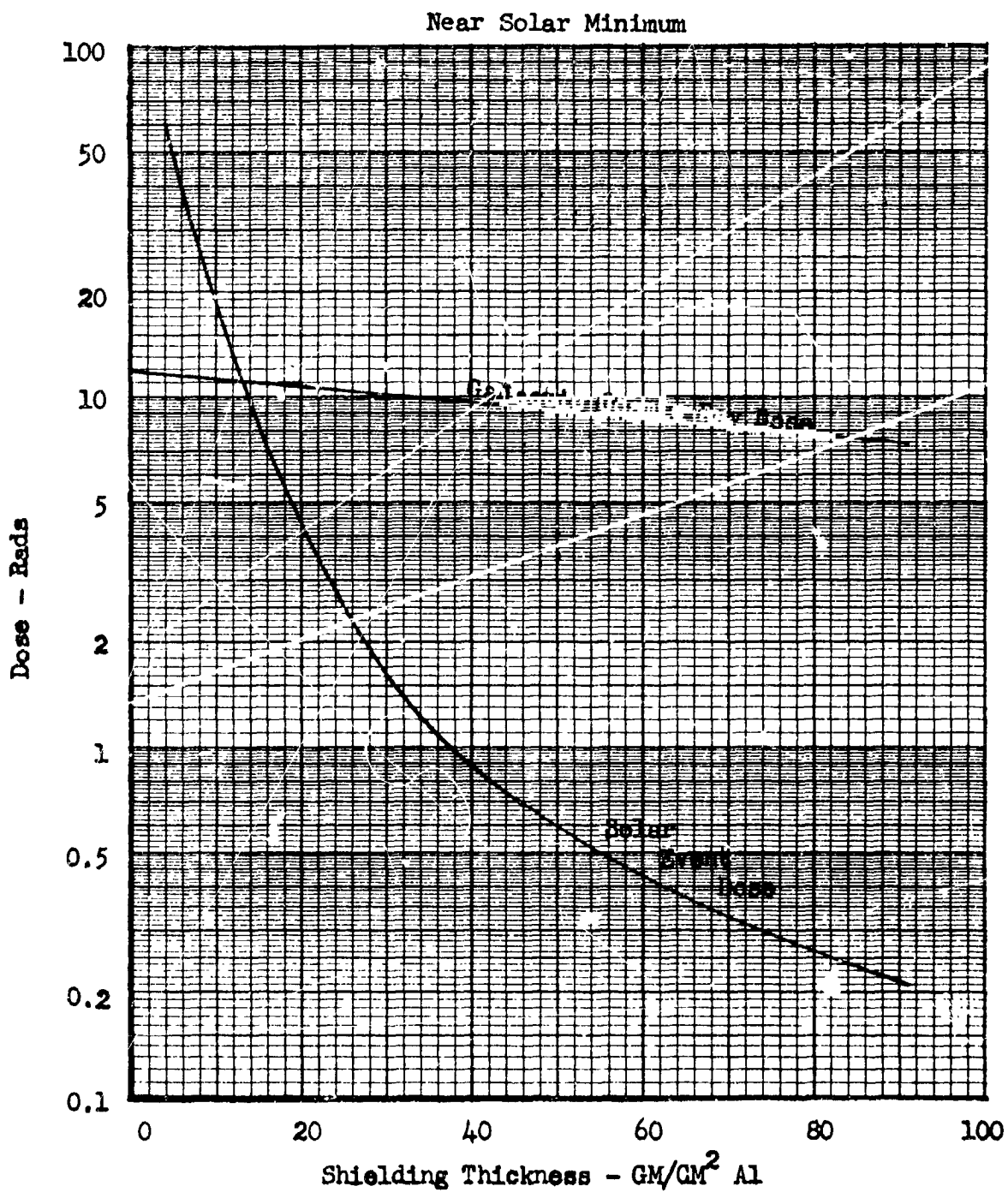


FIGURE 4.3-2 YEARLY DOSE - SYNCHRONOUS ORBIT

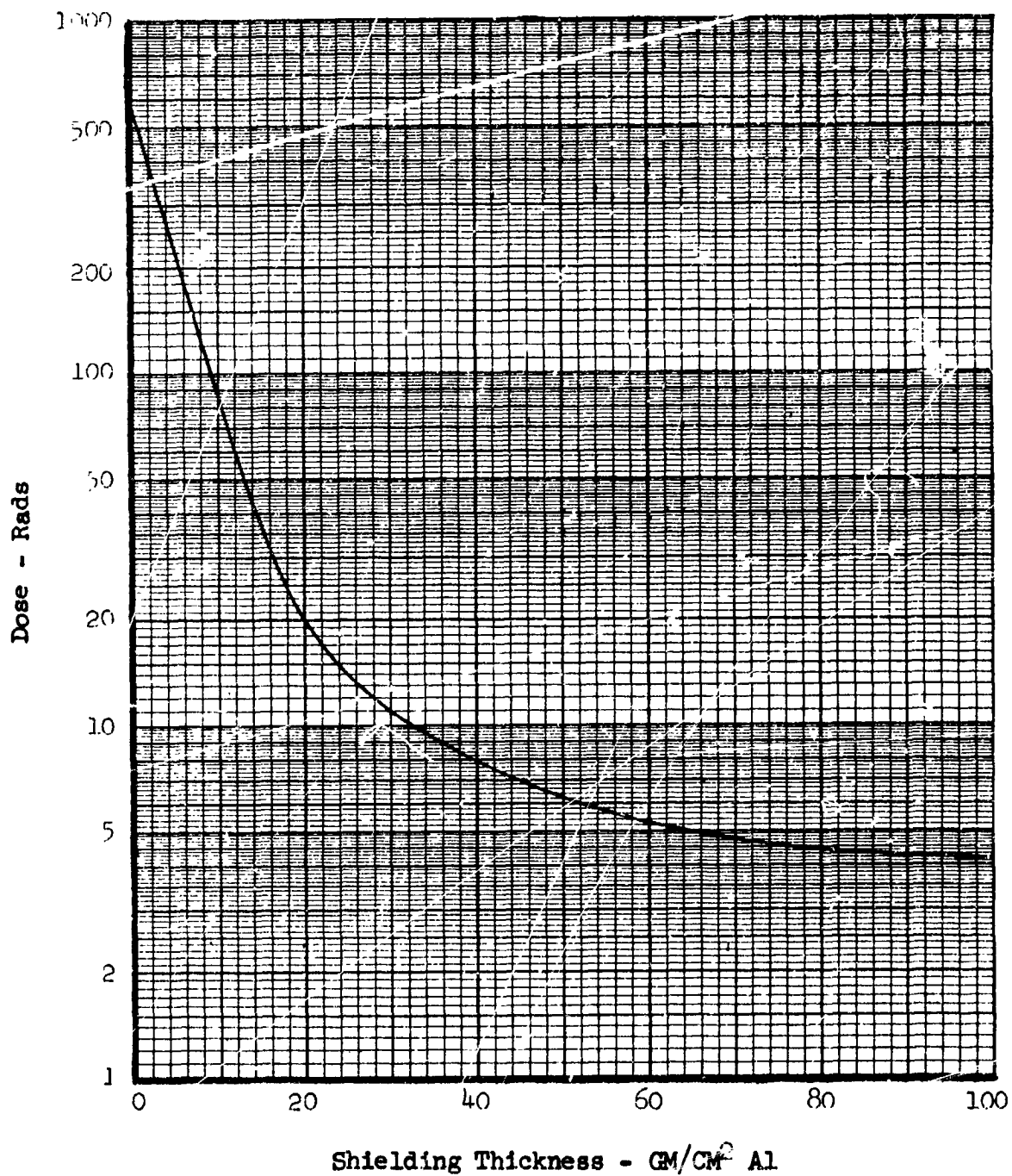


FIGURE 4.3-3 250 N MI YEARLY TRAPPED PROTON DOSE

incorporates data taken during solar minimum. Since the variation with the solar cycle is uncertain and since only low-energy protons are affected, the HEP will be used throughout. The HEP thus provides a conservative estimate of the high-energy trapped-proton environment.

The low-energy-proton environment in low Earth orbit must be extrapolated to zero energy for use in evaluating surface degradation. The result of this extrapolation is a flux of approximately  $5 \times 10^9$  protons/cm<sup>2</sup>/day above zero energy.

#### 4.3.2 Radiation Shielding for Man and Film

The emphasis of this section is on the shielding of film because film is much more sensitive to radiation than man. No radiation data are available on Types 103 and II films. Plus-X Aerecon film has film speed and granularity similar to Type 103, so the radiation response of Plus-X Aerecon has been used to estimate the radiation fogging that will be encountered. Radiation sensitivity is greater for higher-speed films. Thus, since Type II is slower than Type 103, the fogging calculated from Plus-X Aerecon should be conservative for Type II. The radiation response of Plus-X Aerecon is shown in Figure 4.3-4. In both orbits, the maximum time any piece of film is stored is 60 days. Thus, in this study, the effect of 60-day exposure to the radiation environment has been explored.

Since the film provides some self-shielding, the following assumptions are used. The film weighs 80 pounds and is stored in a 1.3-cubic-foot cubic box, allowing 20 percent of the volume for partitions, etc. Thus, the film at the center of the box has self-shielding of approximately 24 g/cm<sup>2</sup> (Al equivalent) in all directions, and the film at the side of the box has self-shielding of approximately 48 g/cm<sup>2</sup> (Al equivalent) over  $2\pi$  steradians.

The radiation tolerances used for man are:

Eyes	27 rad per year
Blood Forming Organs	54 rad per year
Skin	233 rad per year

These are the AEC radiation worker's lifetime tolerance compressed into a 5-year career.

**4.3.2.1 Shielding for Synchronous Orbit** — The synchronous-orbit version of MORL is designed with a biowell to adequately shield the crew during a 180-day stay time, based on Douglas data from Reference 9. The shielding for man in MORL at synchronous-orbit altitude, therefore, will not be considered in detail in this study. The dose received by man while in the MOT will not be significantly different from the dose he would receive in the MORL, as long as he is not in the MOT during a solar event. The heavier shielding of MORL does not affect the galactic cosmic-ray dose, and the trapped dose is minimal in both cases.

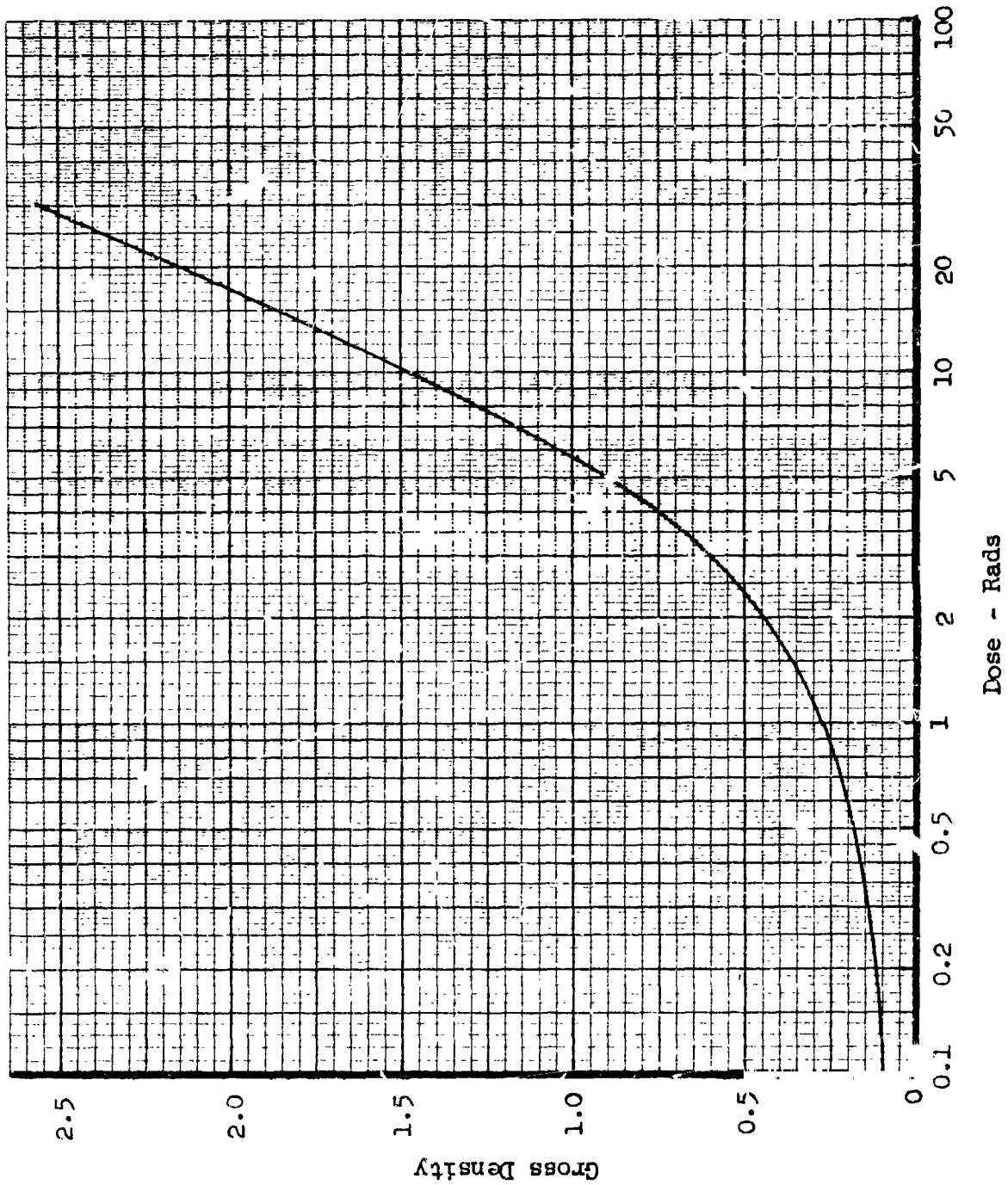


FIGURE 4.3-4 RADIATION RESPONSE OF PLUS-X AERCON



The film is stored in the biowell to take advantage of the biowell's shielding of  $10.5 \text{ g/cm}^2$  (Al equivalent). The density change due to radiation fogging during 60-day storage is presented in Figure 4.3-5 as a function of additional shielding provided by the box. The curves are drawn at constant probability of getting a given density change or greater. The probability is directly related to the solar events probability analysis shown in Figure 4.3-1. Also included are the effects of galactic cosmic-ray dose and the dose received during transfer. The dose from trapped protons, trapped electrons, and Bremsstrahlung are negligible at total shielding thicknesses of about  $50 \text{ g/cm}^2$ .

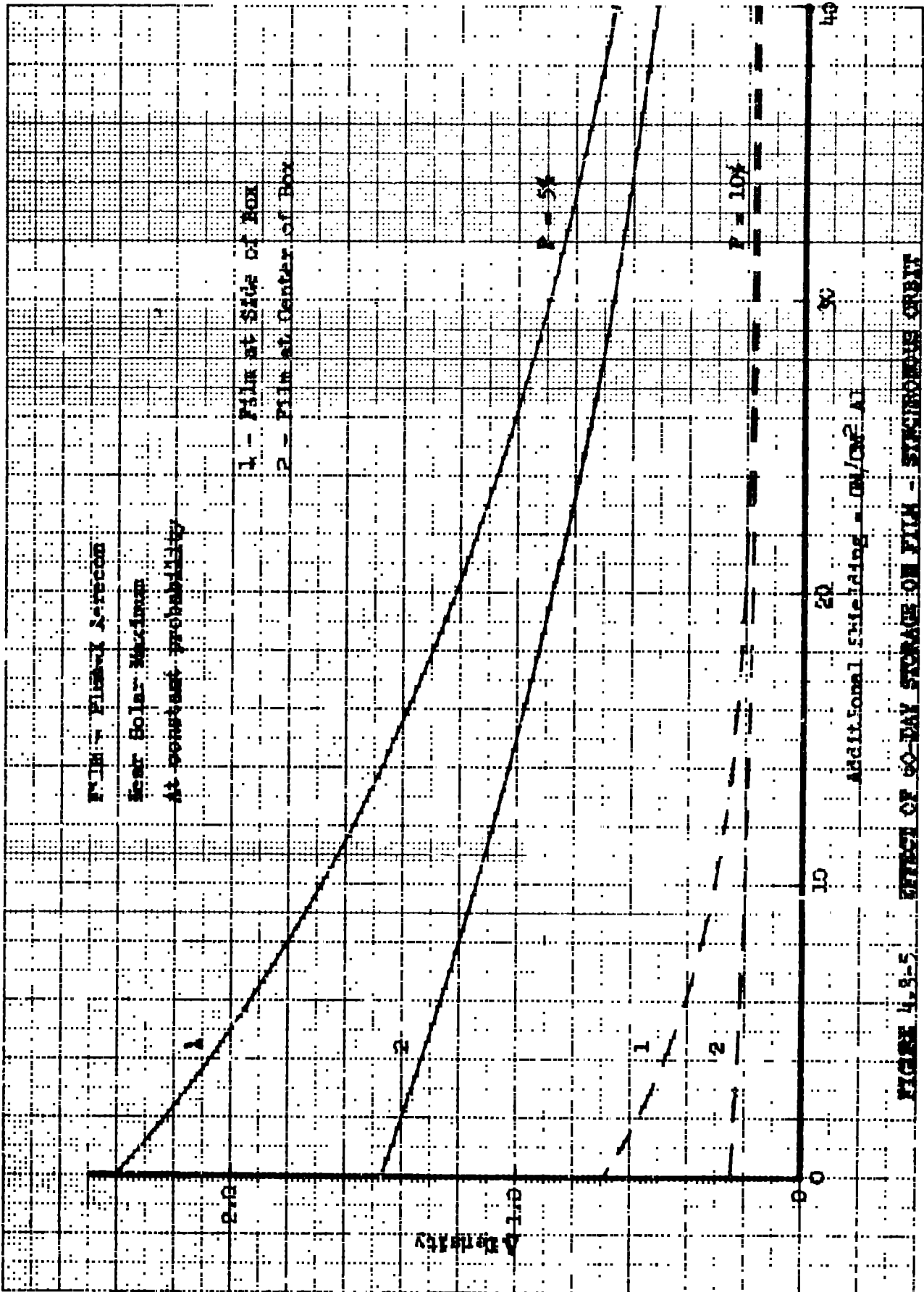
A shield of  $40 \text{ g/cm}^2$  Al, in addition to the biowell, is recommended for the film. As can be seen from Figure 4.3-5, additional shielding greater than this amount results in little gain. Curve flatness at these thicknesses is due to the galactic cosmic-ray contribution, against which it is practically impossible to shield.

The maximum time that any piece of film spends in the MOT is 9 days. During this time, the film receives essentially no dose from the trapped belts. The biggest contributor is Bremsstrahlung with a dose of 0.2 rad for the 9 days. The galactic cosmic rays will contribute approximately the same dose, whether the film is in storage or in the camera. In the event of a solar flare, there is enough warning to move the film to storage if desired. However, the option remains to leave the film in the MOT, since the amount of film lost would not be great.

Figure 4.3-6 shows the fogging as a function of shielding during solar minimum. As can be seen from Figure 4.3-2, the dose is due primarily to galactic cosmic rays. Thus, fogging is nearly independent of shield thickness.

4.3.2.2 Shielding for Low Earth Orbit — The low-Earth-orbit MORL configuration is estimated to be equivalent to a uniform sphere of  $2 \text{ g/cm}^2$  Al in thickness. Figure 4.3-7 shows the change in density due to fogging in 60-day storage as a function of shielding added to the  $2 \text{ g/cm}^2$  sphere. This fogging is due primarily to trapped protons since the contributions from trapped electrons, Bremsstrahlung, cosmic rays, and solar events are negligible. Additional shielding to bring the film storage shielding to  $50 \text{ g/cm}^2$  is proposed. The spectrum of high-energy trapped protons makes the curve fairly flat at these thicknesses so that greater shielding has little effect.

The time the film spends in the MOT is also of importance because the MOT is loss heavily shielded than the film storage area. The following table depicts film shielding inherent in the MOT.



**FIGURE 4.3-5. EFFECT OF 60-DAY STORAGE ON FILM - ESTIMATED DATA**

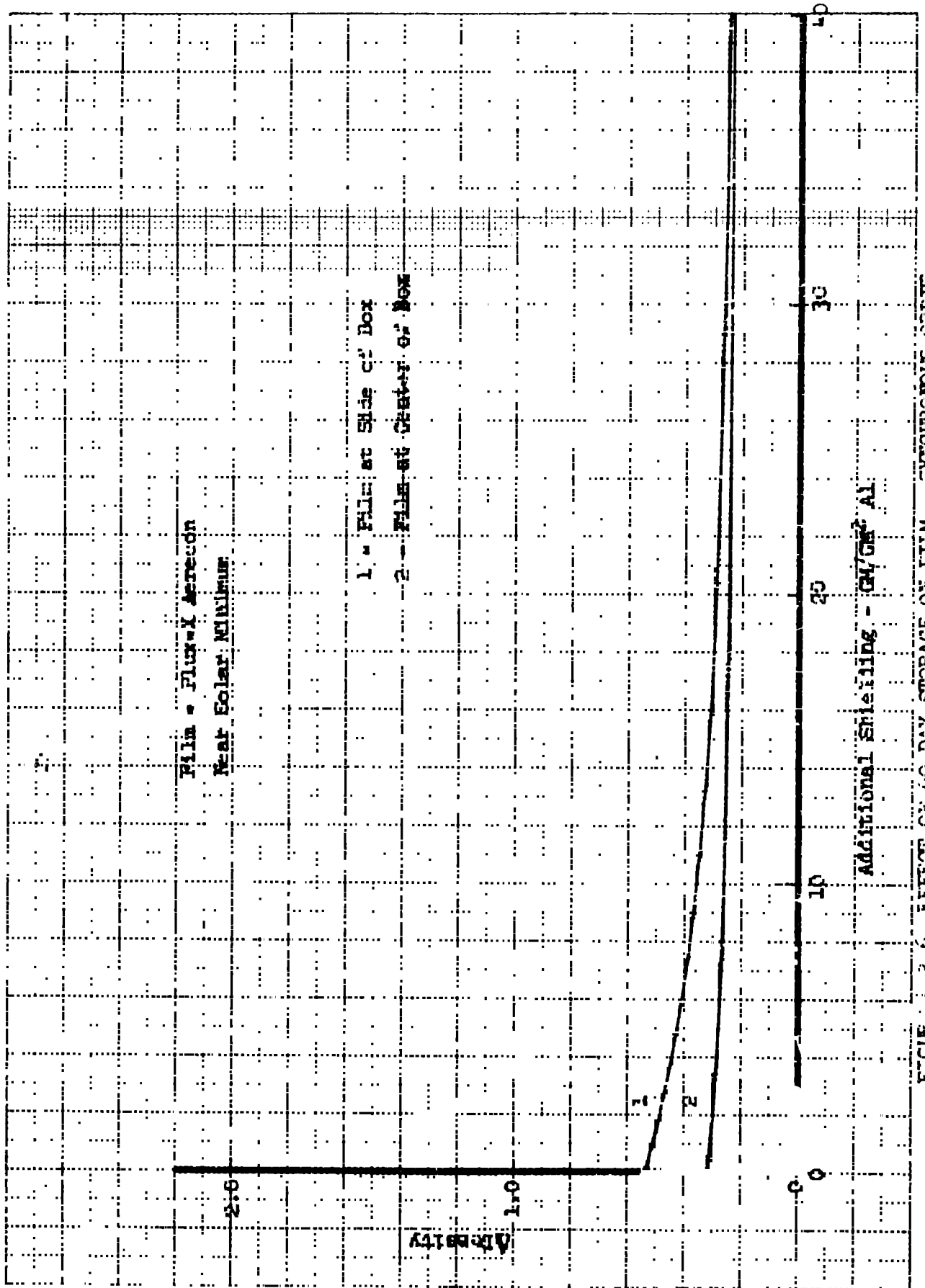


FIGURE 4.3.6 EFFECT OF 60-DAY STORAGE ON FILM - SYNCHRONOUS ORBIT

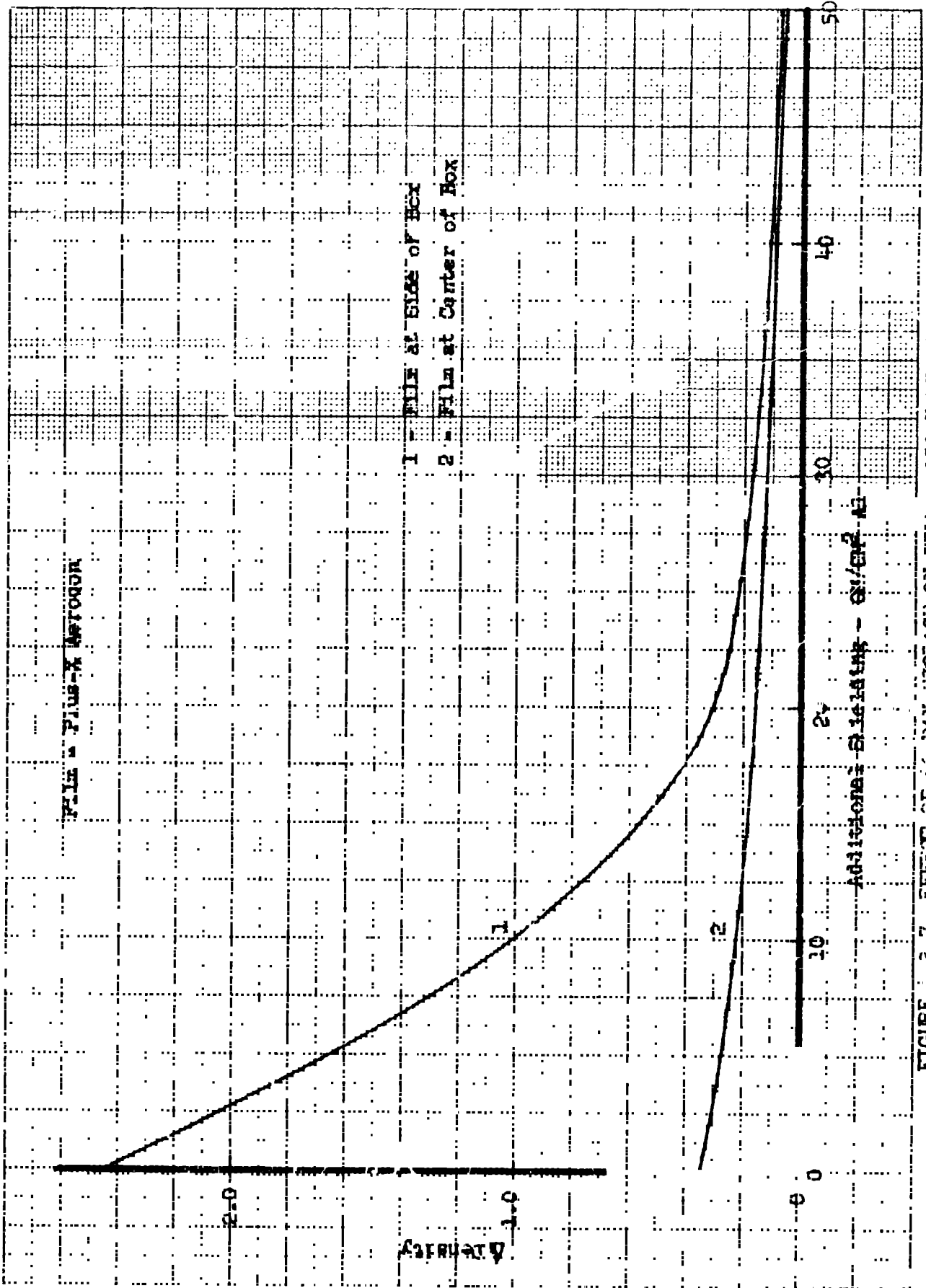


FIGURE 2.3-7 EFFECT OF 50-DAY STORAGE ON FILM - 250 N MI ORBIT

	<u>% Solid Angle (<math>\sim 1 \text{ g/cm}^2</math>)</u>	<u>% Solid Angle (<math>\sim 20 \text{ g/cm}^2</math>)</u>
Detached Mode	46	54
Soft-Gimbal Mode	24	76

The shielding figures for the two modes differ because the MORL provides shielding in the gimbal mode but not in the detached mode. This is the only significant difference between the two modes in either orbit from the radiation standpoint.

The shielding inherent in the MOT is inadequate for the protection of the film in the cameras. If the thinly shielded sectors are increased to  $15 \text{ g/cm}^2$ , the dose rates are 0.06 rad per day and 0.05 rad per day for the detached and soft-gimbal modes, respectively. For comparison, if the shielding were only increased to  $10 \text{ g/cm}^2$ , the film would receive a dose during 9 days in the camera comparable to the 60-day storage dose. Thus, the  $15 \text{ g/cm}^2$  increase provides the minimum acceptable shielding.

The shielding inherent in the MORL is not adequate to protect him in the 250-nautical-mile mission. The dose to man during the 180-day crew cycle is:

Eyes	85 rads
Blood Forming	25 rads
Skin	85 rads

Thus, the eyes receive more than their tolerance of 25 rads. If the crew wears  $6.5 \text{ g/cm}$  (approximately 0.8-inch glass) goggles during passes through the trapped belts, the eye dose will be reduced to tolerance level. Inherent in these dosage figures is the assumption that the crew is in MORL during transit through the trapped belts. If the crew were to spend time in the MOT during some of these transits, heavier goggles would be necessary (approximately  $7.5 \text{ g/cm}^2$ ).

4.3.2.3 Recommendations and Conclusions — The sensitivity of film requires that additional shielding for storage in the MORL be provided for both the synchronous- and low-Earth-orbit missions in the amounts of approximately  $40 \text{ g/cm}^2$  and  $48 \text{ g/cm}^2$ , respectively. If this shielding is a heavy aluminum box, the weight penalty in either case is approximately 1000 pounds. This figure could be reduced somewhat by a detailed study of each configuration and strategic placement of the container to take advantage of inherent shielding. In both cases the total storage shielding is approximately  $50 \text{ g/cm}^2$ .

Additional shielding for the MOT is needed only for the low-Earth-orbit mission. This shielding is placed around the film in the cameras and should bring the minimum shielding to  $15 \text{ g/cm}^2$ .

Additional shielding is not provided for the MOT in synchronous orbit because of the long-range unpredictability of the solar events environment. It is more

practical to use the short-term warning provided by monitoring the Sun's activity. If an event occurs, the film in MOT must either be moved to storage or abandoned. Hence, continual monitoring of solar activity must be a part of the operational procedures. There is also a chance that an event will occur that is large enough to require replacement of the stored film. Data obtained from monitoring the Sun is necessary to determine how soon replacement is practical.

In comparing film damage under the present assumptions, it is noted that the film in the synchronous orbit is more degraded simply because more radiation is expected in the synchronous orbit. Two points deserve re-emphasis, however:

- 1) Fogging estimates are based on limited data:
- 2) Results are quoted for the worst cases because of uncertainties in film properties and environment (primarily the solar event contribution).

The difference in fogging between synchronous and low Earth orbits are only important in that the fogging at synchronous orbit is greater at low Earth orbit. The foggings predicted for the two missions are so similar that the uncertainties involved preclude any more-detailed comparison. Uncertainties in the predicted fogging points up the great need for research in the area of film response to radiation. The magnitude of the predicted fogging indicates that desensitization of film to radiation must be explored. As an example of the last approach, people who use nuclear emulsions have had some success storing their film in a humid atmosphere. The only other approaches to the reduction of fogging are the use of more shielding, less sensitive film, or shorter storage periods. These approaches all involve penalties in weight or operational timeline.

The only additional shielding required for man in low Earth orbit are goggles to be worn when the vehicle passes through the trapped belts. The synchronous-orbit version of the MORL provides for human protection against two solar flares through the use of laboratory shielding and a biowell. Weight of this additional shielding for an available crew stay time of 180 days is 14,200 pounds. However, since the MORL study was based on a higher eye-dose tolerance than used in this study, it is recommended that goggles of approximately 15 g/cm<sup>2</sup> thickness be provided. With these goggles, the probability that the 27-rad tolerance will be exceeded is reduced to 3 percent; hence, the biowell constitutes the only difference between the two missions in terms of the shielding required to protect man.

Protection of man imposes some restrictions on operation timelines of both missions. At synchronous-orbit altitudes, man must be in the biowell during an event; at 250 nautical miles, man must wear goggles during transit through the belts.

Thus, the main differences between the two missions are: the film receives a greater dose in synchronous orbit than in low Earth orbit; the synchronous-orbit mission requires a biowell whereas the low Earth orbit does not.

### 4.3.3 Degradation of Radiated Surfaces

4.3.3.1 Optical Surfaces — MOT performance over a period of time can degrade because of deterioration of the optical surfaces by particle radiation discussed in Section 4.3.1.

MOT configuration considered for the purposes in this discussion is that shown on Page 133 in Reference 1. Since the 120-inch primary mirror cannot be entirely shielded from radiation, it is the most critical optical surface in regard to degradation by particle radiation.

Because of the location of the secondary and folding mirrors, their exposure to particle radiation is unlikely. The secondary mirror is shielded by the mount and by its surface facing the primary mirror — away from the incoming radiation. The folding mirrors are shielded by their location within the cabin and could be further protected by a light shield to baffle out stray light. This shield would be a cone projecting forward from the hole in the primary mirror.

The primary mirror considered for the MOT consists of the mirror structure (assumed beryllium) with a plating of Kanigen nickel, polished optically and coated with a vacuum-deposited reflective film of aluminum (References 37 through 40). The aluminum may have an overcoat of magnesium fluoride. Figure 4.3-8 illustrates the stacking of these surfaces. The purpose of the magnesium fluoride ( $MgF_2$ ) coating is threefold: abrasion resistance, oxidation protection, and enhancement of reflectivity in the ultraviolet portion of the spectrum.

The concern about particle radiation centers on the vapor-deposited aluminum and magnesium fluoride coatings because most of the low-energy protons will expend their energy in these coatings.

Aluminized Surfaces — Because Kanigen nickel has a low reflectivity, a thin layer of aluminum must be evaporated on the nickel. Much research has been reported concerning reflectance coatings and their characteristics (References 41 and 42). Aluminum is considered to be the best candidate material (Reference 43). Figure 4.3-9 illustrates the reflectance of aluminum compared with several other candidate metals.

The aluminum film is deposited at a pressure preferably no greater than  $1$  to  $2 \times 10^{-5}$  mm Hg on a substrate at a temperature no higher than  $50^\circ C$ . The film is deposited rapidly ( $< 15$  seconds) to a thickness of 600 to 900 Å. The thickness should be between 600 to 700 Å, especially on heated substrates because the specular reflectance decreases noticeably in the extreme ultraviolet with thick films (Reference 44).

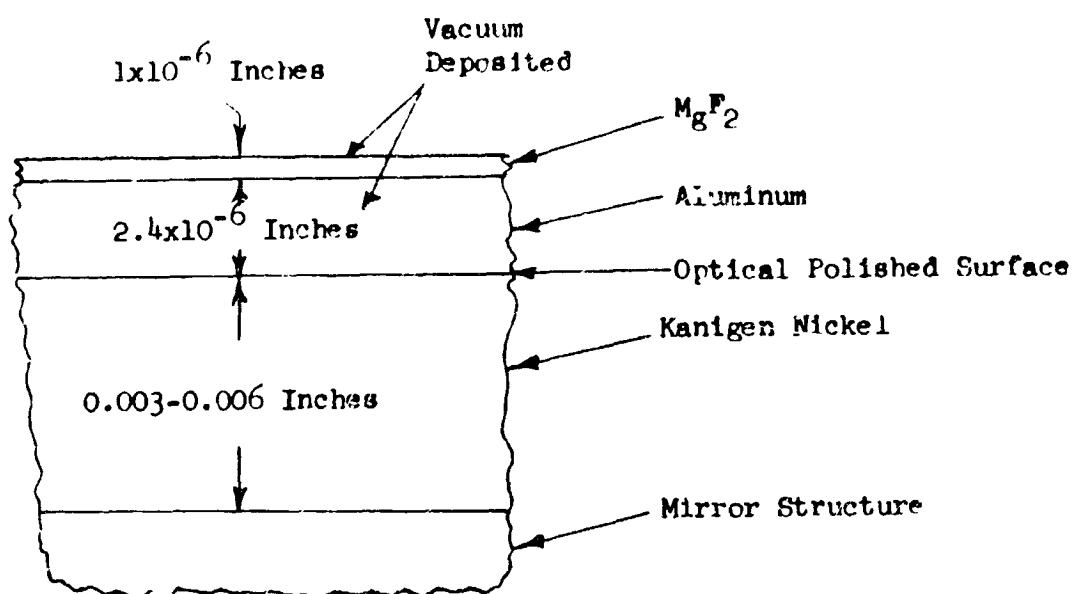


FIGURE 4.3-8 STACKING OF OPTICAL COATINGS

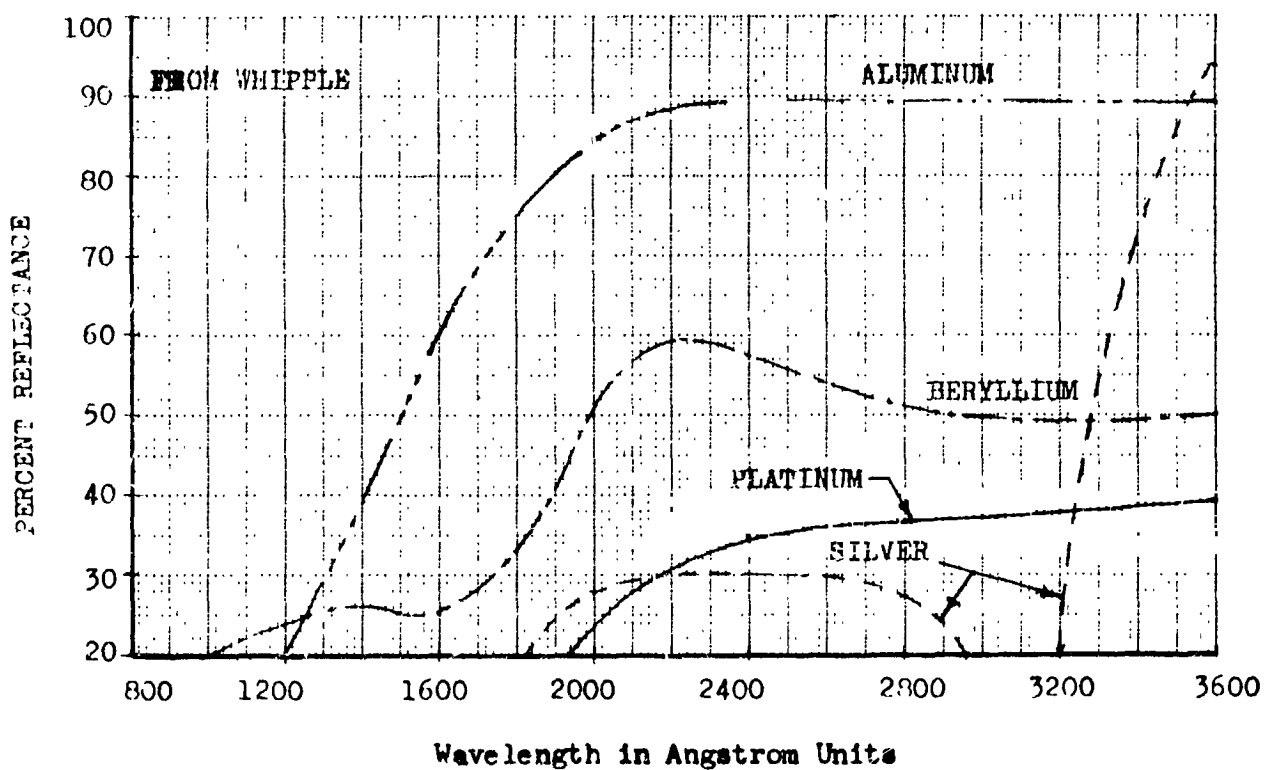


FIGURE 4.3-9 COMPARISON OF REFLECTANCE OF ALUMINUM WITH SEVERAL OTHER METALS



Mirror Overcoating — It is necessary to overcoat aluminum to prevent oxidation unless the aluminizing of the MOT mirrors is performed in space. Figure 4.3-10 illustrates the decrease in reflectance as a function of aging for several wavelengths in the ultraviolet for evaporated aluminum without an overcoat. Figure 4.3-11 illustrates the reflectance as a function of thickness of the oxide layer in the extreme ultraviolet generated by aging.

Another advantage to overcoating with magnesium fluoride ( $\text{MgF}_2$ ) is that it enhances the reflectance in the extreme ultraviolet wavelengths. Figure 4.3-12 shows this enhancement for two thicknesses of  $\text{MgF}_2$  coating compared with fresh aluminum only. Aging of the  $\text{Al}+\text{MgF}_2$  mirrors for 6 months showed no measurable decrease in reflectance, whereas the plain aluminum mirrors decreased approximately 38 percent at  $\lambda = 1216 \text{ \AA}$  (Reference 45).

An alternate method of protecting mirrors for use in the extreme ultraviolet has been to use lithium fluoride ( $\text{LiF}$ ) coatings. These coatings have been used where the main scientific interest was in the study of the profile of the Lyman- $\beta$  line of hydrogen at  $\lambda = 1025.7 \text{ \AA}$ . As can be seen in Figure 4.3-13,  $\text{LiF}$  has a higher reflectance in this region at some sacrifice of reflectance at longer wavelengths.  $\text{Al}+\text{LiF}$  mirrors show very little aging when stored in a laboratory at humidity of 40 percent or less. However, when the humidity was increased to 50 percent, a decrease in reflectance occurred compared with no change for an  $\text{Al}+\text{MgF}_2$  mirror under the same conditions (Reference 46).

Deterioration due to the solubility of  $\text{LiF}$  in water can be greatly reduced by adding a thin (15  $\text{\AA}$ ) film of  $\text{MgF}_2$  over the  $\text{LiF}$ . The addition of  $\text{MgF}_2$  reduced the reflectance by 4 percent, but the loss in reflectance was only 1 percent after a 4-day exposure to 50-percent humidity compared to a loss of 12 percent for an  $\text{Al}+\text{LiF}$  mirror without the  $\text{MgF}_2$ .

Another alternate protective film is silicon monoxide that has been treated by ultraviolet irradiation for 5 hours. Such a mirror has a reflectance of 92 percent at  $\lambda = 2200 \text{ \AA}$ , compared to approximately 40 percent without the ultraviolet treatment. No values are published for  $\lambda < 2200 \text{ \AA}$ ; therefore, the use in the extreme ultraviolet is questionable (Reference 47).

The preceding discussed the recommended optical coatings — the reflective and overcoat. If additional evidence indicates the  $\text{Al}+\text{MgF}_2$  mirrors deteriorate with approximately 5 keV proton irradiation, the alternative coatings may suffice with some compromise of performance. Another approach would be to protect the Kanigen and do the coating in space.

Radiation Effects — Data concerning effects of proton irradiation of approximately 5 keV on the particular types of optical surfaces discussed above is not available. However, a brief review of the effects of proton irradiation of higher energies on several of the different types of optical surfaces, including  $\text{Al}+\text{MgF}_2$

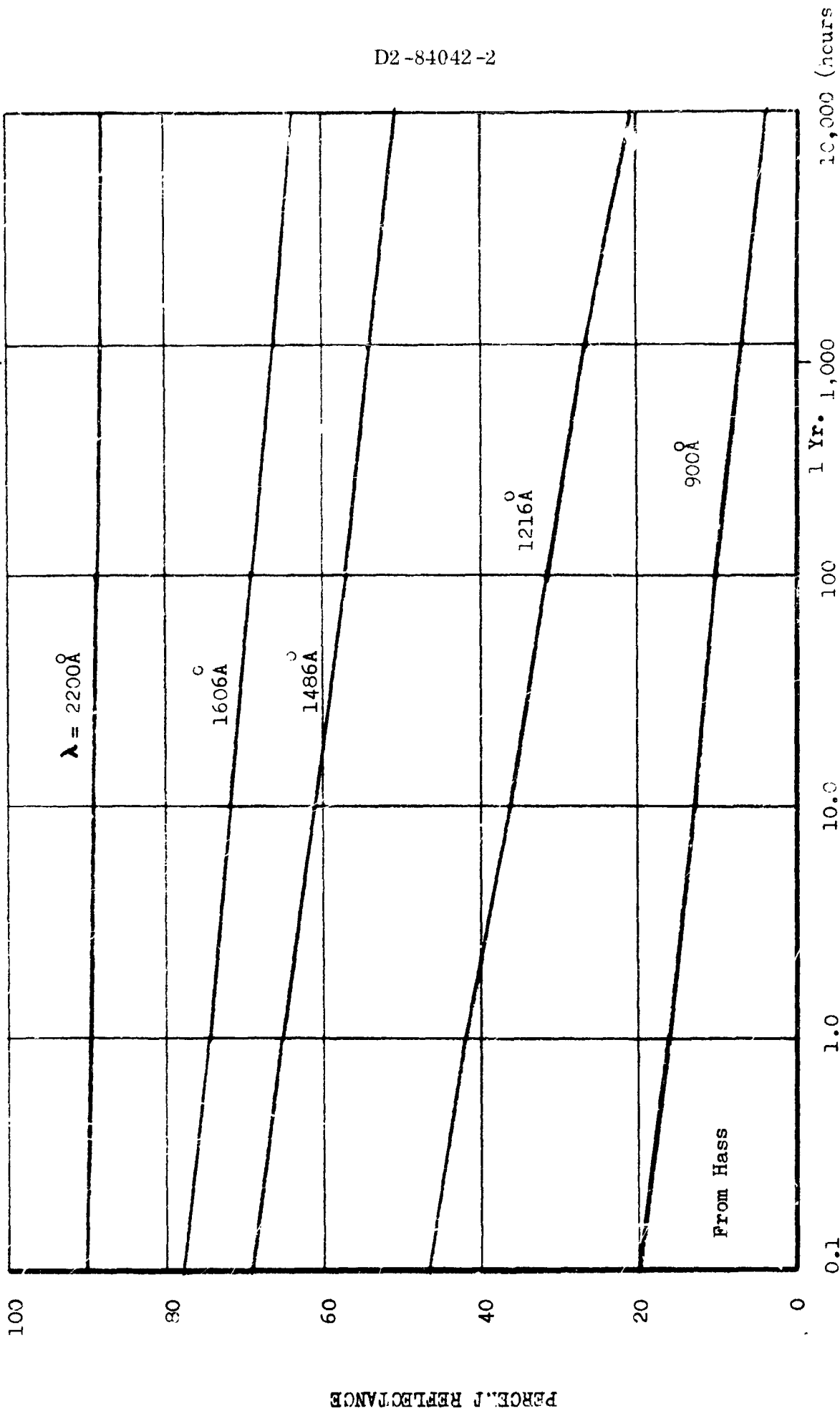


FIGURE 4.3-10 - DECREASE IN REFLECTANCE IN THE EXTREME ULTRAVIOLET AS A FUNCTION OF AGING

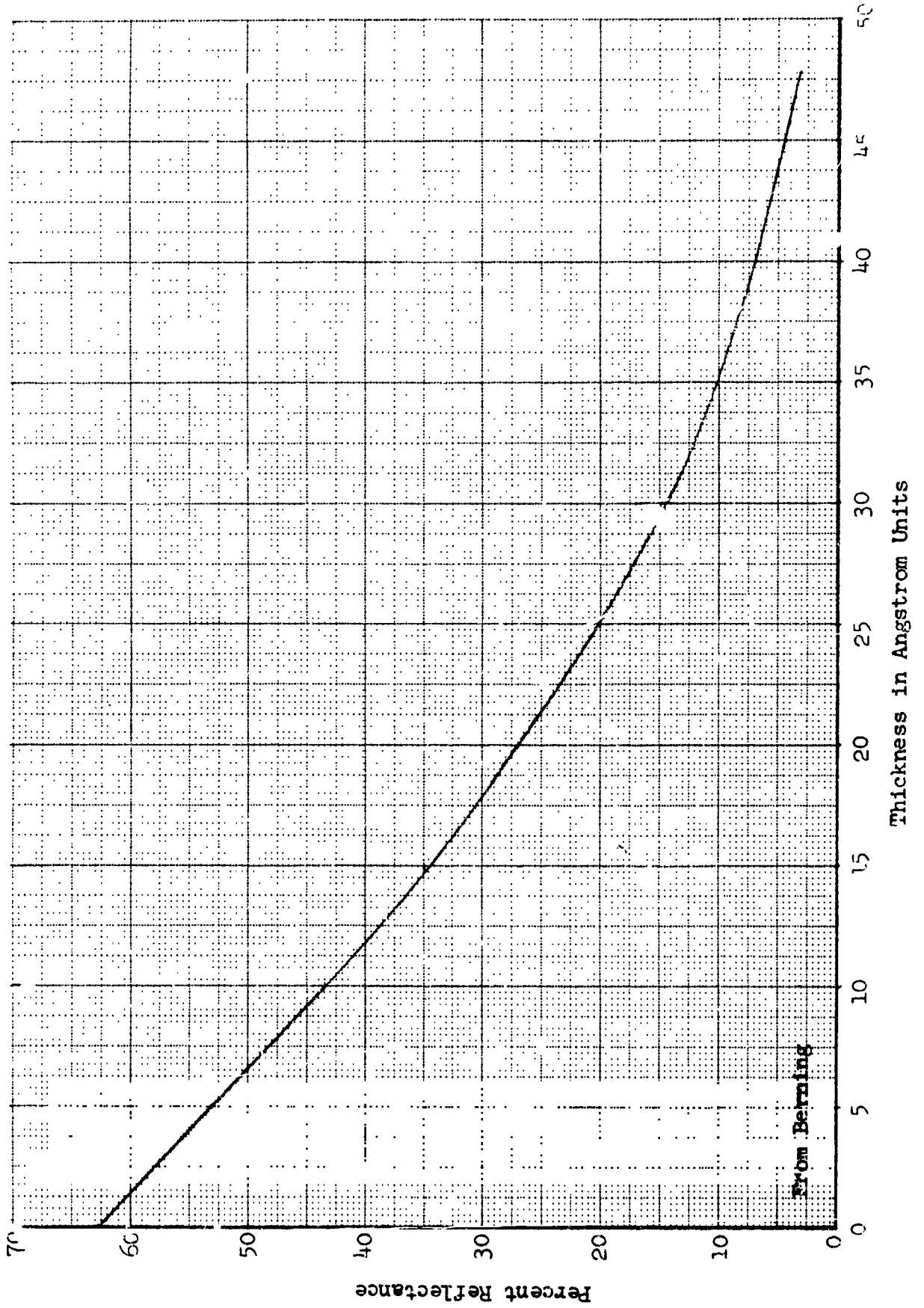


FIGURE 4.3-11 REFLECTANCE AS A FUNCTION OF THICKNESS OF ALUMINUM OXIDE LAYER AT  $\lambda = 1216 \text{ \AA}$

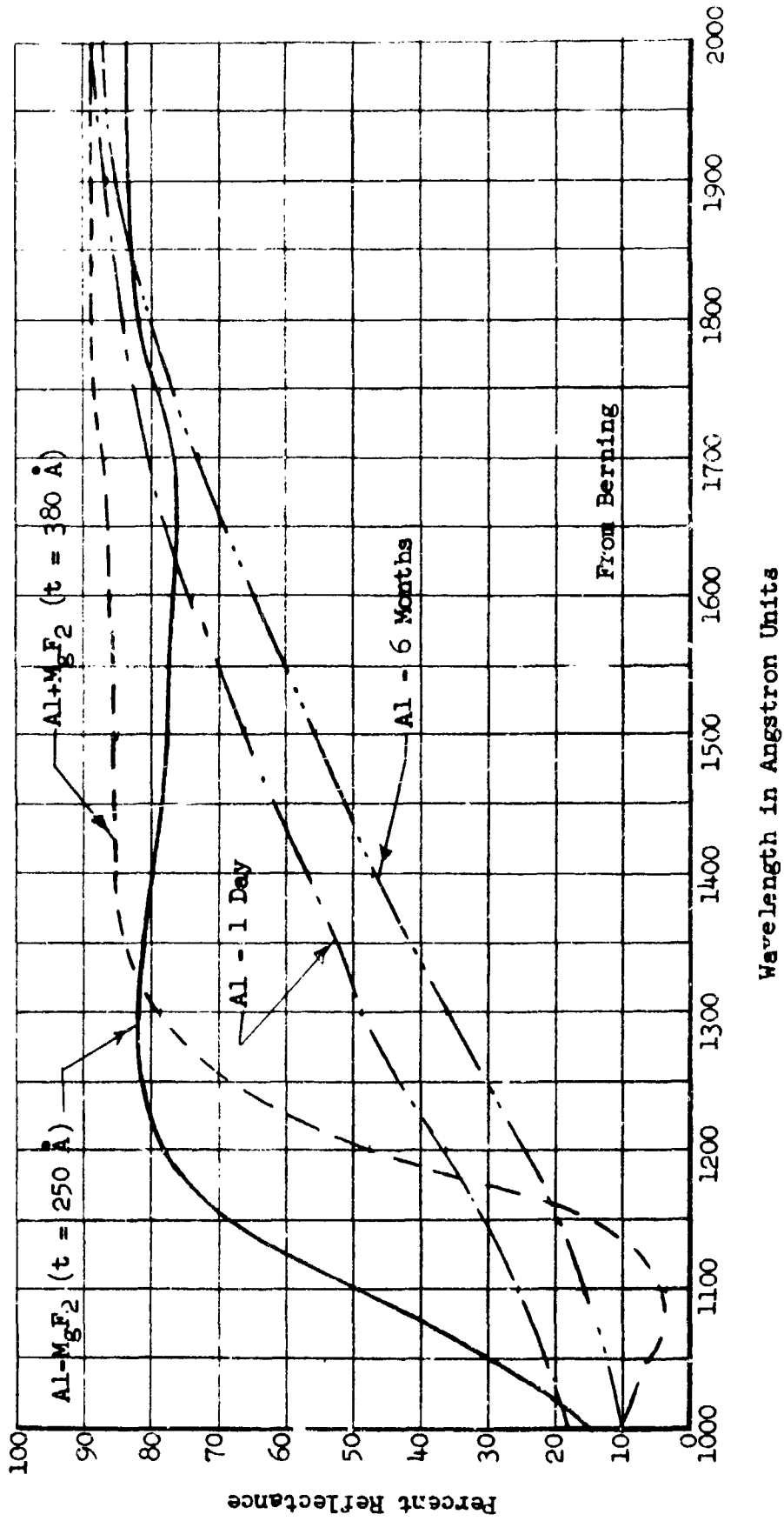


FIGURE 1.3-12 ENHANCEMENT OF REFLECTANCE OF EVAPORATED ALUMINUM MIRROR PROTECTED WITH MgF<sub>2</sub> COMPARED WITH AGED FILM WITH MgF<sub>2</sub> FILM

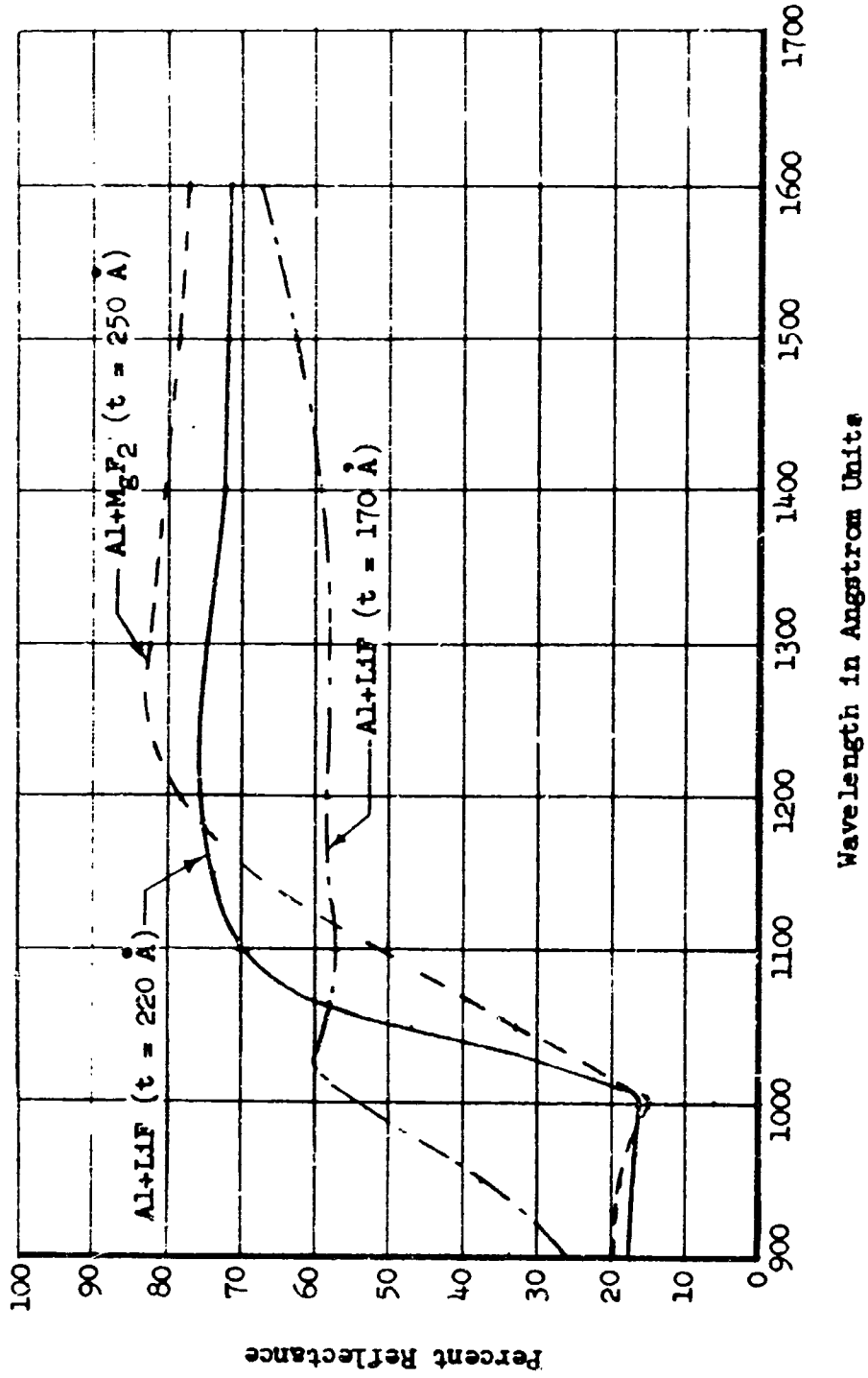
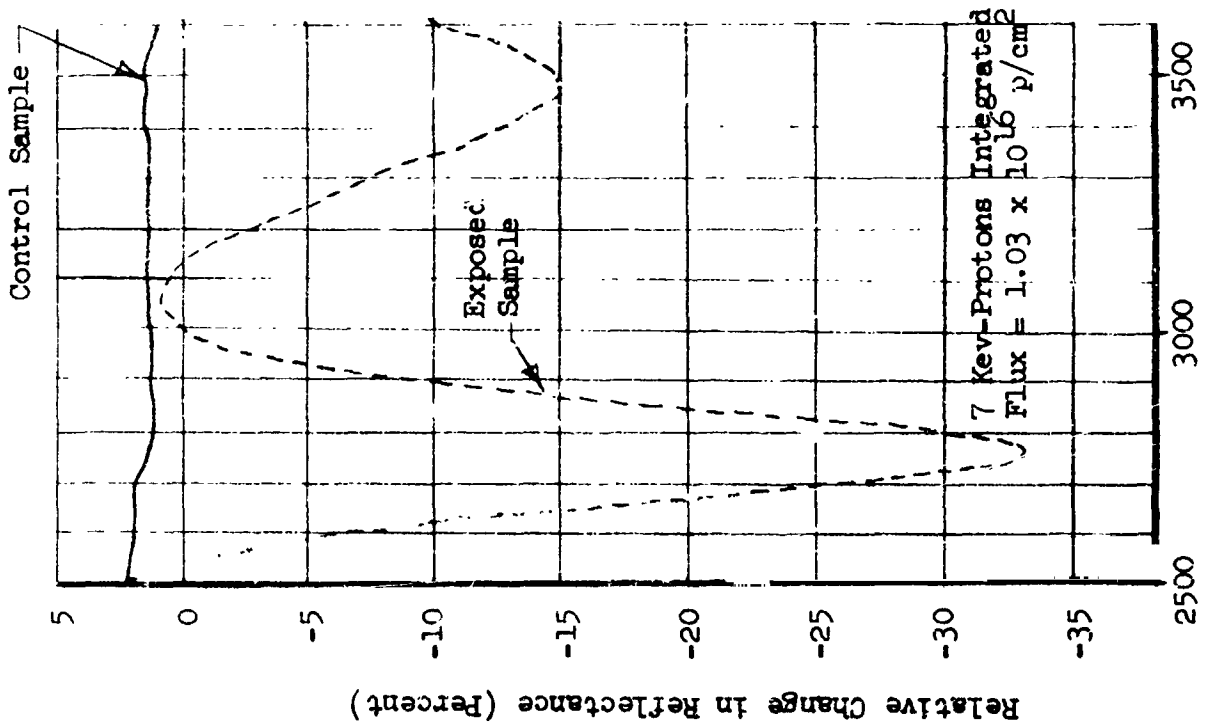
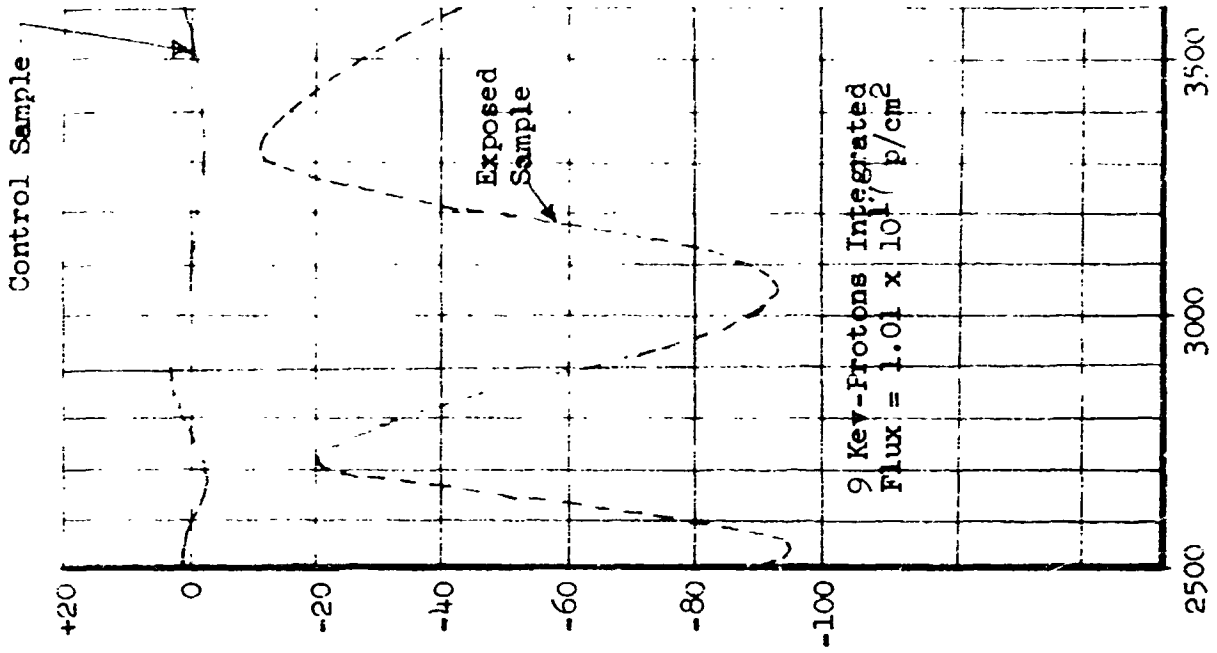


FIGURE 4.3-13 REFLECTANCE OF EVAPORATED ALUMINUM COATED WITH LiF COMPARED WITH ALUMINUM COATED WITH MgF<sub>2</sub>

mirrors is available and is presented here. Only enough information is available to estimate the loss in spectral reflection and surface deformation as a function of integrated proton flux. The following summary of radiation-effects data illustrates the need for further experimentation.

- Anodic Coated Aluminum — Boeing has conducted an experimental program to verify the stability of the Boeing-developed barrier-layer anodized-aluminum reflecting surfaces in a simulated Earth-Mars charged-particle radiation environment (Reference 48). One type of reflector was the low-emittance anodic reflector. The reflector was chemically brightened and anodized per the procedure outlined in Reference 48. The anodized layers ranged from 0.35 to 0.7 micron in thickness. Figure 4.3-14 shows the relative reflectance of the kev-proton irradiated and control samples as measured by the Beckman DK-2A reflectometer. Although the integrated flux is considerably higher than expected for the MOT lifetime, it is obvious the surfaces are ruined for near-ultraviolet wavelengths. The cause for the shift of reflectance minima and the change in reflectance is not obvious; it could be due to an increase in the refractive index, an increase in film thickness, and deposition of a thin film onto the anodic film.
- Chemically Brightened Aluminum — Chemically brightened samples were also irradiated in the experimental program (Reference 48). The surfaces chemically brightened to represent the reflector surface immediately prior to anodizing. Figure 4.3-15 gives the results of the reflectance tests after the samples were exposed to 8.2-kev protons of fluxes of  $4.6 \times 10^{15}$  protons/cm<sup>2</sup> and  $6.1 \times 10^{15}$  protons/cm<sup>2</sup>. Examination of the surfaces by electron photomicrograph revealed that low-energy protons caused blistering of the surface. The size of the largest blisters (irradiated to an integrated flux of  $6.1 \times 10^{15}$  protons/cm<sup>2</sup>) were about 0.3 micron in diameter.
- Vapor-Deposited Aluminum — Samples consisting of chemically brightened aluminum substrates with a coating of vacuum-deposited aluminum to a thickness of 1 micron were irradiated (Reference 48). After irradiation with kev protons, the aluminum surface was almost completely covered with small blisters similar to the chemically brightened sample. The blisters were predominantly approximately 0.2 micron in diameter with some large blisters ranging in size from 0.6 to 3.0 microns. The height of blisters that were approximately 3 microns in diameter was approximately 0.5 micron. Electron micrographs of a blistered surface cross-section are consistent with the range of 7.4-kev protons, being 0.2 micron. The blisters are believed to be formed by gas bubbles formed within the deposited film. The deposited aluminum film is thicker than the normal optical aluminum film by a factor of 10. The blisters were evidently formed at a depth greater than twice the optimum film thickness; therefore, it is possible that a significant amount of the kev protons would pass through, depositing their energy in the Kanigen nickel.



Wavelength (Angstroms)

Wavelength (Angstroms)

FIGURE 4.3-14 RELATIVE CHANGE IN REFLECTANCE CAUSED BY KEV-PROTON IRRADIATION ON ANODIC COATED ALUMINUM

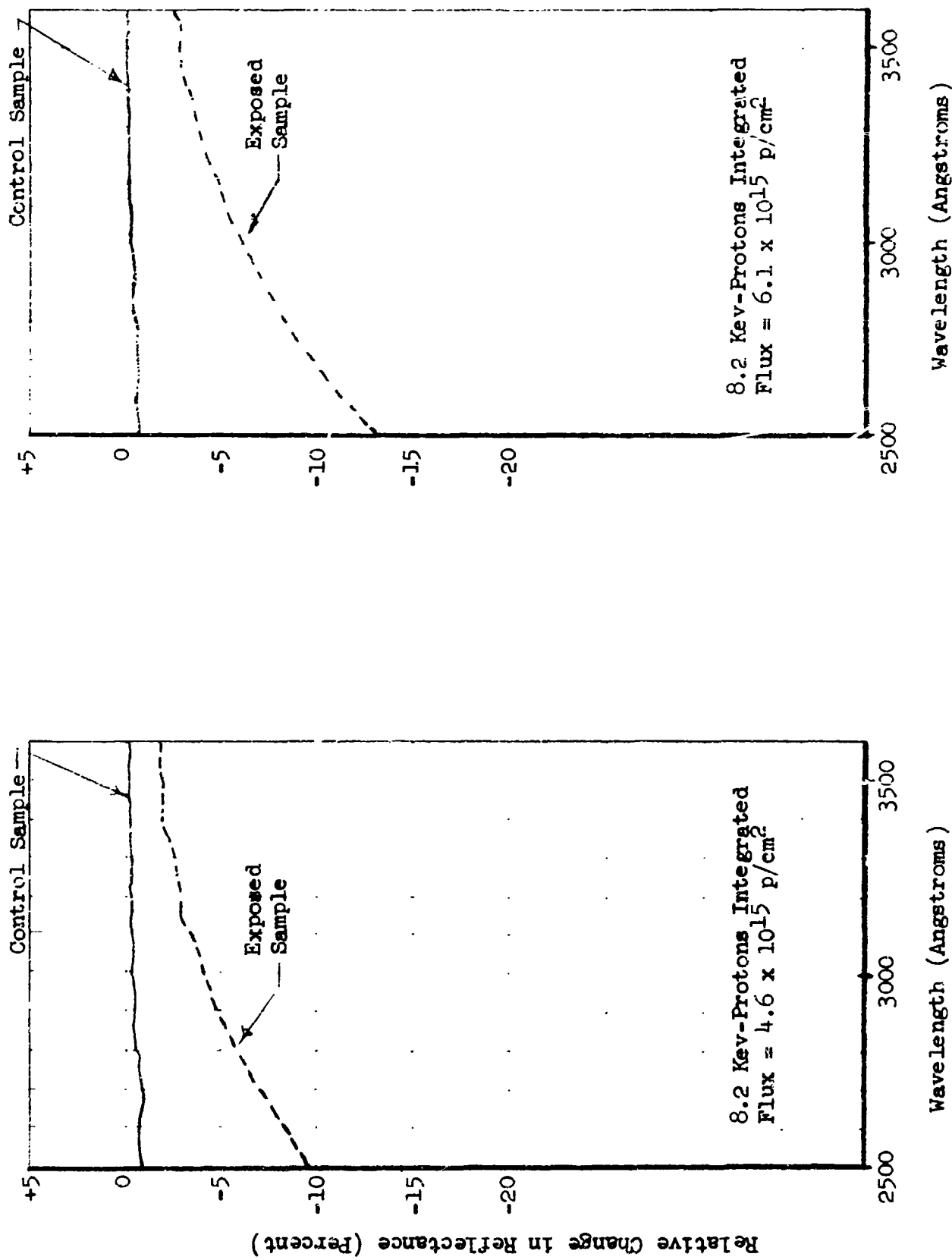


FIGURE 4.3-15 RELATIVE CHANGE IN REFLECTANCE CAUSED BY KEV-PROTON IRRADIATION ON CHEMICALLY BRIGHTENED ALUMINUM



- **MgF<sub>2</sub> - Protected Aluminum Mirrors** — Recent irradiation studies of Al-MgF<sub>2</sub> mirrors on glass substrates have been published that indicate an insignificant change in reflectance. The samples were exposed to a fluence of  $1 \times 10^{12}$  protons/cm<sup>2</sup> of 5-mev protons. Although there was only a change of 0.2 percent in reflectance at  $\lambda = 1216 \text{ \AA}$  as seen in Figure 4.3-16, the glass substrate is reported to have become dark brown.

If a 5-mev proton flux of 50 protons/cm<sup>2</sup>-sec is assumed for a  $2\pi$  surface in space at a synchronous-orbit altitude, the flux per steradian is 8 protons/cm<sup>2</sup> - sec-ster. The telescope housing will stop the low-energy particles so the area of concern is the acceptance cone from the open end of the telescope to the mirror. This solid angle is approximately 0.069 steradian. Using a proton flux of 8 protons/cm<sup>2</sup>-sec-ster, a flux of 0.55 protons/cm<sup>2</sup>-sec is obtained. The fluence on the irradiated Al-MgF<sub>2</sub> mirrors was  $1 \times 10^{12}$  protons/cm<sup>2</sup>. This would correspond to an irradiation time of:

$$\text{Time} = \frac{1 \times 10^{12} \text{ protons/cm}^2}{0.55 \text{ proton/cm}^2\text{-sec}} = 1.82 \times 10^{12} \text{ seconds}$$

$$\text{or } 5.8 \times 10^4 \text{ years}$$

Reference 49 indicates this radiation, which has a very damaging effect on silicon solar cells, is of no danger to Al-MgF<sub>2</sub> coatings used in astronomical satellites exposed to the artificial radiation belt. It must be realized, however, that these samples were irradiated with 5-mev protons, which pass through the coatings and are stopped by the substrate. The radiation that may damage the optical coatings have energies of a few kev.

- **Silicon-Oxide Protected Reflectors** — An experimental study is currently in progress at Boeing under Contract NAS1-5251, NASA/Langley Research Center, to evaluate the effects of ultraviolet radiation and protons on the specular and diffuse reflectance of various solar concentrator coatings and substrates. Typical samples of stretch-formed aluminum and electroformed-nickel solar concentrators are being procured and tested. Coatings such as chromium, SiO, Al, Si<sub>2</sub>O<sub>3</sub>, and SiO<sub>2</sub> are to be tested in several combinations on both the substrates, stretch-formed aluminum and electroformed-nickel. The samples will be irradiated with 2-, 4-, 8-, and 16-kev protons. Details of the experimental studies and progress are reported in References 50 and 51. Data is not available to date of the proton radiation effects on the samples.

**Performance Degradation** — Proton radiation apparently damages the reflective surfaces in such a manner as to cause blistering. The blistering causes irregularities on the optical surface, which in turn produce deformations of the spherical wavefront forming the image. Since light travels perpendicular to the wavefront, these wavefront deformations will vary the normal direction of the image-forming light. The greater the magnitude of the wavefront deformations or the higher their spatial frequency, the more scattered the direction of the light becomes, thus making the

<u>Sample Number</u>	<u>Percent R At 1216 Å Before Irradiation</u>	<u>Percent R At 1216 Å After Irradiation</u>	<u>Total Dose (e/cm<sup>2</sup>)</u>	<u>Exposure (Time-Sec)</u>
147	82.5	82.3	$2 \times 10^{14}$	1 000
2K	77.9	77.8	$2 \times 10^{14}$	1,000
146	82.0	82.1	$2 \times 10^{15}$	10,000
4K	78.3	78.5	$2 \times 10^{15}$	10,000
153	81.5	81.6	$1 \times 10^{16}$	1,000
7/2/62	76.5	76.3	$1 \times 10^{16}$	1,000
<hr/>				
148	80.9	80.7	$1 \times 10^{12}$ protons/cm <sup>2</sup>	

Figure 4.3-16: REFLECTANCE OF  $MgF_2$ -PROTECTED ALUMINUM MIRRORS BEFORE AND AFTER IRRADIATION WITH 1-MEV ELECTRONS AND 5-MEV PROTONS

the point image larger. Hufnagel (Reference 52) has presented a mathematical description of such wavefront disturbances and how to determine the modulation transmission factor,  $M$ . The modulation transfer function of MOT can then be multiplied by the modulation transmission factor  $R M_P$  ( $M = R M_P$  for radiation effects) to produce the average modulation transfer function,  $\langle T \rangle$ .

The performance of a system can be obtained by multiplying its modulation,  $M_S$ , by the factor  $R M_P$  to obtain a new  $R M_S$  that would be the modulation considering the radiation effects. If  $M_S$  includes the modulation transfer function of the optical system, film, and image motion, a new photographic image diameter can be determined as a function of radiation effects.

To obtain an estimate of the time in orbit before the telescope mirror suffers significant damage, an extrapolation was made from the results given in Reference 48. Many tests were made on anodic-coated aluminum at various particle fluxes; the surface damage that resulted was similar to that on the evaporated aluminum surface. It was therefore assumed that the rate at which surface damage occurred in the aluminized surface was similar to that of the anodic coating. Then, using  $10^{16}$  p/cm<sup>2</sup> as the reference point for locating this curve, Figure 4 3-17 was obtained.

Since the criteria being used for wavefront deviation to remain within the theoretical resolution limit is  $1/4 \lambda$ , or a surface variation of  $1/8 \lambda$ , it can be seen from Figure 4. 3-17 that the maximum tolerable fluence (integrated flux) is  $2.5 \times 10^{14}$  p/cm<sup>2</sup>.

Since the 120-inch primary mirror for the MOT cannot be entirely shielded from radiation, it is the most critical optical surface, and was used in determining the limit. It is assumed that the secondary and folding mirrors of the MOT are sufficiently shielded from radiation. The telescope housing will stop the low-energy particles, so the area of concern is the acceptance cone from the open end of the telescope to the mirror. This solid angle is 0.069 steradian. Using a proton flux of  $10^8$  p/cm<sup>2</sup>-sec-ster, we obtain  $6.9 \times 10^6$  p/cm<sup>2</sup>-sec. With a maximum allowable fluence of  $2.5 \times 10^{14}$  p/cm<sup>2</sup>, we get:

$$\frac{2.5 \times 10^{14} \text{ p/cm}^2}{6.9 \times 10^6 \text{ p/cm}^2\text{-sec}} = 3.6 \times 10^7 \text{ sec} = 417 \text{ days}$$

Taking into consideration the assumptions made, the lack of data for the specific case, and the use of maximum particle levels, it can be assumed that the mirror will be useful for a somewhat longer period than that given above.

Using the  $1/4 \lambda$  criteria, the modulation transmission factor ( $M$ ) for the mirror can be estimated using a random wavefront variation method (Reference 52). With  $1/4 \lambda$  peak-to-valley wavefront variation, the rms wavefront variation will be  $1/20 \lambda$ . The rms surface deviation will then be  $1/40 \lambda$ , or  $1/8 \lambda$  peak-to-valley deviation. Using Hufnagel's equation, the modulation transmission factor for the mirror due to radiation damage ( $R M_P$ ) will be:

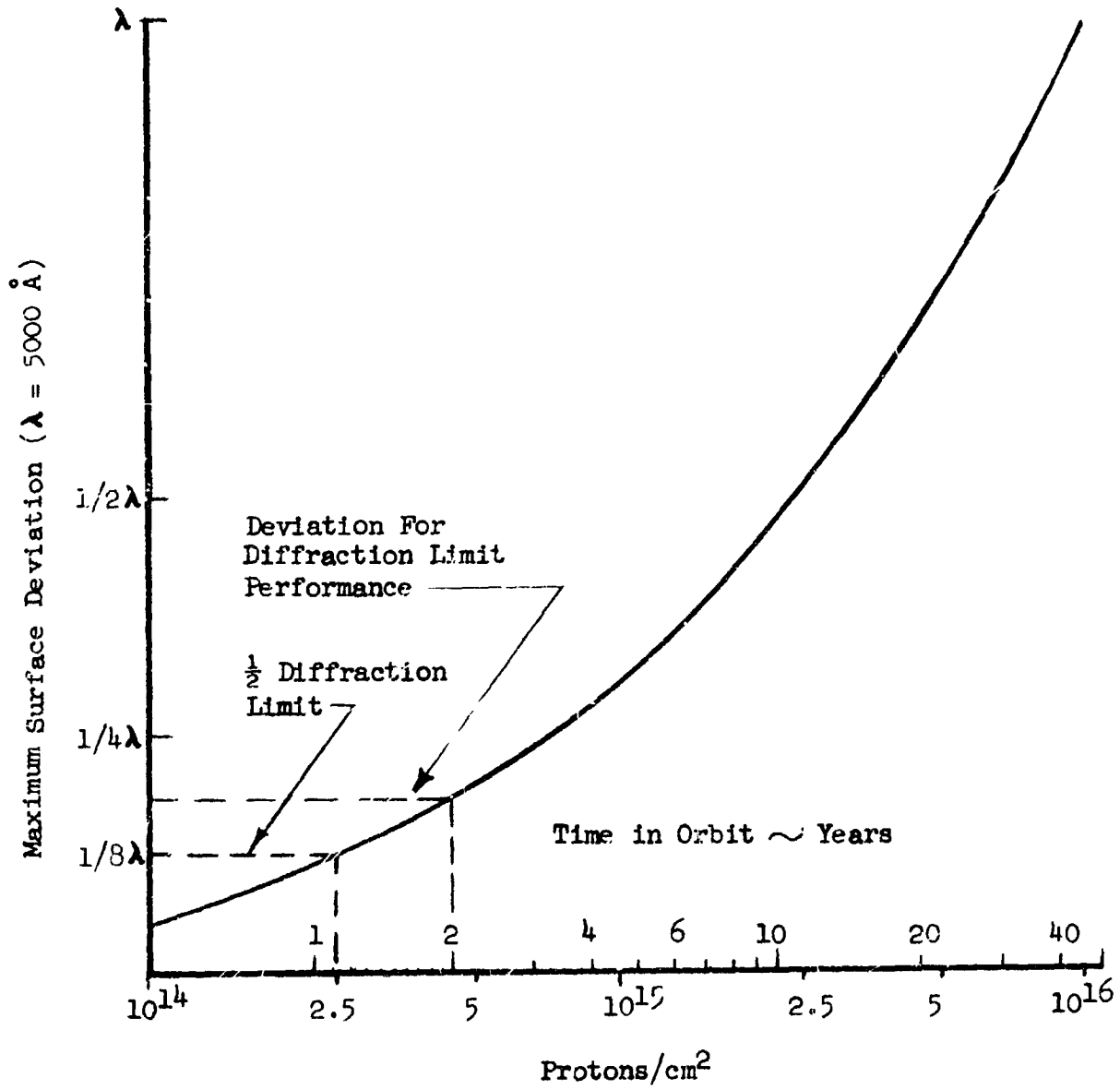


FIGURE 4.3- 17 SURFACE DAMAGE TO PRIMARY MIRROR BY LOW ENERGY PROTONS (7.4 KEV)

$$R_{MP} = \left[ \exp - \frac{4\pi^2}{\lambda^2} (\text{rms wavefront variation})^2 \right]$$

$$R_{MP} = \left[ \exp - \frac{4\pi^2}{20^2} = 0.906 \right]$$

The modulation transfer function curves of Reference 1, Pages 32 and 35, can be multiplied by  $R_{MP}$  and a new photographic image diameter determined. This new photograph disk diameter in magnitudes is

$$\Delta m_{\phi} = 2.5 \log \frac{d_1}{d_2}$$

where  $d_1$  = diameter of original photographic disk

$d_2$  = diameter of photographic disk after radiation effects are included

Use of the  $\lambda_4$  criteria in Hufnagel's equation results in performance equivalent to one-half the Rayleigh limit. If the mirror were permitted to degrade to the full Rayleigh limit of  $R_{MP} = 0.8$  or an rms surface deviation of  $\sim \lambda/30$ , the life would be extended to approximately 2 years.

Figures 4.3-18 and 4.3-19 show the estimated radiation effect on the modulation transfer curves for ef/15 and ef/30. Five-year radiation effects in synchronous orbit result in a limiting stellar magnitude of 22.6 for ef/15 and 22.3 for ef/30 compared to 22.8 and 22.5, respectively, for the 250-nautical-mile orbit. Since the flux at 250-nautical-mile orbit is approximately 1/1000 that of synchronous orbit, the effects are insignificant.

It is quite obvious that considerable experimental effort is required in this area to understand and determine more accurately the degradation that can be expected. Figure 4.3-20 is a block diagram of the type of experimental program recommended. Mirror samples should be evaluated by interferometric techniques to determine the surface deformation. Tests should be performed on samples before and after irradiation, and on control samples, to determine performance in terms of modulation transfer function, resolution limit, and the limiting stellar magnitude using spectrographic films.

#### 4.3.3.2 Exterior Thermal Coatings

Radiation tests and reflectance measurements on thermal coatings considered for the exterior surfaces of the MOT have indicated that a radiation level of  $10^{15}$  proton/cm<sup>2</sup> will not damage the thermal control surface or result in a major change in the emittance of the coating.

Ultraviolet radiation over extended periods can change the solar absorptance of a coating. The external thermal coatings being considered are the most stable ultraviolet coatings available at this time.

FIGURE 4.3-18 ESTIMATED RADIATION EFFECTS ON MODULATION FUNCTION AT  $ef/15$

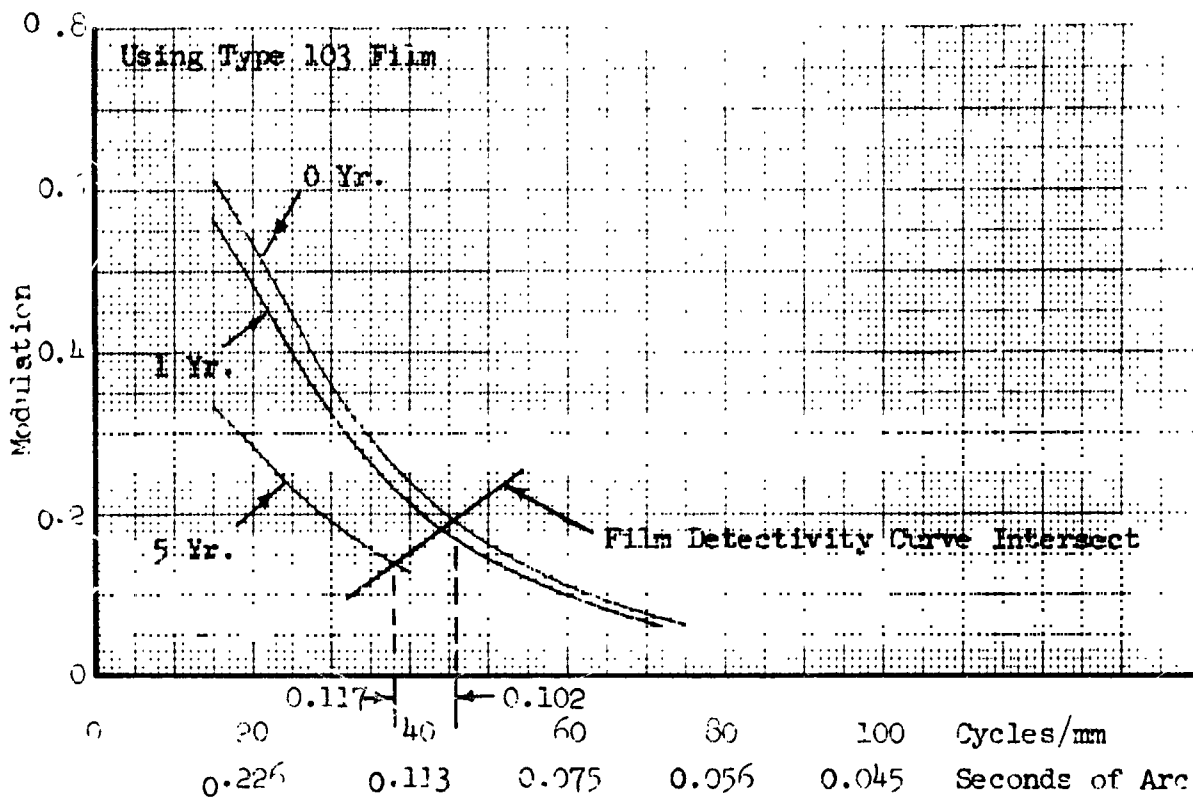
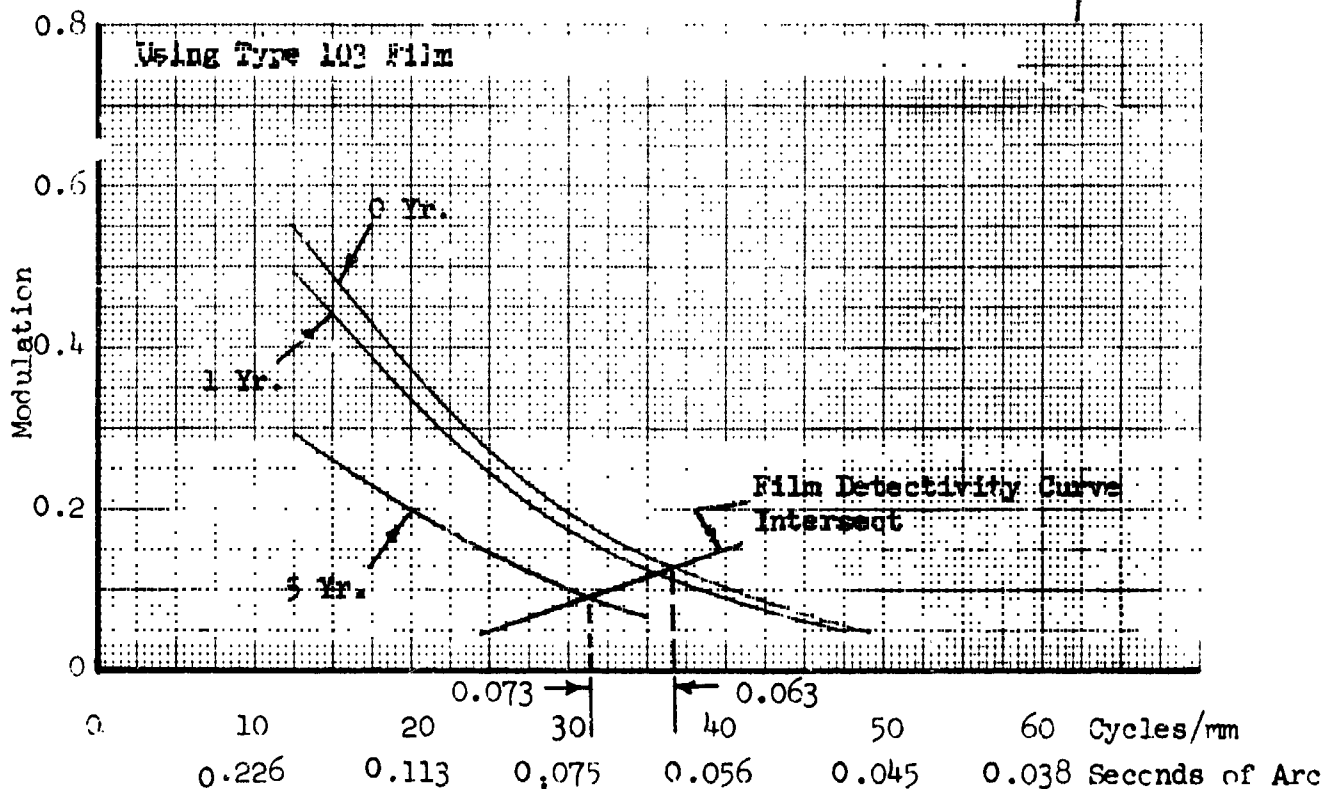


FIGURE 4.3-19 ESTIMATED RADIATION EFFECTS ON MODULATION FUNCTION AT  $ef/30$



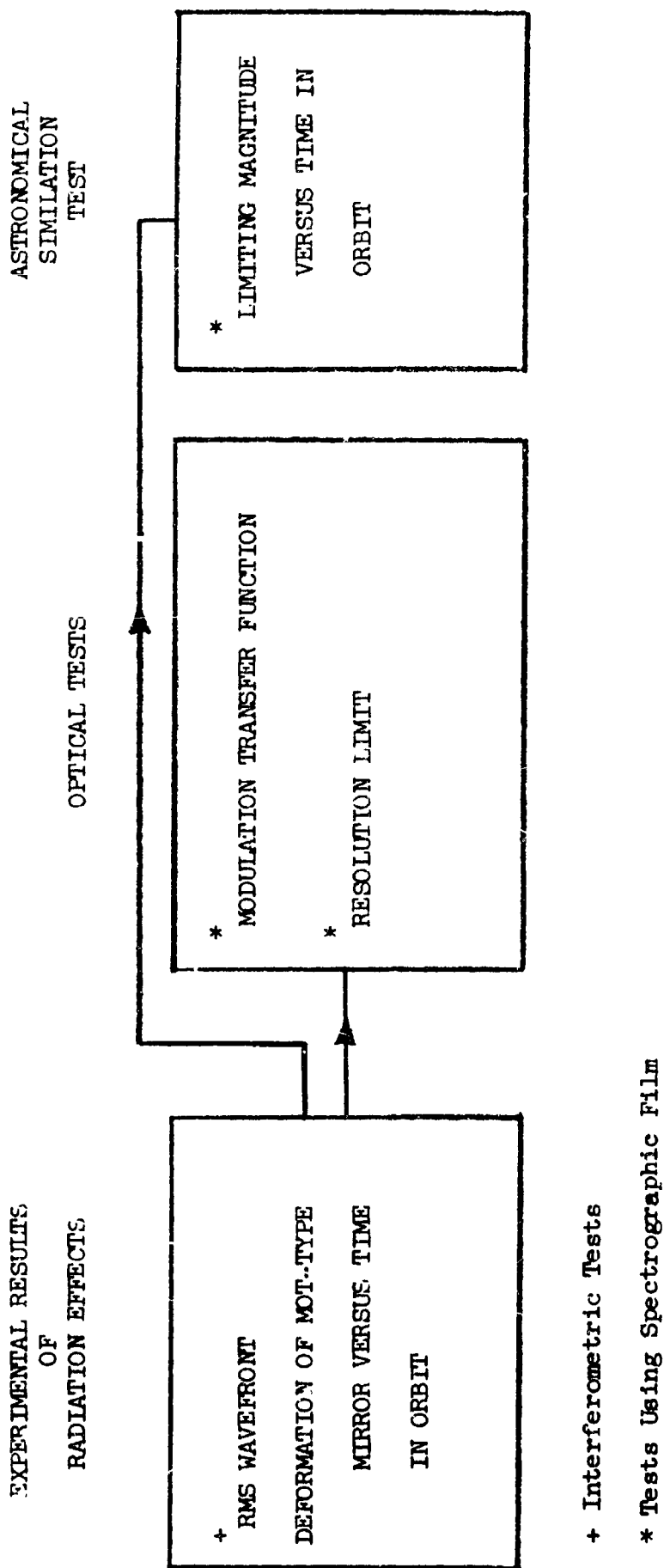


FIGURE 4.3-20 RECOMMENDED STUDY OF KEV-PROTON RADIATION EFFECTS

#### 4.3.4 Performance Degradation of Film

The radiation environment to which a photographic emulsion is subjected greatly influences the photographic results. Exposure to bombardment by high-energy radiation can cause undesirable changes in the sensitometric and image quality characteristics of an emulsion. These changes depend on the nature of the emulsion and the duration of exposure to the radiation. Coarse-grained, high-speed materials are more sensitive to radiation than are the finer-grained, slower-speed materials. As the magnitude and duration of the radiation increases, the effect on the film is greater. The effects, however, are not a direct product of magnitude and time as in the image-forming exposure. The following is a discussion of film degradation due to radiation exposure for both a synchronous orbit and one at 250-nautical-mile altitude. Film degradation is discussed in terms of limiting magnitude that may be photographed.

Some assumptions are made because of the lack of radiation data available on Type 103 spectroscopic film. Some data is available on Plus-X Aerecon (E. K. 8401) which closely matches Type 103 in speed and granularity. The response of Plus-X Aerecon film to radiation is used to estimate the amount of degradation.

The photographic emulsion is sensitive to high-energy radiation, both corpuscular and electromagnetic. The radiation environment at synchronous-orbit altitude poses the greatest hazard. The photographic emulsion at this altitude will be subjected to galactic cosmic rays (very-high-energy protons) and solar event particles (following a solar flare). At the lower altitude, the latter is negligible. Emulsion exposure to this radiation appears to produce the same basic effects: an increase in fog level, a decrease in gamma, and a change in film speed. The magnitude of the effect is dependent on the energy level and duration of the exposing radiation (Reference 53).

Film sensitivity to radiation necessitates that additional shielding be provided for both a synchronous- and a low-Earth-orbit mission. The shielding proposed is about 40 g/cm<sup>2</sup> of aluminum for the high-altitude and 48 g/cm<sup>2</sup> for the 250-nautical-mile orbit. This shielding is only partially successful in protecting the film, so some fogging will still result (see Section 4.3.2). Figure 4.3-21 shows how the sensitometric characteristics are affected at both the high and low altitudes with the amount of shielding indicated above. From these curves, the increase in fog level is apparent.

Limiting photographic magnitude is determined by the following formula (References 54 and 55):

$$pg^m_L = m_L - 2.5 \log \frac{8(ef/n)^2}{T} - \Delta pg^m_s$$



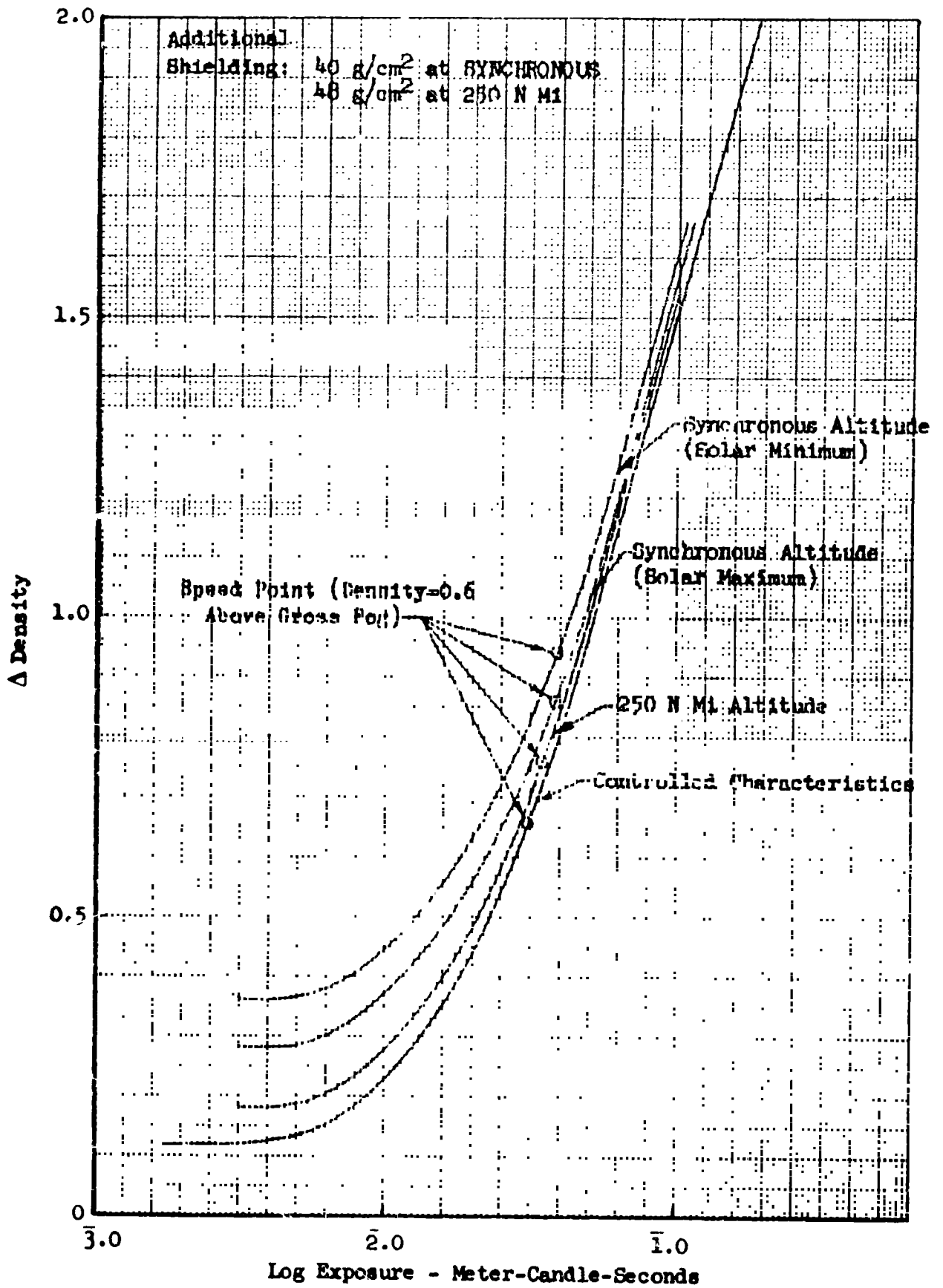


FIGURE 4.3-21 EFFECTS OF RADIATION ON TYPE 103 SPECTROSCOPIC FILM

where  $p_{gmL}$  = limiting magnitude desired to photograph

$m_L$  = limiting detectable stellar magnitude

$ef/n$  = equivalent focal ratio

$T$  = exposure time in minutes

$\Delta_{pgm_s}$  = change in magnitude due to a change in sensitivity

This formula is based on the normal sensitivity of E. K. Type 103 film.

The limiting stellar magnitude of the telescope,  $m_L$ , is dependent on the average sky brightness and diameter of the photographic disk (Reference 55). Sky brightness will not change appreciably from the low Earth orbit to synchronous-orbit altitude. The photographic disk diameter is determined as a result of the modulation transfer function (MTF) computations. The intersection of the film detectivity curve and the MTF curve determines the resolution and, therefore, the size of the disk. The film detectivity or threshold curve is proportional to the gamma and granularity of the film. From Figure 4.3-21 it can be seen that gamma (the slope of the linear portion of the curve) varies slightly. If it is assumed that gamma remains constant, granularity does not change, and resolution is unaffected, the size of the photographic disk is unchanged. With these assumptions, the limiting stellar magnitude remains constant.

As radiation dosage is increased, the speed or sensitivity of the film is decreased. The term for the change in magnitude due to a change in sensitivity is not zero for Type 103 film subjected to radiation due to this sensitivity change. The formula for this term is:

$$\Delta_{pgm_s} = 2.5 \log \frac{S_{A1}}{S_{A2}}$$

$S_A = \frac{1}{E}$  where  $E$  is exposure in meter-candle-seconds

$S_{A1}$  = sensitivity of Type 103 film

$S_{A2}$  = sensitivity due to radiation exposure

The speed point for films used for astronomical work is taken at a density of 0.6 above gross fog (Reference 56). Gross fog for the Type-103-controlled characteristic curve is about 0.1. Exposure of the emulsion to radiation increases the gross fog level as shown in Figure 4.3-21. If the density above fog is maintained at 0.6, the exposure changes, which in turn causes a change in speed. The following table shows how speed changes for the four cases given in Figure 4.3-21.

	Log Exposure	Speed
Controlled	$\bar{2}.495$	32
250 Nautical Miles	$\bar{2}.541$	28
Synchronous (Solar Maximum)	$\bar{2}.583$	26
Synchronous (Solar Minimum)	$\bar{2}.590$	25

Making the suitable corrections for changes in film sensitivity due to radiation exposure, the limiting photographic magnitude,  $pg_{mL}$ , is computed for type 193 spectroscopic film at two effective focal ratios. The values are for an exposure of 40 minutes. The following table summarizes these computations.

	ef/15	ef/30
Controlled	22.8	22.5
250 Nautical Miles	22.6	22.3
Synchronous Altitude (Solar Maximum)	22.5	22.2
Synchronous Altitude (Solar Minimum)	22.5	22.2

Conclusions and Recommendations — The results of this investigation show that limiting photographic magnitude is affected by exposure of the film to radiation. The film is degraded to a higher extent at synchronous altitude; at this altitude the limiting magnitude that may be photographed is reduced by 0.3. The computations were based on the assumptions that: (1) the fogging estimates were obtained from limited film data; and (2) the size of the photographic disk was assumed to be affected by radiation exposure.

The reduction in resolution due to the increase in fog level has not been determined in this investigation due to lack of data. In addition to affecting the sensitometric characteristics of the emulsion, however, it does appear that the radiation also has an effect on image quality. Gamma and granularity were assumed in this study to be unaffected. Further investigation must be conducted to determine the extent that gamma and granularity changes with radiation dosage. If gamma

decreases, causing a reduction in contrast, this results in a loss of detail as the film loses its ability to record subtle brightness differences. This loss in contrast in turn lowers the resolution capability of the film. In addition, the increased fog level increases the overall density of the recorded data, effectively shifting the exposure up on the characteristic curve. This could result in an overexposed scene, with a resultant loss in resolution and acuity.

Another significant effect results if there is an increase in graininess produced by radiation. The increase in graininess decreases the signal-to-noise ratio of the image and produces a loss in detail. The increased graininess effect is more severe in the low-contrast areas of the scene. In these areas, a decrease in signal-to-noise ratio can result in detail being below the visible threshold, therefore, effectively lost (Reference 53).

The shortage of data showing the effects of radiation exposure to spectroscopic films and plates indicates the need for further investigation in this field. The relationship between fog and resolution loss must be investigated to determine the fog level that can be tolerated without serious degradation of performance.

#### 4.3.5 Micrometeoroid Protection

4.3.5.1 Meteoroid Environment — The environment and design criteria governing the meteoroid shielding for the low Earth orbit are discussed in Reference 1. These same criteria will apply to the synchronous-orbit MOT (except for the Earth shadow factor, which would increase from 0.75 to 1.00).

The effect of the change in the Earth shadow factor on the primary mirror damage is shown in Figure 4.3-22.

The probability of no penetration of the walls of the baseline configuration in synchronous orbit during a period of 3 years is:

For wall gage = 0.01 inch,  $P(O) = 0.929$

For wall gage = 0.02 inch,  $P(O) = 0.988$

The probability of penetration of the telescope walls within 3 years, as a function of wall thickness is shown in Figure 4.3-23 for the synchronous-orbit and the 250-nautical-mile orbit cases.

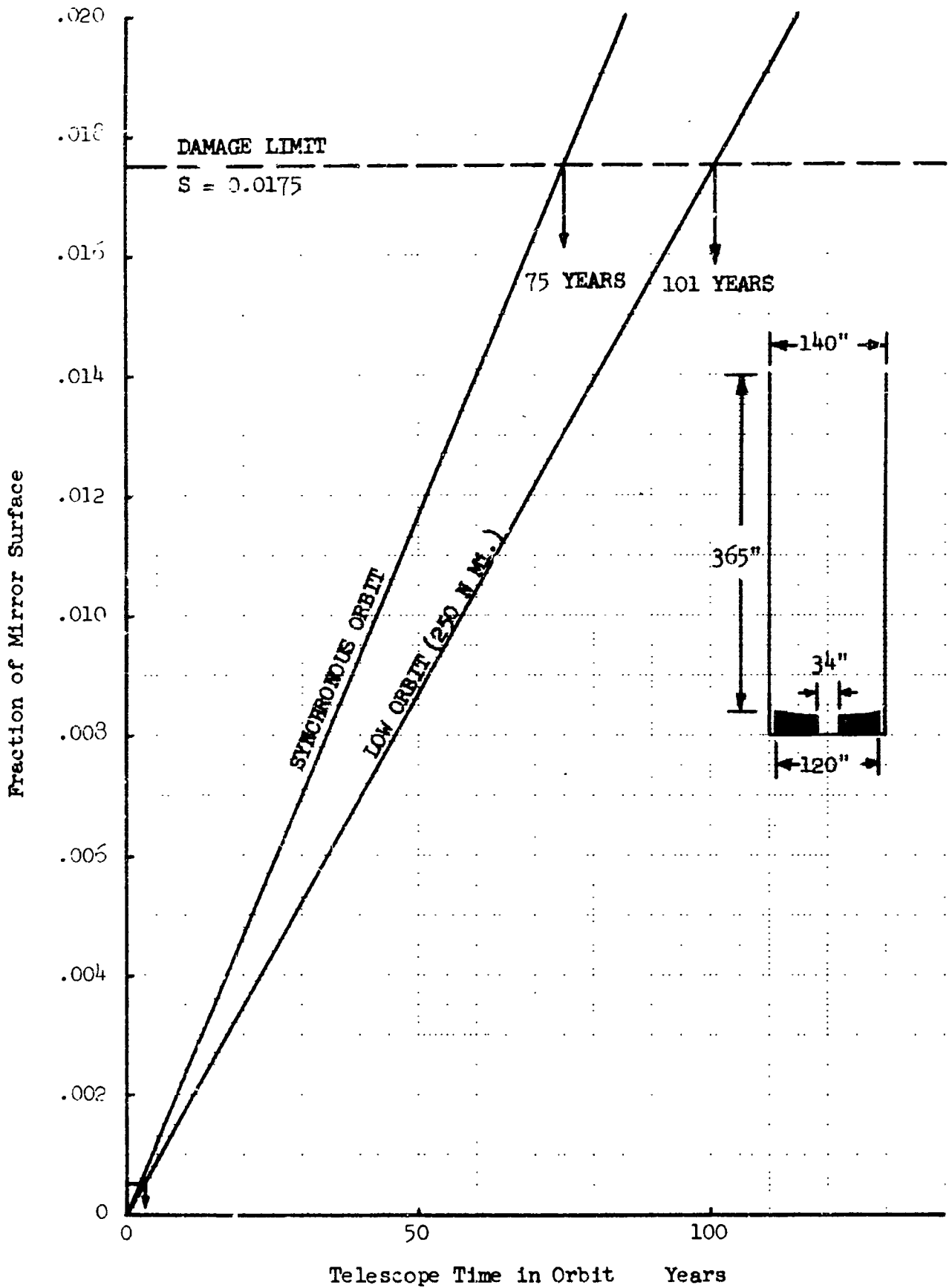


FIGURE 4.3-22 DIRECT METEOROID DAMAGE TO PRIMARY MIRROR

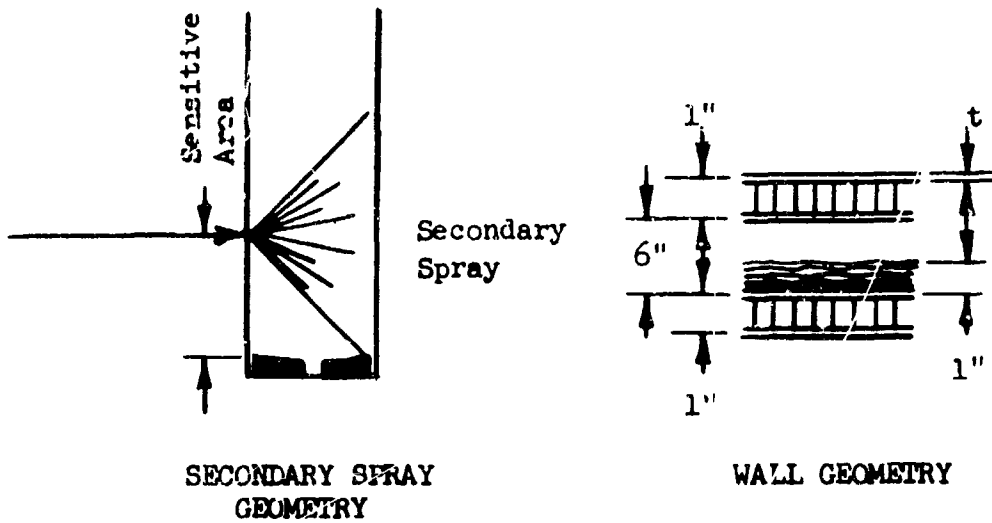
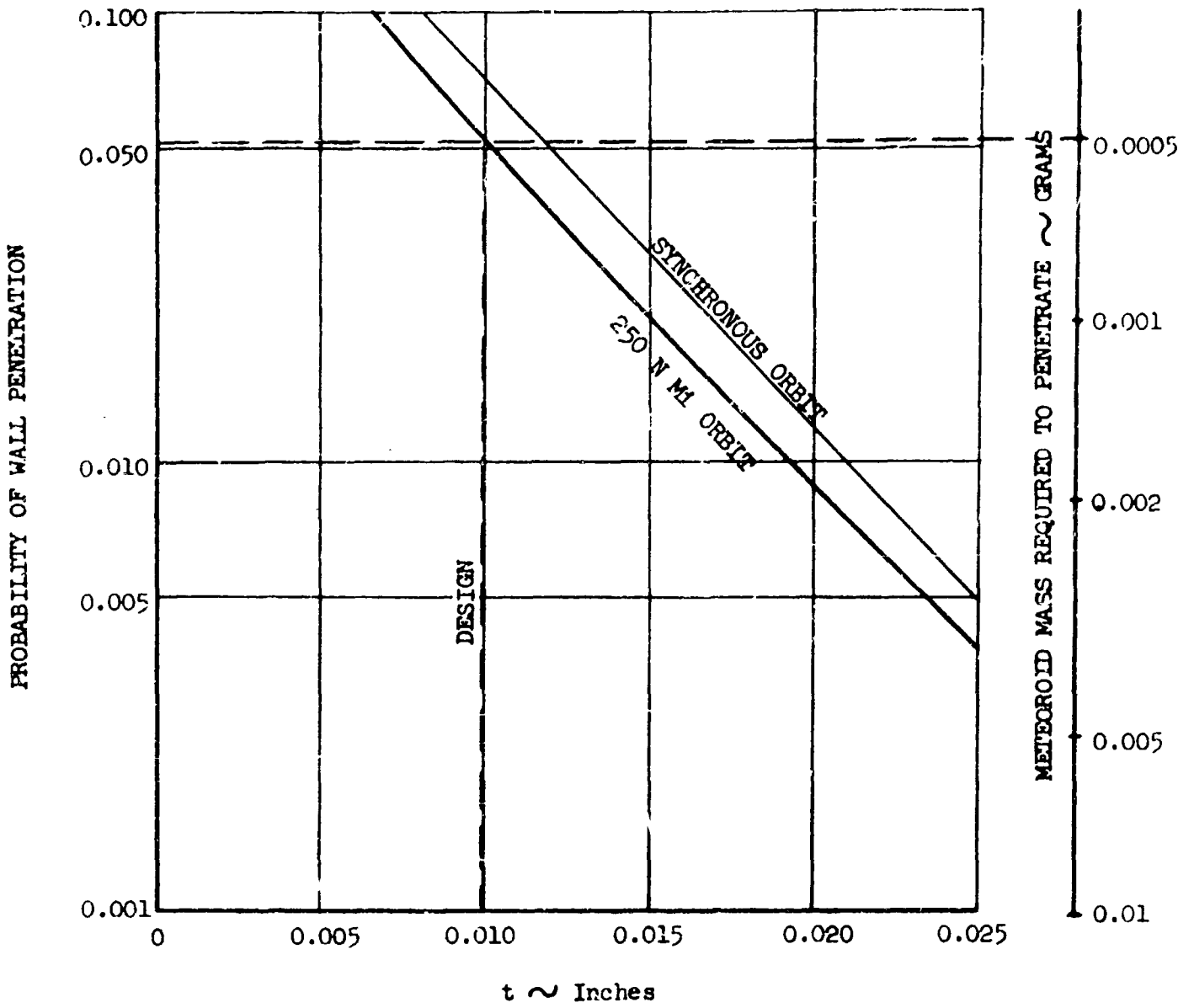


FIGURE 4.3-23 PROBABILITY OF METEOROID PENETRATION OF TELESCOPE WALL

#### 4.4 DATA MANAGEMENT, COMMUNICATIONS, NAVIGATION AND GUIDANCE, AND ELECTRICAL POWER

##### 4.4.1 Data Management

Data management includes the acquisition and handling of MOT data in the MOT, in the MORL, and on the ground.

4.4.1.1 MOT Data Management — As presented in Section 5.6.1 of Reference 1, the MOT is only slightly dependent on the configuration of the integrated MORL-MOT system (i. e., basically the same whether the soft gimbal or the detached mode is used) because the MOT is required to communicate only with the MORL and from distances not in excess of 1 mile. Since neither the MOT mission nor the MOT-MORL relationship is dependent on altitude and since there is no direct contact between MOT and Earth, the MOT data management subsystem is independent of altitude.

4.4.1.2 MORL Data Management — MORL handling of MOT data is not a problem in either the soft-gimbal or the detached mode at either the low Earth or the synchronous-orbit altitude. If there is an advantage, however, it occurs with the synchronous-orbit altitude. The 24-hour-per-day contact with the ground station removes need for efficient communication, which is based on available time between MORL and the ground receiving station. The MORL can then be designed to handle MOT data without being constrained by need for an efficient MORL-Earth communication link.

4.4.1.3 Ground Data Management — All provisions needed to perform ground-system data handling functions for MOT are also required to support the proposed MORL configuration, described by Douglas (References 2 through 28). The provisions for ground handling of MOT data are independent of the coupling mode between MORL and MOT (soft-gimbal or detached) and, with one possible exception, are independent of altitude. The possible exception is that in the synchronous mode there is no constraint on contact time between MORL and Earth.

MOT data is derived from imagery, telemetry and voice sources. Imagery is physically returned to Earth on film and also is obtained via MORL relay from a slow-scan vidicon in the MOT. The technique for reconstruction of images on the ground is essentially the same for data derived from the MORL film projection-scanner system and for data derived from the MOT vidicon. The only difference is that the MOT data is one frame each 6 seconds and has 1150 resolution lines per frame, whereas that from the MORL is one frame each 4 seconds with 2000 resolution lines per frame.

All MOT telemetry is pulse-code modulated (PCM) in a format that conforms to IRIG standards (Reference 57). General purpose telemetry ground stations that can accommodate IRIG PCM formats can, therefore, be used without modification.

MOT voice communication is the same as the proposed MORL voice communication with the additional requirement that any MOT-to-Earth or Earth-to-MOT voice must be relayed through the MORL.

#### 4.4.2 Communications

MOT-MORL communication, as proposed in Reference 1, is independent of altitude and, because MOT does not communicate directly with Earth, substitution of a synchronous altitude for a low-Earth altitude does not affect the design of the MOT communications subsystem.

4.4.2.1 Rf Communications Link — MORL-Earth communication is affected in that the quantity of data that can be transferred increases over 18 times. That is, the data rate of all MORL channels is (by Section 4, Reference 9) the same in both synchronous and low Earth orbits. For the synchronous orbit, a high-gain directional antenna is substituted for the omnidirectional MORL antenna used for near-Earth telemetry. The available contact time between MORL and Earth then increases from 77 minutes per day to 24 hours per day, and the quantity of data that can be transferred increases by the same proportion (to  $6.6 \times 10^9$  bits per day over Channel F).

The sum of the maximum MOT communication ( $0.1 \times 10^9$  bits per day) and the maximum MORL communication ( $0.3 \times 10^9$  bits per day) is very small compared to the available capacity. Therefore, a synchronous orbit eliminates the requirement that efficient communication be used to transfer all presently planned data in the available contact time.

The increase in available capacity of the MORL communications links afforded by the synchronous orbit would permit closer surveillance of MOT experiments by ground personnel. At the expense of crew time, exposed and developed film can be scanned by the MORL film projector/scanner system and transmitted to Earth over the TV link. A 2- x 2-inch film (similar to that proposed for large scale photography) could be transmitted in 4 seconds with a line resolution of approximately 1400 elements and a grey-scale (density) resolution of five to eight levels. Film sizes to 9 x 9 inches (possibly, with additional modification of the MORL film scanner, to 16 x 16 inches) could be transmitted with the same resolutions. While these resolutions do not exploit the capability of the proposed film (Kodak spectrographic film Type 103 or equivalent) to 42 photographic lines per millimeter with up to 10 density levels, there would be sufficient information content to substantially ease the task of ground supervision of the experiment program.

4.4.2.2 Laser Communication-Link Considerations — Recent advances in laser techniques and equipment have made space-to-ground laser communication links feasible. Although laser systems can provide greater bandwidth than can rf systems, they are not currently recommended because:

- 1) Laser systems do not provide all-weather communication capability;



- 2) Incorporation of laser systems would require a modification of the MORL; this modification is not warranted since the rf link can accommodate data requirements presently proposed for both low-Earth- and synchronous-orbit missions:
- 3) Tracking requirements imposed on the ground equipment are severe, particularly for nonsynchronous orbits.

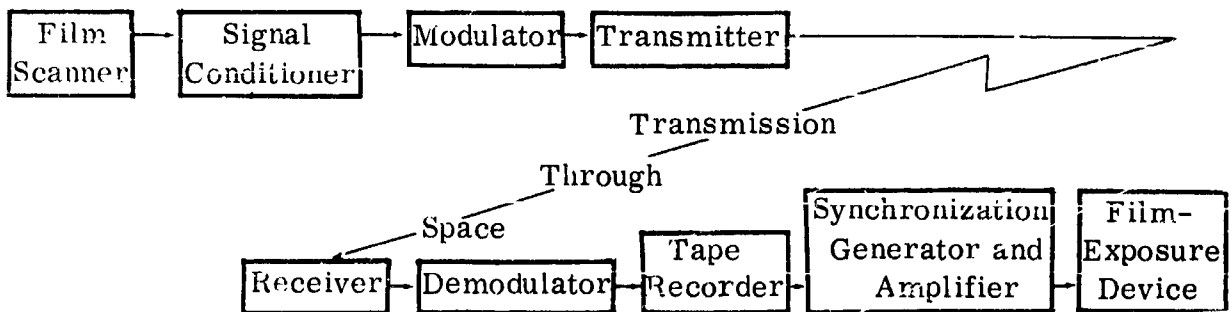
4.4.2.3 Photoscan Techniques — Both conventional and laser type scanners were studied.

Conventional Scanning Techniques — To demonstrate the capability of the 1-mc data link associated with the MORL photoscan unit, the number of images that could be transmitted per day as a function of film size was tabulated. For this exercise, it is assumed that the MORL is in synchronous orbit and that the scanner can convert the filmed image to an electric analog with negligible distortion. If there is a nominal allowance of 50 percent for Keil factor and film handling (12 of 24 hours), then the maximum number of pictures of any one size at 42 line-pairs per millimeter that can be transmitted over the 1-Mc data link is:

Film Size (inches)	16 x 16	1.4 x 21	2 x 2	0.6 x 0.6
Number of images per 24 hours	80	690	5100	56,000

Any requirement to physically bring film back to Earth is not the result of inadequate capacity in the rf link — a 1-year accumulation of photographs could be transmitted in a few days. The requirement that film be physically returned to Earth is based on the assumption that distortions of the film record are unacceptable. This assumption is supported by the practice of using correlation techniques to enhance the signal-to-noise ratio of the photographs that contain images partially or completely masked by noise. The assumption is also supported by the need for dimensional stability so that measurements between astronomical bodies can be made.

A typical imagery transmission link is described to aid in identification of distortion sources. The link converts filmed images to an electric analog, transmits the electric analogs to Earth, and converts the received electric analogs back into filmed images.



The film scanner contains a light source; intensity of the light output is modulated by the density of the element of film being scanned. The modulated light beam is directed by a lens system to a photomultiplier tube or other device that produces an electric output proportional to the intensity of the incident light. The signal conditioner digitizes, pre-emphasizes, or otherwise modifies the output of the scanner, thus providing an electrical analog that describes the density of the film element. The modulator converts this analog into another that is suitable for transmission. This analog is typically an rf signal modulated in amplitude, frequency, or phase. The transmitter amplifies the rf analog for transmission to the ground station where the receiver rejects signals and noise that are outside the bandwidth of the channel and amplifies the desired acceptable signals. The demodulator, the functional inverse of the modulator, converts the rf analog into the signal-conditioner analog form. If nonreal-time image reconstruction is employed, the demodulated analog is temporarily stored by a magnetic-tape recorder. The sync generator and amplifiers accept the output of the tape recorder or the demodulator (as selected by the ground operator) and decodes, de-emphasizes, amplifies, etc. as necessary to drive the film-exposure unit. The film-exposure unit — the functional inverse of the film scanner — causes a light beam to be intensity-modulated proportional to the received electric analog. The light exposes the film so that, ideally, the density of the element of film after development is the same as the density of the corresponding element of film in the film scanner.

In the film scanner, the light beam, film, or both, are moved so that each element of the film is scanned, and the positions of the light beam or film are encoded with the film readout. On the ground, the light beam and the film in the film exposure unit are moved in synchronism (except delayed in time) with the light beam and the film in the film scanner by means of the position data. The ideal result is generation of filmed images on the ground that exactly duplicate the filmed images at the data source.

In practice, the reproduced images are not exactly like the filmed images at the data source. Sources of image distortion are discussed in the following paragraphs.

**Differences in Minimum Resolution Element —** Distortion occurs when the minimum resolution element in the reproduced image is greater than the minimum resolution element of the original film. Resolution is degraded whenever the maximum dimension of the light beam approaches the size of the minimum resolution element on the original film and whenever the information bandwidth of the link restricts the transmission of the electric analogs.

If the light source is a cathode ray tube (CRT) beam, the minimum spot size is limited by the target phosphor decay time, by the thickness of the phosphor, by the smoothness of the phosphor, and by the ratio of acceleration voltages to the velocity dispersion of electrons emitted from the cathode material. The result is about 1000 to 2000 resolvable elements per sweep with grey resolution of 5 to 8 levels. A similar result is realized if a vidicon is substituted for the CRT and the associated photomultiplier.

If the light source is fixed and the light beam is focused by lenses, spot size is determined by how much the source of light approximates a point source, how closely the film can be held to the point of focus, and how small are the aberrations in the lenses. Again, 1000 to 2000 resolvable elements per sweep can be obtained.

The minimum bandwidth of the link cannot be less than the reciprocal of the sweep rate of the light beam expressed in the number of resolution elements swept per second; otherwise, noise will partially or completely mask the smaller resolution elements required for satisfactory transmission of data. It must be noted that more noise is admitted as the bandwidth is increased. That is, excess bandwidth penalizes the system by permitting the noise threshold to rise.

**Mechanical and Signal Irregularities**—Dimensional distortion is introduced by irregularities in mechanical devices that move the spot and the film (both in the scanning and reproduction equipment), and by irregularities in signals to control spot and film position.

**Response and Dynamic Range**—Grey-level resolution is limited by the dynamic range of the phototube and amplifier, the response of the light source and phototube combination as a function of spatial frequency, and by the response of the video amplifiers in the link.

Although the distortion of each element of the imagery-transmission link is small, the cumulative errors are significant. Today's technology permits photo-scan reproductions of film with a resolution about 1000 to 2000 TV elements per scan line, and a dimensional stability of a few resolution elements. This low-resolution data is useful as a crude check on the MOT experiments, but will not permit optimum use of MOT equipment. In fact, much of the expected optical gain of four magnitude will be lost in the phototube process unless the scanned format is restricted to a small area. For instance, a star image on the film with signal-to-noise ratio of 10 is discernable with the eye. After scanning, the reproduced image is completely lost in the noise if the effective scanning aperture exceeds ten times the diameter of the original star image.

**Laser Photo-Readout**—A new generation of photoscanners, in which a laser is used as the light source, is being developed by Perkin-Elmer Corp., Stanford Research Institute, Boeing, and others. The laser photoscanner uses an electrically or mechanically scanned laser beam to read out or record data on photographic film. Advantages of the laser system over conventional TV scanners are:

- 1) The laser is more than 1000 times brighter than any conventional source.
- 2) The lateral coherence of the laser beam permits focusing to a very small spot whose diameter is limited by diffraction effects alone. The diameter of the central maximum (between nulls) is  $2.44F\lambda$ , where  $F$  is the focal length divided by the effective aperture of the focusing optics, and  $\lambda$  is the

laser wavelength. The effective scanning aperture (spot size) can easily be much smaller than the star image diameter on the MOT film.

- 3) The number of resolved elements per line can exceed that of the Type 103 film by a factor of 5 or more. As an example, A. Kozma (Reference 53) reported on a laser recorder that recorded 30,000 resolvable spots per line on 9-inch film.
- 4) The extreme coherence length of the laser permits interference effects over large distances. Part of the laser beam can be tapped off and used in an interferometric mechanical alignment control subsystem.
- 5) The laser beam itself can be used as the electromagnetic carrier, rather than a radio-frequency carrier. This technique removes several possible noise sources from the data link.

As with TV scanners, readout and recording can be accomplished with closely related devices. Figure 4.4-1 illustrates the subsystem components. The critical elements are the beam steering and format drive units.

The electro-optic effect can be used for limited electrical steering of the laser beam, but the number of resolvable spots per scan ( $\sim 100$ ) is at present much too low for application to the MOT problem. Mechanical techniques that appear more useful within the MOT timescale are variations of those used in high-speed streak cameras; rotating mirrors, discs, and drums are used to impart relative motion between the focused laser beam and the film.

Since the full diameter of an Airy disc at  $f/15$  is approximately 0.001 inch, the beam position must be known to within a few ten-thousandths of an inch to maintain geometric relationships. This distance measurement accuracy is well within the capability of interferometric systems. The Airborne Instrument Division of Cutler-Hammer manufactures a digital laser interferometer that measures linear distances to an accuracy of ten-millionths of an inch.

The angular position of the rotating element may be determined with a state-of-the-art shaft encoder. For example, if the 16-inch-square film is placed in a 6-inch-diameter drum for readout, a 16-bit shaft encoder will, in the absence of vibrations, determine the spot position on the circumference to an accuracy of 3 ten-thousandths of an inch.

Reproduction of the original grey scale is basically a function of the film used for recording. The transmission of each resolved spot can be determined to an accuracy of about 1 percent by measuring the attenuation of the laser beam. This is more than adequate. At the recorder, however, the density that results from a particular spot intensity will fluctuate because of the statistical distribution of the silver halide crystals and their low quantum efficiency. The smaller the spot, the greater the relative fluctuation. For this reason, the film used for recording must have smaller grains than the MOT film.

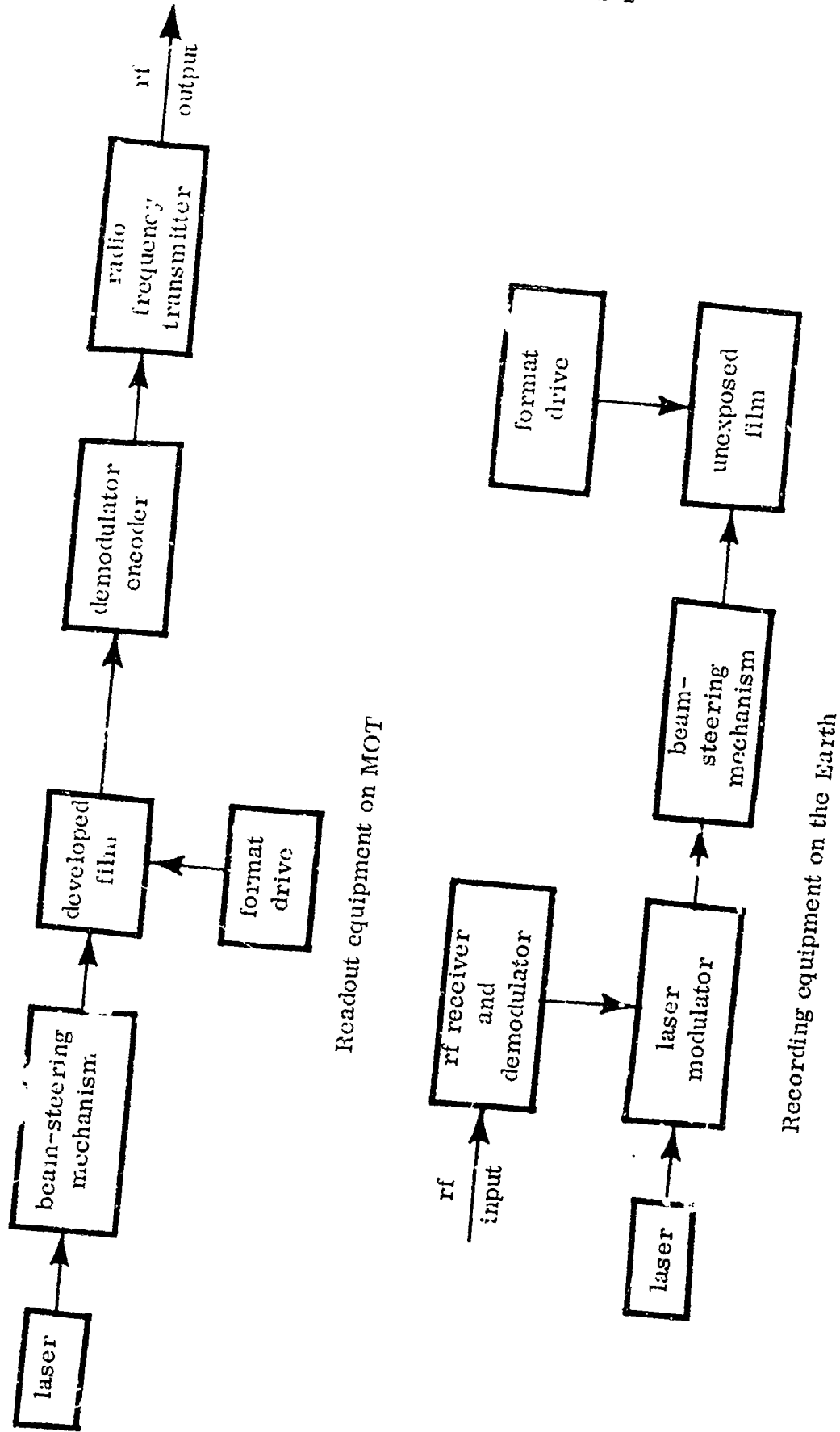


Figure 4.4-1: BLOCK DIAGRAM OF LASER-SCANNER SUBSYSTEMS WITH RADIO FREQUENCY DATA LINK

A representative laser photo-scan system is described below.

The MOT film-negative is placed inside of an optically polished fused quartz drum driven by a servo motor. The film is fastened to the drum so that it can, under the action of the centrifugal force, expand over the inner surface of the cylinder. An optical system focuses a laser beam onto the film plane. The light spot is moved parallel to the axis of the drum with constant velocity. The spot-drive mechanism is also part of a two-beam digital interferometer. The angular position of the drum is readout with a 16-bit digital shaft encoder. The digital rate generated by the interferometer is approximately 100 times the analog bandwidth of the film readout. The digital rate from the shaft encoder is three times the analog bandwidth. These digital signals and the analog film readout signal are encoded and transmitted to the ground station. Although these digital rates are high, the bandwidth requirements are low since the bandwidth is set by the magnitude of fluctuations from the mean drive and scan rates.

At the Earth receiving station a similar laser scanning subsystem is used for recording. The recorder on Earth is synchronized with the readout subsystem through interferometer and encoder outputs. Residual error in the instantaneous position of the recorder spot is corrected by an open-loop beam-deflection mechanism. The received video signal is demodulated, equalized, amplified, and used to drive an electro-optic light modulator. The modulated laser beam is focused on the unexposed film held by the recorder drum.

The minimum transmission time for a 16- by 16-inch negative is approximately 10 minutes. There is a trade between transmission time and reproduction accuracy, so slower picture transmission may be desirable.

4.4.2.4 Conclusions and Recommendations -- It is considered technically feasible to build a laser photo-scan system that is fully responsive to MOT pictorial-transmission needs. Economic feasibility cannot be established without further study. If development of laser photo-scan systems is accelerated, it will be possible to translate photographs into electrical analogs such that degradation of picture quality is not discernable for scientific usage within the time scale of the MOT-MORL system.

It is recommended that images be transmitted to the ground over a photo scan data link. The use of a laser-scan system, if available, will permit optimum use of MOT equipment. If conventional techniques are used, the reconstructed pictures still can be obtained in sufficient quantity to monitor progress of the experiment program, even though full realization of the experimental objectives must be delayed until the original film is transported to Earth (perhaps every 90 days).

#### 4.4.3 Navigation and Guidance

In general, navigation and guidance problems for the synchronous-orbit MOT are unlike those for the MOT in low Earth orbit. There are, despite the differences, several similarities in the navigation and guidance systems for both types of orbits.

Navigation — Ground-based radar tracking will be used to generate the navigational measurements for the MOT-MORL system in both low Earth and synchronous orbits, although hardware for and operation of the two navigation systems are completely different. The synchronous-orbit navigation profile and system description are discussed in Sections 4.4.3.1 and 4.4.3.2. In the low-Earth-orbit navigation system (Reference 7) operation, the vehicle is tracked for the first three passes of a day (total of about 0.5 hour) over the manned spacflight network (MSFN) station at Corpus Christi, Texas. An ephemeris is computed on the ground and transmitted to the vehicle. Thereafter, navigation information is obtained by on-board extrapolation with periodic update from more accurate ground-based extrapolation until the next day's tracking. The position error envelope is always less than 5 nautical miles.

In discussing navigational problems, stationkeeping should be considered since the MOT-MORL detached-mode concept requires stations to be not more than 1 mile apart. Stationkeeping navigation for the synchronous orbit is discussed in Section 4.4.3.2, and for the low Earth orbit in detached mode of operation in Reference 1. Briefly, the MORL rendezvous radar is used to measure range and range rate to the MOT, and the MORL computer is used to compute the relative drifts and necessary velocity impulses. The radar must operate continuously because stationkeeping impulses are required every 9 hours for worst-case ballistic coefficients.

Guidance — The MOT mission profile for both low Earth and synchronous orbits dictates that the MOT rendezvous with MORL, which is already in orbit. Even in the detached mode, the MOT must first rendezvous with and dock to the MORL for initial setup and alignment. The MOT vehicle performs the rendezvous and docking maneuvers because it is lighter and because perturbation of the MORL is to be avoided.

The rendezvous-guidance profile is intimately associated with the trajectory. For this reason, rendezvous guidance problems differ for the synchronous and low Earth orbits (see Sections 4.4.3.1 and 4.4.3.3 and References 1 and 7). In the low Earth orbit, the chaser vehicle (MOT) is injected into an elliptical phasing orbit. A series of apogee-velocity increments, based on tracking and ground-based computation, allow rendezvous. When the vehicles are relatively close (less than 100 nautical miles apart) the rendezvous radar is activated, and terminal rendezvous and braking are controlled by vehicle-based measurements and computations. Docking is achieved visually with radar assistance.

4.4.3.1 Synchronous Orbit Navigation and Guidance Profile — Section 3.4 of this document presents the trajectory and propulsion requirements for launching the MOT into a synchronous orbit. The navigation and guidance requirements for ascent, rendezvous, and telescope operation are described in this section.

Guidance during the boost to the 100-nautical-mile parking orbit is handled by the Saturn V inertial system. The vehicle is tracked throughout its 77 minutes in the parking orbit, and the velocity maneuver necessary for transfer to the synchronous orbit is calculated by ground facilities. During vehicle ascent in the transfer orbit, tracking continues, and the velocity maneuver necessary for insertion into synchronous orbit is determined. Insertion into the synchronous orbit is performed with an accuracy of approximately 20 nautical miles ( $1 \sigma$ ) in position and 33.3 fps ( $1 \sigma$ ) in velocity. If uncorrected, these errors grow to 231 nautical miles ( $1 \sigma$ ) in position and 50.2 fps ( $1 \sigma$ ) in velocity after 8 hours when the MOT nominally makes rendezvous with the MORL at the line of nodes of the two orbits. Therefore, a midcourse trajectory correction is made as soon as possible — about 2.5 hours after entering the synchronous orbit. When the MOT arrives at the relative line of nodes of the two orbits on its corrected trajectory, another velocity maneuver is performed by the MOT to make the MOT and MORL orbits coplanar, and to establish a closing velocity that is favorable for the terminal rendezvous phase. Terminal rendezvous and docking are then performed with on-board systems.

4.4.3.2 Synchronous Orbit Navigation System — The manned spaceflight network (MSFN) ably meets all of the navigation tracking requirements of the MOT synchronous orbit mission. The MSFN, which presently supports the Gemini and Apollo programs, consists of the mission control center (MCC) at Cape Kennedy, the integrated mission control center (IMCC) at Houston, and communication network for data and voice transmission between these facilities and remote sites that provide tracking, telemetry-data-acquisition, command, and air-to-ground communication functions. There are 19 remote ground sites, two Atlantic Missile Range ships, one Pacific Missile Range ship, and any supporting aircraft needed to simultaneously track two spacecraft. The global location of MSFN stations, their excellent facilities, plus the fact that the MSFN was designed to support manned spacecraft missions make it well suited for MOT mission tracking support.

During the boost to the parking orbit the MSFN stations of the Atlantic Missile Range track the vehicle. MSFN stations in Africa, Australia, and Hawaii and the mobile ship-based MSFN stations track the vehicle in its parking orbit. During the transfer from parking to synchronous orbit, the vehicle is tracked by MSFN stations in the United States and by the very-long-range stations at Bermuda and Antigua. When the vehicle is in its inclined synchronous orbit, three MSFN stations (Ascension Island, Antigua, and Bermuda) provide continuous 24-hour tracking. These three stations are equipped with the very-long-range (maximum 32,000 nautical miles) FPQ-6/TPQ-18 radar system. Because the MOT range to these stations varies between 19,000 and 21,000 nautical miles, the vehicle is well within their tracking capability. In addition, Ascension Island is equipped with a Univac 1206 computer for vehicle ephemeris computations.



Navigation System Accuracy — A navigation analysis of the synchronous orbit was conducted using the Boeing computer program, "Parameters Estimation from a Set of Observations" (PESO III). Tracking measurements with FPQ-6/TPQ-16 radar systems were simulated at 10-minute intervals and processed in smoothing blocks of 25 measurements. Six smoothing blocks (total of 150 measurements) were processed. Total tracking time was 89,400 seconds, or approximately 24.8 hours. This simulates the long-term tracking of the MOT-MORI system after boost and rendezvous to determine vehicle ephemeris. Inputs to the program included: (1) the FPQ-6/TPQ-16 radar system measurement errors of 0.15 milliradian ( $1 \sigma$ ) for random angular (azimuth and elevation) measurements and 20 feet ( $1 \sigma$ ) for random range measurements (Reference 60) and, (2) initial uncertainties in position and velocity after insertion into synchronous orbit which are the injection errors of 20 nautical miles ( $1 \sigma$ ) in position and 33.3 fps ( $1 \sigma$ ) in velocity.

Results show residual uncertainties at the end of the tracking time for: (1) the Ascension Island station of 0.89 nautical mile ( $1 \sigma$ ) and 0.372 fps ( $1 \sigma$ ) in velocity; and (2) the Antigua station of 1.05 nautical miles ( $1 \sigma$ ) in position and 0.416 fps ( $1 \sigma$ ) in velocity. The Ascension Island station yields smaller uncertainties because of geometrical considerations due to its more central location with respect to the orbit trace on the surface of the Earth. Although results for the Bermuda station were not determined with the PESO program, they are expected to be a little worse than the Antigua results because Bermuda is the least centrally located station. If the results from the Ascension Island and Antigua stations are combined, the resulting uncertainties are 0.67 nautical mile ( $1 \sigma$ ) in position and 0.272 fps ( $1 \sigma$ ) in velocity.

A second series of PESO runs were made with the measurements made at 1-minute intervals. Once again measurements were processed in smoothing blocks of 25, and 6 smoothing blocks were processed for a total of 150 measurements. Total tracking time was 8940 seconds or about 2.48 hours. This was to simulate short-term tracking of the MOT after insertion into synchronous orbit in order to evaluate the required velocity corrections. Results show residual uncertainties at the end of the tracking period were: (1) 2.75 nautical miles ( $1 \sigma$ ) in position and 3.04 fps ( $1 \sigma$ ) in velocity for the Ascension Island site, and (2) 2.81 nautical miles ( $1 \sigma$ ) in position and 3.15 fps ( $1 \sigma$ ) in velocity for the Antigua site. If tracking data from Ascension Island and Antigua are combined, the resulting uncertainties are 1.82 nautical miles ( $1 \sigma$ ) in position and 2.05 fps ( $1 \sigma$ ) in velocity. These uncertainties are larger than for the one-measurement-per-10-minutes results even though 150 measurements were processed in both cases because tracking takes place for only about 0.1 of the orbit while the one-measurement-per-10-minutes results involve tracking over the entire orbit. Figures 4.4-2 through 4.4-5 are graphs of navigation position and velocity uncertainties as a function of tracking time for the Ascension Island tracking site for both long- and short-term tracking. Note the leveling off of the long-term tracking position and velocity curves, which indicates that longer tracking time would decrease the uncertainties only slightly.

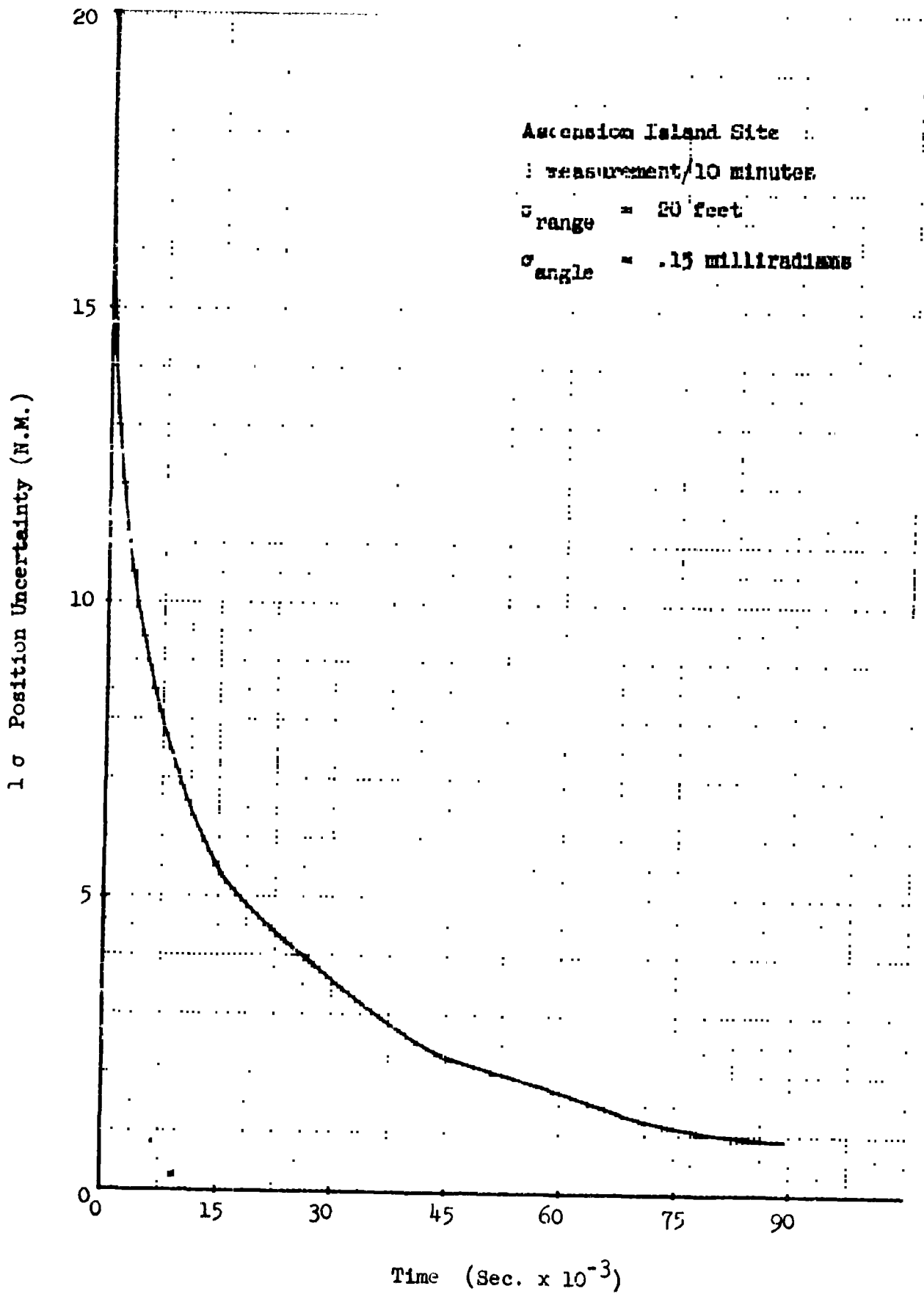


FIGURE 4.4-2 POSITION UNCERTAINTY VS. TIME - LONG TERM TRACKING

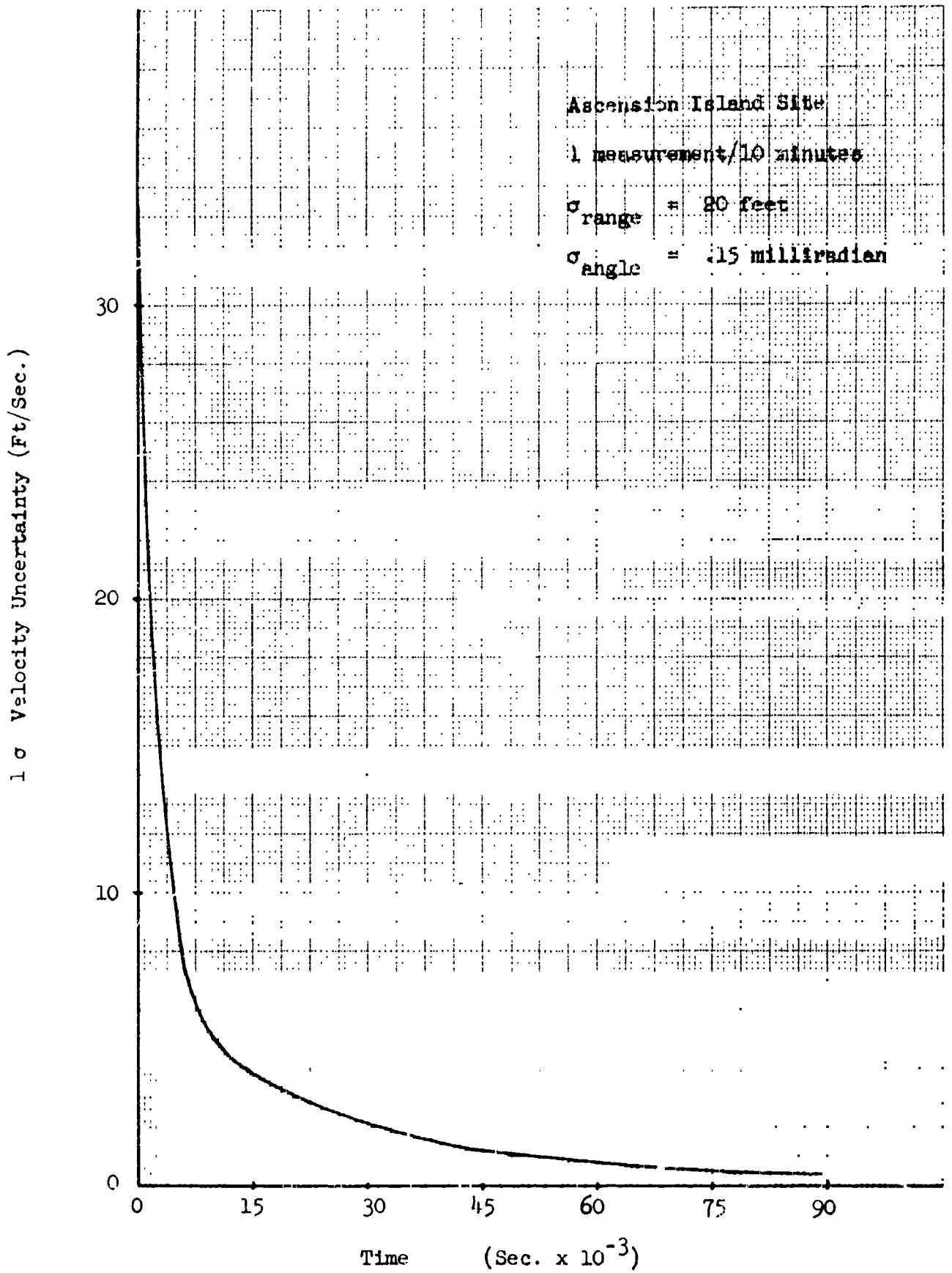


FIGURE 4.4-3

VELOCITY UNCERTAINTY VS. TIME - LONG TERM TRACKING

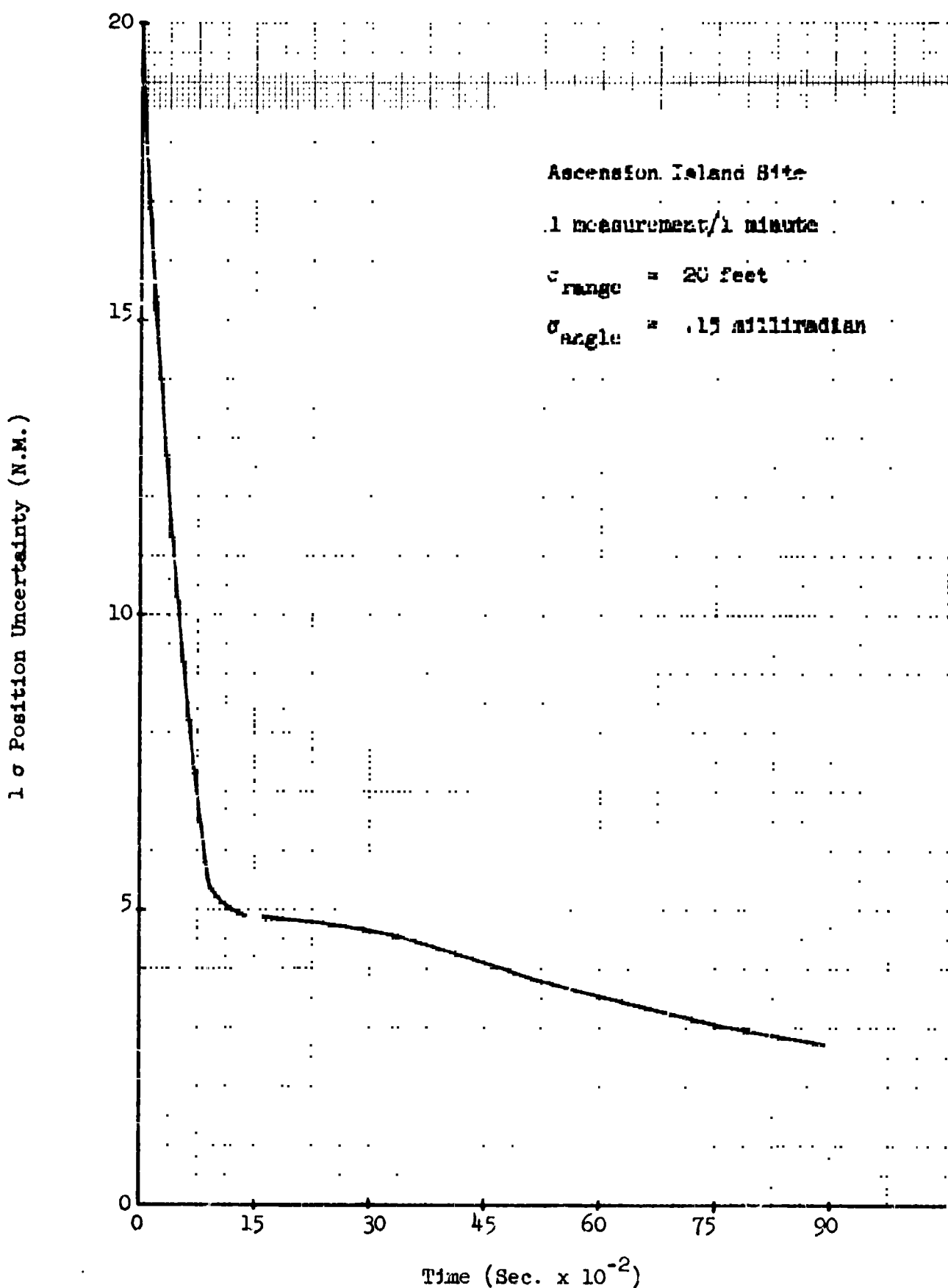


FIGURE 4.4-4 POSITION UNCERTAINTY VS. TIME - SHORT TERM TRACKING

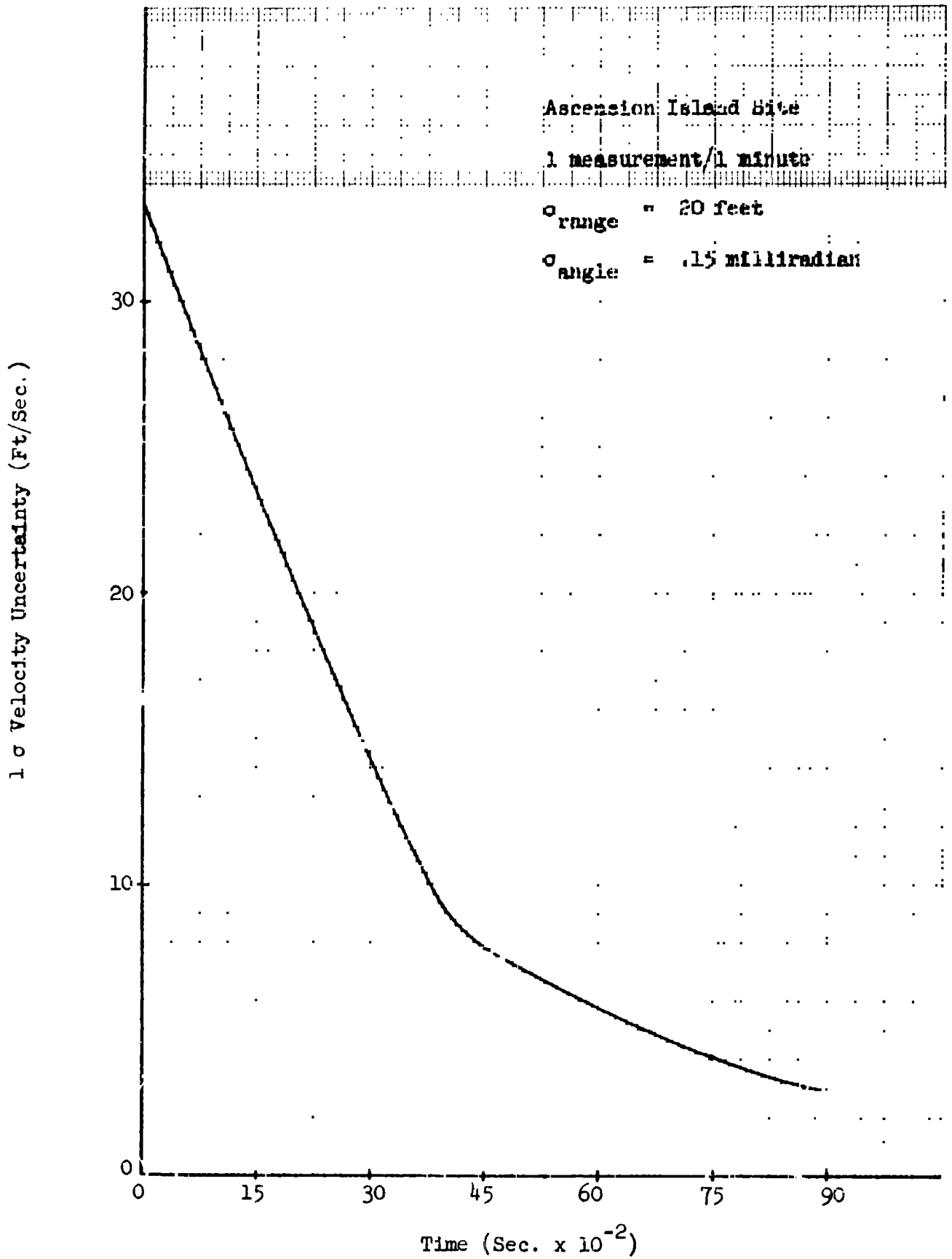


FIGURE 4.4-5 VELOCITY UNCERTAINTY VS. TIME - SHORT TERM TRACKING

Navigation System Problems: Detached Modes versus Soft Gimbal — Long-term navigation for the MOT-MORL system in the soft-gimbal mode presents no special problems. The tracking radar will track a single transponder of the combined vehicle. In the detached mode, the two vehicles are never to be more than 1-nautical-mile apart; thus, both vehicles are within the ground radar beamwidth. It is impossible for the radar to differentiate between the two vehicles. Even if the radar command coder is used to separately interrogate the MOT and MORL transponders and then simultaneously track the two vehicles, position determination with ground tracking is only good to 0.67 nautical mile ( $1 \sigma$ ) (two radar combined) — a distance insufficient to meet the 1-nautical-mile specification for vehicle separation. It is proposed to use the rendezvous radar to measure the relative range and range rate between the MOT and MORL and to use the MORL computer to: (1) process the data to determine the relative position and velocity of the two vehicles; and (2) to determine if and when stationkeeping velocity impulses are necessary. It is concluded (see Section 3.4) that stationkeeping requirements for the synchronous orbit are greatly reduced because aerodynamic drag is no longer a significant perturbation. It is therefore probable that the rendezvous radar will not have to be run continuously for stationkeeping measurement purposes.

4.4.3.3 Synchronous Orbit Rendezvous Guidance Description — The baseline ascent and rendezvous-trajectory profile presented in Section 3.4 indicates that MOT-MORL rendezvous should occur at the relative line of nodes of the MOT and MORL orbits, 8 hours (120 degrees downrange) after insertion of the MOT into synchronous orbit. Accuracy for the MOT insertion in synchronous orbit is 20 nautical miles ( $1 \sigma$ ) in position and 33 fps ( $1 \sigma$ ) in velocity. These position and velocity errors correspond to orbit errors of 0.36 hour ( $3 \sigma$ ) in period, 0.6 degree ( $3 \sigma$ ) in inclination, and 0.0074 ( $3 \sigma$ ) in eccentricity. If left uncorrected these errors will propagate during the 8 hours of travel to reach the rendezvous point. Figures 4.4-6 through 4.4-11 are plots of the propagation of the initial injection-altitude, altitude-rate, downrange, downrange-rate, crossrange, and crossrange-rate errors along the orbit. At the nominal rendezvous point 120 degrees downrange (15 degrees of arc corresponds to 1 hour, thus 120 degrees represents 8 hours) the insertion errors will have grown to 231 nautical miles ( $1 \sigma$ ) in position and 50.2 fps ( $1 \sigma$ ) in velocity. This position error at the rendezvous point is entirely too large and indicates the necessity for performing a velocity correction maneuver. The large 231-nautical-mile ( $1 \sigma$ ) position error at the rendezvous point is almost entirely caused by the initial insertion-velocity error of 33.3 fps ( $1 \sigma$ ), which, in turn, results primarily from control errors during the insertion maneuver.

Analysis of the Velocity Correction — After insertion into synchronous orbit, the MOT will be tracked at the fast tracking rate (one measurement per minute) for 8940 seconds (about 2.48 hours). The velocity correction will then be made. At this point the insertion errors have propagated to 54.3 nautical miles ( $1 \sigma$ ) in position and 38.4 fps ( $1 \sigma$ ) in velocity. Navigation uncertainties are 2.25 nautical miles ( $1 \sigma$ ) in position and 3.04 fps ( $1 \sigma$ ) in velocity for tracking from

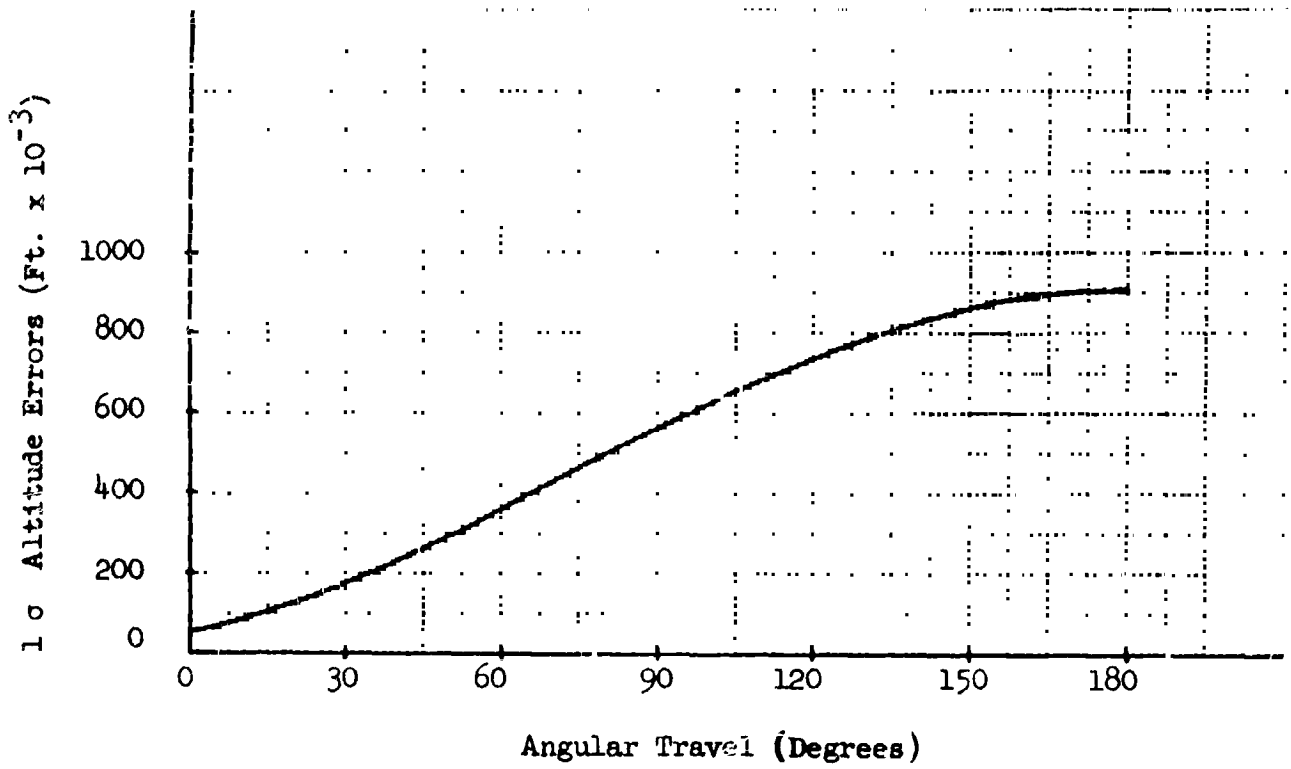


FIGURE 4.4-6 PROPAGATION OF INJECTION ALTITUDE ERRORS

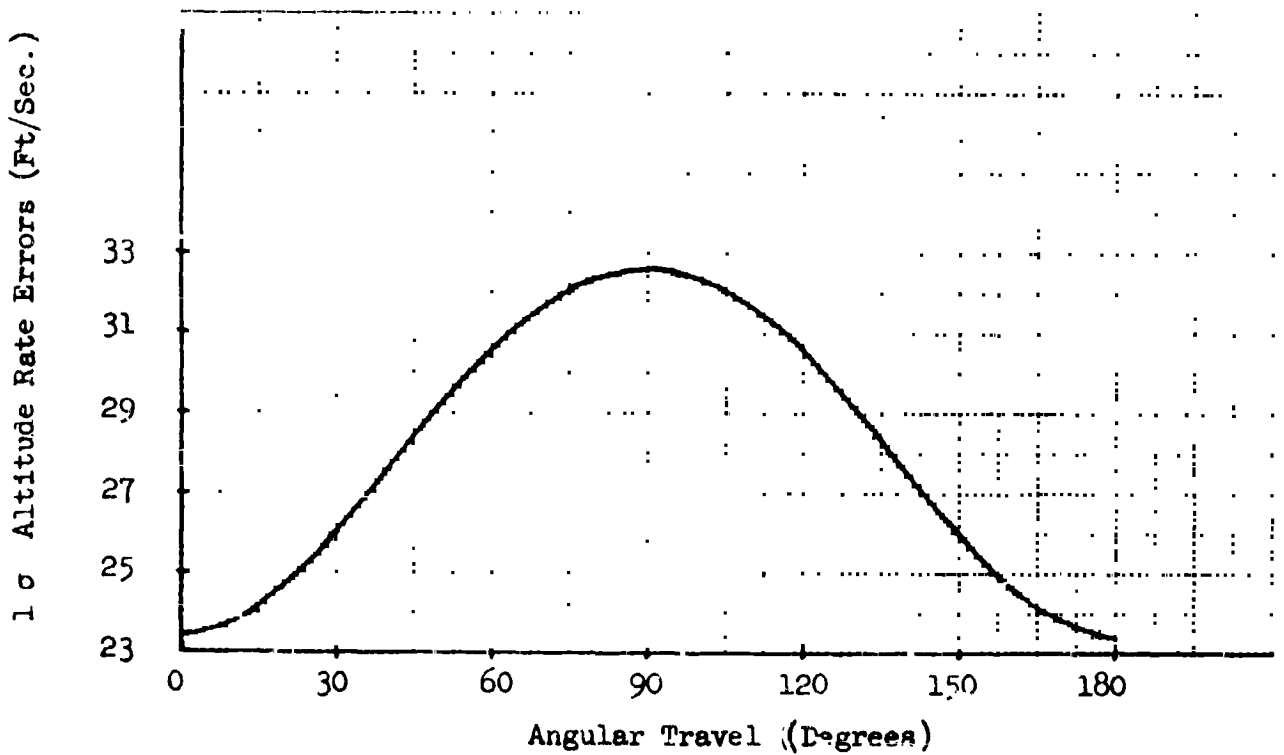


FIGURE 4.4-7 PROPAGATION OF INJECTION ALTITUDE RATE ERRORS

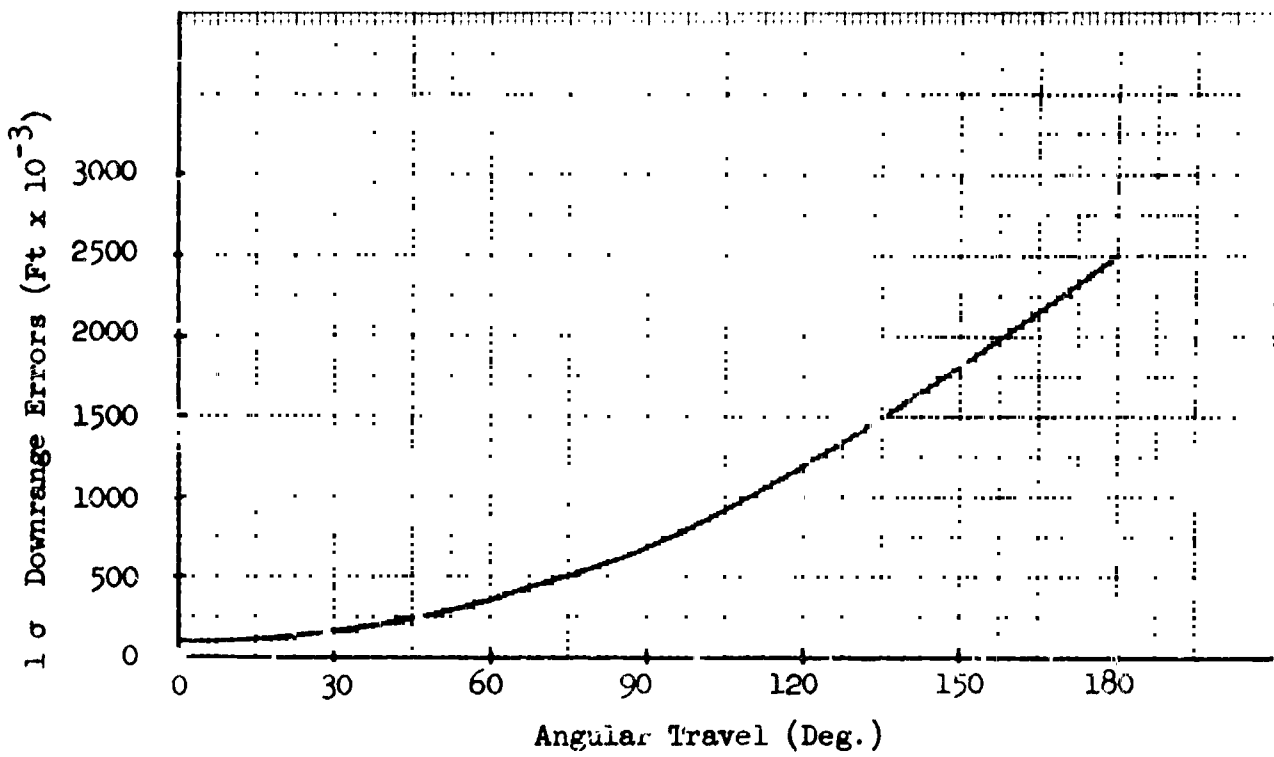


FIGURE 4.4-8 PROPAGATION OF INJECTION DOWNRANGE ERRORS

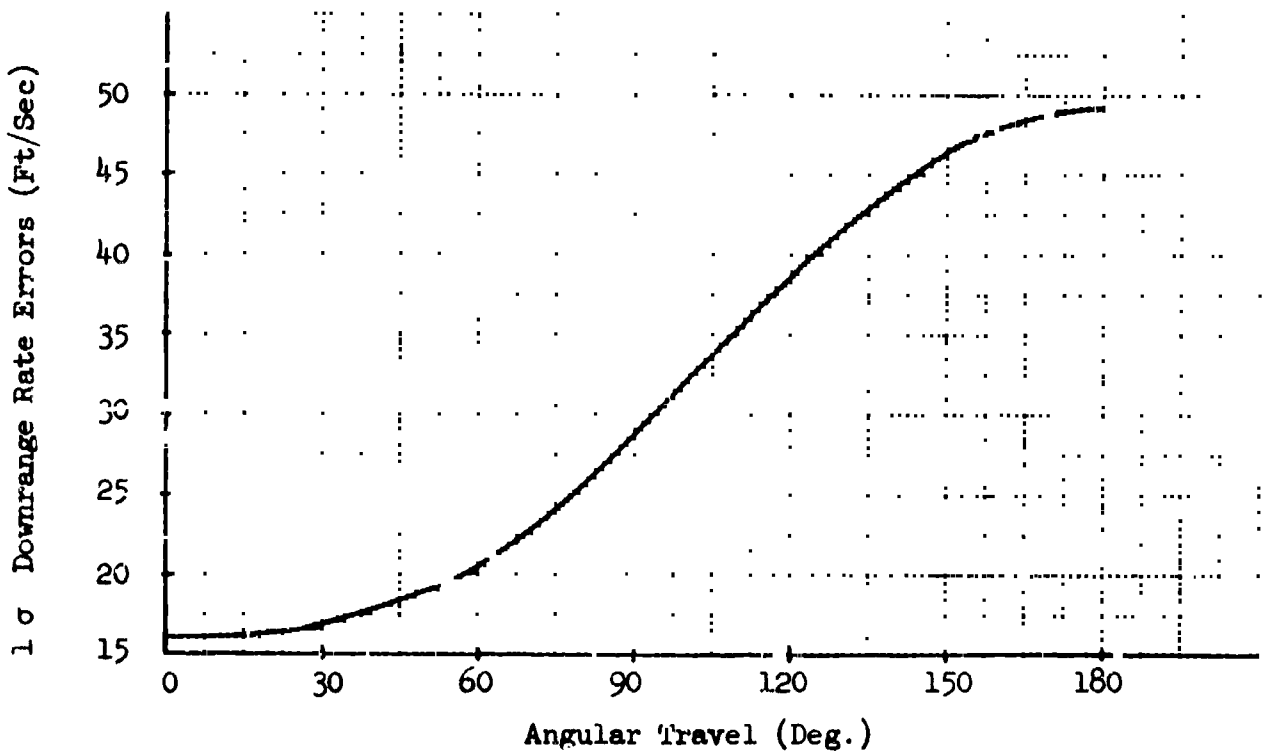


FIGURE 4.4-9 PROPAGATION OF INJECTION DOWNRANGE RATE ERRORS



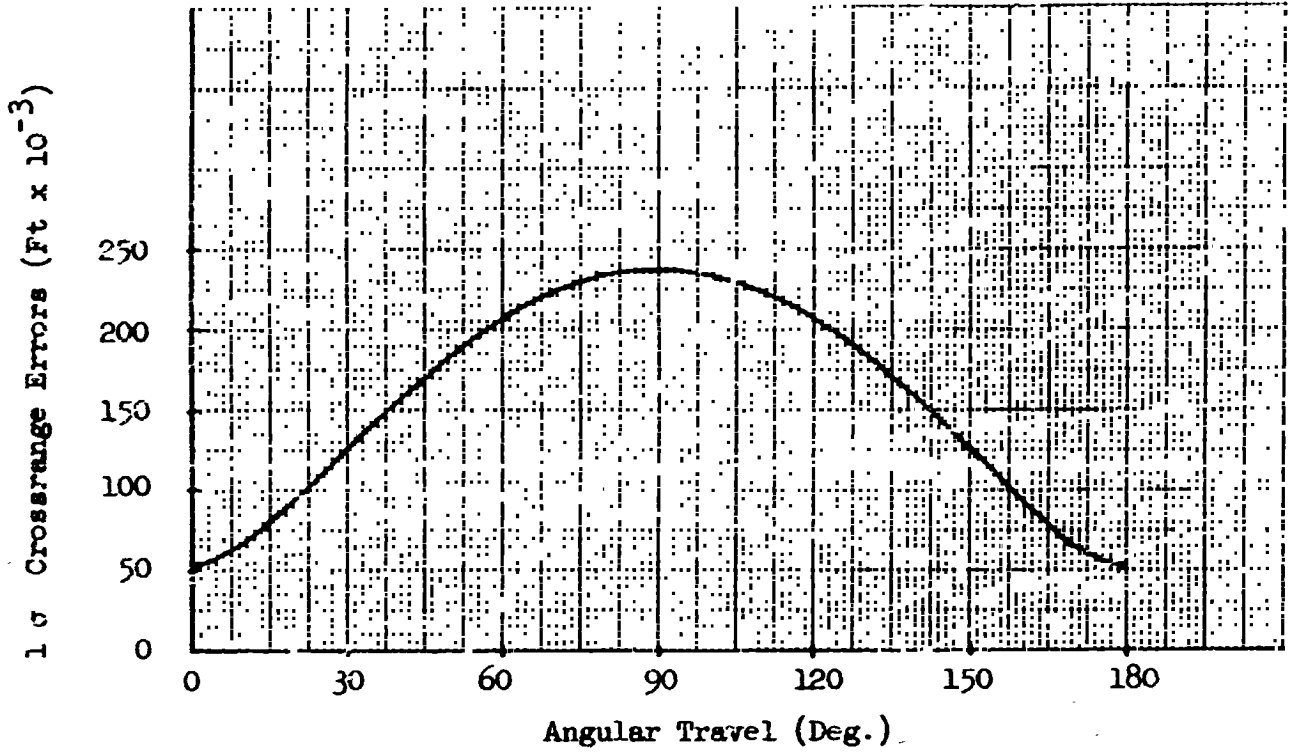


FIGURE 4.4-10 PROPAGATION OF INJECTION CROSSRANGE ERRORS

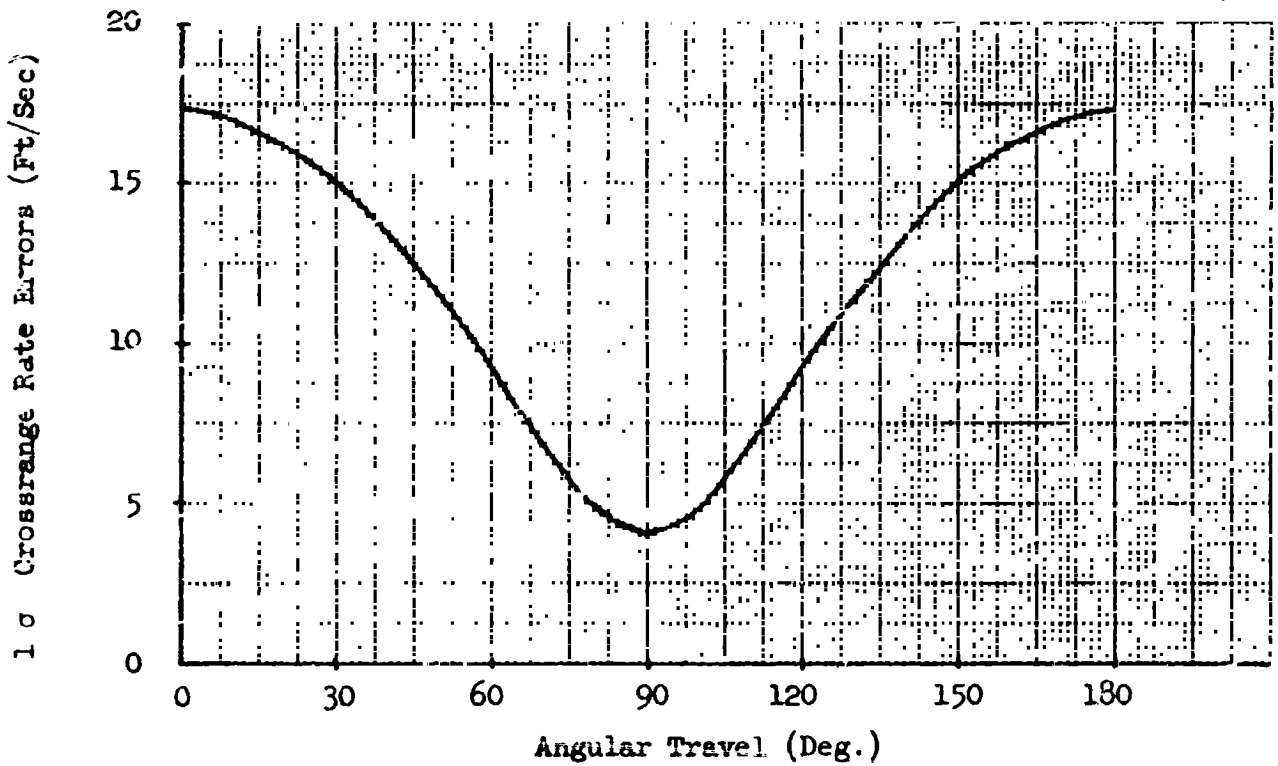


FIGURE 4.4-11 PROPAGATION OF INJECTION CROSSRANGE RATE ERRORS

Ascension Island and 1.82 nautical miles ( $1 \sigma$ ) in position and 2.05 fps in velocity for combined tracking from Ascension Island and Antigua. Control uncertainties of 1 percent ( $1 \sigma$ ) in velocity magnitude and 0.01 radian ( $1 \sigma$ ) pointing accuracy were selected as realistic control errors for the projected 1980 time period.

The above numbers were used as input to the Boeing Orbital Mission Analysis Program (BOMAP). The program computed the required velocity correction and the errors resulting at rendezvous due to navigation and control uncertainties. The required velocity correction was 56.1 fps ( $1 \sigma$ ). This velocity correction resulted in a velocity error at rendezvous of 19.9 fps ( $1 \sigma$ ). Control errors caused position and velocity errors at rendezvous of 3.63 nautical miles ( $1 \sigma$ ) and 1.82 fps ( $1 \sigma$ ), respectively. Navigation uncertainties produced errors at rendezvous of 18.7 nautical miles ( $1 \sigma$ ) in position and 8.58 fps ( $1 \sigma$ ) in velocity for tracking from Ascension Island only and 12.7 nautical miles ( $1 \sigma$ ) in position and 5.88 fps ( $1 \sigma$ ) in velocity for tracking from both sites combined. Total control and navigation errors are 19.0 nautical miles ( $1 \sigma$ ) in position and 8.77 fps ( $1 \sigma$ ) in velocity for Ascension Island tracking and 13.2 nautical miles ( $1 \sigma$ ) in position and 6.18 fps ( $1 \sigma$ ) in velocity for combined tracking. The total velocity error at rendezvous is 21.74 fps ( $1 \sigma$ ) for Ascension Island tracking or 20.83 fps ( $1 \sigma$ ) for combined tracking. This number represents the one-sigma braking velocity impulse that must be applied, at rendezvous point, to the MOT to ensure that it returns to the proper circular synchronous orbit.

In addition, the relative inclination difference between the MOT and MORL orbits must be zeroed. This difference occurs from two sources — launch-window effects, and crossrange injection errors. Velocity requirements are 150 fps (maximum) to eliminate launch-window inclination effects and 128 fps ( $3 \sigma$ ) to eliminate injection inclination errors. When these numbers are root sum squared with the three-sigma required braking-velocity correction, the magnitude is obtained of the total velocity impulse required at the rendezvous point, which is 207.7 fps. (The difference is negligible, 206.9 fps, for combined site tracking). After the rendezvous-velocity impulse the vehicles will be in the same orbital plane with a separation of no more than 19 nautical miles ( $1 \sigma$ ) and a very small velocity difference ( $\approx 2$  fps ( $1 \sigma$ )). At this point, the MORL rendezvous radar will be used and, on the basis of radar measurements, MORL computer computations and visual observations, the MORL crew will operate the MOT controls via a data link to dock the vehicles. It is conservatively estimated that 50 fps will be required to effect the terminal rendezvous and docking maneuver. Adding the first three-sigma velocity corrections (168.3 fps since  $1 \sigma$  is 55.1 fps), the rendezvous velocity impulse, and the  $\Delta V$  required for docking, 426 fps is obtained as the maximum  $\Delta V$  required for rendezvous and docking.

Detached Mode Rendezvous -- In addition to the docking of the MOT to the MORL for initial setup and alignment, it will be necessary to dock the vehicles periodically for routine maintenance purposes when in the detached mode. Since the vehicles will be within 1 nautical mile of each other at all times, the docking will be done visually with range and range rate information determined by the rendezvous radar. Because vehicle separation is small, only a few feet per second should be required to effect docking.

4.4.3.4 Conclusions and Recommendations — No special difficulties in navigation and guidance are anticipated for the proposed synchronous orbit MOT. In fact, synchronous-orbit operation exhibits certain advantages from a navigation and guidance viewpoint.

Navigation — The MOT-MORL system is always in view of three radar tracking sites so that continuous tracking is possible. For very-long-term tracking (from 3 days to several weeks), only slight improvement in position accuracy is anticipated in excess of the 24.8-hour tracking accuracies discussed in Section 4.4.3.2. Even the 24.8-hour tracking accuracy is good enough to suggest routine tracking from only one site, preferably Ascension Island. If certain experiments require very precise navigation information, tracking information from all three sites could be combined. With three sites, the improvement over the 0.67-nautical-mile position accuracy of two sites would be relatively slight since Bermuda would add the least accurate data.

It is concluded that long-term synchronous-orbit navigation appears to yield more accurate position and velocity information than navigation in the low Earth orbit, principally because on-board extrapolation is unnecessary for synchronous-orbit operation. This also reduces on-board computer requirements.

Stationkeeping requirements for detached-mode operation are considerably reduced for the synchronous orbit, because aerodynamic drag is not a significant perturbation. Operation time of the rendezvous radar to provide relative-motion data can be reduced with the resulting benefits of longer radar life, lower power requirements, and reduced on-board computation requirements. Fuel consumption for stationkeeping is also greatly reduced.

Guidance — As previously noted, guidance and rendezvous profiles differ considerably for the synchronous and low Earth orbits. Synchronous-orbit-injection errors impose a requirement for a velocity correction to reduce terminal position errors at rendezvous. It is advisable to provide tracking from two radar sites to minimize navigation uncertainties prior to the velocity correction. This will reduce the position error at rendezvous, caused by control errors, and navigation uncertainties by reducing the contribution of the dominant navigation uncertainties. Synchronous-orbit rendezvous requires a maximum  $\Delta V$  of 426 fps (2-hour launch window).

#### 4.4.4 Electrical Power

The electrical power subsystem concepts selected for the soft-gimbal and the detached modes of the MOT synchronous orbits are based on general MOT constraints. The specific power system constraints and assumptions are:

- 1) Power is supplied by an on-board power system during launch, rendezvous, docking, and operational phases for the detached mode.
- 2) Power for the soft-gimbal mode is supplied by an on-board power source during launch, rendezvous, and docking and by MORL during the operational phase.

- 3) Power load profiles for the soft-gimbal and detached modes of the synchronous orbit are essentially the same for the low Earth orbit; however, the load profiles for Sun-occultation periods are changes (see Figures 4.4-12 and 4.4-13 for the synchronous orbit).
- 4) The solar cell panels are oriented to the Sun by articulation of the panels with respect to the MOT pitch axis and by rolling the MOT about the roll axis.

4.4.4.1 Soft-Gimbal Mode — An on-board power source is required for the soft-gimbal mode only during the launch, rendezvous, and docking and power is supplied from MORL during the operational phase. The power subsystem load profiles are the same for the soft-gimbal modes of the synchronous orbit and the low-Earth-orbit missions during launch, rendezvous, and docking. Hence, the primary silver-zinc battery specified for the low Earth orbit soft-gimbal mode is also suitable for the soft-gimbal synchronous mission.

The on-board power subsystem will provide:

- 1) On-board power supply, consisting of two primary silver-zinc batteries capable of supplying 4800 watt-hours of electrical energy for launch, rendezvous, and docking; estimated weight of batteries is 110 pounds;
- 2) 28-volt d. c. bus and associated circuit breakers, control, and protection; circuit breakers will include direct-current load breakers, battery breakers, and MORL-MOT d. c. -system tie breakers and disconnects.
- 3) 115/200 volt, 3-phase, 400 cps alternating-current bus and associated circuit breakers, control, and protection. Circuit breakers will include alternating-current load breakers, and MORL-MOT alternating-current system tie breakers and disconnects.

4.4.4.2 Detached Mode — Figure 4.4-14 summarizes the power subsystem characteristics and shows differences in the requirements of the synchronous orbit and the low-Earth-orbit missions. Figure 4.4-15 is a schematic diagram of the on-board electrical power subsystem centerline concept selected for the synchronous orbit. This system supplies power requirements during all phases of the mission. The power system basic concept is the same as the low-Earth-orbit mission. However, some component ratings and sizes, and type of battery are changed.

Assumptions used to calculate power source and equipment sizes to meet the requirements shown in Figures 4.4-12 and 4.4-13 are discussed below.

The battery supplies the total energy (including losses) of launch, rendezvous, and docking. This requirement is essentially a single battery discharge-charge cycle of 4800 watt-hours.

The battery also supplies the energy pulses (including losses) of 2820 watt-hours, for about 80 depressurization cycles.

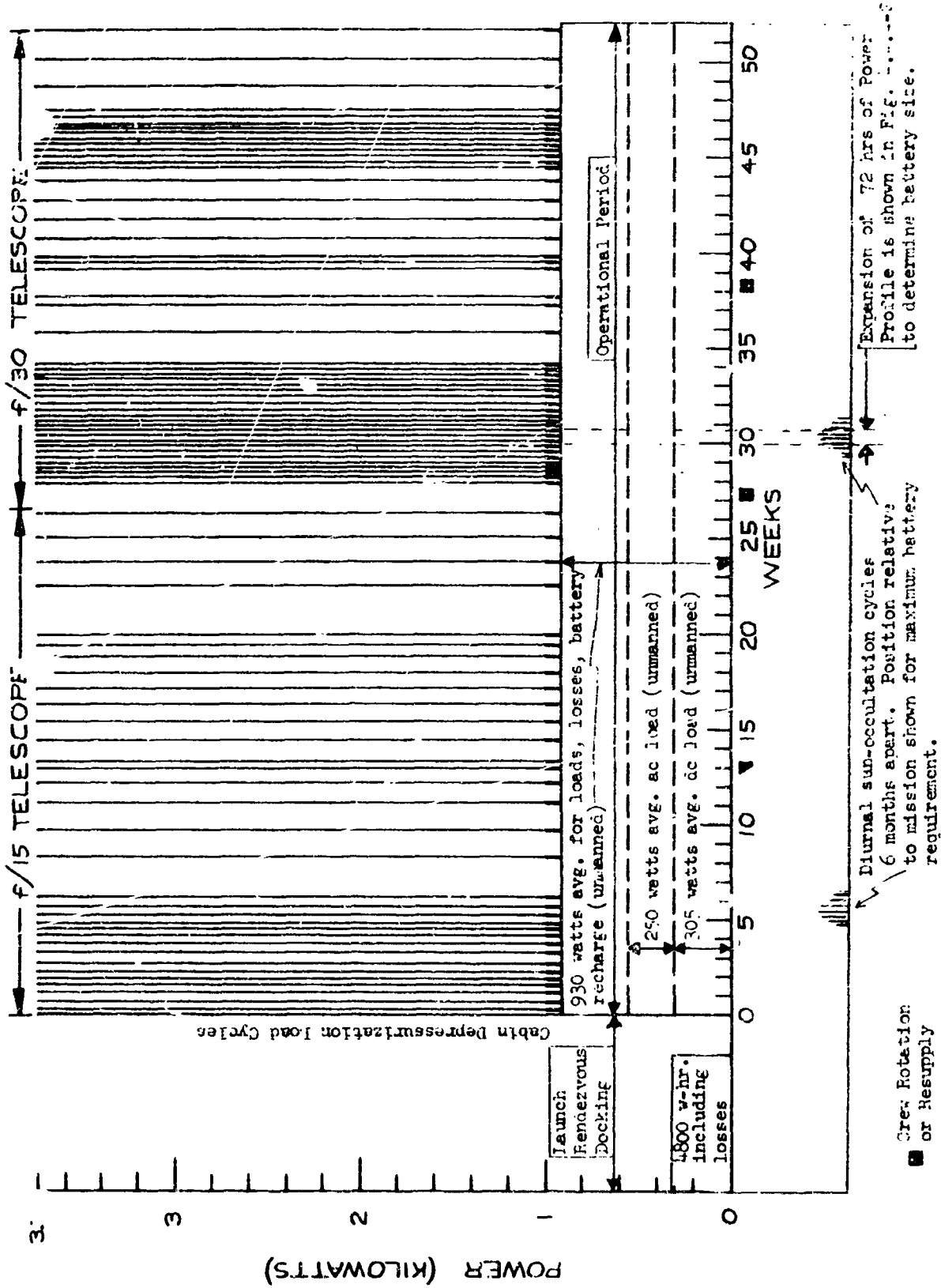


Figure 4.4-12 DETACHED MODE POWER PROFILE

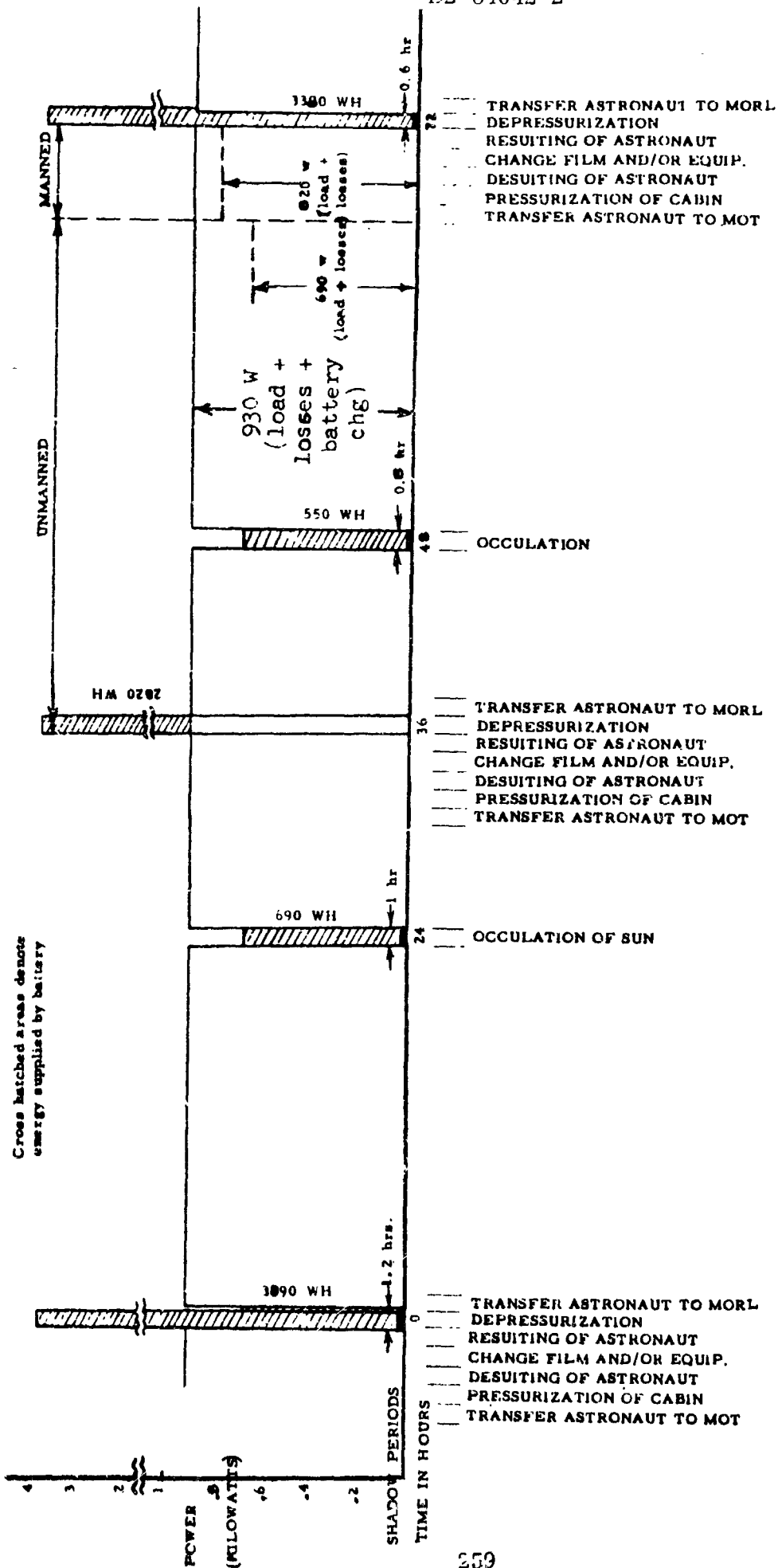


Figure 4.4-13 Detached Mode Expanded Power Profile

Item	Rating		Size		Weight (lbs)	
	Synchro- nous	Low Earth	Synchro- nous	Low Earth	Synchro- nous	Low Earth
Solar Panels	930w	1515w	132 ft <sup>2</sup>	216 ft <sup>2</sup>	196	324
Batteries and Installation	3890wh (AgZn)	3430wh (AgCd)	1.3 ft <sup>3</sup>	4.5 ft <sup>3</sup>	212	593
Regulators	5000w	5000w	2140 in <sup>3</sup>	2140 in <sup>3</sup>	75	75
Inverters	4500w	4500w	5150 in <sup>3</sup>	5150 in <sup>3</sup>	180	180
Battery Chargers	220w	745w	165 in <sup>3</sup>	430 in <sup>3</sup>	8	15
Distribution System	—	—	—	—	250	250
Total	—	—	—	—	921	1437

AgZn = Silver-Zinc Rechargeable Battery

AgCd = Silver-Cadmium Rechargeable Battery

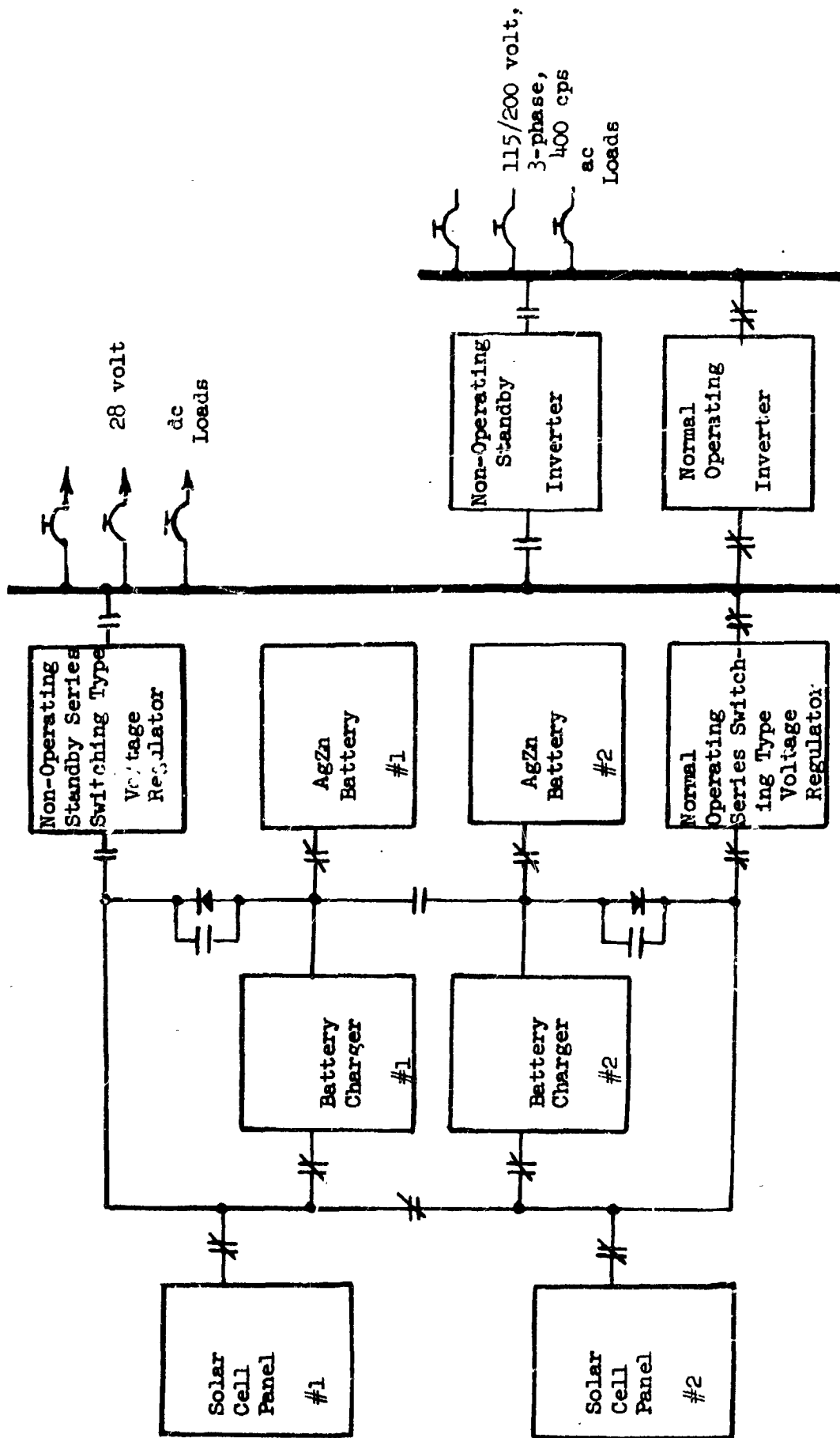
Figure 4.4-14: ELECTRICAL SUBSYSTEM SUMMARY

During Sun-occultation periods of the mission (maximum of 1.2 hours every 24 hours) all power is supplied by the battery. Figure 4.4-13 shows the relationship between depressurization load pulses and Sun occultations and shows the energy blocks that must be supplied during a few occultation cycles, beginning with a maximum battery energy demand occurring when a depressurization cycle is coincident with the longest occultation time. Battery sizing is based on the maximum requirement of 3890 watt-hours and 100 cycles of service. Most battery cycles will be about 30 percent less than the 3890 watt-hours; however, this maximum condition is assumed in the battery rating to ensure a 3890 watt-hour capability, with ample margin of safety, as the mission end.

Battery selection and sizing to meet the maximum duty were based on:

- 1) Sealed and rechargeable with 1-year life;
- 2) Silver-zinc usable wh/lb = 20 based on 60 percent depth of discharge for 100 charge-discharge cycles;
- 3) Silver-cadmium usable wh/lb = 13 based on 80 percent depth of discharge for 100 charge-discharge cycles.

The solar cells must supply the maximum power of 930 watts, which includes load, battery recharge, and losses. Sizing of solar panels is based on 7 watts per square foot and 1.5 pounds per square foot including extension and orientation mechanisms and support structure. Solar panel radiation degradation is



Circuit Breaker Positions Shown For Normal Operating Condition (Non-Occultation Condition)

FIGURE 4.4-15 ELECTRICAL POWER SUBSYSTEM SCHEMATIC - DETACHED MODE



greater at synchronous-orbit altitudes than at low-Earth-orbit altitudes; however, 7 watts per square foot is considered conservative even for the synchronous mission. Battery charger and solar panel requirements for battery charging are based on a capability of full battery recharge in 23 hours.

Efficiencies used in the calculation of losses are:

- 1) Battery charge-discharge = 78 percent;
- 2) Battery charger = 90 percent;
- 3) Voltage regulator = 90 percent;
- 4) Inverter = 90 percent;
- 5) General distribution = 94 percent.

4.4.4.3 Conclusions and Recommendations — The power subsystem electrical load profiles are essentially the same for the synchronous orbit and the low-Earth-orbit missions. The load profiles differ, however, relative to the Sun-occultation periods. The following conclusions point out significant comparisons between the power subsystem concepts of the synchronous and low-Earth orbits.

- 1) The primary silver-zinc battery, specified for the low Earth orbit soft-gimbal mode on-board power supply, is also suitable for the soft-gimbal synchronous mission.
- 2) The centerline solar-cell/secondary-battery power system basic concept, selected for the low-Earth detached mode, is also suitable for the synchronous detached mode.
- 3) A smaller number of battery charge-discharge cycles is required in the detached mode of the synchronous mission. The selected silver-zinc secondary battery weighs 380 pounds less than the silver-cadmium battery required to meet the relatively large number of battery load cycles of the low-Earth mission.
- 4) In the synchronous orbit, more time is available and less power is required for battery recharge. As a consequence, the solar panel area required for synchronous orbit is about 40 percent less than the low-Earth requirements.
- 5) Weight of the total power subsystem for synchronous orbit (detached mode) is 515 pounds less than the corresponding system for the low-Earth mission.

The following recommendation is submitted relative to load-profile/power-system optimization: the depressurization cycles should be scheduled to avoid the longest Sun-occultation periods. This power profile optimization can result in a further reduction of battery weight and solar panel area requirements for battery recharge.

#### 4.5 FLIGHT-PERFORMANCE COMPARISON— LOW EARTH ORBIT VS SYNCHRONOUS ORBIT

Primarily because the S-IB and the S-V boosters are well-suited for both the low-Earth- and the synchronous-orbit MOT operations, respectively, neither operation encounters serious flight-performance problems. Use of the Apollo command module also facilitates these operations, especially the synchronous-orbit operation. As a consequence, neither operation is distinctly inferior or superior to the other, so the selection of the MOT orbit can be based on other criteria.

The following paragraphs discuss flight-performance differences of the low-Earth- and synchronous-orbit operations; but, none of these differences are considered to be of decision-making magnitude.

##### 4.5.1 Launch and Rendezvous

Comparison of the synchronous- and low-Earth-orbit MOT operations with the usual flight-performance  $\Delta V$  figure of merit is not sufficient because different boosters are used for the high and low orbits. More significant constraints in this case of different boosters are payload margin and overall mission costs.

The time required to rendezvous is different for low-Earth- and synchronous-orbit operations. In itself, time required to rendezvous is not of great significance; but, its impact on subsystems and supporting systems can be significant. The time required from launch to rendezvous in the synchronous orbit is nominally 15 hours (about 7 hours if a coplanar launch is achieved). The time required to rendezvous in the low Earth orbit can be kept to about 1 to 2 hours by means of non-coplanar launches. In this mode of operation for the low Earth orbit, the rendezvous vehicle is launched as near coplanar with the MORL as possible, but with the exact launch time determined by the phasing of the target, i. e., phasing is achieved by holding on the launch pad rather than in a phasing orbit. All possible phasing of the MORL will occur in one MORL orbit period; thus, it is necessary to have a launch window of only one orbit period to ensure the desired phasing. With a 28.5-degree inclined MORL orbit, the maximum plane change that will occur during this launch window is less than 0.5 degree. This amount of plane change can be handled by the S-IB booster by turning during boost at a cost of only 200 pounds of payload, relative to a due east, coplanar launch. Therefore, the subsystems aboard the logistics vehicle must be operational for about 15 to 20 hours for the synchronous-orbit mission and operational for only 1 to 4 hours for the low Earth orbit.

With the out-of-plane ascent mode for the low Earth mission, the ground tracking and communications networks need not be any more extensive than for the synchronous-orbit mission during ascent and rendezvous. If a phasing orbit is used for low-Earth-orbit rendezvous, long wait times in the phasing orbit can be encountered; this wait would tie up extensive tracking facilities, including ships.

#### 4.5.2 Orbit Keeping

Due to aerodynamic drag, 575 pounds of propellant are required per year to maintain a detached MOT in a 250-nautical-mile orbit. Due to gravity perturbations of the Sun and Moon, 500 pounds of propellant are required to maintain a detached MOT in synchronous orbit. This difference in orbit-keeping propellant requirements for these two modes is not sufficient to conclude that one mode is superior to the other.

In the synchronous orbit, orbit-keeping corrections are necessary only every 30 days, i. e., just before each rendezvous, whereas, in the 250-nautical-mile orbit, orbit-keeping maneuvers are necessary at least every 45 days and, on occasion, as frequently as every 15 days. Even this may not be a significant difference.

The  $\Delta V$ 's required for stationkeeping beyond those required for orbit-keeping at these two orbit altitudes are insignificant; however, the frequency of maneuver may be significant because at 250 nautical miles, stationkeeping may be necessary as frequently as 9 hours; but, at synchronous-orbit altitude, stationkeeping due to external disturbances is necessary no oftener than 30 days.

The above discussion similarly applies to the soft-gimbal configuration.

#### 4.5.3 Re-Entry

The environment of entry from synchronous orbit is far more severe than the environment of entry from a 250-nautical-mile orbit, and the entry corridor is more restricted when returning from synchronous orbit. However, the Apollo system is designed for entry from the Moon; this entry is more severe and restricted than entry from synchronous orbit. By the time the MOT is operational, the capability of the Apollo to enter from the Moon will have been demonstrated so that entry should present no serious threat to the feasibility of the synchronous-orbit MOT.

The recovery zone for return from synchronous orbit is relatively small (see Figure 3.4-1) irrespective of where the synchronous orbit is departed. The recovery zone for return from a low Earth orbit is somewhere between 28.5° N latitude and 28.5° S latitude depending on orbit departure. However, if the same time for return is allowed from the low Earth orbit as from synchronous orbit (about 6 hours), the longitude of the recovery site can be similarly localized or, stated another way, greater flexibility in recovery zone location is possible from the low Earth orbit.

#### 4.5.4 Conclusions

There is no serious flight-performance problem that threatens the feasibility of either the low-Earth-orbit MOT operation or the synchronous-orbit MOT

operation. As a consequence, neither operation enjoys a distinct superiority over the other with respect to flight-performance considerations.

The synchronous orbit may have a slight operational advantage in that station-keeping operations are required less frequently.

In case of adversities during deorbit maneuvers, a safe Earth return from the low Earth orbit is more probable than from the synchronous orbit.

Selection of the MOT orbit can be based on criteria other than flight performance.

#### 4.6 OPERATIONAL COMPARISON

Before comparing the capabilities of the MOT in synchronous orbit with those in the low Earth orbit, it was necessary to establish common baselines. This required updating the low-Earth-orbit program to the same criteria used for the synchronous-orbit study. This updating included consideration of the effect of radiation on the photographic film and reallocation of the percentage of time assigned to high-dispersion UV and visible observations. It was determined after the initial (low-Earth-orbit) study that it was more realistic to devote more time to high-dispersion UV observations by the MOT. Figure 4.6-1 reflects the updated 1-year program summary for the low Earth orbit, including these revisions plus consideration for large-scale photography of planetary objects. The latter item was omitted from the previous study, but represents an important astronomical capability from an orbiting telescope.

The comparison then was based on the same experiments being conducted for the same percentage of time per year. There are two approaches in determining the number of trips required between the MORL and MOT to replace the film. Either the number of trips is nearly doubled in synchronous orbit to be compatible with the increased observation capability, keeping the size of the film cassettes the same, or the number of trips is kept similar and the size of the cassettes increased. The larger film pack is considered to be of a reasonable size. The increase in number of trips required between the MORL and MOT results in a penalty in terms of time and expendables. Therefore, the frequency of trips was kept the same and the capacity of the film packages increased. Therefore, there is no difference in the typical program represented on Figure 3.5-6 for the synchronous orbit as compared to the low Earth orbit.

From an operational standpoint then, the relative differences occur in the observation time available and in the amount of data obtained, neglecting the MORL crew time differences that would exist for developing, analyzing, and handling the greater volume of data. Detailed analysis of crew duty aboard the MORL is not included as an objective of this study.

##### 4.6.1 Observation Time

Potentially, 24 hours per day are available for observations (from synchronous orbit) of stellar objects and 22.4 hours per day for planetary targets. From the low Earth orbit, 45 minutes during each 90-minute orbit or a total of 12 hours per day is available. Approximately twice as much observation time is therefore available from the synchronous orbit as from the low Earth orbit; this is shown by comparing the data in Figures 3.5-7 and 4.6-1 for the synchronous orbit and low Earth orbit respectively.

	EFF. NO.	PERCENT OF TIME	NO. OF DAYS	NO. OF ORBITS	NO. OF TRIPS		USEFUL ORBITS	OBSERVATION TIME AT 4.5 MKR. PER ORBIT	ORBITS PER TARGET	NO. OF OBSERVATIONS PER TARGET	NO. OF TARGETS
					EQUIPMENT SETUP & CHECKOUT	REPLACE FILM					
WIDE FIELD PHOTOGRAPHY	15	13	47	752	1	15	717	536 HRS	3	3	139
LOW DISPERSION SPECTRA SPECTROMETER & SPECTROGRAPH	15	14	52	832	1	0	809	607 HRS	23	4	15
HIGH DISPERSION SPECTRA ULTRAVIOLET	15	15	55	880	2	6	858	643 HRS	5	1	171
PHOTOELECTRIC PHOTOMETRY	30	3	11	176	1	1	169	127 HRS	10	1	17
LARGE SCALE PHOTOGRAPHY	30	15 } 18 3 }	66	1056	2	32	982	736 HRS	2	2-4 **	482 ---
HIGH DISPERSION SPECTRA VISIBLE	30	8	29	464	1	5	449	337 HRS	18	3	20
HIGH DISPERSION IR	30	3	11	176	1	1	169	127 HRS	1	1	100
THERMOELECTRIC MEASUREMENTS	30	4	21	336	1	2	327	245 HRS	10	1	33
		80	292		10	71	4480	3360 HRS			
OPEN ROTATION (REHEZVOUS, DOCKING, ETC)		1	2								
MAINTENANCE & REPAIR REQUIREMENTS											
<u>SCHEDULED</u>		3	12	192							
<u>SCIENTIFIC EQUIPMENT</u>		1	4	64							
CHANGE SECONDARY MIRROR		15	54	864							
<u>UNSCHEDULED</u>											15*

- NOTES:
- SLIDING & FILM STABILIZATION REQUIRED FOR EACH NEW TARGET
  - TRIPS TO REPLACE FILM, SLIDES, OR TAPE - 3 HRS (2 ORBITS)
  - TRIPS TO SETUP & CHECKOUT EQUIPMENT - 7.5 HRS (5 ORBITS)
  - ROUTINE MAINTENANCE - 3 DAYS APPROXIMATELY EVERY 3 MONTHS
  - 1 ORBIT = 90 MINUTES - POTENTIAL OBSERVATION TIME/ORBIT = 45 MINUTES
- \* ESTIMATED NUMBER OF TRIPS BETWEEN MAINT & WGT TO ACCOMPLISH UNS. SCHEDULED MAINTENANCE
- \*\* EXPOSURE TIME FOR PLANETARY TARGETS IS RELATIVELY SHORT, BUT THE NUMBER OF EXPOSURES PER PLANET, SUCH AS FOR MARS, ARE IN THE ORDER OF THOUSANDS (TIME LAPSED)

FIGURE 4.6-1 ONE-YEAR ASTRONOMICAL PROGRAM SUMMARY - LOW ORBIT

#### 4.6.2 Experiment Expendables

The principal function of the MOT is to make scientific observations of planetary and stellar bodies and to provide a permanent record of these observations. Material for these records constitutes the experiment expendables.

Observations fall into four general classifications: photography, photometry, spectrometry, and polarimetry. Photography is further divided into the three subcategories of narrow-field, wide-field, and large-scale photography. Photometry is subdivided into photoelectric and thermoelectric processes. Spectrometry is subdivided as low-dispersion, high-dispersion (UV), and high-dispersion spectra (IR). Polarimetry is subdivided as thermoelectric measurement and photoelectric photometry.

Recorders and recording media for the various scientific observations are presented in Figure 4.6-2.

Wide-field photography is recorded on roll film (16- by 16-inch format) and large-scale photography is recorded on 2- by 2-inch plates. Low-dispersion spectrographic data is recorded on 0.6- by 0.6-inch slides; high-dispersion spectrographic data is recorded on roll film 1.4 inches wide. The remainder of the data is recorded on rolls of 0.5-inch-wide magnetic tape.

The number of exposures for each type of observation and the resultant number and size of recording media cassettes are shown in Figure 4.6-3. The approximate size, volume, and weight of recorder media are illustrated in Figure 4.6-4.

Data for large-scale photography of planetary objects is omitted from Figures 4.6-3 and 4.6-4 because the potential quantity of exposures for observation of the planets is very large due to the relatively short exposure time (1 to 15 seconds) per photograph. It is assumed that even though the quantity of exposures may be in the thousands, a 70-millimeter camera could be used, thus placing the weight and volume of film considered within the 100-percent growth allowance for logistics.


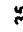




#### 4.6.3 Conclusions and Recommendations

When comparing the telescope use time provided in the soft-gimbal mode and in the detached mode, it was assumed that shuttle travel would be accomplished in parallel with telescope operation. This would not reduce the potential observation time for the detached mode. Docking, pressurization of the MOT cabin, and the crew-transfer operation would then be identical for both modes. This may be a reasonable assumption for normal operation; but, in event of an emergency or malfunction that halted telescope operation, the shuttle entry, checkout, and transit time to the MOT would subtract from the total time available. Also, additional manhours are expended for crew transfer in the detached mode.

GENERAL SCIENTIFIC OBSERVATION	SPECIFIC SCIENTIFIC OBSERVATION	SCIENTIFIC OBSERVATION RECORDER	RECORDER MEDIA
Photography	*Narrow Field Photography *Wide Field Photography *Large Scale Photography	Narrow Field Camera Wide Field Camera Large Scale Camera	Film Film Film
Photometry	Photoelectric Photometry Thermoelectric Photometry	Photoelectric Photometer + T.R. Thermoelectric Photometer + T.R.	Tape Tape
Spectrometry	Low Dispersion Spectra High Dispersion Spectra (UV) High Dispersion Spectra (IR)	Low Dispersion Spectrometer + T.R. Low Dispersion Spectrograph High Dispersion Spectrometer + T.R. High Dispersion Spectrograph High Dispersion Spectrometer + T.R.	Tape Film Tape Film Tape
Polarimetry	Thermoelectric Measurements Photoelectric Photometry	**Photometer + Polarimeter + T.R. **Photometer + Polarimeter + T.R.	Tape Tape
* T.R. **	Synonomous Tape Recorder Adapter Hardware which is used in conjunction with Photometers		

FIGURE 4.6-2 SCIENTIFIC OBSERVATION - RECORDER MEDIA



SCIENTIFIC OBSERVATION RECORDER	Recorder Media			NUMBER OF EXPOSURES						APPROXIMATE SIZE - INCHES						
	FLM	PLATES	TAPE	Media Format	Low Orbit		Synchronous Orbit		Low Orbit		Synchronous Orbit		Low Orbit		Synchronous Orbit	
					PER CASSETTE	PER YEAR	PER CASSETTE	PER YEAR	PER CASSETTE	NO. OF CASSETTE	PER CASSETTE	NO. OF CASSETTE	PER CASSETTE	NO. OF CASSETTE		
Wide Field Camera	X			16" x 16"	45	717	90	1431	3 x 3 x 16	16	3 x 4 x 16	16	3 x 4 x 16		16	
Large Scale Camera	X	X		2" x 2"	85	2916	145	4920	2.5x5.0x16	34	5 0x5.0x16	34	5 0x5.0x16		34	
Stellar Planetary	X				--	17	--	34	--	--	--	--	--		--	
Photoelectric Photometer + T. R.			X		--	35	--	70	--	--	--	--	--		--	
Low Dispersion Spectrometer + T. R.	X			0.6 x 0.6	11	105	21	210	1 x 1 x 2	10	1 x 2 x 2	10	1 x 2 x 2		10	
Low Dispersion Spectrograph			X		--	169	--	313	--	--	--	--	--		--	
High Dispersion Spectrometer (IR) + T. R.			X		--	171	--	343	--	--	--	--	--		--	
High Dispersion Spectrometer (UV) + T. R.	X			1.4" x 21"	13	75	12	150	3 x 3 x 1.5	6	3 x 6 x 1.5	6	3 x 6 x 1.5		6	
High Dispersion Spectrograph			X		--	33	--	63	--	--	--	--	--		--	
Thermoelectric Photometer + T. R.			X		--		--		--	--	--	--	--		--	


 2 RECORDERS INCLUDING 2/100 FT OF 1/2" TAPE TO BE USED ALTERNATELY

FIGURE 4.5-3 MOT SCIENTIFIC RECORDER MEDIA SIZE

SCIENTIFIC OBSERVATION RECORDER	Recorder Media			APPROXIMATE VOLUME-CUBIC INCHES						APPROXIMATE WEIGHT - POUNDS					
	FILM	PLATES	TAPE	Low Orbit		Synchronous Orbit		Low Orbit		Synchronous Orbit		Low Orbit		Synchronous Orbit	
				PER CASSETTE	PER YEAR	PER CASSETTE	PER YEAR	PER CASSETTE	PER YEAR	PER CASSETTE	PER YEAR	PER CASSETTE	PER YEAR		
Wide Field Camera	X			144	2304	192	30??	4	64	8	128				
Large Scale Camera															
Stellar	X	X		200	6800	400	13,600	5	170	10	340				
Planetary	X														
Photoelectric Photometer + T. R.			X												
Low Dispersion Spectrometer + T. R.			X												
Low Dispersion Spectrograph	X			2	20	4	40	0.25	2.5	0.5	5.0				
High Dispersion Spectrometer (IR) + T. R.			X												
High Dispersion Spectrometer (UV) + T. R.			X												
High Dispersion Spectrograph	X			14	84	28	168	2.5	15.0	5.0	30				
Thermoelectric Photometer + I. R.			X												
SUBTOTAL				9208		16,880		251.5		503.0					
GROWTH ALLOWANCE (100%)				9208		16,880		251.5		503.0					
TOTAL				18,416		33,760		503.0		1006.0					

2 RECORDERS INCLUDING 2400 FT OF 1/2" TAPE TO BE USED ALTERNATELY

FIGURE 4.6-4 MOT SCIENTIFIC RECORDER MEDIA VOLUME & WEIGHT

Therefore, on the basis of these considerations, the soft-gimbal concept is the most favorable mode.

A primary factor in the comparison of low Earth versus synchronous orbit, from the operational standpoint, is the available observation time. As discussed in Section 4.6, approximately twice the amount of time is available from synchronous orbit as from low Earth orbit. Figures 3.5-7 and 4.6-1 indicate that the available observation time per year from low Earth orbit is approximately 3360 hours compared to 6657 hours from synchronous orbit. A significant advantage from synchronous orbit is the capability of obtaining continuous observation during a 24-hour orbit as compared to a maximum of 45 minutes out of each 90 minutes when in the low Earth orbit. Therefore, a comparison based on telescope use or observation time indicates that the synchronous-orbit concept would be the recommended mode.

## 4.7 SYSTEM EVALUATION

Definition of the comparison criteria for the MORL-MOT concepts is presented in the following sections together with a summary comparison of the four MOT operational concepts. Advantages and disadvantages are discussed for the MOT operating in the soft-gimbal mode versus the detached mode and for operation at synchronous-orbit altitude versus a low-Earth-orbit altitude of 250 nautical miles.

### 4.7.1 Comparison Criteria

The following defined criteria are those considered significant for comparison of the various MOT concepts of operation. In general, the criteria are similar to those used for evaluation of the basic study low-Earth-orbit concepts and documented in Section 4.8 of Reference 1.

**Technical Risk** — defined as the probability of systems not meeting design or operational requirements by a specified operational date. Technical risk is measured by assessing new and unsolved design problems that are required for each concept.

**Reliability** -- defined as the probability that the vehicles and subsystems will be available for operations.

**Safety** — measured as the probable number of fatal accidents per year of operation. The major safety hazards result from: (1) docking the MOT; Apollo, and the shuttle vehicles; (2) repositioning of the Apollo, logistics modules, and the shuttle vehicle; (3) radiation and micrometeoroids; and (4) handling propellants, gases, and electrical equipment.

**Flexibility** — defined as the ability of a system to perform alternate missions without major modification to vehicles or equipment.

**Accessibility to Man** — reflects the ease with which the crew can accomplish servicing, checkout, and maintenance tasks.

**Man's Ability to Perform Assigned Tasks** — measured by the manhours required to perform MOT servicing, setup and checkout, and maintenance operations.

**Logistics Weight** — defined as the weight of logistics supplies required to support the MOT for 1 year of operation.

**MORL Interface Problems** -- evaluated in terms of the ability to perform MORL experiments in addition to the MOT experiments.

Observation Time — defined as the total hours available per day and per year for observation with the telescope and as the maximum available time per continuous exposure.

Thermal Distortions — defined as physical distortions of the primary mirror and the telescope tube caused by temperature gradients throughout the components.

Micrometeoroid Hazard — measured in terms of potential damage to the primary mirror and probability of penetration of the walls of the baseline configuration.

Radiation Hazard - measured in terms of shielding requirements for the crew and photographic film, the extent of performance degradation of the exposed optical surfaces and thermal coatings and effects on system operations.

Attitude-Stability-and-Control Requirements — measured in terms of the magnitude of the disturbance environment and the resultant requirements on the attitude stability and control system physical characteristics.

Flight Performance — defined in terms of (1) time to rendezvous, (2) frequency of stationkeeping reboost, (3) time to return to Earth, (4) recovery area requirements, and (5) entry corridor characteristics.

Data Management, Communications, and Guidance and Electrical Power — defined in terms of vehicle and ground system requirements and complexity.

Cost — measured in dollar cost of launch vehicles and launch support. Costing of the other factors of the MORL-MOT systems is beyond the scope of this study and is not considered essential to a comparison of the system differences. Except for the different launch vehicles required for operation in synchronous orbit as compared to low Earth orbit, the MORL-MOT systems are judged to be similar in relative cost.

#### 4.7.2 Systems Comparison

A summary comparison of the four MOT operation systems is presented in the following sections with regard to the choice of mode of operation and the choice of orbit altitude.

4.7.2.1 Mode of Operation — The criteria that affect the choice of mode of operation are:

- 1) Technical Risk;
- 2) Reliability;
- 3) Safety;

- 4) Flexibility;
- 5) Accessibility to Man;
- 6) Man's Ability to Perform Assigned Tasks;
- 7) Logistics Weight;
- 8) MORL Interface Requirements;
- 9) Attitude Stability and Control.

Of these criteria, only the logistics weight and the attitude-stability-and-control system are significantly affected by the operational orbit altitude. Operation in the detached mode requires less logistics support (measured in pounds of spares and expendables) for the low-Earth-orbit case, while the synchronous-orbit-case is favored by operation in the soft-gimbal mode. The detached mode is somewhat preferred in the synchronous-orbit case with respect to attitude-stability-and-control system requirements because of the reduced disturbance environment. However, the penalty for operation in the soft-gimbal mode is small.

Pro and con discussions of the remainder of the criteria listed above apply equally well to operation in either orbit; these are presented in Section 4.8 of Reference 1. In the low-Earth-orbit study the soft-gimbal mode was determined to be preferable. The effects of logistics weight and stability and control-system characteristics, as discussed above, are not considered to be large enough to change the preference for the soft-gimbal mode in a synchronous orbit. The advantages of direct access to the MOT from the MORL, elimination of requirements for stationkeeping of the MOT with respect to the MORL, elimination of the shuttle vehicle, and elimination of a self-sufficient electrical power system from the MOT are considered to be worth development of the soft-gimbal system.

4.7.2.2 Orbital Altitude — The comparison criteria pertinent to the selection of an operational altitude include:

- 1) Observation Time;
- 2) Thermal Distortions;
- 3) Micrometeoroid Hazard;
- 4) Radiation Effects;
- 5) Attitude-Stability-and-Control System Requirements;
- 6) Flight Performance;
- 8) Logistics Weight;

- 8) Data Management, Communications, Guidance, and Electrical Power Systems Characteristics;
- 9) Cost.

Observation Time — The available observation time for the telescope is discussed in detail in Section 3.5 and in Reference 1 for operation in synchronous orbit and in the low Earth orbit, respectively. The more significant results are presented in Figure 4.7-1. In general, approximately twice as much time is available for observations from a synchronous orbit as from a low Earth orbit.

	Low Earth Orbit	Synchronous Orbit
Potentially Available Time Per Year	3360 hrs	6657 hrs
Total Available Time Per Day (24 Hrs)	12 hrs	24 hrs
Type of Observation Per 24-Hour Day	Intermittent	Continuous
Available Time Per Continuous Exposure	45 minutes	Virtually Unlimited

Figure 4.7-1: OBSERVATION TIME COMPARISON

Thermal Distortions — Degradation of the primary mirror performance by thermal distortion in synchronous orbit is reduced considerably from that in the low Earth orbit. The RMS deviation is reduced by a factor of approximately 4.5 to 7.5 as shown in Figure 4.7-2, however, the performance in low Earth orbit is within the acceptable limit.

	RMS Deviation
<u>Synchronous Orbit</u>	
Perpendicular to Solar Vector	$\lambda/332$
Parallel to Solar Vector — Dawn	$\lambda/226$
Parallel to Solar Vector — Noon	$\lambda/372$
<u>Low Earth Orbit</u>	
Perpendicular to Solar Vector	$\lambda/50$
● Minimum Required Primary Mirror Quality $\lambda/30$ at 5000 Å	

Figure 4.7-2: PRIMARY MIRROR THERMAL DISTORTIONS

Micrometeoroid Hazard — Direct meteoroid damage to the primary mirror in synchronous orbit is somewhat greater than in the low-Earth-orbit case. However, the effect on the useful life of the telescope in either case is negligible. The useful life before the damage limit is reached is approximately 75 years for the synchronous-orbit case and 101 years for the low-Earth-orbit case. The probability of meteoroid penetration of the telescope wall increases approximately 50 percent in the synchronous orbit over that experienced in the low Earth orbit, but is still a minor consideration.

Radiation Effects -- Radiation shielding requirements for operating in synchronous and in low Earth orbits are compared in Figure 4.7-3. Protection of the crew in synchronous orbit for a 180-day stay time requires the addition of a biowell and extra laboratory shielding to the MORL — a subsequent weight increase of approximately 14,200 pounds. In addition, 15-g/cm<sup>2</sup> goggles must be worn during solar events. Operation in a low Earth orbit requires wearing of 7-g/cm<sup>2</sup> goggles while passing through the belts of trapped radiation particles.

Radiation sensitivity of film is such that shielding is required at both orbital altitudes and the useful life of the film is limited to approximately 60 days in either case. Film storage for 60 days in synchronous orbit will require shielding equal to a 40-g/cm<sup>2</sup>-thick aluminum box located within the MORL biowell, an additional weight penalty of approximately 1000 pounds. Protection in the low Earth orbit will require shielding equivalent to a 48-g/cm<sup>2</sup> aluminum box in the MORL without the biowell. Film in the MOT in synchronous orbit will require no additional shielding during a 7 to 9 day period of use; but, occasionally this film will be degraded by radiation from a solar flare; shielding against this hazard is impractical. For operation in low Earth orbit, a shield of 10 to 15 g/cm<sup>2</sup> will be used around MOT instrumentation containing film.

The primary mirror performance in synchronous orbit is degraded slightly more by radiation effects than for operation in a low Earth orbit. In 5 years the limiting star magnitude is reduced to 22.6 for ef/15 and 22.3 for ef/30 in synchronous orbit, as compared to 22.8 and 22.5 respectively, for the low Earth orbit.

Radiation effects on the MOT external thermal coatings are not significant in either orbit.



	Synchronous Orbit	Low Earth Orbit
Man 180 Days	15 g/cm <sup>2</sup> goggles (to be worn during solar events, additionally) biowell shielding = 10 g/cm <sup>2</sup>	7 g/cm <sup>2</sup> goggles to be worn when passing through trapped belts (MORL = 2 g/cm <sup>2</sup> )
Film Storage 60 Days	40-g/cm <sup>2</sup> -thick box located in biowell	48-g/cm <sup>2</sup> -thick box
Film in MOT	None	10 to 15 g/cm <sup>2</sup> around cameras

Figure 4.7-3: ADDITIONAL RADIATION SHIELDING REQUIREMENTS

Attitude Stability and Control — External disturbance torques are two orders of magnitude less in synchronous orbit than in low Earth orbit. Within limits, disturbance torques are beneficial in that constant precession of the control moment gyros is required, thus reducing stiction and, subsequently, pointing errors. The external disturbance effects in synchronous orbit are quite minimal.

Control-moment-gyro momentum capability required in synchronous orbit is approximately one-half that required for the low Earth orbit, considering the reduced disturbances and longer exposure times in synchronous orbit.

The difficulty of attitude control is not particularly sensitive to orbit altitude; however, a slight advantage is indicated for the synchronous orbit. Control within the required 0.01 arc-second appears feasible in either orbit.

Flight Performance — A comparison of the flight-performance characteristics for the low-Earth- and the synchronous-orbit MOT systems is summarized in Figure 4.7-4. The time to rendezvous is greater for the synchronous orbit than for the low Earth orbit by a factor between 5 and 8.

Reboost for stationkeeping in the low Earth orbit is required approximately each 9 hours, due primarily to aerodynamic drag. In synchronous orbit, corrections are required only once each 30 days.

Minimum elapsed time for return to Earth from orbit is approximately 1 hour from the low Earth orbit and increases to approximately 6 hours from synchronous orbit.

The landing and recovery area for vehicles returning from the generally fixed position in a synchronous orbit is a relatively small portion of the Earth's surface located in the western Pacific Ocean. Therefore, a relatively small recovery

force is needed; but, return through a narrow entry corridor is required. If immediate deorbit and descent from a low Earth orbit is made, recovery may be anywhere throughout a 57-degree-wide band extending around the Earth's equator.

<u>Criteria</u>	<u>Low Earth Orbit</u>	<u>Synchronous Orbit</u>
Time to rendezvous	1 to 4 hours	8 to 20 hours
Stationkeeping boost frequency (worst case)	9 hours	30 days
Time to return to Earth	1 hour	6 hours
Recovery zone	Anywhere between 30°N and 30°S latitude for 1-hour return  Selected latitude or longitude for 3-hour return	Longitude localized and inflexible
Entry corridor	Broad	Narrow

Figure 4.7-4: FLIGHT PERFORMANCE COMPARISON

Logistics Weight — The logistics vehicle weight requirements for the synchronous orbit are less severe with regard to booster capability than for the low Earth orbit, primarily because of the increased booster capability and the decreased propellant cargo (for attitude control, stationkeeping, and orbit-keeping) requirements for synchronous orbit. Propellant requirements for the low Earth orbit are approximately double those for the synchronous orbit. Resupply launches are reduced from one each 90 days for the low Earth orbit to one each 180 days for the synchronous orbit. A weight summary of the logistics vehicles for the two orbits is shown in Figure 4.7-5.

	<u>180-Day Supply Cycle</u>		<u>90-Day Supply Cycle</u>	
	<u>Synchronous Orbit</u>		<u>Low Earth Orbit</u>	
	<u>Gimbal</u>	<u>Detached</u>	<u>Gimbal</u>	<u>Detached</u>
CSM	36,225	36,475	13,027	13,027
MMM	8,438	8,583	6,151	6,201
Cargo	11,284	13,198	8,755	8,481
Launch Weight	55,947	58,256	27,933	27,709
Capability	79,600	79,600	36,000	36,000
Excess	+23,653	+21,344	+ 8,067	+ 8,291

Figure 4.7-5: LOGISTICS VEHICLE WEIGHT SUMMARY

Data Management and Communications — The MOT data management subsystem and the MOT-MORL communication links are basically independent of orbit altitude, being concerned with transfer of information between the MOT and the MORL only.

MORL data management and communications are improved by operation in synchronous orbit in that continuous communication with a single ground station is possible. The low-Earth-orbit system requires two ground stations and achieves a contact time of only an average of 77 minutes per day. For the synchronous-orbit case, much of the data storage may be located on the ground because of the continuous contact with the MOT and MORL.

The single ground station associated with the synchronous orbit makes all electronically transmitted data available at one site without relay, requires the MORL to maintain contact with only one slowly moving (relative) ground station, eliminates the need for rapidly slewing space-borne antenna, and reduces the amount of redundant data that must be transferred.

Physical return of film-recorded data is required from either orbit altitude.

Electrical Power — The electrical power subsystem used in synchronous orbit is essentially the same as that for low Earth orbit, but considerable reduction in system size and weight is gained by operation in synchronous orbit.

In the synchronous orbit, detached mode, the solar panels are without sunlight a maximum of 1.2 hours per 24 hours, while for the low Earth orbit they are without sunlight for 35 minutes out of each 1.5-hour orbit. This allows a reduction of approximately 40 percent in the solar panel size — from 216 square feet to 132 square feet — with a weight reduction of 128 pounds.

Since the batteries in synchronous orbit are cycled only 90 times per year as compared to 6759 times per year for the low Earth orbit, silver-zinc batteries weighing 212 pounds are used in synchronous orbit instead of the 595 pounds of silver-cadmium batteries used in low Earth orbit.

Cost — Both the synchronous-orbit and low-Earth-orbit MOT-MORL systems require launchings each 90 days and use similar vehicles except for the launch vehicles. Therefore, the significant cost difference is the launch vehicles used. Nominally, six launchings are required per year to assemble the MOT-MORL system in orbit and maintain it in operation for 1 year of a continuous 5-year period.

The low-Earth-orbit MOT-MORL system uses the Saturn-IB launch vehicle with a cost of approximately \$20.5 million per launch or \$123 million for a 1-year period. The synchronous-orbit MOT-MORL system uses a Saturn V vehicle with a launch cost of approximately \$63 million per launch or \$378 million for one year. These typical values of cost per launch include launch services and are

based on a use rate of 10 per year for a period of 5 years, beginning January 1968.

Although the launch vehicle cost is approximately tripled for operation in synchronous orbit, the useful observation time of the telescope is essentially doubled, resulting in an effective launch-vehicle-cost to observation-time ratio of approximately 1.5 to 1. Since the launch vehicle cost is only part of the overall system cost, the relative increase in system cost and observation time is less than 1.5; but, a complete and detailed cost analysis is beyond the scope of this study.

A complete system cost analysis and comparison will include consideration of additional factors such as detailed design, development, and qualification of spacecraft hardware. Operational support systems, such as tracking systems, communications requirements, and data handling facilities will have to be defined in detail and cost charges determined. These will be dependent upon the extent of mutual use of these facilities among the MOT and other operational space systems of the same time period. An extensive plan of program development will disclose cost factors that are not discernable at the present time.

#### 4.7.3 General Conclusions and Recommendations

4.7.3.1 Mode of Operation — The study results indicate that the soft-gimbal mode is preferred over the detached mode for both the synchronous orbit and the low earth orbit.

- The choice of mode has essentially no effect on the time available for observation.
- The soft-gimbal mode is preferable with respect to crew utilization, safety, accessibility, and overall logistics requirements because of the direct access between the MORL and the MOT.
- The detached mode is preferable with respect to technical risk because it is dependent on relatively well-developed docking and shuttle techniques. Use of the soft-gimbal mode will require design, development, testing, and qualification of a specialized and critical unit of hardware.

4.7.3.2 Operational Altitude — Operation in synchronous orbit is preferred to a low Earth orbit, and the mode of operation has only a small influence on this choice.

- Available observation time is virtually doubled in synchronous orbit over that in low Earth orbit.
- Long uninterrupted periods of observation are available to synchronous orbit.
- The decrease disturbance environment allows the attitude-control system size to be reduced in synchronous orbit.
- The decreased thermal gradients in synchronous orbit result in less distortion of the telescope structure and primary mirror.

- Electrical-power subsystem requirements are reduced in synchronous orbit for the detached mode.
- Increased radiation protection is required in synchronous orbit for the crew and film with the risk of occasional loss of film in the MOT by radiation from a solar flare.
- Cost of operation in synchronous orbit is higher but may be offset by operational advantages.

4.7.3.3 Recommended Follow-On Studies — It is recommended that future studies of the manned orbital telescope include the following:

- Design, manufacture, and development of a 120-inch primary mirror.
- Investigation of the attitude-control system in detail beyond that of the present studies.
- Design and further evaluation of soft-gimbal hardware.
- Further definition and integration of astronomical and astrophysical requirements with regard to use of a large space-borne telescope.
- Definition of a development program plan and a detailed costing analysis.

## 5.0 REFERENCES

1. "A System Study of a Manned Orbital Telescope," Boeing Document D2-84042-1, October 1965.
- 2--28 "Report on the Optimization of the Manned Orbital Research Laboratory (MORL) System Concept," Volumes I through XXVII, Douglas Aircraft Company, September 1964.

<u>Reference</u>	<u>Vol</u>	<u>Title</u>	<u>Report</u>
2	I	Technical Summary	SM-46072
3	II	Systems Analysis — Mission Analysis and Results	SM-46073
4	III	Systems Analysis — Experimental Program	SM-46074
5	IV	System Analysis — Flight Crew	SM-46075
6	V	Systems Analysis — Operations	SM-46076
7	VI	Systems Analysis — Mission Profile Data	SM-46077
8	VII	Systems Analysis — Reliability and Safety	SM-46078
9	VIII	Effectiveness Studies — Alternate Missions	SM-46079
10	IX	Effectiveness Studies — MORL and Unmanned Concepts	SM-46080
11	X	Effectiveness Studies — MORL and Other Manned Concepts	SM-46081
12	XI	Laboratory Configurations and Interiors	SM-46082
13	XII	Laboratory Mechanical Systems — Structures	SM-46083
14	XIII	Laboratory Mechanical Systems — Artificial Gravity	SM-46084
15	XIV	Laboratory Mechanical Systems — Environmental Control and Life Support	SM-46085
16	XV	Laboratory Mechanical Systems — Stabilization and Control	SM-46086
17	XVI	Laboratory Mechanical Systems — Propulsion and Reaction Control	SM-46087
18	XVII	Laboratory Electrical and Electronic Systems — Electrical Power	SM-46088
19	XVIII	Laboratory Electrical and Electronic Systems — Alternate Power Systems	SM-46089

<u>Reference</u>	<u>Vol</u>	<u>Title</u>	<u>Report</u>
20	XIX	Laboratory Electrical and Electronic Systems — Communications and Telemetry	SM-46090
21	XX	Logistics System	SM-46091
22	XXI	Alternate Logistics System	SM-46092
23	XXII	Experiment Briefs, Part I, II, and III	SM-46093 SM-46094 SM-46095
24	XXIII	Experimental Program — Tabulation of System Requirements	SM-46096
25	XXIV	Technology Studies	SM-46097
26	XXV	Preliminary Program Plan	SM-46098
27	XXVI	Reliability, Safety, and Quality Program Plan	SM-46099
28	XXVII	Cost Plan	SM-46100
29.		"Saturn V Design Data Book for Space Propulsion Systems," Boeing Document D5-10059.	
30.		"Supporting Data for the Attitude Stability and Control of a Manned Orbital Telescope," Boeing Document D2-84039-1, October 1965.	
31.		Laverty, N. P., "The Comparative Performance of Electron Tube Photo-detectors in Terrestrial and Space Navigation Systems," IEEE Transactions on Aerospace and Navigational Electronics.	
32.		Evans, W. J., "Aerodynamic and Radiation Disturbance Torques on Satellites Having Complex Geometry," Chapter 5 of <u>Torques and Attitude Sensing in Earth Satellites</u> , Singer SF, Academic Press, 1964.	
33.		Hanson, W. B., "Structure of the Ionosphere," Chapter 2 of <u>Satellite Environment Handbook</u> by F. S. Johnson, Stanford University Press, 1965.	
34.		Whipple, F. C., "On Meteoroids and Penetration," 9th Annual American Astronautical Society Meeting, Los Angeles, California, January 1963, revised version.	
35.		D'Astolo, "Meteoroid Hazard in Near Earth and Deep Space," NASA TM-X 50116.	
36.		Valley, Shea L., <u>Handbook of Geophysics and Space Environments</u> , Office of Aerospace Research, AFRL, 1965.	
37.		Saxton, J. H., "Aluminum-Nickel Mirrors," <u>Journal of the Optical Society of America</u> , Vol 48, No. 3, August 1958.	

38. "Study and Analysis of Lightweight Optical Elements," Perkin-Elmer Corporation Report 5857, under Contract AF33(616)-6877, October 1961.
39. Ullom, James R., "Recent Developments in Large High-Quality Optical Mirrors," Paper presented at the Society of Photographic Instrumentation Engineers, Los Angeles, California, April 9, 1962.
40. "Final Report — Feasibility Study of 120-Inch Orbiting Astronomical Telescope AE-1148, Prepared for Langley Research Center of the National Aeronautics and Space Administration by J. W. Fecker Division of American Optical Company, under Contract NAS T-1305-18.
41. Holland, L., Vacuum Deposition of Thin Films, John Wiley & Sons, Inc., New York, 1956.
42. Hass, Georg, Physics of Thin Films, Vol I, Academic Press, New York and London, 1963.
43. Whipple, Fred L. and Robert J. Davis, "Proposed Stellar and Interstellar Survey," The Astronomical Journal, Vol 65, No. 5, June 1960.
44. Hass, Georg and Richard Tousey, "Reflecting Coatings for the Extreme Ultraviolet," Journal of the Optical Society of America, Vol 49, No. 6, June 1959, p. 593.
45. Berning, P. H., G. Hass, and R. P. Madden, "Reflectance-Increasing Coatings for the Vacuum Ultraviolet and Their Applications," Journal of the Optical Society of America, Vol 50, No. 6, June 1960, p. 586.
46. Angel, D. W., W. R. Hunter and R. Tousey, "Extreme Ultraviolet Reflectance of LiF-Coated Aluminum Mirrors," Journal of the Optical Society of America, Vol 51, No. 8, August 1961, p. 913.
47. Hall, Joseph F. and Robert C. Allen, "Reflectance of Oxidized Silicon Monoxide Films Deposited onto Aluminum Mirrors Compared with Silicon Monoxide Evaporated in High Vacua," Journal of the Optical Society of America, Vol 51, No. 3, March 1961, p. 367.
48. Gillette, R. B. and R. R. Brown, "Space Radiation Tests on Reflecting Surfaces," Boeing Document D2-36359-1, Contract JPL 950998, June 2, 1965.
49. Canfield, L. R., G. Hass and J. E. Waylonis, "Further Studies on MgF<sub>2</sub>-Overcoated Aluminum Mirrors with Highest Reflectance in the Vacuum Ultraviolet," Applied Optics, Vol 5, No. 1, January 1966, p. 45.
50. Gillette, Roger B., "Experimental Studies and Investigation of Ultraviolet-Proton Radiation Effects on Solar Concentrator Reflective Surfaces," Boeing Document D2-84083-1, Contract NAS 1-5251, Quarterly Progress Report 1, July 1, 1965 through October 1, 1965.
51. Gillette, Roger B., "Experimental Studies and Investigation of Ultraviolet-Proton Radiation Effects on Solar Concentrator Reflective Surfaces," Boeing Document D2-84083-2, Contract NAS 1-5251, Quarterly Progress Report 2, October 1, 1965 through January 1, 1966.



52. Hufnagel, R. E. , "The Practical Application of Modulation Transfer Functions," Perkin-Elmer, Norwalk, Conn. , March 6, 1963.
53. Itek Corporation, Palo Alto Division, Photographic Reconnaissance Systems Study, Sections II and III (Secret), Appendix I (Unclassified), Document Control No. PA-466, prepared for Boeing.
54. Selwyn, E. W. H. , Photography in Astronomy. Eastman Kodak Company, Rochester, N. Y . 1950.
55. Fredrick, Laurence W. , editor. "Final Report -- Applications in Astronomy Suitable for Study by Means of Manned Orbiting Observatories and Related Instrumentation and Operational Requirements," Volumes I and II, Supported by NASA Grant NsG-480.
56. Kodak Plates and Films for Science and Industry Catalog P-9, Eastman Kodak Company. 1962.
57. Document 106-60, Telemetry Standards, Inter-Range Instrumentation Group, June 1962.
58. Kozma, A. , "Introduction to Optical Data Processing," University of Michigan Engineering Summer Conference Notes, Chapter 4, May 1965.
59. Annette, W. P. and D. G. Bradshaw, "Compilation of Data on Satellite Tracking Networks and Navigation Error Analysis Digital Computer Programs," Aerospace Group, The Boeing Company, May 19, 1965.
60. Mann, H. P. , "The Accuracy of AMR Instrumentation," Air Force Missile Test Center Technical Documentary Report MTC-TDR-64-1, Patrick Air Force Base, Florida, December 13, 1963.
61. Spitzer, Lyman, Jr. , "Space Telescopes and Components," The Astronomical Journal, Vol 65, No. 5, June 1960, p. 242.